2019

ANALYSIS AND DESIGN OF CASTELLATED BEAMS

Elaiwi, Sahar Sahib

UNIVERSITY OF PLYMOUTH

ANALYSIS AND DESIGN OF CASTELLATED BEAMS

By

SAHAR SAHIB ELAIWI

A thesis submitted to the University of Plymouth
in partial fulfilment for the degree of

DOCTOR OF PHILOSOPHY

School of Engineering

October 2019

Copyright Statement

This copy of the thesis has been supplied on condition that anyone who consults it is understood to recognise that its copyright rests with its author and that no quotation from the thesis and no information derived from it may be published without the author's prior consent.

ANALYSIS AND DESIGN OF CASTELLATED BEAMS

Sahar Sahib Elaiwi, Doctor of Philosophy, 2019

School of Engineering, University of Plymouth

ABSTRACT

The castellated beam is one of the steel members which uses less material, but has equal performance as the I-beam of the same size. Most of the castellated beams are fabricated from a standard universal I-beam or H-column, by cutting the web on a half hexagonal line down the centre of the beam, then these two halves are moved directly across by a half unit of spacing and re-joined by welding. This process leads to increasing the beam's depth and thus the bending strength and stiffness about the major axis, without adding additional materials. This allows castellated beams to be used in long-span applications with light or moderate loading conditions for supporting floors and roofs. In addition, the fabrication process creates openings on the web, which can be used to accommodate services.

Existing studies have shown that the resistance of the castellated beam is influenced by shear stresses, particularly those around web openings and under the T-section, which could cause the beam to have different failure modes. Therefore, web openings may reduce the shear resistance of the castellated beam. However, previous studies confirm that the method of analysis and design for the solid beam, may not be suitable for the castellated beam. Design guidance on the strength and stiffness for castellated beams is available in most countries, but also, some of them do not take into account the shear effect because as far as the bending strength is concerned, neglecting the shear effect may not cause direct problems. However, for the buckling and calculation of serviceability, the shear weakness due to web openings in castellated beams, could affect the performance of the beams and thus needs to be carefully reconsidered.

The aims of this study are, firstly to investigate the effect of web openings on the transverse deflection and lateral-torsional buckling of castellated beams, by using both analytical and numerical methods, whilst also adopting some of the previous studies for validating the

analytical results. The second aim, is to focus on the effect of both the geometric nonlinear and material inelasticity on castellated beams, under uniformly distributed load within different boundary conditions, through investigating the load-deflection curve and predicting the value of lateral-torsional buckling moment capacity, by using nonlinear numerical analysis method. The third aim, is to study the free vibration, static buckling and dynamic instability of castellated beams, w subjected to transverse periodic loading by developing analytical solutions.

The purpose of developing analytical solutions, which adopt the classical principle of minimum potential energy, is for the design and practical use; while the numerical solutions developed using the commercial software ANSYS are for the validation of the analytical solutions. By examining the results of analytical and numerical solutions obtained, a number of important features of the castellated beams are identified. This study has contributed to enhancing the knowledge of the effect of web openings on the performance of castellated beams subjected to uniformly distributed transverse loads with/or without being exposed to elevated temperatures. Data provided in these studies, can essentially be used by structural designers for providing better, economical and safe structures.

Keywords: castellated beam; shear effect, transvers deflection; lateral torsional buckling; dynamic analysis; finite element; linear and nonlinear; energy method; uniformly distributed loads; non-uniform temperature; simply supported; pinned-fixed supported.

ACKNOWLEDEMENTS

I'm so glad to have studied at the **University of Plymouth**. During my time in Plymouth city, I have gained a lot of friends, and studying there was like being in my hometown. My sincere gratitude to everyone for all the encouragement during my study. I want to tell all of them, thank you so much for everything, you have helped me.

AUTHOR'S DECLARATION

At no time during the registration for the degree of Doctor of Philosophy has the author been registered for any other University award without prior agreement of the Doctoral College Quality Sub-Committee.

Work submitted for this research degree at the University of Plymouth has not formed part of any other degree either at University of Plymouth or at another establishment.

Paper presentations were given at relevant conferences and several papers have been published.

Word count of main body of thesis: 34,956 words.

Figure count of the thesis: 69 figures.

Table count of the thesis: 16 tables.

Signed ……………Sahar. S. Elaiwi…**Date**………………7/oct/2019………

PAPERS AND CONFERENCES

This thesis is based on the following papers published in Journals/ conferences, which will be referred to in the text by their Roman numerals.

I.   Elaiwi, S., Kim, B. and Li, L. (2017). "Analysis and Design of Castellated Beams." The 2nd Annual International Conference on Structural Engineering and Mechanics 19-22 June, Athens, Greece. (Oral Presentation).

II.   Elaiwi, S., Kim, B. and Li, L. (2017). "Bending Analysis of Continuous Castellated Beams." World Congress on Advances in Structural Engineering and Mechanics (ASEM17) 28Augest-1September, llsan (Seoul), Korea. (Oral Presentation).

III.   Elaiwi, S., Kim, B. and Li, L. (2018). "Linear and Nonlinear Buckling Analysis of Castellated Beams." Eighth International Conference on Engineering Failure Analysis 8th-11th July, Budapest, Hungary. (poster Presentation)

IV.   Elaiwi, S., Kim, B. and Li, L. (2018). "Bending Analysis of Continuous Castellated Beams." Proceedings (pp. 1-14) of the 2017 World Congress on Advances in Structural Engineering and Mechanics (ASEM17) 28Augest-1September, 2017, llsan (Seoul), Korea.

V.   Elaiwi, S., Kim, B. and Li, L. (2019). "Bending Analysis of Castellated Beams." Athens Journal of Technology and Engineering, 6(1): 1-16.
       DOI: https:// doi=10.30958/ajte.6-1-1

       PEARL (OA): http://hdl.handle.net/10026.1/13030

VI.   Elaiwi, S., Kim, B. and Li, L. (2019). "Dynamic instability of castellated beams subjected to transverse periodic loading." Challenge Journal of Structural Mechanics, 5(1): 9-18. ISSN: 2149-8024.
       DOI: http://dx.doi.org/10.20528/cjsmec.2019.01.002

       PEARL (OA): http://hdl.handle.net/10026.1/13384

VII.   Elaiwi, S., Kim, B. and Li, L. (2019). "Linear and Nonlinear Buckling Analysis of Castellated Beams." International Journal of Structural and Civil Engineering Research, 8(2): ISSN: 2319-6009.

DOI: http://dx.doi.org/10.18178/ijscer.8.2.83-93

PEARL (OA): http://hdl.handle.net/10026.1/14327

LIST OF CONTENENTS

LIST OF TABLES

LIST OF FIGURES

CHAPTER ONE

1. INTRODUCTION

1.1. Motivation and background

Technological developments in all areas of construction are encouraging researchers and engineers as well as designers in the field to improve the performance of structural members of construction. This requires the development of detailed specifications for various individual structural members to be used in construction. The purpose of developing such high-quality standards is to improve the durability, safety, and serviceability of the structure as well as to reduce the materials and construction costs. **Figure 1-1** shows two images of the application examples of castellated beams used in the construction of Exchange House in London (photos were taken by Sahar Elaiwi).

Figure 1-1 Images of application examples of castellated beams in building construction in Exchange House in London

Steel is widely utilized in the structural field because of its advantages in material and mechanical properties as well as time saving in construction, which makes it preferable in most structures, particularly those used in high-rising buildings. However, due to the rapidly gaining appeal for steel construction especially in recent years, the steel cost becomes higher. Owing to the fact that the steel materials have poor fire resistance, buildings made from steel structures require the use of high-quality fireproof materials to protect steel members from fire, which further increases its cost.

Engineers and researchers have tried various methods to reduce the material and construction costs to help optimise the use of the steel structural members. The castellated beam is one of the steel members, which uses less material but has equal performance as the I-beam of the same size (Harper, 1991). In some of the publications (Altifillisch et al., 1957), the castellated beam is also referred to as the open-web expanded, perforated steel beam with web openings. The castellated beam is fabricated from a standard universal I-beam or H-column by cutting the web on a half hexagonal line down the centre of the beam. The two halves are moved across by a half unit of spacing and then re-joined by welding. This process increases the depth of the beam and hence the bending strength and stiffness about the major axis without adding additional materials. This allows castellated beams to be used in long span applications with light or moderate loading conditions for supporting floors and roofs. In addition, the fabrication process creates openings on the web, which can be used to accommodate services (see **Figure 1-2**). As a result, the designer does not need to increase the finished floor level. Thus, despite the increase in the beam depth the overall building height may actually be reduced. When compared with a solid web solution where services are provided beneath the beam, the use of castellated beams could lead to savings in the cladding costs. Moreover, because it is light-weight, the castellated beam is more convenient in transportation and installation than the normal I-beam.

The web openings in the castellated beam, however, may reduce the shear resistance of the beam. Existing studies have shown that the resistance of the castellated beam is influenced by shear stresses (Redwood and Demirdjian, 1998), particularly those around web openings and under the T-section, which could cause the beam to have different failure modes. There is evidence (Boyer, 1964; Kerdal and Nethercot, 1984;

Demirdjian, 1999) that the method of analysis and design for the solid beam may not be suitable for the castellated beam. Design guidance on the strength and stiffness for castellated beams is available in some countries. However, again, most of them do not take into account the shear effect. As far as the bending strength is concerned, neglecting the shear effect may not cause problems. However, for the buckling and for the calculation of serviceability, the shear weakness due to web openings in castellated beams could affect the performance of the beams and thus need to be carefully considered.

The previous researches showed that the responsibility of flange is to resist a large part of the flexural forces. In contrast, according to (Anupriya and Jagadeesan, 2014), most of the shear forces are carried by the web. The web openings will not only lead to a decrease of web in carrying shear forces, but also a decrease in torsional stiffness of castellated beams; the latter is concerned in relation to lateral torsional buckling. Clause 4.15.4.5 of BS 5950-4 demonstrates some guidance for the determination of the lateral–torsional buckling moment of members with web openings. It states that the method used to determine the lateral buckling resistance moment of solid web beams can be used for beams with web openings using the section properties at the centreline of an opening, i.e. the reduced cross-section properties. Therefore, the calculations of the safe design of castellated beams should take into account the influence of the lateral-torsion buckling which depends on cross-sectional properties and the depth of the beam such as the consideration of the effect of flexural and shear capacity.

The design of castellated beams requires the consideration of the lateral-torsion buckling in addition to the flexural and shear capacity. The previous studies explained that the cross-sectional properties and the depth of the beam can affect the lateral-torsional buckling. The castellated beam is more sensitive to lateral-torsional buckling because it is deeper and more slender than traditional I-beam and the presence of web openings reduces the torsional stiffness of the web. Note that for long span beams, it is the beam stiffness that dominates the loading capacity of the beam.

1.2. The problem statement and objectives

The transverse deflection and lateral-torsional buckling of structural members are usually caused by dead loads and live loads such as the weight of the building and human activities. In castellated beams' structure, the problem associated with transverse deflection and lateral-torsional buckling is also influenced by the web openings. Traditionally, the main serviceability criteria are to limit deflection under a design load as a percentage of the length of the beam (i.e., for example, $l/250$ where l is the beam length). Therefore, the designing procedure of beam needs to consider three different issues. The first issue is the strength, the second is the deflection and the last one is the lateral torsional buckling.
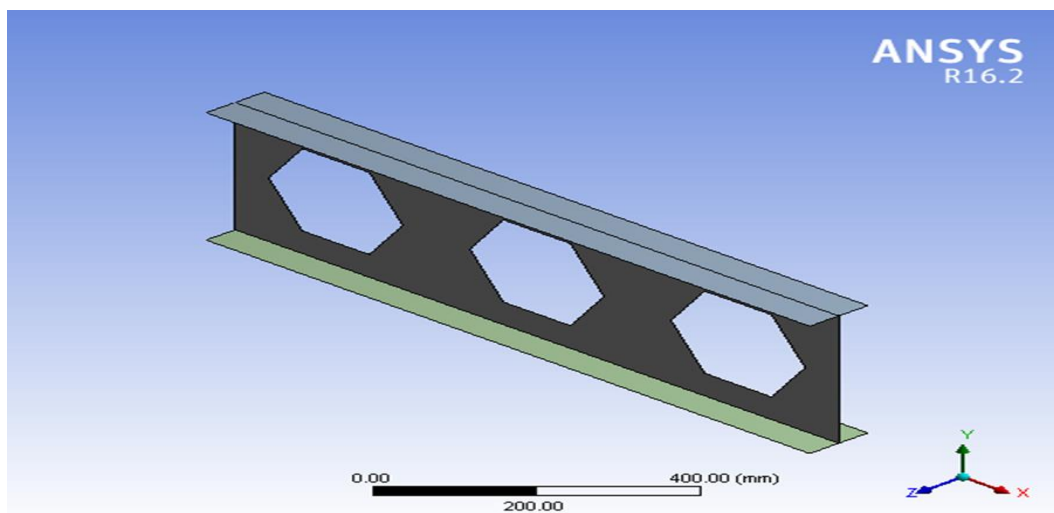
Figure 1-2 A typical castellated beam

At the present time, three different methods (Pritykin, 2015) are used to determine the deflections of castellated beams; one is based on the theory of composed bars, one is using the theory of Vierendeel truss, and one is the finite element method (FEM). The first two are the simplified empirical methods; whereas the last one is the numerical method which could provide more accurate results. However, the use of FEM is quite complicated and needs to have skills and experience. The FEM software are also expensive, the use of which requires some training. In contrast, the analytical solution is simple, easy to use and can be used directly and its key for validating FEM model.

The aim of this study is firstly to investigate the effect of web openings on the transverse deflection and lateral-torsional buckling of castellated beams by using both analytical and numerical methods. The second aim is to focus on the effect of both the geometric nonlinearity and material inelasticity on castellated beams under uniformly distributed loads with different boundary conditions, through investigating the load-deflection curve and predicting the value of lateral-torsional buckling moment capacity by using nonlinear numerical solution. The third aim is to study the free vibration, static buckling and dynamic instability of castellated beams subjected to transverse periodic loading by developing analytical solutions.

The purpose of developing analytical solutions is for the design and practical use, while the numerical solutions to be developed are for the validation of the analytical solutions. The analytical solution will be developed using the classical principle of minimum potential energy, whereas the numerical solutions will be obtained using the commercial software ANSYS. The detailed objectives of the research are as follows:

➢   To investigate the effect of web openings on the transverse deflection of castellated beams subjected to a uniformly distributed transverse load.

➢   To develop analytical solutions of transverse deflection of castellated beams subjected to a uniformly distributed transverse load with/without non-uniform temperature.

➢   To evaluate the shear-induced transverse deflection of castellated beams subjected to a uniformly distributed transverse load.

➢   To perform linear and nonlinear finite element stress analyses of castellated beams using 3D linear 4-Node thin shell elements (SHELL181) and to validate the analytical solutions.

➢   To enhancing the knowledge of the effect of web openings on the lateral-torsional buckling of castellated beams subjected to a uniformly distributed transverse load.

➢   To develop analytical expressions for the critical load of lateral-torsional buckling of castellated beams subjected to a uniformly distributed transverse load.

➢ To perform linear and nonlinear finite element also inelastic behaviour lateral-torsional buckling analyses of castellated beams using three-dimensional shell elements and to validate the analytical expressions of the critical load of lateral-torsional buckling.

➢ To develop analytical expressions for the free vibration (frequency of the lateral-torsional vibration), static buckling and dynamic instability of castellated beams subjected to transverse periodic loading by developing analytical solutions.

1.3. Methodology

The main focus of the present study is on the castellated beam for providing economical and safe design to prevent the beams from the shear, flexural and buckling failures. The outline of the research program was summarized in **Figure 1-3**.

The first term of the research program is to calculate the maximum deflection of the castellated beam subjected to a uniformly distributed load by developing the linear analytical solution, which is derived, based on the principle of minimum potential energy. Moreover, linear 3D finite element method is performed by adopting program ANSYS Mechanical 17.2 software for validation the results of analytical solution.

In the second term, the second order of total potential energy principle is presented to develop the analytical method for calculating the critical load of lateral-torsional buckling of the castellated beam subject to a uniformly distributed load. In addition, linear finite element method is used in the numerical analysis where a commercial program ANSYS Mechanical 17.2 software package is used to model the castellated beam in 3D for the validation of the analytical solutions.

Nonlinear finite element method is also used in this thesis to enhance different research objectives and to understand the behaviours of castellated beams subjected to a uniformly distributed load in linear elastic and nonlinear performance. Nonlinear analysis, which takes into account the effect of both the geometric nonlinearity and material inelastic, was conducted by using a commercial program ANSYS Mechanical 17.2 software package.

Another aim of the thesis is to investigate the free vibration, static and dynamic instability of castellated beams subjected to transverse periodic loading. Bolotin's method is used to perform the dynamic instability analysis.

Furthermore, this thesis has presented a tool called 'solution Tools' that enhances the efficiency of the solution process during stages of analytical and numerical analysis. The 'solution Tools' includes some of the mathematical programming, such as Maple, and MS Excel spread sheets.

The analytical results are compared and discussed. The details of research methods used are listed below:

➢   The principle of minimum potential energy theory is used to develop the analytical method for determining the maximum deflection of castellated beams subjected to a uniformly distributed load with/without non-uniform temperature distribution.

➢   Second order of the total potential energy theory is used to develop the analytical method for determining the critical load of lateral-torsional buckling of castellated beams subjected to a uniformly distributed transverse load.

➢   Bolotin's method is used to perform the dynamic instability analysis of castellated beams subjected to transverse periodic loading. By assuming the instability modes, the mass, stiffness, and geometric stiffness, matrices are derived using the kinetic energy, the strain energy and the potential of applied loads.

➢   Maple mathematical program is used for solving and simplifying the equations of analytical solution and coupled to MS Excel, which is used to collect characters' analysis input (load cases, lengths, dimensions of cross-sections, moment of inertia and area of the section) to find the results and show it in tables and figures.

➢   Linear and nonlinear finite element method (FEM) is used for validating the analytical solutions.
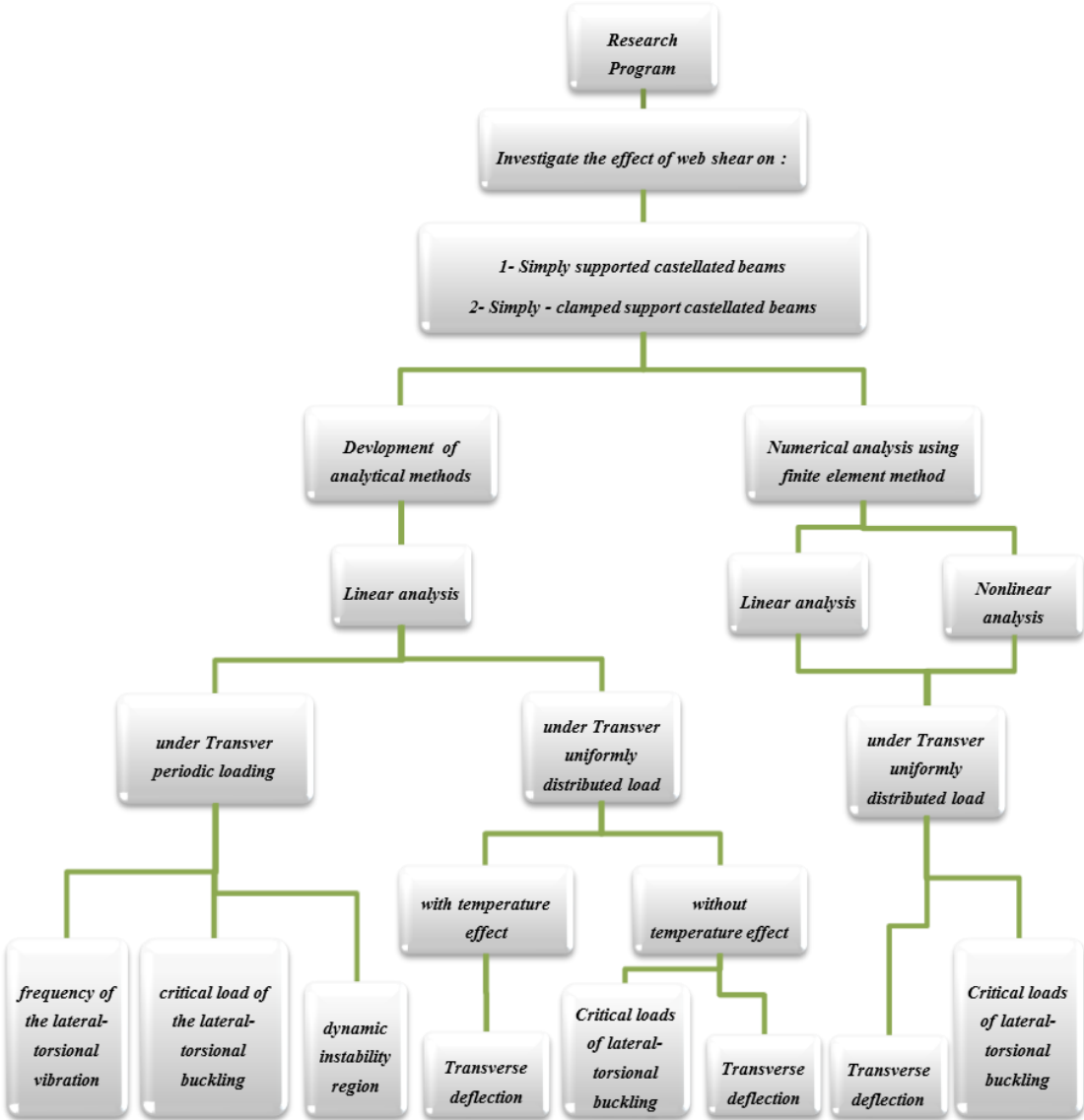
Figure 1-3 Methodology and research program

1.4. Organization of thesis

The thesis is organized into seven main chapters (see **Figure 1-4**). **Chapter 1** provides a brief background about the castellated beam, the general assumptions used for this study and the motivation of the research.

Chapter 2 contains a literature review of castellated beams, which presents a complete overview of failure modes, analysis and design methods of castellated beams. This chapter focuses on several previous studies about castellated beams and theoretical

analysis methods of castellated beams. Internet search engines (Google scholar, TU Delft repository, American Institute of Steel Construction (AISC), Science Direct etc.) are used to find the resources of relevant studies. The knowledge gap and context for the contributions of this research are also presented at the end of this chapter.

Chapter 3 introduces the approach of the analytical method, which is used in this study. The calculation of maximum deflection of the castellated beam subjected to uniformly distributed loads, with/without non-uniform temperature distribution, with different boundary conditions, takes into account the shear effect of web openings. The comparison of results obtained from the analytical and numerical methods are also provided in this chapter.

Chapter 4 covers a literature review of lateral-torsional buckling castellated beams that discusses a complete overview of factors that influence lateral-torsional buckling, and current design philosophy of lateral-torsional buckling resistance of I-beam with web openings. This chapter focuses on several previous studies about the calculation methods of lateral-torsional buckling resistance of castellated beams. In addition, the focuses are on the second-order elastic analysis to develop a simple method to predict the critical load of lateral-torsional buckling of castellated beams subjected to a uniformly distributed transverse load. The comparison of results obtained from the analytical and numerical methods are also provided in this chapter.

Chapter 5 presents the nonlinear finite element numerical analyses of castellated beams subjected to a uniformly distributed transverse load. Moreover, the nonlinear results are compared with the linear analytical and linear numerical solutions given in Chapter 4 for investigating the load–deflection relation characteristics and lateral-torsional buckling of castellated beams under uniformly distributed transverse load.

Chapter 6 discusses the dynamic instability of castellated beams. In addition, analytical solutions for calculating the free vibration, static buckling and dynamic instability of castellated beams subjected to transverse periodic loading, are developed. Some important features of the castellated beams in association with dynamic loading are highlighted in this chapter.

Chapter 7 presents the main conclusions that are drawn from this study and provides the suggestions and recommendations for future study.
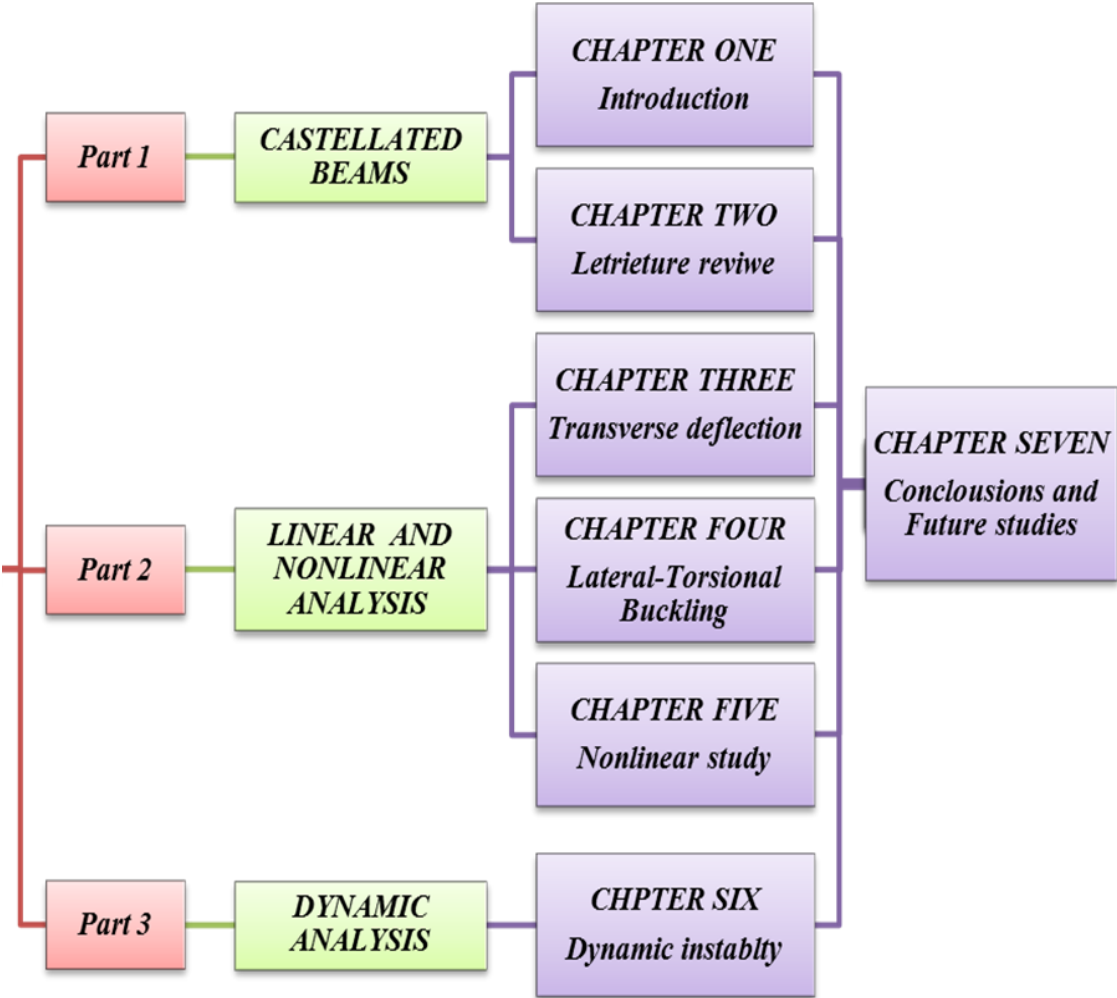
Figure 1-4 Organisation diagram of thesis

CHAPTER TWO

2. LITERATURE REVIEW

2.1. History of development of fabrication method

It was reported by Seimaini and Das in 1978 (Bake, 2010), that the first use of the castellated beam was in 1910 in USA by Horton, who was working on the Chicago Bridge and Iron Works. This process consisted of cutting the web of the beam and re-joining the two parts by welding to get a beam that has more strength. However, the more general concept of fabricating a castellated beam was adopted in 1935 by the engineer Boyd, who was working in the British Structural Steel Company, Argentina (Knowles, 1991). According to Knowles, Boyd found a solution to strengthen a beam by using a simple way; that is to cut the beam web and weld another, which he cut and welded in the same method. As a result, the new beam has the capacity of flexural resistance more than the original beam by approximately 20-30% because of increasing the depth by about 50% according (Sherbourne and Van Oostrom, 1972). In 1940, this product was marketed in the UK and known as the Boyd beam. Later, this beam's name was replaced by 'castle-like' or 'battlemented', which refers to the pattern of cutting along the centreline of the web in a zigzag. (Knowles, 1991)

After the Second World War, the castellated beam was used throughout Europe because the cost of manufacture was not expensive where the cost of labour was cheap and the price of material was high. In other words, the ratio of labour cost to material cost is low. The number of sections of beams, which were available in European factories, was also limited at that time.

Increasing demand for castellated beams led to finding a way to make the fabrication process more accurate and fast. Litzka Stahlbau Boyer (1964) developed a process called the Litzka process, which is very efficient using equipment that gives the designers more suitable design requirements such as the depth of beam, the dimensions of openings, the angle of openings, the shape of the opening and the spacing between the openings (Bradley, 2003).

Nowadays the fabrication method of castellated beams is done by cutting the web of hot rolled I-sections according to a regular alternating pattern along the web by using either oxy cutting or plasma cutting and then welding teeth of the tee-sections of halves after one of the halves is shifted. The whole process is controlled automatically by a computer. **Figure 2-1** shows a typical example of the process of a castellated beam.
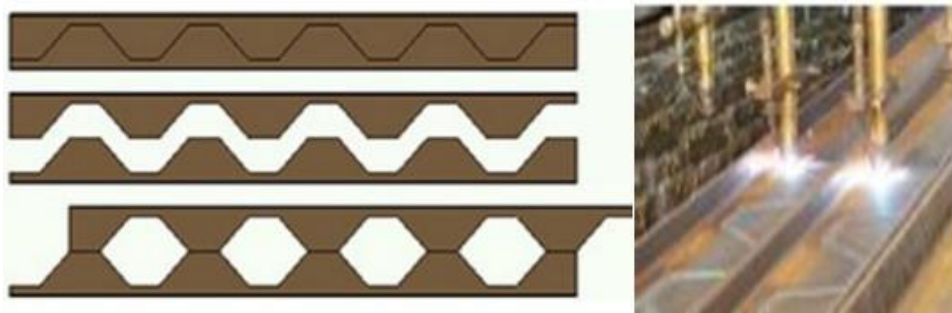
Figure 2-1 Fabrication of a castellated beam starting from a plain-webbed parent section.(Sonck,2014)

2.2. The failure modes of castellated beams

For many years, castellated beams have been used in construction because the responsibility of a construction engineer is to design the structure according to safety and serviceability considerations, while considering functional requirements according to the use for which the construction is intended. Extensive study has been carried out by researchers who are working in the construction field to identify the behaviour of castellated beams when they are loaded with different types of loads. It was found that the castellated beam could fail in various different modes depending on the dimensions of the beam and the type of loading as well as the boundary

conditions of the beams. Kerdal and Nethercot (1984) informed the potential failure modes, which possibly take place in castellated beams. Also, they explained the reasons for the occurrence of these failure modes. For instance, shear force and web weld rupture cause a Vierendeel mechanism and web post-buckling. Additionally, they pointed out that any other failures whether caused by a flexural mechanism or a lateral-torsional instability is identical to the equivalent modes for beams without web opening.

2.3. Local failure modes

The aim of this section is to highlight the failure modes of castellated beams occurred due to web openings, which is normally located near the opening in the web posts of the beam. These failures are called local failure modes (Verweij, 2010), which have been observed and documented in existing studies. In a study done by Sonck (2014) four different failure modes were defined, namely, the Vierendeel mechanism caused by web opening, the web post failure also caused by web opening, the shear and flexural failure caused by beam shear force, and the flexural failure by bending moment.

2.3.1. Vierendeel failure mode

Altifillisch et al. (1957) and Toprac and Cooke (1959) explained the Vierendeel failure mode of the castellated beam. This failure mode occurs when a castellated beam is subjected to high shear forces, which generate the primary moment that is the conventional bending moment and the secondary moment that is called a Vierendeel moment. These loads are carried by parts of the beam, which are located between the openings where they behave as an assembly of individual structural components, consisting of vertical web posts, upper and lower horizontal T-sections. Halleux (1967); Hosain and Spiers (1973); (Chung et al. (2001); Liu and Chung (2003); (Durif et al. (2011); Tsavdaridis and D'Mello (2012) and (Durif et al. 2013) also discussed the Vierendeel failure mechanism of beams with various different shapes of openings.

In the castellated beam, the global bending moment is redistributed as two axial forces over the horizontal upper and lower T-sections. The global shear force is divided into two shear forces over the upper and lower T-sections. The location of these forces in the components is determined by supposing an inflection point in the middle of each horizontal T-section, where the local bending moment is zero assuming that the shear forces in both part sections are equal. According to the static equilibrium equation, the results of local forces in the upper, lower and middle of the T-section will be a Vierendeel moment at both T-sections. Therefore, the increase of horizontal opening length causes an increase in the Vierendeel moment.

Because of the arrival of the T-sections around an opening to the maximum resistance against the local forces and secondary bending, the castellated beam will fail by the Vierendeel mechanism which is dominant in the section openings due to the formation of plastic hinges in the four corners of these openings. **Figure 2-2** illustrates Vierendeel Truss Analogy and Vierendeel effect.

Kerdal and Nethercot (1984) investigated the Vierendeel failure mechanism by using both analytical and experimental methods. They identified the parameters that are related to the Vierendeel failure mode, such as members with short spans (for which shear dominates), wide openings (with large secondary bending moments) or shallow tee sections (low plastic resistance of the tees), etc.
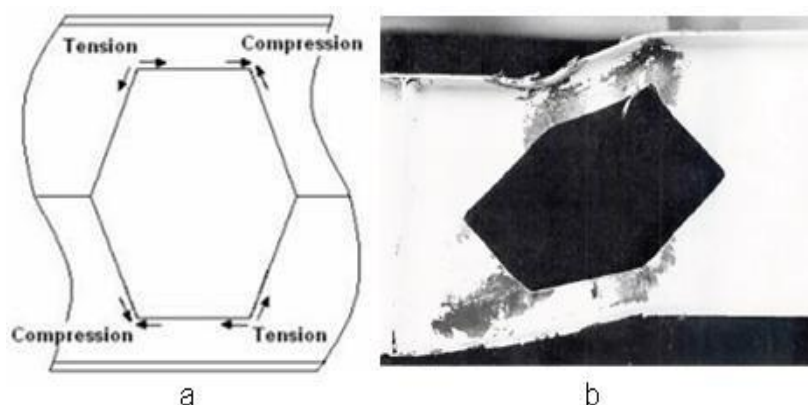
Figure 2-2 Vierendeel failure (a) Vierendeel Truss Analogy, (b) Local failure - Vierendeel effect (Hosain and Spiers 1973)

2.3.2. Web post failure

Slender web-posts in association with deep I-sections present instability in regions between web openings, which are called web posts. Web post failure is the consequence of the presence of the axial and shear forces due to the global moment and global shear force as well as the local Vierendeel moments that encourage compression in the web post.

2.3.3. Web post buckling

The possibility of the buckling of the web post occurring between web openings of castellated beams (Zaarour and Redwood, 1996) is due to the presence of the couple of the horizontal shear forces effective at mid-depth of the web-post, which is combined with double curvature bending over the height of the post, leading to a complex failure mode, which is called web post buckling. The technique of the web post buckling failure mode thought to be caused by one of opening edge of the web will behave under tension stress but the opposite edge in compression stress. In other words, the buckling will happen across the compression line, as shown in **Figure 2-3**. At a result, the buckling will cause a twisting effect of the web-post across its height. Kerdal and Nethercot (1984) stated that shear force and web weld rupture can cause the Vierendeel failure mode and also web post-buckling.
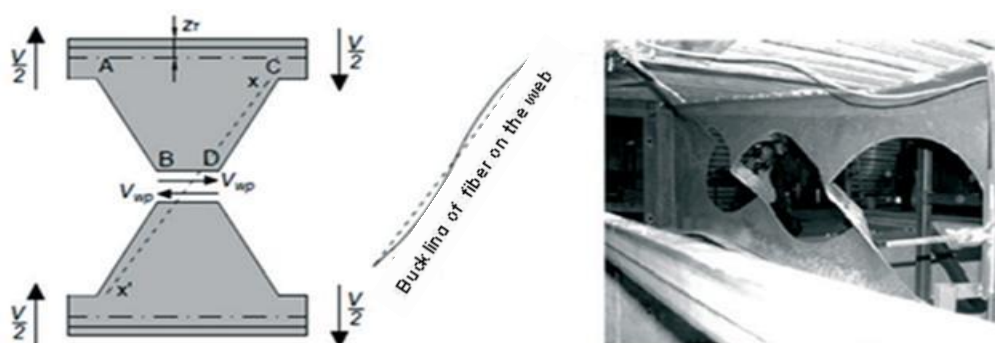
Figure 2-3 Web buckling due to shear (Badke-Neto et al., 2015)

Pourbehi and Pirmoz (2015) also reported the web-post buckling is due to the shear response and presented some important factors used for the design of castellated beams. Their data was collected from a numerical study on 300 castellated beam

models. Besides the work mentioned above, the web post buckling failure mode in castellated beams has also been investigated by other researchers. Hosain and Spiers (1973); Redwood and Demirdjian (1998) and Tsavdaridis and D'Mello (2011) also investigated the web post buckling failure mode occurred in castellated beams.

2.3.3.1. Compression buckling of web post

In 1990 Ward (Sonck, 2014) stated that – in order to reduce the effect of bearing and buckling, stiffeners should be used at the reaction location and stress concentrated points, which can be applied directly at the web post of the castellated beams. Hosain and Spiers (1973) did an investigation on 12 simple castellated beams and reported that because of the action of concentrated load, web buckling causes premature failure (see **Figure 2-4**). This failure can occur in local loading areas or reaction force region (Kerdal and Nethercot, 1984). While the buckling behaviour of the beam of solid web is not affected by the loaded region size, the buckling behaviour of the castellated beam is affected by the concentrated loads (Okubo and Nethercot, 1985).
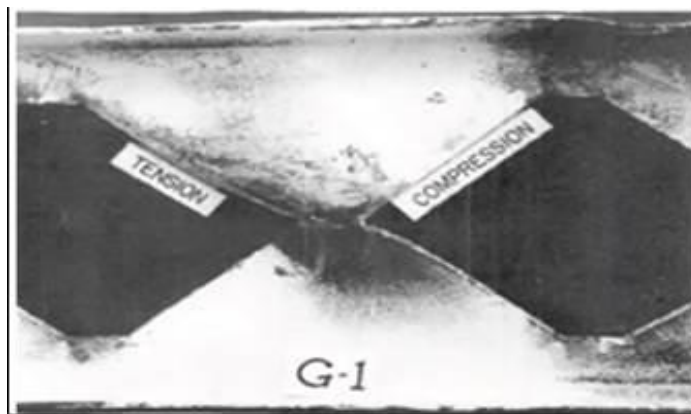
Figure 2-4 Web buckling due to compressive stress (Hosain and Spiers, 1973).

2.3.3.2. Bending of web post failure due to moments in web-posts

Bending of web posts failure has investigated by a number of researchers and have obtained that this failure occurs in castellated beams because the in-plane bending resistance of the web post of castellated beams will be reduced by the present

bending moment in the web post (Müller et al, 2006). He found that the web posts bending failure can be avoided by increasing the web post width.

2.3.3.3. Web welds failure

Hosain and Spiers (1971) investigations are concerned about the failure at weld joint area between two segments of a web post in castellated beams (Kerdal and Nethercot, 1984). Practically, the horizontal shear stresses located in the web post may potentially exceed the yield strength of the welded throat, which can thus cause the web welds to fail within a web-post. Note that the web weld failure becomes more vulnerable if the length of weld throat is short (Maalek, 2004). **Figure 2-5** shows the web welds failure, which occurred during an experimental test, carried out by Hosain and Spiers (1973).
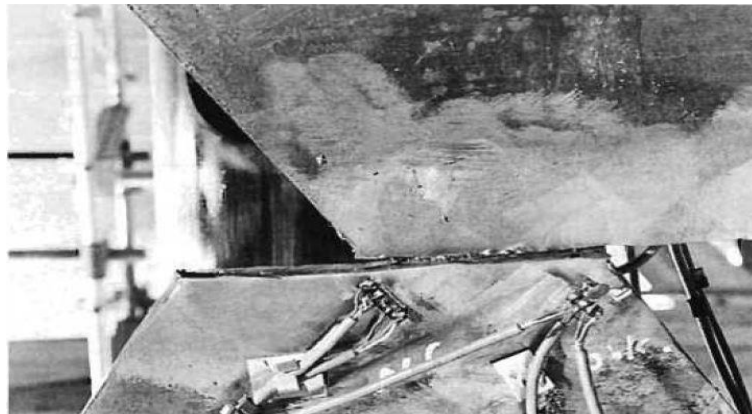
Figure 2-5 Web welds failure (Erdal and Saka, 2013).

2.3.4. Shear resistance

2.3.4.1. Shear failure

Reduction of the local carrying capacity of web posts causes shear failure of the beam (Müller et al., 2006) and (Tsavdaridis and D'Mello, 2011). It has been reported that the shear resistance of castellated beams can be determined by the sum of the vertical shear capacity of top and bottom flanges. However, this state of failure is

affected by the cross section of web openings and Vierendeel effects (Demirdjian, 1999).

2.3.4.2. Web shear buckling

Aglan and Redwood (1974) discussed the effect of the spacing between web openings on the appearance of web shear buckling failure. Redwood and Demirdjian (1998) reported that high shear forces in a castellated beam could cause the web shear buckling failure. Demirdjian (1999) also carried out similar investigation.

2.3.4.3. Flexural failure

Toprac and Cooke (1959) and Halleux (1967) discussed the flexural failure mode of castellated beams (see **Figure 2-6**). It was reported that applying high bending moment on the castellated beam can lead to flexural failure.
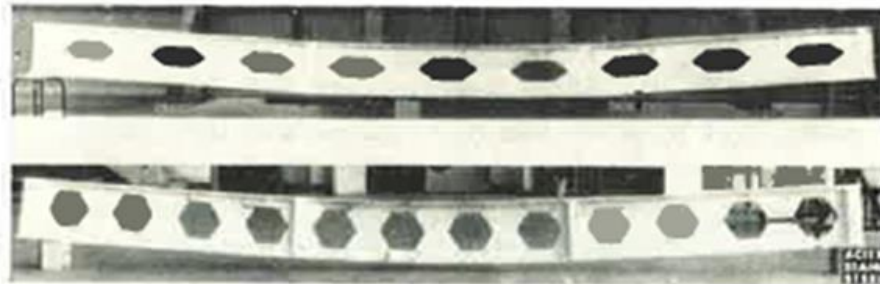
Figure 2-6 Flexure mechanism (Halleux, 1967).

2.4. Global failure modes

The global failure modes are those caused by global buckling such as flexural buckling, lateral-torsional buckling, and lateral buckling of the beams (Verweij, 2010).

2.4.1. Lateral-torsional buckling

It was reported that the castellated beam with long span often leads to buckling laterally prior to reaching maximum flexural strength, when sufficient lateral support is not provided (Demirdjian, 1999). Lateral-torsional buckling failure of slender beams has been studied extensively since 1980 (Kim et al., 2016). Kerdal and Nethercot (1984); Korrani et al., (2010) and Sonck et al., (2014) explained the lateral-torsional buckling mechanism. The fact that the castellated beam has a large bending stiffness around one axis and a small bending stiffness around other axis leads the castellated beam to be vulnerable to lateral-torsional buckling unless some restraints are provided.

Additionally, the presence of web openings causes a decrease of the overall sectional torsional stiffness, which further decreases the resistance of the beam to lateral-torsional buckling failure. Kerdal (1982) and Demirdjian (1999) reported that the torsional stiffness of the web is affected by deeper and more slender section properties. **Figure 2-7** illustrates the shape of castellated beams at lateral-torsional buckling failure. Mohebkhah and Showkati (2005) used finite element method to investigate the effects of slenderness on the moment-gradient factor and of elastic lateral bracing stiffness on the flexural torsional buckling. Zirakian and Showkati (2006) carried out an investigation by using experimental and finite elements method to examine the lateral torsional or distortional buckling behaviour of castellated beams. Sonck and Belis (2016) determined the weak-axis flexural buckling resistance of castellated beams and cellular beams. The modified diagrams of castellated beams and cellular beams and the modified residual stress pattern effect are examined. In this study, critical buckling load and the buckling resistance of simply support castellated beams and cellular beams are studied using a numerical method.
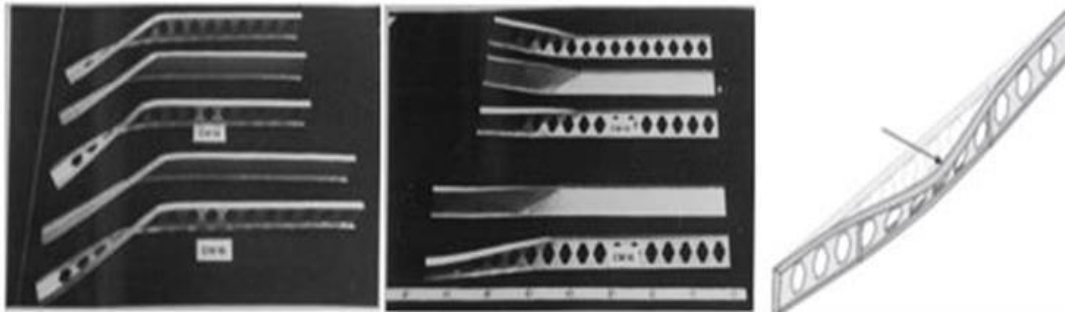
Figure 2-7 Lateral-torsional buckling (Kerdal, 1982).

2.4.2. Lateral buckling failure due to moments in web-posts

A beam that has a large slenderness and significant web openings, like the long span castellated beam, can easily fail in a form called lateral buckling of web posts (Radić. and Markulak, 2007). A number of researchers have investigated the lateral buckling of web posts of castellated beams and obtained corresponding critical moments to cause the lateral buckling of web posts. Hosain and Spiers (1973); Pattanayak and Chesson (1974) and Aglan and Redwood (1974) found that, for most castellated beams the lateral buckling of web posts comes after the yielding starts in the web, which indicates that the failure is a combined one of material yield and buckling. Müller et al. (2006) found that the lateral buckling of the web posts could be avoided by increasing the web post width. **Figure 2-8** shows the shape of lateral buckling failure of castellated beam (Showkati et al., 2012).
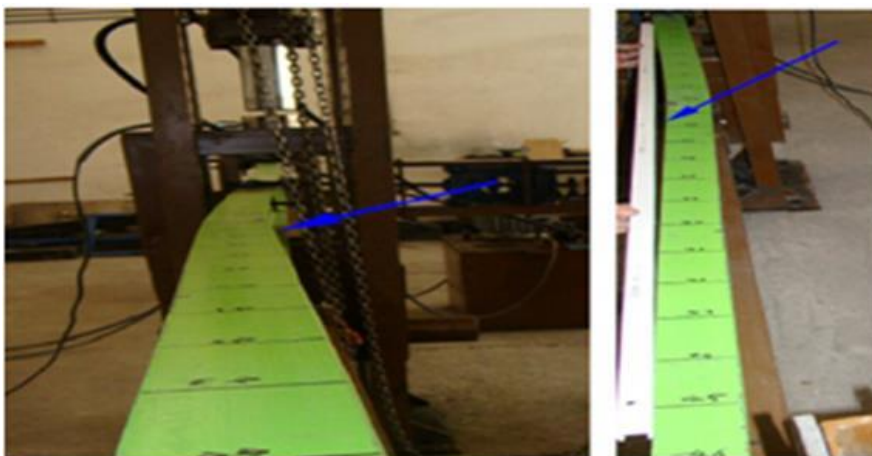
Figure 2-8 Lateral buckling (Showkati, et al. 2012).

2.5. The studies about deflection and shear effect

Sherbourne and Van Oostrom (1972) developed a numerical computer program for the analysis of castellated beams considering both elastic and plastic deformations by using practical lower limit relationships for shear, moment and axial force interaction of plasticity.

Hosain et al. (1974) demonstrated that the finite element method is a suitable method for calculating the deflection of symmetrical section castellated beams. They divided the castellated beams into an assemblage of elements, which are used to get the stiffness matrix.

Srimani and Das (1978) conducted an analysis on five experimental groups of castellated beams to determine the deflection by using finite element method. Because of symmetry, only one half of the beam was modelled. The numerical results obtained were compared with experimental data obtained by other researchers.

Knowles (1991) clarified the previous methods, which have been adopted to determine design ultimate load and deflection by performing elastoplastic analysis. He also discussed the design curves used for the castellated beam design.

Zaarour and Redwood (1996) carried out experiments on 12 simply supported castellated beams with a concentrated load applied at the mid of span which gives a low moment-to-shear ratio. It demonstrated the possibility of the occurrence of the buckling of the web posts between web openings. Nonlinear finite element analysis, taking into account plastic deformation, was conducted to calculate the buckling loads. A comparison was made between the results they obtained and the results of previous studies.

Maalek (2004) calculated the shear deflection of the straight-sided tapering cantilever of the rectangular cross section by using a theoretical method. The formulae he used were based on Timoshenko's beam theory and virtual work

method. His results were compared with the results obtained from finite element analysis.

El-Sawy et al. (2009) mentioned that the influence of shear deformation on castellated beams is directly proportional to the web openings depth and inversely proportional to the length of the castellated columns and web post width. The wide range of castellated columns with different cross sections, lengths, and restricted conditions are examined to estimate the resistance of buckling about the major axis by using a simplified procedure which is presented in his study. The analytical results were validated with results obtained by finite element analysis.

Gholizadeh (2011) utilized artificial intelligence technologies called back-propagation (BP) neural network and adaptive neuro fuzzy inference system (ANFIS) methods to build a program for predicting the critical load of castellated beams susceptible to web-post buckling. To validate his results, he also carried out the nonlinear finite element analysis using NASTAN software and examined the failure load and failure mode of the beams. It was found that the BP network and ANFIS methods are able to predict accurate results for the web-post buckling of castellated beams.

Aminian et al. (2012) proposed new design formulas for calculating the load carrying capacity of castellated beams by using linear genetic programming and integrated search algorithms. It was found that the use of machine learning system is an active method to validate the failure load of castellated beams.

Soltani et al. (2012) studied the effect of nonlinearity in material and/or geometry on the failure model prediction of castellated beams. Their study was done by using MSC/NASTRAN software to find out bending moments and shear load capacity, which are compared with those published in literature.

Erdal and Saka (2013) analysed the cellular beams with different numbers of web openings and spacings by using nonlinear finite element method, which was carried out by using ANSYS software. It was found that the combined local buckling, web-

post buckling, and Vierendeel failure occur on cellular beams due to the externally applied loads in different positions and the lateral supports. They also conducted the experimental tests on 12 cellular beams and the experimental results were used to validate the numerical results.

Based on Vierendeel failure, Panedpojaman and Rongram (2014) conducted a study to predict the load carrying capacities by using SCI P100's method and Chung et al.'s formula. The results were compared with those obtained from the finite element analysis method. The load carrying capacities were presented in terms of the moment-shear interaction curve for studying Vierendeel's effect on the overall behaviour of the cellular beams. Moreover, the investigations that were carried out on 120 non-linear finite element models of cellular beams with beam section sizes and opening ratios of 0.5 and 0.8 are reported. The results showed that the FE interaction curve's shape is slightly affected by the sizes of the steel sections. The study suggested a simple quadratic equation to estimate the interaction based on Vierendeel failure.

Recently, Wang et al. (2014) conducted a parametric study on the large deflection analysis of castellated beams at high temperatures. They used finite element method to calculate the growth of the end reaction force, the middle span deflection, and the bending moments at susceptible sections of castellated beams. The results were compared with those of corresponding solid beams to examine the effect of web openings.

Axial compression buckling of castellated columns was investigated by Yuan et al. (2014), who derived an analytical solution for critical load based on stationary potential energy and considering the effect of the web shear deformations on the flexural buckling of simply supported castellated column. The analytical solution was validated by using the numerical results obtained from finite element analysis.

Menkulasi et al. (2015) analysed 30 models of castellated beams subjected to concentrated loads with different cross sections and loading positions for evaluating the resistance of castellated beams to the concentrated load with and without

stiffeners. The study was carried out by employing nonlinear finite element analysis method.

Morkhade and Gupta (2015) discussed the effect of the dimensions and positions of web holes and locations of stiffeners around the holes on the behaviour of the perforated steel I beam with rectangular web holes. The study showed that the load carrying capacity of the beam is affected by the positions of holes. Experimental and finite element analysis methods were employed in this study. The nonlinear finite element analysis was carried out by using ANSYS software.

More recently, Sonck et al. (2015) presented a comprehensive comparison between the deflection results of cellular and castellated beams obtained from numerical analysis and those obtained from different simplified design codes. The beams studied involve various web opening dimensions, different parent sections and different span lengths. The comparison showed that the design codes are not accurate for short span beams and conservative for long span beams.

Yuan et al. (2016) adopted the principle of minimum potential energy to derive an analytical method to calculate the deflection of castellated/cellular beams with hexagonal/circular web openings, subjected to a uniformly distributed transverse load. The analytical results were validated by using numerical results obtained from finite element analysis using ANSYS software.

Lei et al. (2017) investigated the buckling behaviour of castellated columns exposed to a fire when they were also subjected to axial compression. In their study, an analytical equation was developed based on the web opening shear effect and the non-uniform cross-section temperature distribution for predicting the critical buckling load of castellated columns.

Martins et al. (2017) investigated the lateral-torsional buckling of cellular beams. Nonlinear geometric and material analyses were developed for modelling the behaviour of cellular beams with different restricted conditions and different loading cases, which are achieved by using ABAQUS 6.12 software. In their study, the

numerical results, which took into account geometric imperfections, were compared with those obtained by using ABNT NBR 8800:2008 standards and by Abreu et al. (2010).

2.6. Research gaps

The goal of the literature review is to identify the research fields, which are needed to further study and investigate. As a result of the previous research efforts, the general behaviour of castellated beams and understanding different failure modes, which occur during the construction and/or loading, were discussed. Due to the geometric particulars of the beam, however, it was remarkable to note that most of the theoretical approximate methods are interested in design calculations of the castellated beams for long span beams where the shear effect is negligible. However, the castellated beams/columns are used not only for long span beams/columns but also for short beams/columns. Owing to the complexity of section profile of the castellated beams, the shear-effect caused by the web opening on the calculation is not fully understood.

In addition, the static load still dominates the current designing of structures for castellated beams, in spite of the significance of the dynamic response to machinery loading and to extreme environmental loads. Actually, there are no accurate calculation methods available in the literature to perform these analyses.

Also, it seems that the significant problem of the castellated beam has remained unresolved. European building standards do not have formulas for design calculations of castellated beams, which include shear deformations at the static and dynamic state.

In literature, researchers have adopted the finite element method to predict the calculations design of castellated beams by using different software programs such as (MS/NASTRAN, ABAQUS, and ANSYS). However, these programs need to be used efficiently because any error could lead to significant distortions in results. In

spite of the potential programs, only the case of simply supported castellated beams has been discussed in most of the studies.

The development of the analytical methods to predict the static and dynamic calculations of the castellated beam took place in the present research. The equations of the analytical solutions are developed based on the principle of minimum potential energy. In order to improve the accuracy and efficiency of this method, shear rigidity factor is determined by using suitable numerical techniques.

CHAPTER THREE

3. DEFLECTION CALCULATION OF CASTELLATED BEAMS

3.1. Introduction

This chapter firstly puts emphasise on the development of an approximate method of deflection calculation of castellated beams subjected to a uniformly distributed transverse load with/without temperature effect. The method is developed based on the principle of minimum potential energy. The analytical method developed here considers the shear effect of web openings. To demonstrate the analytical method, comparisons between the analytical results, previous studies from the literature, and linear FEA numerical computations are also provided.

3.2. Analytical philosophy of deflection analysis of castellated beams

An approximate method of deflection analysis of castellated beams under a uniformly distributed transverse load is presented in this chapter. The method is developed based on the principle of minimum potential energy.

Because of the presence of web openings, the cross-section of the castellated beam is now decomposed into three parts to calculate the deflection and stress, two of which represent the top and bottom T-sections, one of which represents the mid-part of the web. The analysis model for this study is illustrated in **Figure 3-1 (a)**.

In this study, the cross-section of the castellated beam is assumed to be doubly symmetric, with the flange width and thickness as b_f and t_f, the web depth and thickness as h_w and t_w, and the half depth of hexagons as a. The half of the distance between the

centroids of the two T-sections is *e* and the hexagonal opening height is 2a. For a 60°

cutting angle the side length of the hexagonal opening is $\left(\frac{2a}{\sqrt{3}}\right)$ and the width of one

sloping edge of hole S_0 is calculated from $\left(\frac{\text{orignal depth of beam}}{\tan 60}\right)$, in which S_0 is $\left(\frac{a}{\sqrt{3}}\right)$.

Hence the distance from the centreline to the centreline of adjacent castellation holes

can be found according to this formulae $S = 2\left(\frac{2a}{\sqrt{3}} + S_0\right)$, which equals to $\left(\frac{6a}{\sqrt{3}}\right)$

(Demirdjian, 1999).

(a)
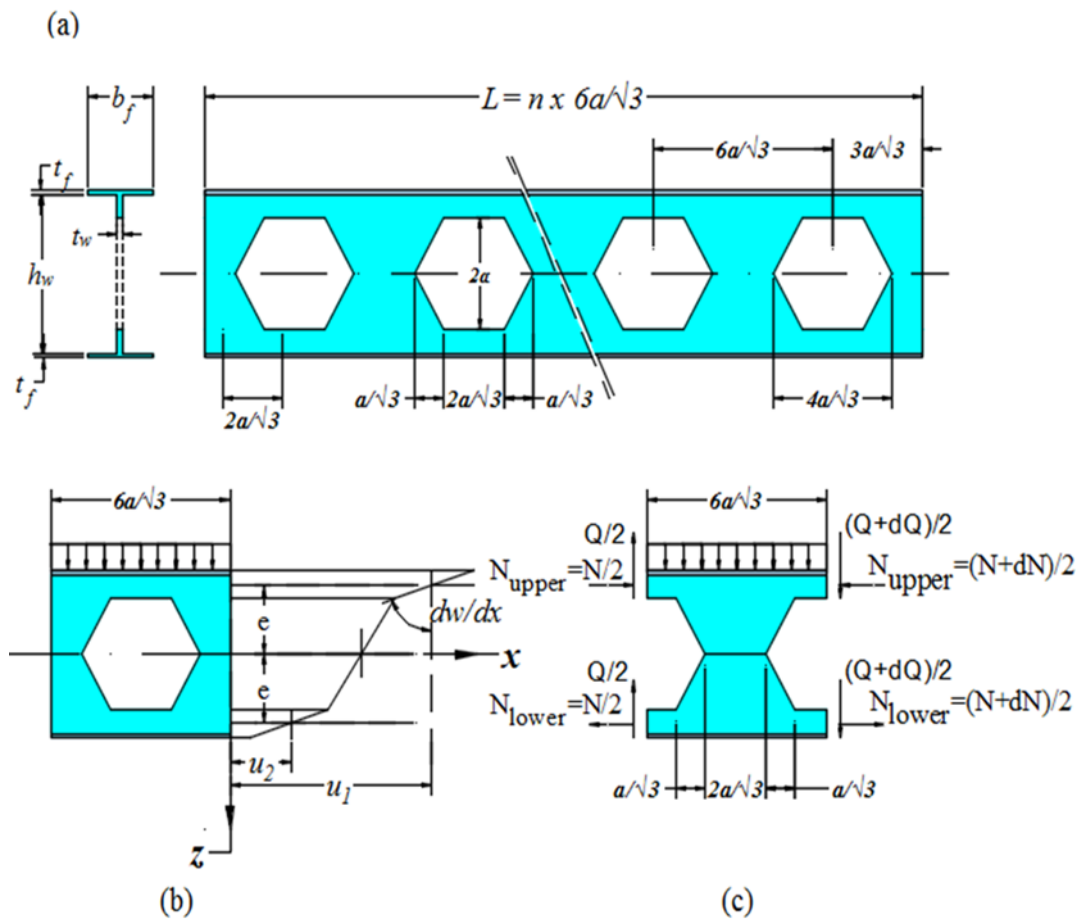
Figure 3-1 (a) Notations used in castellated beams, (b) displacements and (c) internal forces

Under the action of a uniformly distributed transverse load, the beam section will have

axial and transverse displacements as shown in **Figure 3-1 (b)**, where (*u₁, w*) and

(*u₂, w*) are the axial displacements and the transverse displacements of the centroids of

the upper and lower T-sections. All points on the section have the same transverse

displacement according to the use of beam model (Yuan et al., 2014). The corresponding axial strains ε_{1x} in the upper T-section and ε_{2x} in the lower T-section are assumed to be linearly distributed, and so do the displacements. Thus, the displacements can be expressed as follows:

In the upper T-section : $-\left(\frac{h_w}{2} + t_f\right) \leq z \leq -a$

$$u(x,z) = u_1(x) - (z + e)\frac{dw}{dx}$$
3-1

In the lower T-section : $a \leq z \leq \left(\frac{h_w}{2} + t_f\right)$

$$u(x,z) = u_2(x) - (z - e)\frac{dw}{dx}$$
3-2

For the middle part between the two T-sections: $-a \leq z \leq a$

$$u(x,z) = \frac{u_1(x) + u_2(x)}{2} - \frac{z}{a}\left(\frac{u_1(x) - u_2(x)}{2} - (e - a)\frac{dw}{dx}\right)$$
3-3

The corresponding axial strains in the two T-sections can be determined by using the strain-displacement relation as follows:

For the upper T-section:

$$\varepsilon_1(x,z) = \frac{du_1}{dx} - (z + e)\frac{d^2w}{dx^2}$$
3-4

For the lower T section,

$$\varepsilon_2(x,z) = \frac{du_2}{dx} - (z - e)\frac{d^2w}{dx^2}$$
3-5

The shear strain γ_{xz} in the middle part between the two T-sections can also be determined using the shear strain-displacement relation as follows:

$$\gamma_{xz}(x,z) = \frac{\partial u}{\partial z} + \frac{\partial w}{\partial x} = -\frac{u_1 - u_2}{2a} + \frac{e}{a}\frac{dw}{dx}$$
3-6

in which,

$$e = \frac{b_f t_f \left(\frac{h_w + t_f}{2}\right) + t_w \left(\frac{h_w}{2} - a\right)\left(\frac{h_w + 2a}{4}\right)}{b_f t_f + t_w \left(\frac{h_w}{2} - a\right)}$$
3-7

For simplicity of presentation, the following two new functions are used:

$$u_\beta = \frac{u_1 + u_2}{2} \qquad\qquad\qquad 3\text{-}8$$

$$u_\beta = \frac{u_1 - u_2}{2} \qquad\qquad\qquad 3\text{-}9$$

For the conservative system in the equilibrium state, the effect of a uniformly distributed transverse load on castellated beams will lead to internal forces. To determine the distribution of internal forces at an opening, Lawson and Hicks (2011) reported that each of the T-sections is subjected to combined axial force, bending and shear. According to **Figure 3-1 (b)** these internal forces can be obtained as follows:

$$N_1 = Eb_f \int_{-(t_f+\frac{h_w}{2})}^{-h_w/2} \varepsilon_{1x}\, dz + Et_w \int_{-\frac{h_w}{2}}^{-a} \varepsilon_{1x}\, dz = EA_{tee}\frac{du_1}{dx} \qquad 3\text{-}10$$

$$M_1 = Eb_f \int_{-(t_f+\frac{h_w}{2})}^{-h_w/2} (z+e)\varepsilon_{1x}\, dz + Et_w \int_{-\frac{h_w}{2}}^{-a} (z+e)\varepsilon_{1x}\, dz = -EI_{tee}\frac{d^2w}{dx^2} \qquad 3\text{-}11$$

$$Q_3 = Gt_w \int_{-a}^{a} \gamma_{xz}\, dz = 2Gt_w(e\frac{dw}{dx} - \frac{u_1 - u_2}{2}) \qquad 3\text{-}12$$

$$N_2 = Et_w \int_{a}^{h_w/2} \varepsilon_{2x}\, dz + Eb_f \int_{\frac{h_w}{2}}^{t_f+h_w/2} \varepsilon_{2x}\, dz = EA_{tee}\frac{du_2}{dx} \qquad 3\text{-}13$$

$$M_2 = Et_w \int_{a}^{h_w/2} (z+e)\varepsilon_{2x}\, dz + Eb_f \int_{\frac{h_w}{2}}^{t_f+h_w/2} (z+e)\varepsilon_{2x}\, dz = -EI_{tee}\frac{d^2w}{dx^2} \qquad 3\text{-}14$$

where E is the Young's modulus and G is the shear modulus, A_{tee} and I_{tee} are the area and the second moment of area of the T-section, which are determined in their own coordinate system as follows:

$$A_{tee} = b_f t_f + t_w \left(\frac{h_w}{2} - a\right) \qquad\qquad 3\text{-}15$$

$$I_{tee} = \frac{b_f t_f^3}{12} + b_f t_f \left(\frac{h_{w+} t_f}{2} - e\right)^2 + \frac{t_w}{12}\left(\frac{h_w}{2} - a\right)^3$$
$$+ t_w \left(\frac{h_w}{2} - a\right)\left(\frac{h_w + 2a}{4} - e\right)^2$$

3-16

$$I_{reduced} = \frac{b_f \left(h_w + 2t_f\right)^3}{12} - \frac{(2a)^3 t_w}{12} - \frac{(h_w)^3 \left(b_f - t_w\right)}{12}$$

3-17

Because the upper and lower T-sections behave according to Bernoulli's theory, the strain energy of the upper T-section U_1 and the lower T-section U_2 caused by a transverse load can be expressed as follows:

$$U_1 = \frac{Eb_f}{2}\int_0^l \int_{-(t_f+\frac{h_w}{2})}^{-\frac{h_w}{2}} \varepsilon_{1x}^2 dzdx + \frac{Et_w}{2}\int_0^l \int_{-(\frac{h_w}{2})}^{-a} \varepsilon_{1x}^2 dzdx$$
$$= \frac{1}{2}\int_0^l \left[EA_{tee}\left(\frac{du_1}{dx}\right)^2 + EI_{tee}\left(\frac{d^2w}{dx^2}\right)^2\right]dx$$

3-18

$$U_2 = \frac{Et_w}{2}\int_0^l \int_a^{(\frac{h_w}{2})} \varepsilon_{2x}^2 dzdx + \frac{Eb_f}{2}\int_0^l \int_{\frac{h_w}{2}}^{(t_f+\frac{h_w}{2})} \varepsilon_{2x}^2 dzdx$$
$$= \frac{1}{2}\int_0^l \left[EA_{tee}\left(\frac{du_2}{dx}\right)^2 + EI_{tee}\left(\frac{d^2w}{dx^2}\right)^2\right]dx$$

3-19

Hence, the total of strain energy of the upper and lower T-sections can be expressed as follows:

$$U_T = \frac{EA_{tee}}{2}\int_0^l \left[\left(\frac{du_1}{dx}\right)^2 + \left(\frac{du_2}{dx}\right)^2\right]dx + EI_{tee}\int_0^l \left(\frac{d^2w}{dx^2}\right)^2 dx$$

3-20

The mid-part of the web of the castellated beam, which is illustrated in **Figure 3-1 (a)**, is assumed to behave according to Timoshenko's theory (Yuan et al., 2014). Therefore, its strain energy due to the bending and shear U_b can be expressed as follows:

$$U_b = \frac{1}{2}\sum K_b \Delta^2$$

3-21

where Δ is the relative displacement of the upper and lower T-sections due to a pair of shear forces and can be expressed as $\left(\Delta = 2a\gamma_{xy}\right)$, while K_b is the combined stiffness of the mid part of the web caused by the bending and shear, and is determined in terms of Timoshenko beam theory as follows: (Timoshenko and Gere,1961)

$$\frac{1}{K_b} = \frac{3l_b}{2GA_b} + \frac{l_b^3}{12EI_b} \qquad\qquad 3\text{-}22$$

where $\left(A_b = t_w\sqrt{3a}\right)$ is the equivalent cross-sectional area of the mid part of the web, $\left(I_b = t_w\left(\sqrt{3}a\right)^3/12\right)$ is the second moment of area, and $\left(l_b = 2a\right)$ is the length of the Timoshenko beam; herein representing the web post length. Note that, the Young's modulus of the two T-sections is $\left(E = 2(1 + v)G\right)$ and the Poisson's ratio is taken as $v = 0.3$, the value of the combined stiffness of the mid part of the web caused by the bending and shear can be determined as follows: (Yuan et al., 2014)

$$K_b = \frac{\sqrt{3}Gt_w}{4} \qquad\qquad 3\text{-}23$$

As a result, for castellated beam the total shear strain energy of the mid-part of the web, U_{sh} due to the shear strain γ_{xy} can be calculated as follows:

$$U_{sh} = \frac{\sqrt{3}}{2}Gt_wa^2\sum_{k=1}^{n}\gamma_{xz}^2 \approx \frac{\sqrt{3}Gt_wa^2}{2\times\frac{6a}{\sqrt{3}}}\int_{0}^{l}\gamma_{xz}^2dx = \frac{Gt_wa}{4}\int_{0}^{l}\gamma_{xz}^2dx \qquad\qquad 3\text{-}24$$

Letting the shear rigidity factor $k_{sh} = \frac{1}{4}$ (Yuan et al., 2014) and substituting Eqs. (3-6) into (3-24), it gives the total shear strain energy of the mid-part of the web:

$$U_{sh} = \frac{Gt_we^2k_{sh}}{a}\int_{0}^{l}\left(\frac{dw}{dx} - \frac{u_\beta}{e}\right)^2 dx \qquad\qquad 3\text{-}25$$

Note that, in the calculation of shear strain energy of Eq. (3-24) one uses the concept of smear model, in which the shear strain energy was calculated first for web without holes. Then by assuming the ratio of the shear strain energies of the webs with and without holes is proportional to the volume ratio of the webs with and without holes, the shear strain energy of the web with holes was evaluated, in which $\left(K_{sh} = \frac{1}{4}\right)$ was obtained. However, by using a two-dimensional linear finite element analysis

the value of the combined stiffness of the mid part of the web of the castellated beam caused by the bending and shears was found to be:

$$K_b = 0.78 \times \frac{\sqrt{3}Gt_w}{4}$$

<div style="text-align: right;">3-26</div>

which is smaller than that above-derived from the smear model. This leads to the shear rigidity factor $\left(K_{sh} = 0.78 \times \frac{1}{4}\right)$. The reason for this is probably due to the smear model used for the calculation of the shear strain energy for the mid-part of the web in Eq. (3-24).

However, it should be mentioned that the factor of (0.78) in Eq. (3-26) was obtained for only one specific section of a castellated beam. It is not known whether this factor can also be applied to other dimensions of the beams. A finite element analysis model for determining the shear rigidity factor K_{sh} is therefore developed (see **Figure 3-2 (c)**), in which the length and depth of the unit are $\left(4a/\sqrt{3}\right)$ and $(2a + a/2)$, respectively. In the unit the relative displacement **(Δ)** can be calculated numerically when a unit load F is applied (see **Figure 3-2 (c)**). Hence, the combined rigidity $\left(K_b = \frac{1}{\Delta}\right)$ is obtained. Note that in the unit model all displacements and rotation of the bottom line are assumed to be zero, whereas the line where the unit load is applied is assumed to have zero vertical displacement. The calibration of the shear rigidity for beams of different section sizes shows that the use of the expression below gives the best results and therefore Eq. (3-27) is used in the present analytical solutions:

$$K_{sh} = \left(0.76 - \frac{b_f}{l}\right) \times \frac{1}{4}$$

<div style="text-align: right;">3-27</div>

Hence the value of the combined stiffness of the mid part of the web of the castellated beam caused by the bending and shear which is adopted in this thesis is:

$$K_b = \left(0.76 - \frac{b_f}{l}\right) \times \frac{\sqrt{3}Gt_w}{4}$$

<div style="text-align: right;">3-28</div>

where l is the length of the beam. Thus, the total potential energy of the castellated beam U is expressed as follows:

$$U = U_T + U_{sh} \qquad\qquad 3\text{-}29$$

The potential of the uniformly distributed load due to the transverse displacement can be expressed as follows:

$$W = q_{max} \int_0^l w \, dx \qquad\qquad 3\text{-}30$$

where q_{max} is the uniformly distributed load, is calculated according to the maximum moment, which can be expressed in terms of design stress $\sigma_y = \frac{M_y(h_w + 2t_f)}{2I_{reduced}}$, as follows:

$$q_{max} = 16 \frac{\sigma_y I_{reduced}}{l^2 (h_w + 2t_f)} \qquad\qquad 3\text{-}31$$

where σ_y is the yield stress of castellated beam.

In summary, the total potential energy of the castellated beam subjected to a uniformly distributed load can be expressed as follows:

$$\Pi = EA_{tee} \int_0^l \left(\frac{du_\beta}{dx}\right)^2 dx + EI_{tee} \int_0^l \left(\frac{d^2w}{dx^2}\right)^2 dx$$
$$+ \frac{Gt_w e^2 k_{sh}}{a} \int_0^l \left(\frac{dw}{dx} - \frac{u_\beta}{e}\right)^2 dx - W \qquad\qquad 3\text{-}32$$
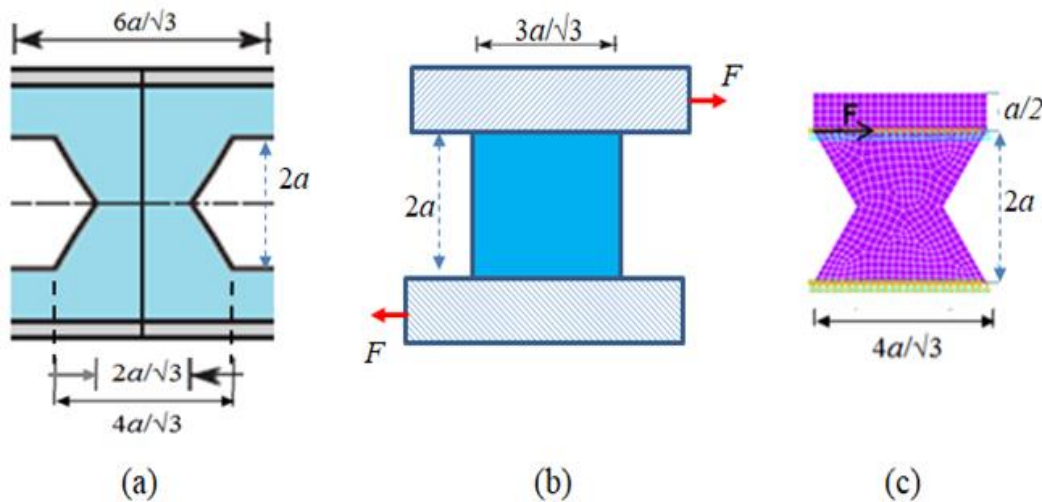
Figure 3-2 Shear strain energy calculation model: **(a)** unit considered, **(b)** shear deformation calculation model and **(c)** finite element model of 4a/√3 length unit and (2a+a/2) depth, loaded by a unit force F.

3.2.1. Deflection of simply supported castellated beam with uniformly distributed loads

For a simply supported castellated beam: $u_\alpha(x)$, $u_\beta(x)$ and $w(x)$ can be assumed as follows:

$$u_\alpha(x) = \sum_{m=1,2,..} A_m \cos\frac{m\pi x}{l} \qquad\qquad 3\text{-}33$$

$$u_\beta(x) = \sum_{m=1,2,..} B_m \cos\frac{m\pi x}{l} \qquad\qquad 3\text{-}34$$

$$w(x) = \sum_{m=1,2,..} C_m \sin\frac{m\pi x}{l} \qquad\qquad 3\text{-}35$$

where A_m , B_m, and C_m ($m = 1,2,...$) are the constants to be determined. It is obvious that the displacement functions assumed in Eqs. (3-33), (3-34) and (3-35) satisfy the simply support boundary conditions, that are $w = \frac{d^2 w}{dx^2} = 0$, and $\frac{du_\alpha}{dx} = \frac{du_\beta}{dx} = 0$ at $x = 0$

and $x = l$.

Substituting Eqs. (3-33), (3-34) and (3-35) into (3-32), according to the principle of minimum potential energy: (Timoshenko, 1961)

$$\delta(U_T + U_{sh} - W) = 0 \qquad\qquad 3\text{-}36$$

The variation of Eq. (3-36) with respect to A_m , B_m and C_m results in the following three algebraic equations:

$$EA_{tee}\left(\frac{m\pi x}{l}\right)^2 A_m = 0 \qquad\qquad 3\text{-}37$$

$$\left[EA_{tee}\left(\frac{m\pi}{l}\right)^2 + \frac{Gt_w k_{sh}}{a}\right]B_m - \left[\frac{Gt_w e k_{sh}}{a}\left(\frac{m\pi}{l}\right)\right]C_m = 0 \qquad\qquad 3\text{-}38$$

$$\left[EI_{tee}\left(\frac{m\pi}{l}\right)^4 + \frac{Gt_we^2k_{sh}}{a}\left(\frac{m\pi}{l}\right)^2\right]C_m$$

$$-\left[\frac{Gt_wek_{sh}}{a}\left(\frac{m\pi}{l}\right)\right]B_m\frac{[1-(-1)^m]q_{max}}{m\pi}$$

3-39

Mathematically Eqs. (3-37) - (3-39) lead to:

$$A_m = 0$$

3-40

$$B_m = \frac{\left[\frac{Gt_wek_{sh}}{a}\left(\frac{m\pi}{l}\right)\right]}{\left[EA_{tee}\left(\frac{m\pi}{l}\right)^2 + \frac{Gt_wk_{sh}}{a}\right]}C_m$$

3-41

$$C_m = \frac{1-(-1)^m}{(m\pi)^5}\frac{ql^4}{EI_{tee} + \dfrac{e^2EA_{tee}}{1 + \dfrac{EA_{tee}a(m\pi)^2}{Gk_{sh}t_wl^2}}}$$

3-42

C_m can be further simplified as:

$$C_m = \frac{ql^4}{E(I_{tee} + e^2A_{tee})}\frac{1-(-1)^m}{(m\pi)^5}\left[1 + \frac{e^2A_{tee}}{I_{tee} + e^2A_{tee}} \times \frac{EA_{tee}a(m\pi)^2}{Gk_{sh}t_wl^2}\right.$$

$$\left.\times\left(1 - \frac{EI_{tee}a(m\pi)^2}{Gk_{sh}t_wl^2e^2}\right)\right]$$

3-43

Therefore, the expression of castellated beam deflection is as follows:

$$w(x) = \frac{ql^4}{E(I_{tee} + e^2A_{tee})}\sum_{m=1,2,..}\frac{2}{(m\pi)^5}\left[1 + \frac{e^2A_{tee}}{I_{tee} + e^2A_{tee}}\right.$$

$$\left.\times\frac{EA_{tee}a(m\pi)^2}{Gk_{sh}t_wl^2}\times\left(1 - \frac{EI_{tee}a(m\pi)^2}{Gk_{sh}t_wl^2e^2}\right)\right]\sin\frac{m\pi x}{l}$$

3-44

The maximum deflection of the beam is at $x = \dfrac{l}{2}$, and thus can be can be expressed as follows:

$$w|_{x=l/2} = \frac{ql^4}{E(I_{tee} + e^2A_{tee})}\left[\sum_{k=1,2,..}\frac{2}{\pi^5}\frac{(-1)^{k+1}}{(2k-1)^5} + \frac{e^2A_{tee}}{I_{tee} + e^2A_{tee}}\times\frac{EA_{tee}a}{Gk_{sh}t_wl^2}\right.$$

$$\left.\times\left(\sum_{k=1,2,..}\frac{2}{\pi^2}\frac{(-1)^{k+1}}{(2k-1)^3} - \frac{EI_{tee}a}{Gk_{sh}t_wl^2e^2}\sum_{k=1,2,..}\frac{2}{\pi}\frac{(-1)^{k+1}}{(2k-1)}\right)\right]$$

3-45

Note that:

$$\sum_{k=1,2,..} \frac{2}{\pi^5} \frac{(-1)^{k+1}}{(2k-1)^5} = \frac{5}{2 \times 384}$$
3-46

$$\sum_{k=1,2,..} \frac{2}{\pi^3} \frac{(-1)^{k+1}}{(2k-1)^3} = \frac{1}{16}$$
3-47

$$\sum_{k=1,2,..} \frac{2}{\pi} \frac{(-1)^{k+1}}{(2k-1)} = \frac{1}{2}$$
3-48

Substituting Eqs. (3-46), (3-47) and (3-48) into (3-45) gives the maximum deflection:

$$w|_{x=l/2} = \frac{5ql^4}{384E(2I_{tee} + 2e^2 A_{tee})} + \frac{ql^2 a}{16G k_{sh} t_w} \times \left(\frac{e A_{tee}}{I_{tee} + e^2 A_{tee}} \right)^2$$
$$\times \left(1 - \frac{2EI_{tee}a}{G k_{sh} t_w l^2 e^2} \right)$$
3-49

It is clear from Eq. (3-49) that the first part indicates the deflection generated by the bending load, which is deemed as that given by Bernoulli-Euler beam, while the second part provides the deflection generated by the shear. Moreover, Eq. (3-49) shows that the shear-induced deflection is proportional to the cross-section area of the two T-sections but inversely proportional to the beam length.

To determine the approximate deflection, the calculation does not consider webs' shear effect, and this is shown in Eq. (3-50).

$$w|_{x=l/2} = \frac{5ql^4}{384EI_{reduced}}$$
3-50

3.2.2. Deflection of pinned-fixed castellated beam with uniformly distributed loads

For pinned-fixed castellated beam $u_\alpha(x)$, $u_\beta(x)$ and $w(x)$ can be assumed as follows:

$$u_\alpha(x) = \sum_{m=1,2,..} F_k \left[(2k-1) \sin\left(\frac{(2k-1)\pi(l-x)}{2l} \right) \right.$$
$$\left. - (2k+1) \sin\left(\frac{(2k+1)\pi(l-x)}{2l} \right) \right]$$
3-51

$$u_\beta(x) = \sum_{m=1,2,\ldots} E_k \left[(2k-1) \sin\left(\frac{(2k-1)\pi(l-x)}{2l}\right) \right.$$
$$\left. - (2k+1) \sin\left(\frac{(2k+1)\pi(l-x)}{2l}\right) \right]$$

3-52

$$w(x) = \sum_{m=1,2,\ldots} D_k \sin\left(\frac{k\pi(l-x)}{l}\right) \sin\left(\frac{\pi(l-x)}{2l}\right)$$

3-53

where F_k, E_k, and D_k ($k = 1,2,\ldots$) are the coefficients to be determined. It is obvious that the displacement functions assumed Eqs. (3-51), (3-52) and (3-53) to satisfy the pinned-fixed support boundary conditions, that is $w = \frac{d^2 w}{dx^2} = 0$, and $\frac{du_\beta}{dx} = 0$ at $x = 0$ and $w = \frac{dw}{dx} = u_\alpha = u_\beta = 0$ at $x = l$.

Substituting Eqs. (3-51), (3-52) and (3-53) into (3-32), and according to the principle of minimum potential energy at Eq. (3-36) it yields:

$$E_k = \frac{128 q k l^5 \, G k_{sh} t_w e \cos(k\pi)\,(1 + 4k^2)}{\pi^4 (16k^4 + 24k^2 + 1)(4k^2 - 1)}$$
$$\times \left(\frac{1}{\left[\begin{array}{l} 4(4k^2 + 1)EG k_{sh} t_w l^2 (A_{tee} e^2 + I_{tee}) \\ + \left(2k^2 + 3 + \frac{1}{8k^2}\right) 8E A_{tee} EI_{tee} \pi^2 a k^2 \end{array} \right]} \right)$$

3-54

$$D_k = \frac{-128 q k l^4 \cos(k\pi)\, Z}{\pi^5 (16k^4 + 24k^2 + 1)(4k^2 - 1)}$$

3-55

where:

$$Z = \frac{\left((2k^2 + 3 + \frac{1}{8k^2}) 8E A_{tee} \pi^2 a k^2 + (4k^2 + 1) 4G k_{sh} t_w l^2 \right)}{\left[4(4k^2 + 1)EG k_{sh} t_w l^2 (A_{tee} e^2 + I_{tee}) + \left(2k^2 + 3 + \frac{1}{8k^2}\right) 8E A_{tee} EI_{tee} \pi^2 a k^2 \right]}$$

3-56

Therefore, the deflection of pinned-fixed castellated beam can be expressed as:

$$\text{w}(x) = \sum_{k=1,2,3} \frac{-128 q k l^4 \cos(k\pi)\, Z \sin\left(\frac{k\pi(l-x)}{l}\right) \sin\left(\frac{\pi(l-x)}{2l}\right)}{\pi^5 (16k^4 + 24k^2 + 1)(4k^2 - 1)}$$

3-57

Clearly, the denominator of Eq. (3-57) is very complicated, and the position of the maximum deflection point is at ($x = 0.375l$) away from the pinned support end, which is obtained by using the zero derivative of the deflection function with respect to coordinate as described in the bending theory of beams (Timoshenko, 1961).The Eq. (3-57) is not easy to simplify but it is regarded as Bernoulli-Euler beam with modifications.

To determine the approximate deflection, the calculation does not consider webs' shear effect, but rather can be employed Eq. (3-58):

$$w_{max} = \frac{ql^4}{185EI_{reduced}}$$ 3-58
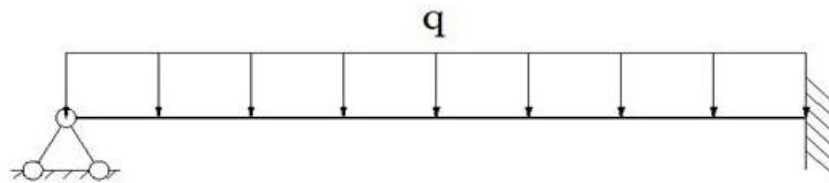
Figure 3-3.Pinned-fixed beam.

3.2.3. Deflection of non-uniform temperature distribution simply supported castellated beam with uniformly distributed loads

Consider a castellated beam that is used in the external floor and wall, in which the beam can be bent about its major axis but is restrained in its lateral direction. When there is fire inside the building, the castellated beam is exposed to a fire on one side. During the fire, the heat will be transferred from the fire into the beam, which causes the beam to have a non-uniform temperature distribution on its cross-section. Consequently, the material properties that depend on the temperature will also not be uniform in the cross-section.

Since the heat is transferred from one flange to another through the web, it is reasonable to assume that the temperature is uniformly distributed in each T-section, although the two T-sections may have different temperatures at the same time.

Note that the thermal expansion induced by temperature was not considered in this study. This is because when a simply support boundary is involved in the beam the axial displacement can be freely expanded so there will be no thermal stresses in the beam. All thermal strains are converted into displacement and thus the thermal expansion does not cause significant deflection
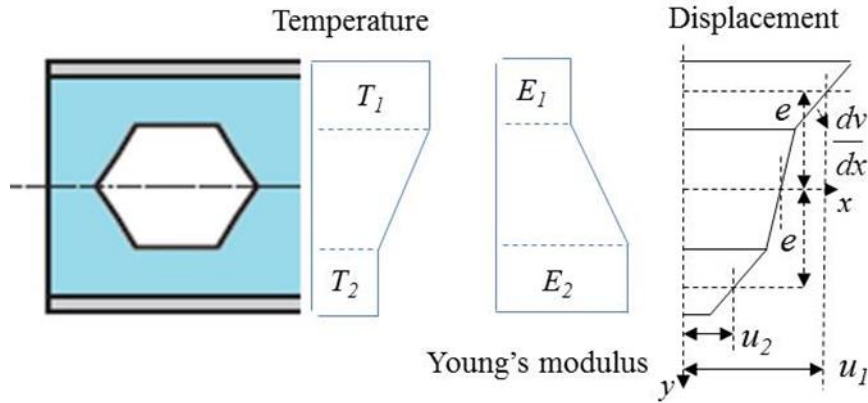
Figure 3-4 Definition of temperature, Young's modulus and displacement component in the cross-section (Lei et al., 2017).

Let (u_1, w) and (u_2, w) be the axial and transverse displacements at the centroid points of the two T-sections (see **Figure 3-4**) The strain energy of the two T-sections of castellated beams U_1 and U_2 due to transverse loads can be expressed as follows:

$$U_1 = \frac{1}{2} \int_0^l \left[E_1 A_1 \left(\frac{du_1}{dx} \right)^2 + E_1 I_1 \left(\frac{d^2 w}{dx^2} \right)^2 \right] dx \qquad 3\text{-}59$$

$$U_2 = \frac{1}{2} \int_0^l \left[E_2 A_2 \left(\frac{du_2}{dx} \right)^2 + E_2 I_2 \left(\frac{d^2 w}{dx^2} \right)^2 \right] dx \qquad 3\text{-}60$$

where A_1 and A_2 are the areas of the two T-sections, E_1 and E_2 are the Young's modulus of the two T-sections and I_1 and I_2 are the second moments of areas of the two T-sections about their own centroid axes, and l is the length of the beam.

The average shear strain of the mid-part of the web γ_{xz} is expressed as follows:

$$\gamma_{xz}(x,z) = \frac{e}{a} \frac{dw}{dx} - \frac{u_1 - u_2}{2a} \qquad 3\text{-}61$$

Thus the shear strain energy of the mid-part of the web U_{sh} is expressed as follows:

$$U_{sh} = \frac{t_w e^2 (E_1 + E_2) k_{sh}}{4(1+v)a} \int_0^l \left(\frac{dw}{dx} - \frac{u_1 - u_2}{2e} \right)^2 dx \qquad \text{3-62}$$

$$\Pi = \frac{1}{2} \int_0^l \left[E_1 A_1 \left(\frac{du_1}{dx} \right)^2 E_1 I_1 \left(\frac{d^2 w}{dx^2} \right)^2 \right] dx$$

$$+ \frac{1}{2} \int_0^l \left[E_2 A_2 \left(\frac{du_2}{dx} \right)^2 E_2 I_2 \left(\frac{d^2 w}{dx^2} \right)^2 \right] dx \qquad \text{3-63}$$

$$\times \frac{t_w e^2 (E_1 + E_2) k_{sh}}{4(1+v)a} \int_0^l \left(\frac{dw}{dx} - \frac{u_1 - u_2}{2e} \right)^2 dx - W$$

$$\delta(U_T + U_{sh} - W) = 0 \qquad \text{3-64}$$

For a simply supported castellated beam: $u_\alpha(x)$, $u_\beta(x)$, and $w(x)$ can be assumed as follows:

$$u_\alpha(x) = \sum_{m=1,2,..} A_m \cos \frac{m\pi x}{l} \qquad \text{3-65}$$

$$u_\beta(x) = \sum_{m=1,2,..} B_m \cos \frac{m\pi x}{l} \qquad \text{3-66}$$

$$w(x) = \sum_{m=1,2,..} C_m \sin \frac{m\pi x}{l} \qquad \text{3-67}$$

where $A_m, B_m,$ and C_m $(m = 1,2, ...)$ are the constants to be determined, it is obvious that the displacement functions assumed Eqs. (3-65), (3-66) and (3-67) satisfy the simply support boundary conditions, that are $w = \frac{d^2 w}{dx^2} = 0$, and $\frac{du_\alpha}{dx} = \frac{du_\beta}{dx} = 0$ at $x = 0$ and $x = l$.

Substituting Eqs. (3-65)- (3-67) into (3-63) by using Eqs. (3-8) and (3-9), according to the principle of minimum potential energy, it yields,

$$A_m = -\frac{E_2}{E_1} B_m \qquad \text{3-68}$$

Note that for castellated beams or columns, $A_1 = A_2 = A_{tee}$ and, $I_1 = I_2 = I_{tee}$. Thus:

$$B_m = \frac{\left[\frac{(E_1 + E_2)I_{tee}(m\pi)^5}{l^4}\right]C_3 - 2q(1 - (-1)^m)}{\frac{2E_2 A_{tee}e(m\pi)^4}{l^3}}$$
<div align="right">3-69</div>

$$C_m = \frac{2q(1 - (-1)^m)l^4}{(m\pi)^5} \left[\frac{1}{(E_1 + E_2)I_{tee} + \left(\frac{4E_2 A_{tee}e^2(E_1 + E_2)E_1 E_2}{(E_1 + E_2)^2 \left(1 + \frac{8aE_1 E_2(1 + v)(m\pi)^2 A_{tee}}{(E_1 + E_2)^2 l^2 t_w k_{sh}}\right)}\right)}\right]$$
<div align="right">3-70</div>

$$C_m = \frac{2ql^4}{(E_1 + E_2)\left[I_{tee} + \frac{4A_{tee}e^2 E_1 E_2}{(E_1 + E_2)^2}\right]} \frac{(1 - (-1)^m)}{(m\pi)^5}\left[1 + \frac{4A_{tee}e^2 E_1 E_2}{I_{tee} + \frac{4A_{tee}e^2 E_1 E_2}{(E_1 + E_2)^2}} \times \frac{8aE_1 E_2(1 + v)(m\pi)^2 A_{tee}}{(E_1 + E_2)^2 l^2 t_w k_{sh}} \right.$$
$$\left. \times \frac{1}{(E_1 + E_2)^2}\right]$$
<div align="right">3-71</div>

Eq. (3-70) can be further simplified as:

Therefore, the expression of the castellated beam deflection is expressed as follows:

$$w(x) = \frac{2ql^4}{(E_1 + E_2)\left[I_{tee} + \frac{4A_{tee}e^2 E_1 E_2}{(E_1 + E_2)^2}\right]} \frac{(1 - (-1)^m)}{(m\pi)^5}\left[1 + \frac{4A_{tee}e^2 E_1 E_2}{I_{tee} + \frac{4A_{tee}e^2 E_1 E_2}{(E_1 + E_2)^2}} \times \frac{8aE_1 E_2(1 + v)(m\pi)^2 A_{tee}}{(E_1 + E_2)^2 l^2 t_w k_{sh}} \right.$$
$$\left. \times \frac{1}{(E_1 + E_2)^2}\right] \sin\frac{m\pi x}{l}$$
<div align="right">3-72</div>

As the maximum deflection of uniformly loaded simply supported beam takes place at $x = \frac{l}{2}$, the maximum deflection can be expressed as follows:

$$w|_{x=l/2} = \frac{2ql^4}{(E_1 + E_2)\left[I_{tee} + \frac{4A_{tee}e^2E_1E_2}{(E_1+E_2)^2}\right]} \left[\sum_{k=1,2,..} \frac{2(-1)^{k+1}}{\pi^5(2k-1)^5}\right.$$

$$+ \frac{4A_{tee}e^2E_1E_2}{I_{tee} + \frac{4A_{tee}e^2E_1E_2}{(E_1+E_2)^2}} \times \frac{8aE_1E_2(1+v)(m\pi)^2A_{tee}}{(E_1+E_2)^2l^2t_wk_{sh}}$$

$$\left. \times \frac{1}{(E_1+E_2)^2} \times \sum_{k=1,2,..} \frac{2(-1)^{k+1}}{\pi^3(2k-1)^5}\right]$$

3-73

Substituting Eqs. (3-46), (3-47) and (3-48) into (3-73) gives the maximum deflection:

$$w|_{x=l/2} = \frac{5ql^4}{384(E_1+E_2)\left[I_{tee} + \frac{4A_{tee}e^2E_1E_2}{(E_1+E_2)^2}\right]} + \frac{ql^2}{(E_1+E_2)} \times \frac{a(1+v)}{t_wk_{sh}}$$

$$\times \left[\frac{2eA_{tee}E_1E_2}{I_{tee} + \frac{4A_{tee}e^2E_1E_2}{(E_1+E_2)^2}(E_1+E_2)^2}\right]^2$$

3-74

Eq. (3-74) reflects the influence of non-uniform material properties caused by the non-uniform temperature on the maximum deflection of the castellated beam when the shear effect is considered.

It is obvious that, the first part of Eq. (3-74) indicates the deflection generated by the bending load but affected by temperature, while the second part provides the deflection generated by the shear load also affected by temperature. Moreover, Eq. (3-74) shows that rising or reducing shear effect depends on the cross-section area of major axis as well as the difference in temperatures between the two T- sections.

3.2.4. Deflection of non-uniform temperature distribution roller- fixed supported castellated beam with uniformly distributed loads.

Note that the thermal expansion induced by temperature was not considered in this study because the axial displacement can be freely expanded at the side of roller boundary in the beam; so there will be no thermal stresses in the beam. All thermal strains are converted into displacement and thus the thermal expansion does not cause significant deflection.

For roller-fixed castellated beam $u_\alpha(x)$, $u_\beta(x)$ and $w(x)$ can be assumed as follows:

$$u_\alpha(x) = \sum_{m=1,2,..} F_k \left[(2k-1) \sin\left(\frac{(2k-1)\pi(l-x)}{2l}\right) - (2k+1) \sin\left(\frac{(2k+1)\pi(l-x)}{2l}\right) \right]$$
<div align="right">3-75</div>

$$u_\beta(x) = \sum_{m=1,2,..} E_k \left[(2k-1) \sin\left(\frac{(2k-1)\pi(l-x)}{2l}\right) - (2k+1) \sin\left(\frac{(2k+1)\pi(l-x)}{2l}\right) \right]$$
<div align="right">3-76</div>

$$w(x) = \sum_{m=1,2,..} D_k \sin\left(\frac{k\pi(l-x)}{l}\right) \sin\left(\frac{\pi(l-x)}{2l}\right)$$
<div align="right">3-77</div>

where F_k, E_k, and D_k (k = 1, 2 …) are the constants to be determined. It is obvious that the displacement functions assumed satisfy the pinned-fixed support boundary conditions, that are $w = \frac{d^2w}{dx^2} = 0$, and $\frac{du_\beta}{dx} = 0$ at $x = 0$ and $w = \frac{dw}{dx} = u_\alpha = u_\beta = 0$ at $x = l$.

Substituting Eqs. (3-75), (3-76) and (3-77) into (3-63), and according to the principle of minimum potential energy, it yields:

$$D_k = \frac{-256qkl^4 Z \cos(k\pi)}{\pi^5 (16k^4 + 24k^2 + 1)(4k^2 - 1)(E_1 + E_2)}$$
<div align="right">3-78</div>

where

$$Z = \frac{\left[16A_{tee}E_1E_2\pi^2 ak^2(1+v)\left(2k^2 + 3 + \frac{1}{8k^2}\right) + k_{sh}t_w l^2(E_1+E_2)^2(4k^2+1) \right]}{\left[\left(16A_{tee}E_1E_2 I_{tee}\pi^2 ak^2(1+v)\left(2k^2 + 3 + \frac{1}{8k^2}\right) + I_{tee}k_{sh}t_w l^2(E_1+E_2)^2(4k^2+1) \right) \\ +4(4k^2+1)A_{tee}k_{sh}t_w l^2 E_1 E_2 e^2 \right]}$$
<div align="right">3-79</div>

$$w(x) = \sum_{k=1,2,3} \frac{-256qkl^4 \cos(k\pi) Z \sin\left(\frac{k\pi(l-x)}{l}\right) \sin\left(\frac{\pi(l-x)}{2l}\right)}{\pi^5 (16k^4 + 24k^2 + 1)(4k^2 - 1)(E_1 + E_2)}$$
<div align="right">3-80</div>

Eq. (3-80) reflects the influence of non-uniform material properties caused by the non-uniform temperature on the maximum deflection of pinned-fixed castellated beam when the shear effect is considered.

Clearly, the denominator of Eq. (3-80) is very complicated, and the position of the maximum deflection point is at ($x = 0.375l$). The Eq. (3-80) is not easy to simplify but it is regarded as Bernoulli-Euler beam with modifications.

3.3. **Numerical analysis**

Finite Element Analysis (FEA) is a numerical method that has been implemented to simulate any physical phenomenon for finding out new concepts. Essentially, it was used for solving cases of structural mechanics, sometimes instead of experimental techniques as well as to validate versus the experimental or analytical solution.

In general, FEA suits for solving the problems such as heat transfer, fluid mechanics, and manufacturing modelling in engineering fields by solving mathematical equations numerically and therefore is named as numerical method.

At present, the accuracy and flexibility of this method have led to it becoming commonplace in the analysis and design of steel structures consisting of thin-walled members with web openings exposed to various types of loading and different boundary conditions.

The ANSYS software is the finite element analysis tool that is adopted in this study for numerical analysis of castellated beams to verify the accuracy of the analytical solutions of transverse deflection of castellated beams subjected to uniformly distributed transverse load.

3.3.1. **The modeling of castellated beams**

ANSYS software library has different types of elements for the analysis of different types of structures. Previous studies have shown that the use of three-dimensional (3D) finite element model was successful in idealizing the structural behaviour of castellated beams (El-Sawy et al., 2009).

The modelling of castellated beams is carried out by using 3D linear 4-Node Thin Shell Elements (SHELL181) depicted in **Figure 3-5.** It is designed for modelling thin-walled members because one dimension of the element is very small compared with another two dimensions; also for linear, large rotation, and/or large strain nonlinear applications. This element presents four nodes with six DOF per node, i.e., translations and rotations on the X, Y, and Z-axis, respectively.
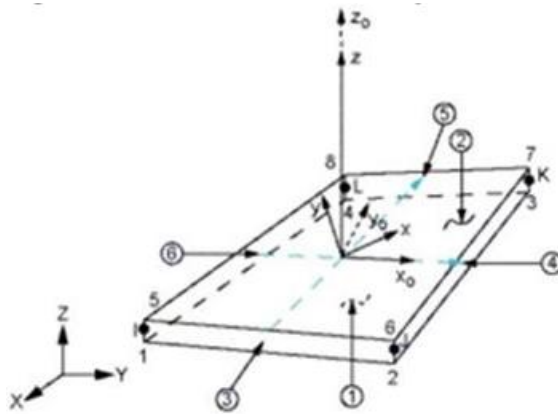
Figure 3-5 Shell element ANSYS library.

3.3.2. Meshing consideration and material model

With regard to the mesh size of the model, the short length beams were meshed by using element size of 5 mm, whereas for the long length beams the element size of 10 mm was used. A typical mesh configuration for castellated beam is shown in **Figure 3-6**. The material model of the castellated beam uses linear elastic material with Young's modulus E = 2.1×10^5 MPa, Poisson's ratio v =0.3 and yield stress σ_y=275 MPa.
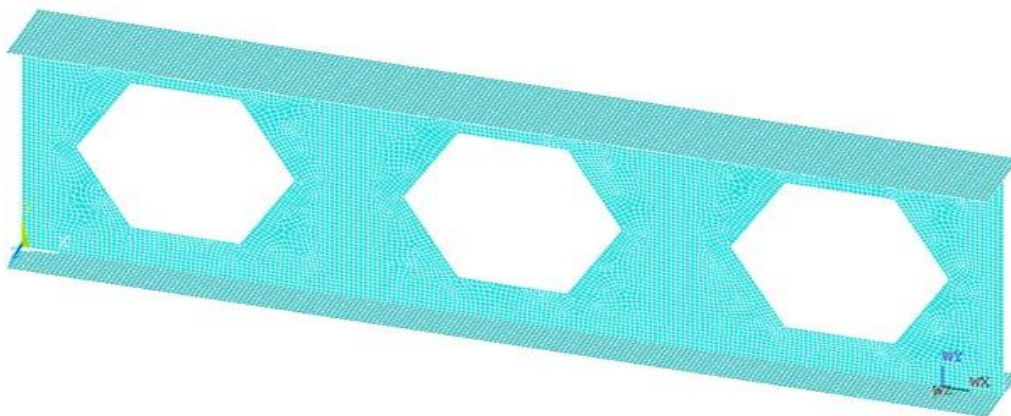
Figure 3-6 A typical mesh configuration

3.3.3. Boundary conditions and loading

3.3.3.1. Simply supported castellated beam

For simply supported beam, a half-length analysis model is used because of the symmetry. Therefore, it has led to reducing the number of elements and nodes, also saving time. The displacement boundary conditions are applied to all nodes at the two ends, as shown in **Figure 3-7**. The lateral and transverse deflections and rotation are restrained ($u_y=u_z=0$ and $\theta_x=0$) at the simply supported end, while the symmetric boundary condition is applied at the other end by restricting the axial displacement and rotations about the two axes within the cross-section ($u_x=0$ and $\theta_y=\theta_z=0$).

A line load is used to model the uniformly distributed transverse load, which acts on the junction of the flange and the web. The uniformly distributed load (q_{max}) is considered after multiplying with beam's half-length and then divided by the numbers of the nodes on the line defining the junction of the flange and the web nodes, which gives the load applying on each node.

3.3.3.2. Pinned-fixed supported castellated beam

The boundaries of one end simply supported and another fixed are applied in the model. Full length of the castellated beam is used. The displacement boundary conditions are applied to all nodes at the two ends, as shown in **Figure 3-7**. The lateral and transverse deflections and rotation are restrained ($u_y=u_z=0$ and $\theta_x=0$) at the simply supported end, while the fixed support boundary condition is applied at the other end by restraining the axial displacement, transverse deflections and rotations around the three axes within the cross-section ($u_x=u_y=u_z=0$ and $\theta_x=\theta_y=\theta_z=0$).

The uniformly distributed load is also applied at the junction between the flange and web as a line load, which is similar to the simply supported beam as described above.
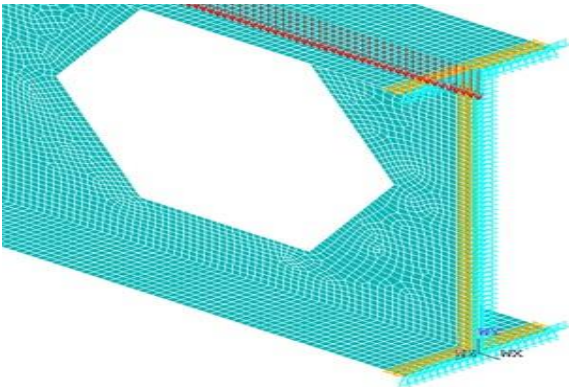
Figure 3-7 The typical loading method and boundary conditions in finite element model of castellated beam.

3.3.4. The dimensions of parameter study and the value of load

Ten groups of selected beams with different lengths are analysed, each of them having different cross sections. The (h_w/t_w) ratio of the selected sections is (37.5) and the (b_f/t_f) ratio of the selected sections ranges from 10 to 25, as tabulated in **Table (3-1)**.

Table 3-1 Parameters of castellated beams groups considered

Group	Name of beam	the opening panel (unit)	l mm	$l/2$ mm	bf mm	tf mm	h_w mm	t_w mm	a mm	q_{max} N/mm
A	A1	2	692.82	346.41	100	10	300	8	100	1739.76
	A2	2	692.82	346.41	150	10	300	8	100	2428.21
	A3	2	692.82	346.41	200	10	300	8	100	3116.67
	A4	2	692.82	346.41	250	10	300	8	100	3805.12
B	B1	4	2078.46	1039.23	100	10	300	8	100	193.31
	B2	4	2078.46	1039.23	150	10	300	8	100	269.80
	B3	4	2078.46	1039.23	200	10	300	8	100	346.30
	B4	4	2078.46	1039.23	250	10	300	8	100	422.79
C	C1	10	3464.16	1732.05	100	10	300	8	100	69.59
	C2	10	3464.16	1732.05	150	10	300	8	100	97.13
	C3	10	3464.16	1732.05	200	10	300	8	100	124.67
	C4	10	3464.16	1732.05	250	10	300	8	100	152.20

Group	Name of beam	the opening panel (unit)	l mm	$l/2$ mm	b_f mm	t_f mm	h_w mm	t_w mm	a mm	q_{max} N/mm
D	D1	12	4156.92	2078.46	100	10	300	8	100	48.33
	D2	12	4156.92	2078.46	150	10	300	8	100	67.45
	D3	12	4156.92	2078.46	200	10	300	8	100	86.57
	D4	12	4156.92	2078.46	250	10	300	8	100	105.69
E	E1	14	4849.74	2424.87	100	10	300	8	100	35.50
	E2	14	4849.74	2424.87	150	10	300	8	100	49.55
	E3	14	4849.74	2424.87	200	10	300	8	100	63.60
	E4	14	4849.74	2424.87	250	10	300	8	100	77.65
F	F1	16	5542.56	2771.28	100	10	300	8	100	27.18
	F2	16	5542.56	2771.28	150	10	300	8	100	37.94
	F3	16	5542.56	2771.28	200	10	300	8	100	48.69
	F4	16	5542.56	2771.28	250	10	300	8	100	59.45
G	G1	18	6235.38	3117.69	100	10	300	8	100	21.48
	G2	18	6235.38	3117.69	150	10	300	8	100	29.97
	G3	18	6235.38	3117.69	200	10	300	8	100	38.48
	G4	18	6235.38	3117.69	250	10	300	8	100	46.98
H	H1	26	9006.66	4503.33	100	10	300	8	100	10.29
	H2	26	9006.66	4503.33	150	10	300	8	100	14.37
	H3	26	9006.66	4503.33	200	10	300	8	100	18.44
	H4	26	9006.66	4503.33	250	10	300	8	100	22.51
I	I1	36	12470.77	6235.38	100	10	300	8	100	5.37
	I2	36	12470.77	6235.38	150	10	300	8	100	7.49
	I3	36	12470.77	6235.38	200	10	300	8	100	9.62
	I4	36	12470.77	6235.38	250	10	300	8	100	11.74
J	J1	42	14549.23	7274.61	100	10	300	8	100	3.95
	J2	42	14549.23	7274.61	150	10	300	8	100	5.51
	J3	42	14549.23	7274.61	200	10	300	8	100	7.07
	J4	42	14549.23	7274.61	250	10	300	8	100	8.63

3.3.5. Comparison of results and discussion

The details of comparisons between the analytical results and finite element analysis results are given in the tables and plotted in the figures. These results indicate the shear effect of web openings on the transverse deflection. It can be noticed from the comparisons that the present analytical solution, taking into account shear, agrees well with the result provided by the finite element analysis.

3.3.5.1. Maximum deflections of simply supported beams subjected to uniformly distributed loads

Table (3-2) shows the results of maximum deflections of simply supported castellated beams with a uniformly distributed load for different lengths with various cross-section dimensions, obtained using Eq. (3-49). In the results, T1 is based on Eq. (3-28); T2 uses$\left(K_{sh} = 0.78 \times \frac{1}{4}\right)$; T3 uses$\left(K_{sh} = \frac{1}{4}\right)$; T4 is obtained from Eq. (3-50); and T5 is the finite element analysis results. The results are also plotted in **Figure 3-8**.

Table (3-3) shows the relative errors of the maximum deflections of simply supported castellated beam with a uniformly distributed load, which are obtained based on the finite element numerical solutions that are described in **Table (3-2),** between analytical solutions using different shear rigidity factors obtained by Eq. (3-49), including one with zero shear factor obtained by Eq. (3-50) for four castellated beams of different flange widths.

Figure 3-8 shows a comparison of the maximum deflections between analytical solutions using different shear rigidity factors including one with zero shear factor and FEA numerical solution for different beam lengths with various flange widths. It can be seen from the figure that, the analytical solution using the proposed shear factor is closest to the numerical solution, whereas the analytical solutions using other shear factors is not as good as the present one. This demonstrates that the shear factor is also affected by the ratio of the flange width to the beam length. In addition, it can be seen from the figure that, the longer the beam, the closer the analytical solution to the numerical solution; and the wider the flanges, the closer the analytical solution to the

numerical solution. **Figure 3-9** shows the relative error of each analytical solution when it is compared with the finite element solution. From the figure it is evident that the error of the analytical solutions using the present shear rigidity factor does not exceed 5.0% for all of discussed four sections in all the beam length range ($l >3$ meters). For beams less than 3 meters the error is about 11.0% which is quite big. However, for most practically used beams the length will be longer than 3 meters. In contrast, the analytical solution ignoring the shear effect or considering the shear effect by using smear model or by using the length-independent shear rigidity factor, will have large error, particularly when the beam is short.

3.3.5.2. Maximum deflection of pinned-fixed castellated beam due to uniformly distributed loads

Table (3-4) shows the results of maximum deflections of pinned-fixed castellated beams with a uniformly distributed load for different lengths with various cross-section dimensions, obtained using Eq. (3-57). In the results, T1 is based on Eq. (3-28); T2 uses$\left(K_{sh} = 0.78 \times \frac{1}{4}\right)$; T3 uses$\left(K_{sh} = \frac{1}{4}\right)$; T4 is obtained from Eq. (3-58); and T5 is the finite element analysis results. The results are also plotted in **Figure 3-10**.

Table (3-5) shows the relative errors of the maximum deflections of pinned-fixed castellated beam with a uniformly distributed load, which are obtained based on the finite element numerical solutions that are described in **Table (3-4)**, between analytical solutions using different shear rigidity factors obtained by Eq. (3-57), including one with zero shear factor obtained by Eq. (3-58) for four castellated beams of different flange widths.

Figure 3-10 shows a comparison of the maximum deflations between analytical solutions using different shear rigidity factors, including one with zero shear factor and FEA numerical solution for different beam lengths with various flange widths. It can be seen from the figure that, the analytical solution using the proposed shear factor again is closest to the numerical solution, whereas the analytical solutions using other shear factors is not as good as the present one. This demonstrates that the shear factor is also

affected by the ratio of the flange width to the beam length. In addition, it can be seen from the figure that, the longer the beam, the closer the analytical solution to the numerical solution; and the wider the flanges, the closer the analytical solution to the numerical solution. **Figure 3-11** shows the relative error of each analytical solution when it is compared with the finite element solution. From the figure it is evident that the relative error of the analytical solutions using the present shear rigidity factor does not exceed 23% for all of discussed four sections in all of the beam length range ($l > 3$ meter) . In contrast, the analytical solution ignoring the shear effect, or considering the shear effect by using smear model or by using the length-independent shear rigidity factor will have large error, particularly when the beam is short. Compared to the simply supported beams, the error of the analytical solution of the pinned-fixed beams seems to be larger. This is probably due to the deflection functions assumed for pinned-fixed beams that have slow convergence.

Table 3-2 Comparison of results of maximum deflections of simply supported castellated beam with a uniformly distributed load obtained using different approaches

b_f mm	Name of beam	T1 mm	T2 mm	T3 mm	T4 mm	T5 mm
100	A1	2.66	2.21	1.86	0.41	3.00
	B1	5.74	5.56	5.19	3.68	6.12
	C1	12.24	12.12	11.74	10.23	12.35
	D1	16.77	16.62	16.24	14.74	16.65
	E1	22.04	21.89	21.46	20.06	21.71
	F1	28.00	28.03	27.70	26.19	27.60
	G1	35.13	34.99	34.66	33.15	34.60
	H1	70.80	71.00	70.67	69.16	69.00
150	A2	3.84	2.86	2.39	0.41	4.18
	B2	6.71	6.24	5.73	3.68	7.11
	C2	13.02	12.79	12.28	10.23	13.40
	D2	17.50	17.30	16.78	14.74	17.75
	E2	22.80	22.62	22.11	20.05	22.88
	F2	28.92	28.76	28.24	26.19	28.81
	G2	35.87	35.71	35.20	33.15	35.50
	H2	70.89	71.73	71.21	69.16	70.00
200	A3	5.53	3.50	2.85	0.41	5.31
	B3	7.74	6.91	6.21	3.68	8.10
	C3	13.85	13.47	12.76	10.23	14.43
	D3	18.29	17.98	17.26	14.74	18.80
	E3	23.57	23.30	22.58	20.05	23.91
	F3	29.69	29.44	28.72	26.19	29.94
	G3	36.63	36.40	35.681	33.15	36.69
	H3	72.59	72.41	71.69	69.16	71.74
250	A4	7.33	4.23	3.43	0.41	6.90
	B4	8.50	7.69	6.81	3.68	9.10
	C4	14.68	14.25	13.37	10.23	15.42
	D4	19.11	18.76	17.87	14.74	19.80
	E4	24.50	24.08	23.19	20.05	25.20
	F4	30.48	30.22	29.33	26.19	31.00
	G4	37.40	37.18	36.29	33.15	37.80
	H4	73.35	73.29	72.30	69.16	72.99
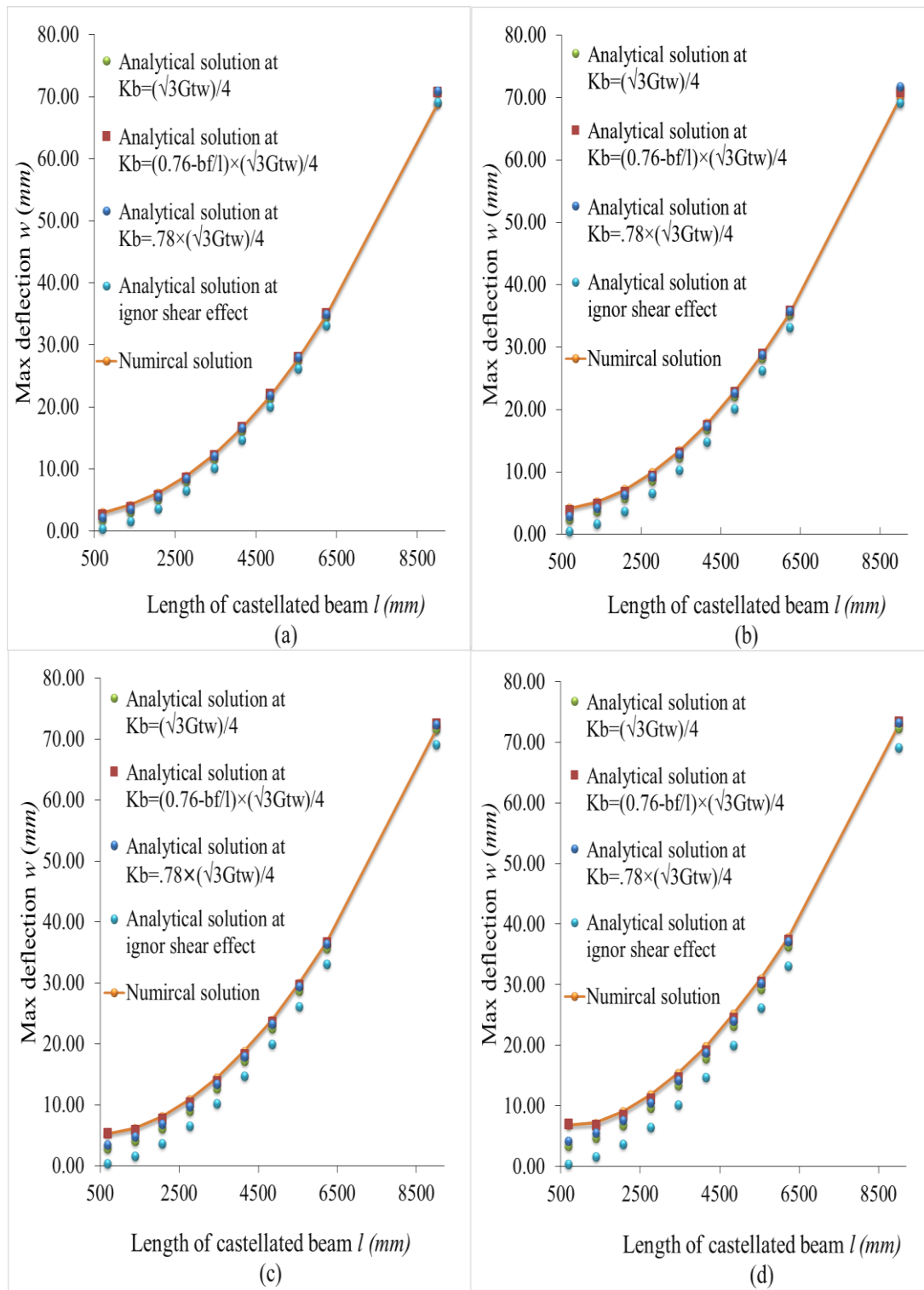
Figure 3-8 Maximum deflections of simply supported castellated beam with a uniformly distributed load between analytical solutions using different shear rigidity factors obtained by Eq. (3-49), including one with zero shear factor obtained by Eq. (3-50) and FEA numerical solution for different beam lengths with various flange widths. (a) bf =100mm, (b) bf =150mm, (c) bf =200mm and (d) bf =250mm. (h_w=300mm, t_f=10mm, t_w=8mm and a=100mm)

Table 3-3 The relative errors of maximum deflections of simply supported castellated beam with a uniformly distributed load obtained based on the finite element numerical solutions

b_f mm	Name of beam	T1	T2	T3	T4
100	A1	0.11	0.26	0.38	0.86
	B1	0.06	0.09	0.15	0.40
	C1	0.01	0.02	0.05	0.17
	D1	-0.01	0.00	0.02	0.11
	E1	-0.02	-0.01	0.01	0.08
	F1	-0.01	-0.02	0.00	0.05
	G1	-0.02	-0.01	0.00	0.04
	H1	-0.03	-0.03	-0.02	0.00
150	A2	0.08	0.32	0.43	0.90
	B2	0.06	0.12	0.19	0.48
	C2	0.03	0.05	0.08	0.24
	D2	0.01	0.03	0.05	0.17
	E2	0.00	0.01	0.03	0.12
	F2	0.00	0.00	0.02	0.09
	G2	-0.01	-0.01	0.01	0.07
	H2	-0.01	-0.02	-0.02	0.01
200	A3	0.00	0.34	0.46	0.92
	B3	0.04	0.15	0.23	0.55
	C3	0.04	0.07	0.12	0.29
	D3	0.03	0.04	0.08	0.22
	E3	0.01	0.03	0.06	0.16
	F3	0.01	0.02	0.04	0.13
	G3	0.00	0.01	0.03	0.10
	H3	-0.01	-0.01	0.00	0.04
250	A4	-0.01	0.39	0.50	0.94
	B4	0.07	0.15	0.25	0.60
	C4	0.05	0.08	0.13	0.34
	D4	0.04	0.05	0.10	0.26
	E4	0.03	0.04	0.08	0.20
	F4	0.02	0.03	0.05	0.16
	G4	0.01	0.02	0.04	0.12
	H4	0.00	0.00	0.01	0.05
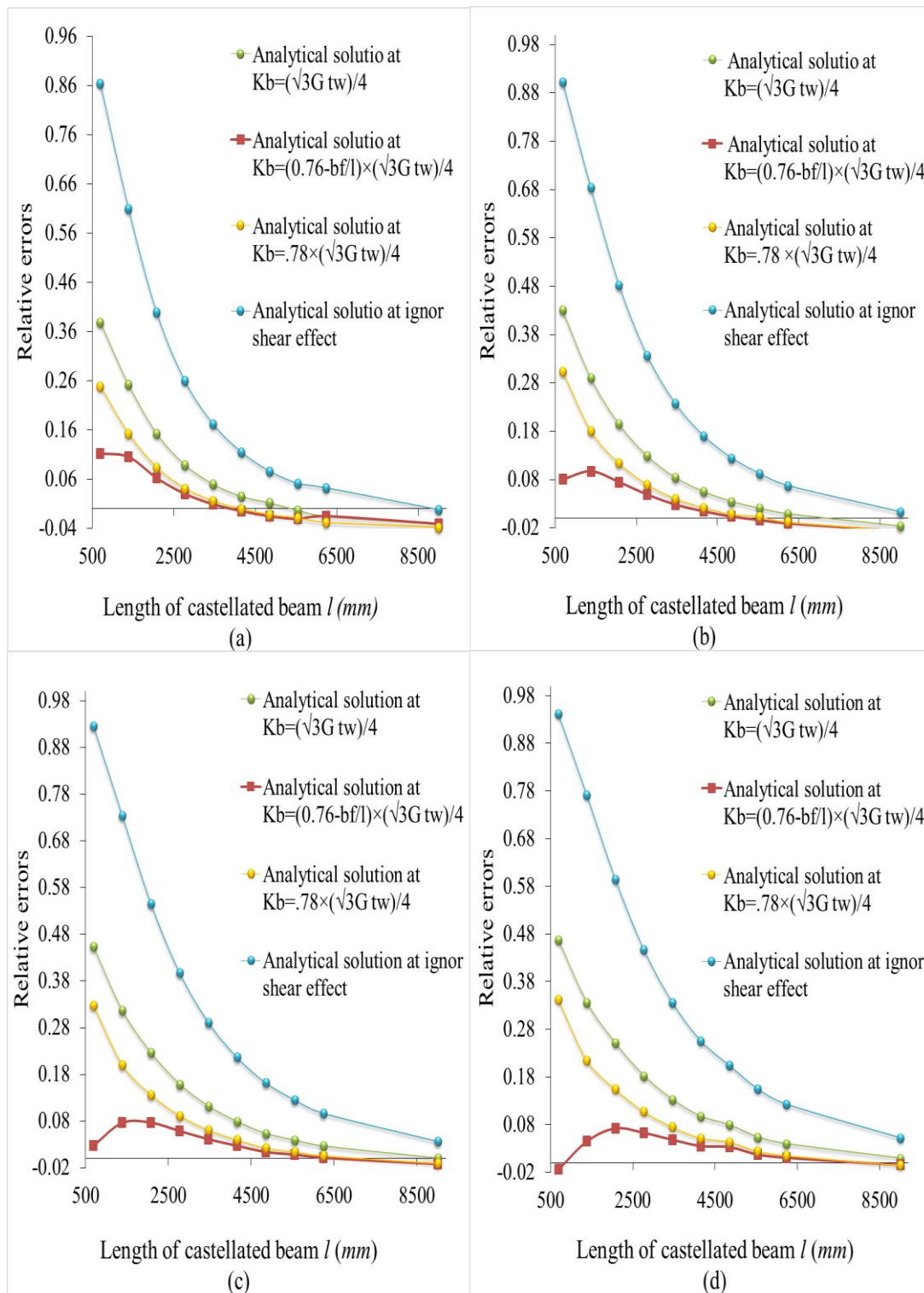
Figure 3-9 Relative errors of maximum deflections of simply supported castellated beam with a uniformly distributed load between analytical solutions using different shear rigidity factors obtained by Eq. (3-49), including one with zero shear factor obtained by Eq. (3-50) and FEA numerical solution for different beam lengths with various flange widths. (a) bf =100mm, (b) bf =150mm, (c) bf =200mm and (d) bf =250mm. (h_w=300mm, t_f=10mm, t_w=8mm and a=100mm)

Table 3-4 Comparison of results of maximum deflections of pinned-fixed castellated beam with a uniformly distributed load obtained using different approaches

b_f mm	Name of beam	T1 mm	T2 mm	T3 mm	T4 mm	T5 mm
100	B1	3.30	3.05	2.71	1.47	4.36
	C1	5.80	5.69	5.35	4.09	6.99
	D1	7.60	7.50	7.15	5.88	8.80
	E1	9.73	9.64	9.29	8.01	10.91
	F1	12.18	12.10	11.75	10.46	13.33
	G1	14.97	14.89	14.54	13.24	16.08
	H1	29.41	29.34	28.99	27.62	30.36
	I1	54.86	54.80	54.45	52.95	55.48
150	B2	4.10	3.62	3.15	1.47	5.39
	C2	6.46	6.27	5.79	4.09	8.06
	D2	8.24	8.08	7.60	5.88	9.92
	E2	10.36	10.21	9.74	8.01	12.06
	F2	12.82	12.68	12.20	10.46	14.52
	G2	15.60	15.47	14.99	13.24	17.30
	H2	30.03	29.92	29.44	27.62	31.78
	I2	55.46	55.37	54.89	52.95	57.23
200	B3	4.88	4.19	3.60	1.47	6.42
	C3	7.14	6.84	6.24	4.09	9.12
	D3	8.91	8.65	8.05	5.88	11.00
	E3	11.02	10.79	10.19	8.01	13.18
	F3	13.46	13.25	12.65	10.46	15.67
	G3	16.24	16.04	15.44	13.24	18.46
	H3	30.65	30.50	29.89	27.62	33.05
	I3	56.08	55.34	55.34	52.95	58.69
250	B4	5.80	4.76	4.04	1.47	7.50
	C4	7.85	7.41	6.69	4.09	10.18
	D4	9.60	9.22	8.50	5.88	12.08
	E4	11.70	11.36	10.63	8.01	14.28
	F4	14.13	13.83	13.10	10.46	16.79
	G4	16.90	16.62	15.89	13.24	19.60
	H4	31.29	31.07	30.34	27.62	34.26
	I4	56.70	56.52	55.79	52.95	60.20
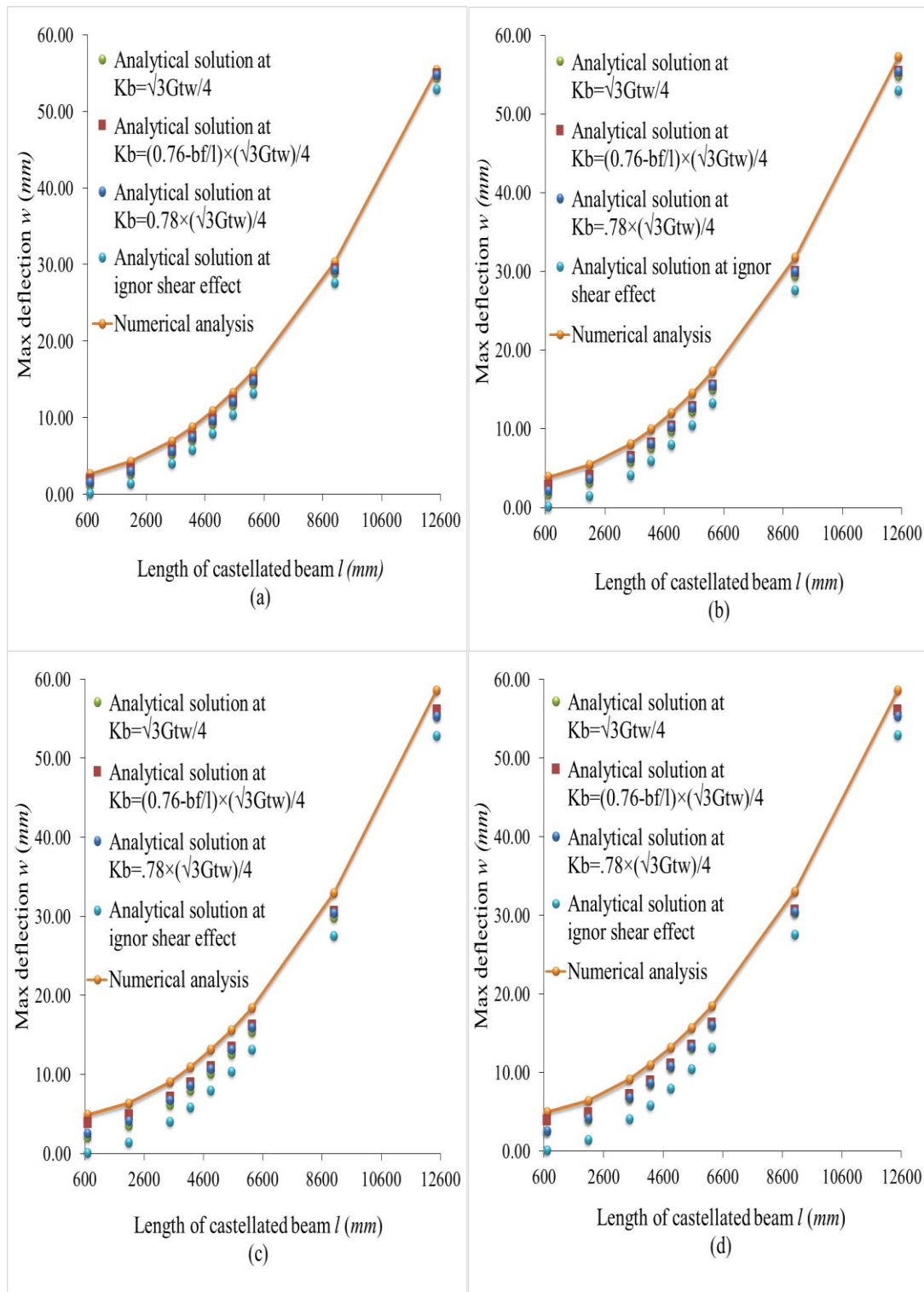
Figure 3-10 Maximum deflections of pinned-fixed castellated beam with a uniformly distributed load between analytical solutions using different shear rigidity factors obtained by Eq. (3-57), including one with zero shear factor obtained by Eq. (3-58) and FEA numerical solution for different beam lengths with various flange widths. (a) $bf = 100$mm, (b) $bf = 150$mm, (c) $bf = 200$mm and (d) $bf = 250$mm. ($h_w = 300$mm, $t_f = 10$mm, $t_w = 8$mm and $a = 100$mm)

Table 3-5 The relative errors of maximum deflections of pinned-fixed castellated beam with a uniformly distributed load obtained based on the finite element numerical solutions

b_f mm	Name of beam	T1	T2	T3	T4
100	B1	0.24	0.30	0.38	0.66
	C1	0.17	0.19	0.24	0.42
	D1	0.14	0.15	0.19	0.33
	E1	0.11	0.12	0.15	0.27
	F1	0.09	0.09	0.12	0.22
	G1	0.07	0.07	0.10	0.18
	H1	0.03	0.03	0.04	0.09
	I1	0.01	0.01	0.02	0.05
150	B2	0.24	0.33	0.41	0.73
	C2	0.20	0.22	0.28	0.49
	D2	0.17	0.19	0.23	0.41
	E2	0.14	0.15	0.19	0.34
	F2	0.12	0.13	0.16	0.28
	G2	0.10	0.11	0.13	0.23
	H2	0.06	0.06	0.07	0.13
	I2	0.03	0.03	0.04	0.07
200	B3	0.24	0.35	0.44	0.77
	C3	0.22	0.25	0.32	0.55
	D3	0.19	0.21	0.27	0.47
	E3	0.16	0.18	0.23	0.39
	F3	0.14	0.15	0.19	0.33
	G3	0.12	0.13	0.16	0.28
	H3	0.07	0.08	0.10	0.16
	I3	0.04	0.06	0.06	0.10
250	B4	0.23	0.37	0.46	0.80
	C4	0.23	0.27	0.34	0.60
	D4	0.21	0.24	0.30	0.51
	E4	0.18	0.20	0.26	0.44
	F4	0.16	0.18	0.22	0.38
	G4	0.14	0.15	0.19	0.32
	H4	0.09	0.09	0.11	0.19
	I4	0.06	0.06	0.07	0.12
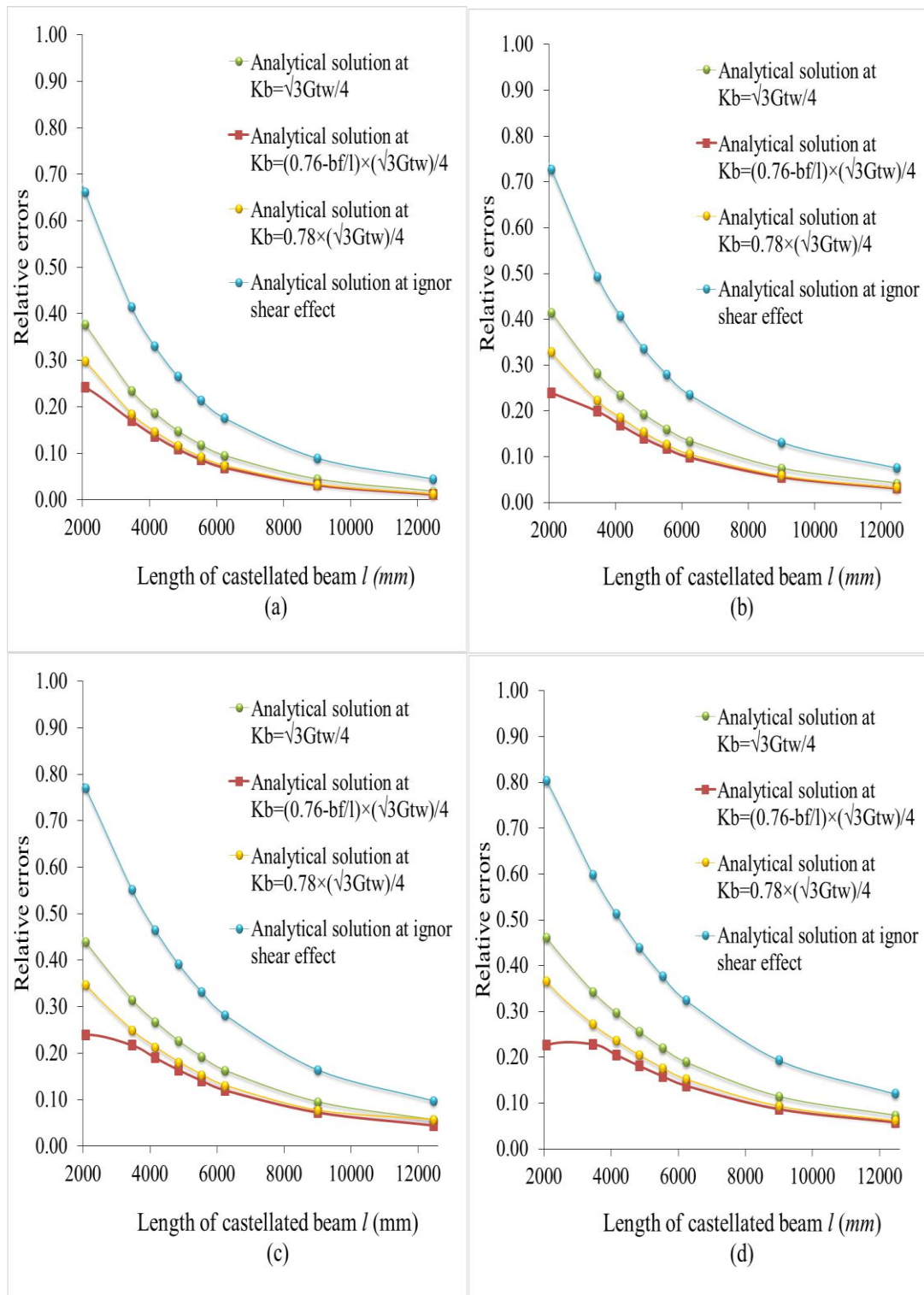
Figure 3-11 Relative errors of maximum deflections of pinned-fixed castellated beam with a uniformly distributed load between analytical solutions using different shear rigidity factors obtained by Eq. (3-57), including one with zero shear factor obtained by Eq. (3-50) and FEA numerical solution for different beam lengths with various flange widths. (a) bf =100mm, (b) bf =150mm, (c) bf =200mm and (d) bf =250mm. (h_w=300mm, t_f=10mm, t_w=8mm and a=100mm)

3.3.5.3. Deflection of simply supported castellated beam due to three fire scenarios with a uniformly distributed load

Table (3-6) shows three fire scenarios with defined temperatures and material properties that were applied on castellated beams.

Table 3-6 Temperatures and Young's modulus in two T- sections (E_o is the Young's modulus at ambient temperature) (BSEN1993-1-2:2005)

Parameter	Case 1	Case 2	Case 3
Temperature, T_1	550 ^{o}C	450 ^{o}C	350 ^{o}C
Temperature, T_2	100 ^{o}C	200 ^{o}C	300 ^{o}C
Young's modulus, E_1	$0.5E_o$	$0.6E_o$	$0.7E_o$
Young's modulus, E_2	E_o	$0.9E_o$	$0.8E_o$

Table (3-7) describes the results of maximum deflections of simply supported castellated beams due to the three fire scenarios with a uniformly distributed load for different beam lengths with various flange widths. These results are determined by Eq. (3-74), including one without fire scenarios obtained by Eq. (3-49) based on Eq. (3-28) for various flange widths: (a) bf =100mm, (b) bf =150mm, (c) bf =200mm and (d) bf =250mm. (h_w=300mm, t_f=10mm, t_w=8mm and a=100mm).

Figure 3-12 shows the maximum deflections of simply supported castellated beam due to the three fire scenarios defined in **Table (3-6)** with a uniformly distributed load between analytical solutions obtained by Eq. (3-74), including one without fire scenarios obtained by Eq. (3-49) based on Eq. (3-28) for various flange widths: (a) bf =100mm, (b) bf =150mm, (c) bf =200mm and (d) bf =250mm. (h_w=300mm, t_f=10mm, t_w=8mm and a=100mm).

The figure reflects the shear effect due to web opening on the deformation of the beam in different fire scenarios when subjected to a uniformly distributed load. It can be seen from the figure that, in each group of flange width, the curves of the maximum deflection have a similar variation pattern. However, the maximum deflection of the

three examined cases is different, in spite of the average temperatures of them being the same. The increase in the deflection is directly proportional to the amount of difference in temperatures between the two T-sections. Thus, case one, which has the largest temperature difference, is the worst case

Table 3-7 Comparison of results of maximum deflections of simply supported castellated beam due to three fire scenarios with a uniformly distributed load

b_f mm	Name of beam	Max. deflection (mm) due to			
		(case 1+q_{max})	(case 2+q_{max})	(case 3+q_{max})	(q_{max})
100	C1	15.32	14.20	13.70	12.24
	E1	30.04	27.84	26.85	22.04
	G1	49.65	46.02	44.39	35.13
	H1	103.59	96.02	92.62	71.12
150	C2	15.33	14.20	13.70	13.02
	E2	30.04	27.84	26.85	22.80
	G2	49.67	46.02	44.39	35.87
	H2	103.62	96.02	92.62	71.85
200	C3	15.33	14.21	13.70	13.83
	E3	30.05	27.84	26.85	23.57
	G3	49.68	46.02	44.39	36.63
	H3	103.64	96.03	92.62	72.59
250	C4	15.33	14.21	13.70	14.68
	E4	30.05	27.84	26.85	24.38
	G4	49.68	46.03	44.39	37.40
	H4	103.66	96.03	92.62	73.35
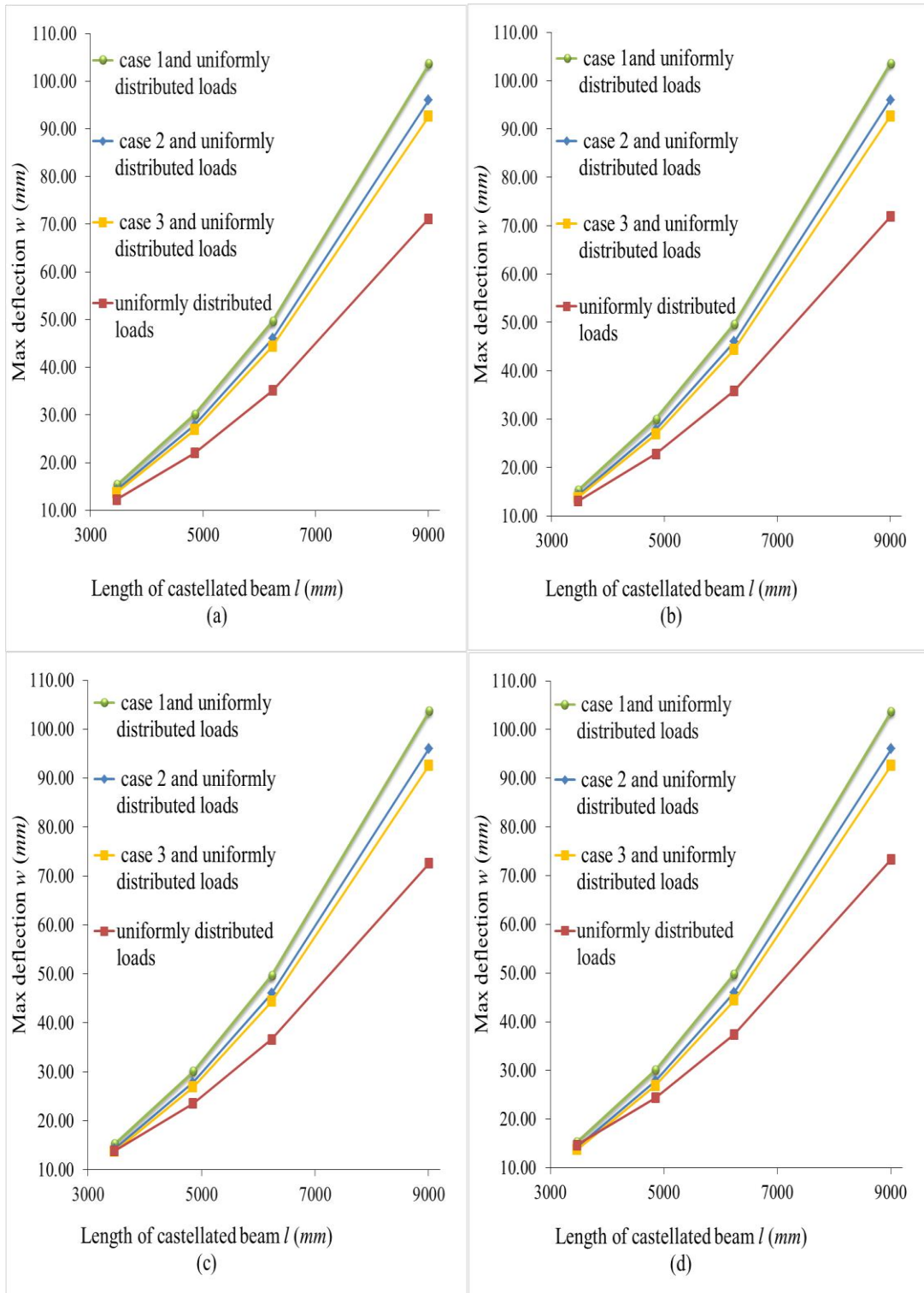
Figure 3-12 Maximum deflections of simply supported castellated beam due to three fire scenarios with a uniformly distributed load between analytical solutions obtained by Eq. (3-74), including one without fire scenarios obtained by Eq. (3-49) for different beam lengths with various flange widths. (a) $bf =100$mm, (b) $bf =150$mm, (c) $bf =200$mm and (d) $bf =250$mm. ($h_w=300$mm, $t_f=10$mm, $t_w=8$mm and $a=100$mm).

3.3.5.4. Deflection of roller-fixed castellated beam due to three fire scenarios with a uniformly distributed

Table (3-8) gives the results of maximum deflections of roller-fixed castellated beams in three different fire scenarios with a uniformly distributed load for different beam lengths with various flange widths. These results are determined by Eq. (3-80), including one without fire scenarios obtained by Eq. (3-57) based on Eq. (3-28) for various flange widths: (a) bf =100mm, (b) bf =150mm, (c) bf =200mm and (d) bf =250mm. (h_w=300mm, t_f=10mm, t_w=8mm and a=100mm).

Figure 3-13 plots the maximum deflections of roller-fixed castellated beams due to the three fire scenarios as given in **Table (3-6),** with a uniformly distributed load, obtained from the analytical solutions presented by Eq. (3-80), including one without fire scenarios obtained by using Eq. (3-57) based on Eq. (3-28) for various flange widths: (a) bf =100mm, (b) bf =150mm, (c) bf =200mm and (d) bf =250mm. (h_w=300mm, t_f=10mm, t_w=8mm and a=100mm).

The figure reflects the shear effect due to web opening on the maximum deflection of castellated beam in different fire scenarios. It can be seen that, in each group of flange width, the curves of the maximum deflection have a similar variation pattern. Moreover, it can be seen that, the maximum deflection of the three examined cases is different, in spite of the average temperatures in them being the same, where the increase in the deflection of the castellated beam is directly proportional to the amount of difference in temperatures between the two T- sections. Thus, case one, which has the largest temperature difference, is the worst case, which reflects that the increase of deflection is influenced by the reduction of Young's modulus.

Table 3-8 Comparison of results of maximum deflections of roller- fixed castellated beam due to three fire scenarios with a uniformly distributed load

b_f mm	Name of beam	Max. deflection (mm) due to			
		(case 1+q_{max})	(case 2+q_{max})	(case 3+q_{max})	(q_{max})
100	C1	8.73	8.27	8.06	5.80
	E1	14.79	13.89	13.48	9.73
	G1	22.89	21.39	20.72	14.97
	H1	45.19	42.06	40.66	29.41
150	C2	9.66	9.20	8.99	6.46
	E2	15.70	14.79	14.38	10.36
	G2	23.79	22.28	21.61	15.60
	H2	46.07	42.93	41.53	30.03
200	C3	10.63	10.17	9.96	7.14
	E3	16.63	15.72	15.31	11.02
	G3	24.70	23.19	22.52	16.24
	H3	46.96	43.82	42.41	30.65
250	C4	11.64	11.17	10.97	7.85
	E4	17.58	16.68	16.27	11.70
	G4	25.63	24.12	23.45	16.90
	H4	47.87	44.72	43.31	31.29
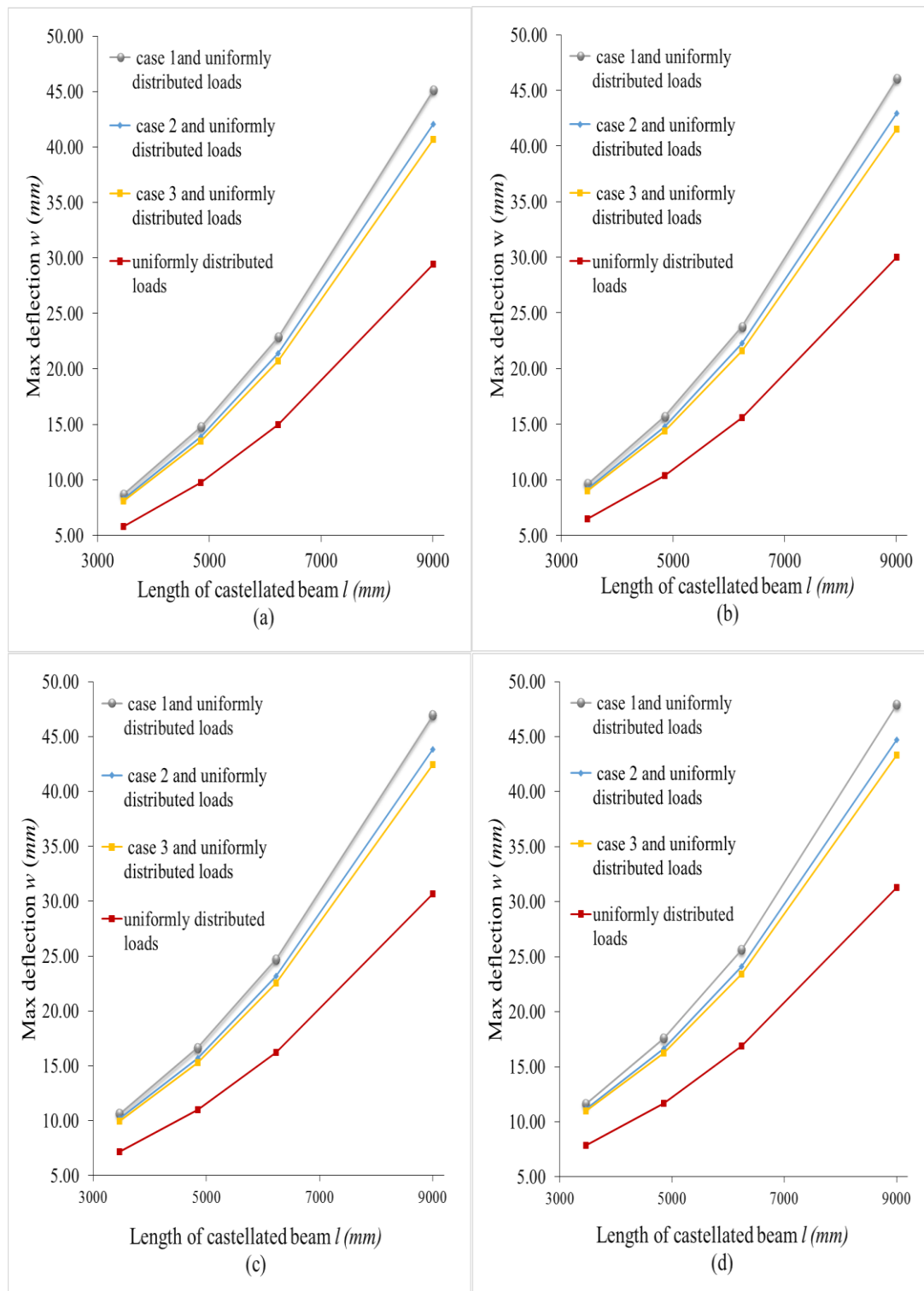
Figure 3-13 Maximum deflections of roller-fixed castellated beam due to three fire scenarios with a uniformly distributed load between analytical solutions obtained by Eq. (3-80), including one without fire scenarios obtained by Eq. (3-57) for different beam lengths with various flange widths. (a) $bf =100$mm, (b) $bf =150$mm, (c) $bf =200$mm and (d) $bf =250$mm. ($h_w=300$mm, $t_f=10$mm, $t_w=8$mm and $a=100$mm).

3.4. Conclusions

In this chapter, a number of equations have been presented for determining the maximum transverse deflection of simply support and pinned–fixed support castellated beams subjected to a uniformly distributed load with/without non-uniform temperature. These equations are derived based on the principle of minimum potential energy. In order to evaluate the analytical results, ANSYS software is used. From these equations and the evaluation, the main conclusions that can be summarized as follows:

➢ The shear-induced deflection caused due to web openings is proportional to the cross-section area of the two T-sections but inversely proportional to the beam length.

➢ The present analytical results are in excellent agreement with those obtained from the finite element analysis, which demonstrates the appropriateness of proposed approach.

➢ Shear effect on the deflection of castellated beams is very important, particularly for short and medium length beams with narrow or wide section. Ignoring the shear effect could lead to an under-estimation of the deflection.

➢ The relative errors between analytical calculation and numerical calculation do not exceed (24%) even for short span castellated beam with narrow or wide section for pinned-fixed.

➢ The effect of web shear on the deflection reduces when castellated beam length increases.

➢ Despite that the numerical solution based on FEA has been widely used in the analysis of castellated beams, it is usually time consuming and limited to specific geometrical dimensions. Thus, a simplified calculation solution that is able to deliver reasonable results but requires less computational effort would be helpful for both researchers and designers.

> ➤ For the same average temperatures, the maximum deflection of the castellated beam under non-uniform temperature distribution with transverse distributed load is directly proportional to the amount of difference in temperatures between the two T- sections of the beam.

CHAPTER FOUR

4. LATERAL-TORSIONAL BUCKLING

4.1. Introduction

In some cases, castellated beams may undergo a lateral-torsional buckling before they reach to their ultimate limit state. Recent evidence explains that due to applying transverse loads on the major axis of the castellated beam, the cross section of the beam is affected by compression and tension stress. Compression stress on the top flange causes the vertical movement of the beam that is in the same direction as the load, which causes lateral moment and thus creating the horizontal movement when the vertical stiffness is bigger than the lateral stiffness. Meanwhile, tension stress that is created on the bottom flange tries to reduce the vertical deflection, which leads to twisting around the major axis when the load exceeds the limit state, as well as causing a torsional moment, in addition to the existing bending moment. The combinations of these effects are prone to produce an instability state called lateral-torsional buckling. Kerdal and Nethercot (1984) indicated that the behaviour of castellated beams is similar to the plain beam but the properties of the cross section should be considered to evaluate the lateral-torsional buckling (see **Figure 4-1**).

This chapter will firstly present the factors affecting the lateral-torsional buckling, and review the current design philosophy that has been adopted for determining the lateral-torsional buckling resistance of I-beams with web openings under bending loads. Secondly, the analytical methods will be presented for elastic critical lateral-torsional buckling loads of castellated beam under a uniformly distributed transverse load on the top flange for two common boundary conditions. The analytical approach will be developed based on the principle of minimum potential energy. Moreover, the linear

FEA numerical computations will be provided for verifying the accuracy of the analytical solutions.
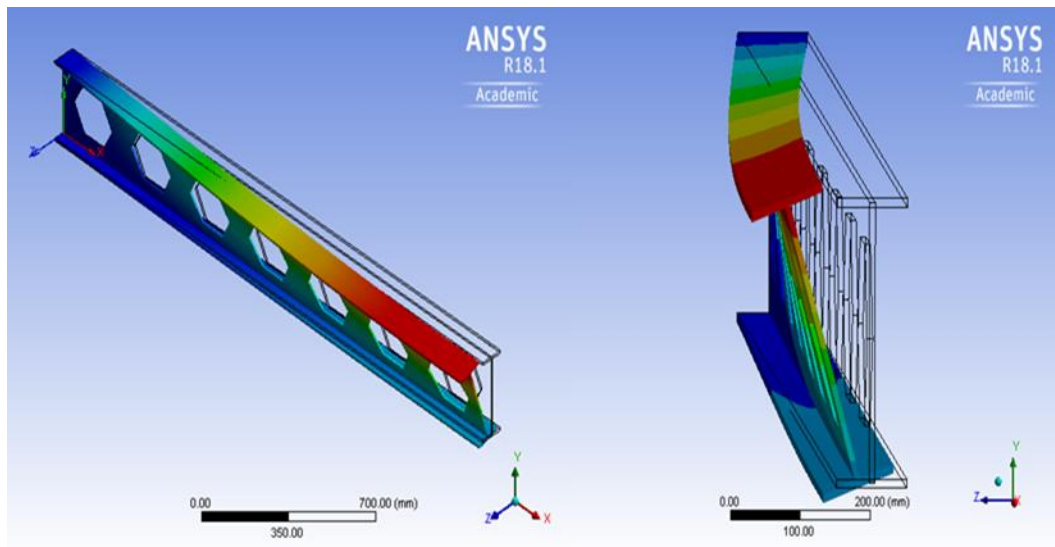
Figure 4-1 The mechanism of Lateral-Torsional Buckling

4.2. Factors influencing lateral-torsional buckling

Numerous experimental, theoretical and numerical investigations have pointed out that some factors have an impact on castellated beam's vulnerability to lateral-torsion buckling (http://www.scirp.org/journal/ojce). The factors include: the distance between the lateral supports to the compression of the flanges; boundary conditions; loading type and position, section type; material properties; magnitude and distribution of the residual stresses and geometric imperfections (Martins et al., 2017).

4.2.1. Effective length (the distance of castellated beam between two laterals supports)

Effective length indicates the distance of castellated beam between two lateral supports; (Korrani et al., 2010) noted that the potential of lateral-torsional buckling occurring is reduced when the effective length is small which leads to prevent the buckling where this occurred because of the instability of compression flange. Therefore, this distance should not exceed the limitations.

4.2.2. Boundary conditions

Actually, the lateral-torsional buckling failure is reduced if the buckling moment is increased which leads to reducing the lateral buckling of the beam, owing to the fact that the lateral buckling consists of three deformation types, namely lateral bending, warping, and twisting, where these deformations are affected by the beam boundary conditions. Hence, the kinds of boundary conditions should be considered to increase the resistance of beam and prevent all these deformations. In BS5950-1:2000 the effective length of beam takes into account the effect of the boundary conditions on lateral-torsional buckling (Sehwail, 2013; Ahnlén. and Westlund, 2013 and New steel construction technical report, 2006).

4.2.3. Loading location

The lateral-torsional buckling is affected by the vertical line extended between the location of applying load and the shear canter of the cross-section of the beam. New steel construction technical report (2006) pointed out that the applying load above the shear centre makes the beam vulnerable to destabilizing load situation, which indicated that the beam is more sensitive to the lateral-torsional buckling failure. On the other hand, the applying load at the shear centre or down leads to decrease the occurrence of this failure which is called non-destabilizing load. The previous research found that applying loading below or above the shear centre can change the load of buckling by ± 40% (Sehwail, 2013).

4.2.4. Loading type

The influence of loading type on the occurrence of a lateral-torsional buckling failure for steel beams is addressed in BS5950-1:2000 by using the equivalent uniform moment factor. The previous researchers pointed out that, where the cross-section is subjected to a uniformly bending moment that is distributed on the length of beam, it resists the buckling less than the same cross section subjected to different bending moment distribution. For this reason, the designers use the equivalent uniform moment factor to modify the design procedure.

4.2.5. Imperfections

Initial imperfections are the lateral displacements and twists along the beam length. The previous investigations stated that these imperfections appear in structural steel sections due to the fabrication process. In addition, the process of loading could be eccentric which urges continuous increase in the lateral deflection and twist at the first stage of loading because the elastic critical moment will be less than yield moment. Unfortunately, another reason for these imperfections occurring, is that the section's properties of beam might change because of distortions and cracks during beam transportation. However, residual stresses may increase because of imperfections (Sehwail, 2013 and Jovi, 2015).

4.2.6. Residual stress

Some previous studies stated that the process of manufacture of steel sections and fabricating castellated beams such as cutting, shifting, and welding could cause a significant lack of beam strength. This phenomenon is called residual stress. It is clear that these stresses can affect physical and mechanical properties of the beams. In other words, the large changes in the temperature during the fabrication process, or erection could affect the residual stresses, and then the section will start to undergo stress at lower moments. Therefore, the yielding will extend through the cross section of the beam concurrently with increased moment. According to the experiments of Sonck et al. (2014), the castellated beams have compressive residual stresses at the flanges more than the original parent does. As a result, ignoring these stresses possibly leads to obtaining unsafe lateral-torsional buckling resistance values (Sehwail, 2013 and Sonck, 2014)

4.2.7. The slenderness

New steel construction technical report (2006) indicates that the slenderness of section is one of the important conditions that should be considered in the steel structural design check for lateral-torsional buckling to provide safe structures. Some of the factors could affect the slenderness of section such as the beam length and the stiffness

of both flange lateral bending and the section torsional. However, the castellated beam is more exposed to the lateral-torsional buckling failure than the I-beam of the same size due to increasing the depth and the web openings.

4.3. Current design philosophy of lateral-torsional buckling resistance of I-beam with web openings

Currently, two basic design philosophies have been adopted for determining the lateral-torsional buckling resistance of I-beam with web openings under bending loads.

The first design philosophy indicates that for I-beam with web openings, the design check of lateral-torsional buckling is decreased to be a lateral flexural buckling check of the compressed T-section at web opening. ArcelorMittal (2008) reports this design philosophy. According to Nseir et al. (2012), this philosophy is conservative because the tension effect of the flange and the stiffness of torsional of the full cross-section are completely ignored.

Nethercot and Kerdal (1982) elicit the other design philosophy. They performed experiments on eight castellated beams and noticed that the lateral-torsional buckling resistance is not affected by the web openings of the beam. Hence the design philosophy of lateral-torsional buckling for I-beam without web openings could be used to the I-beam with web openings, taking into consideration that the properties of the cross-sectional should be calculated at the centre of the castellation.

Now today, the design specifications such as BSEN1993-1-1:2005; BS5950-1:2000; Australian standards AS4100 and American standard AISC provide methods, which are derived, based on the above philosophies, to determine the lateral-torsional buckling resistance for I-beams with web openings. Many articles found in the literature have used this design specification.

4.4. The calculation methods of lateral-torsional buckling resistance of castellated beam

Mohebkhah (2004) developed a nonlinear finite element method for simulating inelastic castellated beams with various loading cases to examine lateral–torsional buckling. The work also discussed the influence of moment gradient on the lateral-torsional buckling of castellated beams. The FEA results of inelastic castellated beams with different slenderness were compared with the results obtained according to the design specifications AISC-LRFD. Mohebkhah reported that the design specifications AISC-LRFD is unsafe because the values of moment gradient factors for inelastic beams provided in AISC are bigger than those determined by nonlinear FEA method.

Zirakian and Showkati (2006) carried out an experimental investigation to examine lateral-distortional buckling mode and discussed the interaction between local buckling and lateral-torsional buckling. In their work, six tests were performed on simply supported castellated beams exposed to a concentrated load. They reported that the interaction of different buckling modes would lead to a distortion of the cross-section of the castellated beam due to lack of strength as assumed during lateral-torsional buckling. The experimental results were compared with the analytical results of the elastic and inelastic lateral buckling loads, which were obtained by applying the South well, modified, and Massey extrapolation techniques to gain more accurate predictions of the critical buckling loads.

Showkati (2008) suggested several empirical formulas to calculate the bending coefficient of unbraced castellated beams. The comparison was made between his results and published data by previous studies. The results show that the elastic-bending capacities of castellated beams, which are subjected to the uniform distributed loads on the top flange, are affected by the section properties.

Kohnehpooshi and Showkati (2009) carried out the numerical investigations using finite element method for the evaluation of the effective flexural and torsional stiffness's, shear and tension effects of castellated beams on the overall failure of the beams when subjected to pure bending. The finite element method was carried out using ANSYS software by using 3-D nonlinear Shell Elements (SHELL181).

Sweedan (2011) utilized ANSYS software for simulating the lateral-torsional buckling of simply supported circular web openings beam. This study applied different cases of loading on simply supported circular web openings beam which associated with wide variety of parameters such as cross-sectional dimensions, lengths of beams and arrangement of web openings to find critical moment values and the moment-gradient factor. According to numerical results, this study reported that the moment-gradient factor is affected by the beam geometry and slenderness. In addition, a simplified approach was proposed to enable accurate determination of a moment modification factor KLB for the cellular beams.

Ellobody (2011) utilized analytical and experimental methods to investigate the interaction of buckling modes in castellated beams. Nonlinear finite element method was utilized to simulate 96 models of the castellated beam by using ABAQUS software. The effects of various characteristics such as cross section dimensions and length of the beam on the failure mechanisms of the castellated beams were examined. It was reported that web distortional buckling occurs on castellated beam because of high strength, but lateral-torsional buckling failure due to the normal strength of castellated beam.

Nseir et al. (2012) used both the experimental and numerical methods to examine the lateral-torsional buckling resistance of circular web opening beams. In addition, they suggested an analytical design method. Three tests were conducted to make a comparison between the experimental and numerical results. Their study used a wide variety of parametric factors, including cross-sectional shape, bending moment distribution, the relative size of the openings, and yield stress.

The design methods provided in the design specifications BS5950-1, 3.1, 4:1985 and 1988 are adopted by Pachpor et al. (2014) to examine the behaviour of circular web opening beams to predict the lateral-torsional buckling resistance.

Panedpojaman (2015) made efforts to calculate the lateral-torsional buckling resistance of I-beams with web openings under a constant bending moment. Two methods, namely General Method and Specific Method, were used. In addition, the section properties for

the calculation were adopted according to Nethercot and Kerdal (1982)'s design principle.

Kim et al. (2016) presented an analytical study with focussing on the web shear effects on the lateral–torsional buckling of simply supported castellated beams liable to pure bending and/or a uniformly distributed load. They performed this study by using the classical principle of minimum potential energy. They also reported that to increase the accuracy of the critical moments' value and loads, the average torsional constant of the full and reduced sections should be considered in calculations, instead of simply taking the average of the critical moments or loads.

Sonck and Belis (2016) presented a nonlinear numerical study to examine the behaviour of the lateral-torsional buckling of doubly symmetric castellated beams subjected to a constant bending moment. For calculations, the study took into account the modified residual stresses and the cross-sectional properties at the centre of the web opening. The calculations for lateral-torsional buckling were based on the design specification BSEN1993-1-1: 2005. The results of the numerical study have been compared with experimental results to assess the effects of geometric imperfections, elastic-plastic material behaviours, and residual stresses.

Kwani and Wijaya (2017) presented a paper to investigate the lateral-torsional buckling of castellated beams. AISC specifications have no equation to determine the critical moment for lateral-torsional buckling for design purposes of castellated beams. Therefore, they adopted the collapse analysis by using finite element method to modify the correction factor of AISC formula for determining the critical moment of the castellated beam.

4.5. Analytical philosophy of lateral-torsional buckling of castellated Beam

The condition of changing the beam from straight stability state to lateral deflection and twist state occurs at the critical loads. A calculation method of elastic critical loads of castellated beams when the beam has a lateral–torsional buckling is presented in this chapter. The method is derived based on the principle of the total potential energy.

According to the model illustrated in, **Figure 4-2 (a)** the beam shear centre will have lateral and transverse displacements, respectively $v(x)$, $w(x)$. Furthermore, the cross-section has an angle of twist $\phi(x)$. In the linear situation, the strain energy stored in the beam involves two parts; the energy caused by the deflection and the energy caused by the twist, which can be written as follows:

$$U_s = \frac{1}{2} \int_0^1 \left[EI_y \left(\frac{d^2w}{dx^2} \right)^2 + EI_z \left(\frac{d^2v}{dx^2} \right)^2 + EI_w \left(\frac{d^2\phi}{dx^2} \right)^2 + GJ \left(\frac{d\phi}{dx} \right)^2 \right] dx \qquad 4\text{-}1$$

where U_s is the strain energy, l is the beam length, E is the Young's modulus, G is the shear modulus and J is the torsional constant; I_y and I_z are the second moments of the cross-sectional area about the y and z axes respectively, I_w is the warping constant. Because of web openings I_y , I_z, I_w and J are introduced as a function of x.

In order to consider the web shear influence to determine the elastic critical lateral-torsional buckling loads in castellated beams, it is assumed that the cross-section of the castellated beam is decomposed into three parts, two of which represent the top T-section and bottom T-section, one of which represents the middle-part of the web. The analysis model for this study is illustrated in **Figure 4-2 (a)**. The second assumption is that the displacements at the shear centres of the top and bottom tee-sections are small. The third assumption is that the warping constants of the top and bottom T-sections and the mid-part of the web are so small and therefore can be ignored. The displacements of the three parts in the castellated beam can thus be expressed as follows (see **Figure 4-2 (b)**) (Kim. et al., 2016):

$$v_1 = v + \frac{h}{2} sin\phi \approx v + \frac{h\phi}{2} \qquad\qquad 4\text{-}2$$

$$v_2 = v - \frac{h}{2} sin\phi \approx v - \frac{h\phi}{2} \qquad\qquad 4\text{-}3$$

$$w_1 = w + \frac{h}{2} (1 - cos\phi) \approx w \qquad\qquad 4\text{-}4$$

$$w_2 = w + \frac{h}{2} (1 - cos\phi) \approx w \qquad\qquad 4\text{-}5$$

where v_1 and v_2 are the lateral displacements of the shear centre of the top and bottom T-section, w_1 and w_2 are the transverse displacements of the shear centre of the top and bottom T-section, (h) is the distance between the shear centres of top and bottom T-sections. Hence, the strain energy of the castellated beam based on the three parts can be written as follows:

$$U_s = \frac{1}{2}\int_0^l \left[EI_{y1}\left(\frac{d^2 w_1}{dx^2}\right)^2 + EI_{z1}\left(\frac{d^2 v_1}{dx^2}\right)^2 + GJ_1\left(\frac{d\phi}{dx}\right)^2 \right] dx$$
$$+ \frac{1}{2}\int_0^l \left[EI_{y2}\left(\frac{d^2 w_2}{dx^2}\right)^2 + EI_{z2}\left(\frac{d^2 v_2}{dx^2}\right)^2 + GJ_2\left(\frac{d\phi}{dx}\right)^2 \right] dx \qquad 4\text{-}6$$
$$+ \frac{1}{2}\int_0^l \left[EI_{y3}\left(\frac{d^2 w_3}{dx^2}\right)^2 + EI_{z3}\left(\frac{d^2 v_3}{dx^2}\right)^2 + GJ_3\left(\frac{d\phi}{dx}\right)^2 \right] dx$$

where $I_{y1} = I_{y2}$ and $I_{z1} = I_{z2}$ are the second moments of the T- sectional area about the y and z axes. $J_1 = J_2$ is the torsional constant of the tee-section, I_{y3} and I_{z3} are the second moments of the cross-sectional area of the mid-part of the web about the y and z axes respectively, and J_3 is the torsional constant of the mid-part of the web.

Hence, the formula of the strain energy of castellated beam (top T- section, bottom T- section and mid-part of the web), which is susceptible to deflection and twist due to uniformly distributed load at the top T- sections, can be obtained by substituting Eqs. (4-2)– (4-5) into Eq. (4-6):

$$U_s = \frac{1}{2}\int_0^l \left[2EI_{y1}\left(\frac{d^2 w_1}{dx^2}\right)^2 + 2EI_{z1}\left(\frac{d^2 v_1}{dx^2}\right)^2 \right.$$
$$+ \frac{h^2}{2}EI_{z1}\left(\frac{d^2 \phi}{dx^2}\right)^2 + 2GJ_1\left(\frac{d\phi}{dx}\right)^2 \Bigg] dx \qquad 4\text{-}7$$
$$+ \frac{1}{2}\int_0^l \left[EI_{y3}\left(\frac{d^2 w_2}{dx^2}\right)^2 + EI_{z3}\left(\frac{d^2 v_2}{dx^2}\right)^2 + GJ_3\left(\frac{d\phi}{dx}\right)^2 \right] dx$$

According to **Figure 4-2 (c)**, I_{y1}, I_{z1} and J_1 are constants, while I_{y3}, I_{z3} and J_3 are depending upon the location of the web openings, therefore they are function of $\textbf{x}$. Hence, from the comparison between Eqs. (4-7) and (4-1), it can be obtained, that:

$$I_y = 2I_{y1} + I_{y3} \qquad\qquad 4\text{-}8$$

$$I_z = 2I_{z1} + I_{z3} \qquad\qquad 4\text{-}9$$

$$I_w = \left(\frac{h}{2}\right)^2 I_z \approx \frac{h^2}{2} I_{z1} \qquad\qquad 4\text{-}10$$

$$J = 2J_1 + J_3 \qquad\qquad 4\text{-}11$$

Note from Eq. (4-10) the warping strain energy cannot be ignored because the displacement compatibility occurs when the two T-sections assemble.

The potential energy, which is the negative value resulting from the applied loads when the lateral-torsional buckling occurs, can be written as follows:

$$W = -\int_0^l \left[M_y \left(\frac{d^2 w}{dx^2}\right) + M_y \phi \left(\frac{d^2 v}{dx^2}\right) + \frac{a_z q_z}{2} \phi^2 \right] dx \qquad\qquad 4\text{-}12$$

where a_z refers to the z-coordinate of the loading point, which is the vertical distance between the loading point and the shear centre of the beam, in this case, $a_z = \frac{h_w}{2} + t_f$ because the uniformly distributed load is applied on the top flange of the beam.

In summary, by using Eqs. (4-7) and (4-12), the equation of the total potential energy of the castellated beam considering lateral-torsional buckling deflection can be expressed as follows:

$$
\begin{aligned}
\Pi = \frac{1}{2}\int_0^l &\left[2EI_{y1}\left(\frac{d^2 w_1}{dx^2}\right)^2 + 2EI_{z1}\left(\frac{d^2 v_1}{dx^2}\right)^2 \right. \\
&\left. + \frac{h^2}{2} EI_{z1}\left(\frac{d^2 \phi}{dx^2}\right)^2 + 2GJ_1\left(\frac{d\phi}{dx}\right)^2 \right] dx \\
&+ \frac{1}{2}\int_0^l \left[EI_{y3}\left(\frac{d^2 w_2}{dx^2}\right)^2 + EI_{z3}\left(\frac{d^2 v_2}{dx^2}\right)^2 + GJ_3\left(\frac{d\phi}{dx}\right)^2 \right] dx \qquad 4\text{-}13 \\
&- \int_0^l \left[M_y\left(\frac{d^2 w}{dx^2}\right) + M_y \phi\left(\frac{d^2 v}{dx^2}\right) + \frac{a_z q_z}{2}\phi^2 \right] dx
\end{aligned}
$$

Figure 4-2 (a) Notations used in castellated beams. **(b)** Loading and displacements of web and displacement of flanges when lateral–torsional buckling occurred **(c)** Section properties of middle-part of web in four different regions. $I_{y3} = I_{y3}^*$, $I_{z3} = I_{z3}^*$, $J_3 = J_3^*$ in region 2, in region 4, $I_{y3} = I_{z3} = J_3 = 0$, section properties vary with x in regions 1 and 3.

4.5.1. Determining the elastic critical buckling loads of simply supported, doubly symmetric castellated beam subjected to uniformly distributed loads

The critical moment M_{cr} of a simply supported castellated beam under a uniformly distributed load applied on the top flange of the beam can be obtained from Eq. (4-14) as follows (Kim et al., 2016),

$$M_{cr} = \frac{-\left(\frac{h_w}{2} + t_f\right) + \sqrt{\left(\frac{h_w}{2} + t_f\right)^2 + \left(\frac{\pi^2}{6} + \frac{1}{2}\right)^2 \left[I_w + \frac{G(2J_1 + kJ_3^*)l^2}{\pi^2 E}\right]\frac{1}{(2I_{z1} + kI_{z3}^*)}}}{\left(\frac{1}{3} + \frac{1}{\pi^2}\right)^2} \qquad \text{4-14}$$
$$\times \frac{E(2I_{z1} + kI_{z3}^*)}{l^2}$$

where

$$M_{cr} = \left(\frac{q_z l^2}{8}\right)_{cr} \tag{4-15}$$

I_{z3}^* is negligible because in most of castellated beams $I_{z3}^* << 2I_{z1}$. Thus, Eq. (4-14) can be simplified as (Kim et al., 2016)

$$\left(\frac{q_z l^2}{8}\right)_{cr} = \frac{-\left(\frac{h_w}{2} + t_f\right) + \sqrt{\left(\frac{h_w}{2} + t_f\right)^2 + \left(\frac{\pi^2}{6} + \frac{1}{2}\right)^2 \left[\frac{I_w}{2I_{z1}} + \frac{G(2J_1 + kJ_3^*)l^2}{2I_{z1}\pi^2 E}\right]}}{\left(\frac{1}{3} + \frac{1}{\pi^2}\right)^2} \times \frac{2I_{z1}E}{l^2} \tag{4-16}$$

$$(q_z)_{cr} = \frac{-\left(\frac{h_w}{2} + t_f\right) + \sqrt{\left(\frac{h_w}{2} + t_f\right)^2 + \left(\frac{\pi^2}{6} + \frac{1}{2}\right)^2 \left[\frac{I_w}{2I_{z1}} + \frac{G\left(2J_1 + kJ_3^*\right)l^2}{2I_{z1}\pi^2 E}\right]}}{\left(\frac{1}{3} + \frac{1}{\pi^2}\right)^2}$$
$$\times \frac{16I_{z1}E}{l^4} \tag{4-17}$$

4.5.2. Determining the elastic critical buckling loads of pinned-fixed castellated beam, doubly symmetric castellated beam subjected to uniformly distributed loads

The buckling displacements of a pinned-fixed castellated beam can be assumed as follows:

$$w(x) = A \sin\left(\frac{k\pi(l - x)}{l}\right) \sin\left(\frac{\pi(l - x)}{2l}\right) \tag{4-18}$$

$$v(x) = B \sin\left(\frac{k\pi(l - x)}{l}\right) \sin\left(\frac{\pi(l - x)}{2l}\right) \tag{4-19}$$

$$\phi(x) = C \sin\left(\frac{k\pi(l - x)}{l}\right) \sin\left(\frac{\pi(l - x)}{2l}\right) \tag{4-20}$$

where A, B, and C are the constants to be determined. It is obvious that the above displacements functions satisfy the boundary conditions, that are $w = v = \phi = \frac{d^2w}{dx^2} = \frac{d^2v}{dx^2} = \frac{d^2\phi}{dx^2} = 0$ at $x = o$ and $w = v = \phi = \frac{dw}{dx} = \frac{dv}{dx} = \frac{d\phi}{dx} = 0$ at $x = l$.

Substituting Eqs. (4-18), (4-19) and (4-20) into Eq. (4-7) yields

$$U_s = \frac{41}{128} \frac{\pi^4}{l^3} \left[E\left(2I_{y1} + kI^*_{y3}\right)A^2 + E\left(2I_{z1} + kI^*_{z3}\right)B^2 + EI_w C^2 \right.$$
$$\left. + \frac{16}{41}\left(1 + \frac{1}{\pi^2}\right) G\left(2J_1 + kJ^*_3\right)\left(\frac{l}{\pi}\right)^2 C^2 \right]$$

4-21

According to Kim.et al. (2016) k refers to the fraction of the volume of the solid and holes in the mid-part of the web beam. For most castellated beams, because of matching of the solid areas and holes in the mid-part of the web have equal area this leads to the value of $k=0.5$.

The internal bending moment for a pinned-fixed castellated beam subject to a uniformly distributed load can be written as follows:

$$M_y(x) = \frac{3}{8} q_z l x - \frac{1}{2} q_z x^2$$

4-22

Substituting Eq. (4-22) into Eq. (4-12) yields an expression for the potential energy of the external loads as:

$$W = \frac{4lq_z}{3\pi} A + \frac{q_z \pi^2 l}{20}\left(\frac{1}{3} + \frac{1}{\pi^2}\right) BC - \frac{a_z l q_z}{8} C^2$$

4-23

Combining Eqs. (4-21) and (4-23) yields an expression for the total potential energy:

$$\Pi = \frac{41}{128} \frac{\pi^4}{l^3} \left[E\left(2I_{y1} + kI^*_{y3}\right)A^2 + E\left(2I_{z1} + kI^*_{z3}\right)B^2 + EI_w C^2 \right.$$
$$\left. + \frac{16}{41}\left(1 + \frac{1}{\pi^2}\right) G\left(2J_1 + kJ^*_3\right)\left(\frac{l}{\pi}\right)^2 C^2 \right] + \frac{4lq_z}{3\pi} A$$
$$+ \frac{q_z \pi^2 l}{20}\left(\frac{1}{3} + \frac{1}{\pi^2}\right) BC - \frac{a_z l q_z}{8} C^2$$

4-24

The variation of Eq. (4-24) with respect to A, B and C results in the following three algebraic equations:

$$\frac{41l}{128}\left(\frac{\pi}{l}\right)^4 \left[2E\left(2I_{y1} + kI^*_{y3}\right)A\right] + \frac{4lq_z}{3\pi} = 0$$

4-25

$$\frac{41l}{128}\left(\frac{\pi}{l}\right)^4 \left[2E\left(2I_{z1} + kI^*_{z3}\right)B\right] = -\frac{q_z \pi^2 l}{20}\left(\frac{1}{3} + \frac{1}{\pi^2}\right) C$$

4-26

$$\frac{41l}{128}\left(\frac{\pi}{l}\right)^4\left[2EI_wC + \frac{16}{41}\left(1+\frac{1}{\pi^2}\right)2G(2J_1 + kJ_3^*)\left(\frac{l}{\pi}\right)^2 C\right]$$
$$= \frac{a_z l q_z}{4}C - \frac{q_z\pi^2 l}{20}\left(\frac{1}{3}+\frac{1}{\pi^2}\right)B$$

4-27

The second-order variation of the total potential energy equation, with respect to *A, B* and *C* should be equal to zero, from which the critical moment/load is obtained

$$\delta^2\prod = \delta^2(U_s + W) = 0$$

4-28

Eq. (4-28) leads to:

$$A = 0$$

4-29

$$E(2I_{z1} + kI_{z3}^*)\left(\frac{\pi}{l}\right)^2 B = \frac{8q_z l^2}{20}\left(\frac{1}{3}+\frac{1}{\pi^2}\right)C$$

4-30

$$\left[\left(\frac{\pi}{l}\right)^2\left(\frac{41}{8}\right)^2 EI_w + G(2J_1 + kJ_3^*)\right]C = \frac{8q_z l^2}{20}\left(\frac{1}{3}+\frac{1}{\pi^2}\right)B + \frac{41a_z l^2 q_z}{4\pi^2}C$$

4-31

Eliminating B in Eqs. (4-30) and (4-31), it yields

$$\left[\frac{8q_z l^2}{20}\left(\frac{1}{3}+\frac{1}{\pi^2}\right)\right]^2 + \frac{41a_z l^2 q_z}{4\pi^2}\left(E(2I_{z1} + kI_{z3}^*)\left(\frac{\pi}{l}\right)^2\right)$$
$$= \left[\left(\frac{\pi}{l}\right)^2\left(\frac{41}{8}\right)^2 EI_w + G(2J_1 + kJ_3^*)\right]\left(E(2I_{z1} + kI_{z3}^*)\left(\frac{\pi}{l}\right)^2\right)$$

4-32

Solving for q_z from Eq. (4-32), it yields

$$\left(\frac{q_z l^2}{8}\right)_{cr} = \frac{-\left(\frac{h_w}{2}+t_f\right)+\sqrt{\left(\frac{h_w}{2}+t_f\right)^2 + \frac{64\pi^2}{20}\left(\frac{1}{\pi^2}+\frac{1}{3}\right)^2\left[\frac{I_w}{64}+\frac{G(2J_1+kJ_3^*)l^2}{41^2\pi^2 E}\right]\frac{1}{(2I_{z1}+kI_{z3}^*)}}}{\frac{64\pi^2}{20}\left(\frac{1}{\pi^2}+\frac{1}{3}\right)^2} \times \frac{41E(2I_{z1}+kI_{z3}^*)}{l^2}$$

4-33

Again, if I_{z3}^* is neglected, Eq. (4-33) can be simplified as follows: (Kim et al., 2016)

$$\left(\frac{q_z l^2}{8}\right)_{cr} = \frac{-\left(\frac{h_w}{2}+t_f\right)+\sqrt{\left(\frac{h_w}{2}+t_f\right)^2 + \frac{64\pi^2}{20}\left(\frac{1}{\pi^2}+\frac{1}{3}\right)^2 \left[\frac{I_w}{64}+\frac{G(2J_1+kJ_3^*)l^2}{41^2\pi^2 E}\right]\frac{1}{(2I_{z1})}}}{\frac{64\pi^2}{20}\left(\frac{1}{\pi^2}+\frac{1}{3}\right)^2} \qquad \text{4-34}$$
$$\times \frac{41E(2I_{z1})}{l^2}$$

$$(q_z)_{cr} = \frac{-\left(\frac{h_w}{2}+t_f\right)+\sqrt{\left(\frac{h_w}{2}+t_f\right)^2 + \frac{64\pi^2}{20}\left(\frac{1}{\pi^2}+\frac{1}{3}\right)^2 \left[\frac{I_w}{64}+\frac{G(2J_1+kJ_3^*)l^2}{41^2\pi^2 E}\right]\frac{1}{(2I_{z1})}}}{\frac{64\pi^2}{20}\left(\frac{1}{\pi^2}+\frac{1}{3}\right)^2} \qquad \text{4-35}$$
$$\times \frac{328E(2I_{z1})}{l^4}$$

4.6. Numerical analysis lateral-torsional buckling of castellated beams due to uniformly distributed load

The main objective herein is to validate the equations of analytical solutions developed in sec 4.6 for calculating critical moment of lateral-torsional buckling of castellated beams subjected to uniformly distributed load on top flange. A linear 3D finite element analysis is carried out by employing ANSYS mechanical (APDL) software for conducting Eigenvalue analysis to determine the critical moment

4.6.1. Modelling consideration, material model and loading

The FEA modelling of castellated beams is done by using 3D linear 4-Node Thin Shell Elements (SHELL181) depicted in **Figure 3-5**, which is suitable for linear and large rotation. This element presents four nodes with six DOF per node, i.e., translations and rotations on the X, Y, and Z-axis, respectively. The beams are meshed using element sizes not exceeding 10 mm**.** A typical mesh configuration is shown in **Figure 3-6**. The mechanical properties used are the elastic material with Young's modulus E = 2.1×10^5 MPa, Poisson's ratio v =0.3, and yield stress σ_y=275 MPa.

The external load is the uniformly distributed load ($q_{max} = 16\frac{\sigma_y I_{reduced}}{l^2(h_w+2t_f)}$) acting on the junction of the upper flange and web. (see **Figure 3-7**)

4.6.2. Boundary conditions

4.6.2.1. Simply supported castellated beam

The displacement boundary conditions are applied to all nodes at the two ends of the beam, as shown in **Figure 3-7**. The lateral and transverse deflections and rotation are restrained ($u_y=u_z=0$, and $\theta_x=0$) at two ends of the simply supported beam. Moreover, another boundary condition is applied by restricting the axial displacement ($u_x=0$) at one node of one end of the simply supported beam.

4.6.2.2. Pinned-fixed castellated beam

The displacement boundary conditions are also applied to all nodes at the two ends of the beam, as shown in **Figure 3-7**. The lateral and transverse deflections and rotation are restrained ($u_y=u_z=0$ and $\theta_x=0$) at the simply supported end, while the fixed support boundary condition is applied at the other end by restricting the axial displacement, transverse deflections and rotations around the three axes within the cross-section ($u_x=u_y=u_z=0$ and $\theta_x=\theta_y=\theta_z=0$).

4.6.3. Comparison of results and discussion

4.6.3.1. Linear lateral-torsional buckling stress results of simply supported due to uniformly distributed load act on top flange

Table (4-1) shows a comparison of the critical loads of lateral-torsional buckling of simply support castellated beam subjected to the uniformly distributed transverse load applying on its top flange between analytical solution and numerical analysis. The analytical solution was obtained directly from Eqs. (4-16) and (4-17), whereas the numerical result was obtained by using linear buckling analysis built in ANSYS software (APDL)**.** The yield moment was calculated by using $M_{yield} = \frac{2\sigma_y I_{reduced}}{h_w+2t_f}$ with $\sigma_y = 275 \frac{N}{mm^2}$ and $I_{reduced}$ was calculated using Eq. (3-17). The results of different castellated beam lengths with various flange widths (see Section 3.3.4) shown in **Table (4-1)** are also plotted in **Figures 4-3, 4-4** and **4-5**, respectively

It can be seen from the figures that, in each group of flange width, the curves of the analytical solution and numerical analysis have a similar variation pattern. The analytical solution is in excellent agreement with the numerical analysis. This indicates that the analytical model developed above for the castellated beam is appropriate for calculating the critical load of lateral-torsional buckling. Moreover, the latter reflects the influence of ignoring the value of the second moment of the cross-sectional area of the mid-part of the web about the z-axis (I_{z3}^*) , and taking account the torsional constant of the cross-sectional area of the mid-part of the web, this is comparable to that of the two T- sections (kJ_3^*) (Kim et al., 2016).

Table 4-1 Comparison of results linear critical lateral-torsional buckling load (q_{cr}, $\mathrm{M_{cr}}$) of simply supported castellated beams with a uniformly distributed act on top flange

b_f mm	Name of beam	Myield N.mm x10⁷	Linear buckling Analytical analysis			Linear buckling Numerical analysis (Ansys)		
			qcr N/mm	Mcr N.mm x10⁷	$\dfrac{\mathrm{Mcr}}{\mathrm{Myield}}$	qcr N/mm	Mcr N.mm x10⁷	$\dfrac{\mathrm{Mcr}}{\mathrm{Myield}}$
100	C1	10.44	35.50	5.33	0.51	34.54	5.18	0.50
	E1	10.44	12.23	3.59	0.34	12.10	3.56	0.34
	G1	10.44	5.68	2.76	0.26	5.40	2.63	0.25
	H1	10.44	1.90	1.93	0.18	1.88	1.90	0.18
	I1	10.44	0.73	1.41	0.14	0.72	1.41	0.13
	J1	10.44	0.45	1.20	0.11	0.45	1.18	0.11
150	C2	14.57	91.28	13.69	0.94	90.56	13.58	0.93
	E2	14.57	28.44	8.36	0.57	28.29	8.32	0.57
	G2	14.57	12.64	6.14	0.42	12.74	6.19	0.42
	H2	14.57	3.99	4.05	0.28	3.86	3.92	0.27
	I2	14.57	1.51	2.94	0.20	1.58	3.07	0.21
	J2	14.57	0.96	2.53	0.17	0.96	2.53	0.17
200	C3	18.70	192.00	28.80	1.54	185.71	27.86	1.49
	E3	18.70	57.11	16.79	0.90	56.04	16.47	0.88
	G3	18.70	23.97	11.65	0.62	23.67	11.51	0.62
	H3	18.70	7.18	7.28	0.39	7.04	7.14	0.38
	I3	18.70	2.61	5.07	0.27	2.61	5.07	0.27
	J3	18.70	1.64	4.33	0.23	1.61	4.26	0.23
250	C4	22.83	356.67	53.50	2.34	317.97	47.70	2.09
	E4	22.83	101.70	29.90	1.31	100.22	29.46	1.29
	G4	22.83	41.15	20.00	0.88	40.79	19.82	0.87
	H4	22.83	11.70	11.86	0.52	11.59	11.76	0.51
	I4	22.83	4.09	79.61	0.35	4.10	7.98	0.35
	J4	22.83	2.53	67.06	0.29	2.51	6.64	0.29
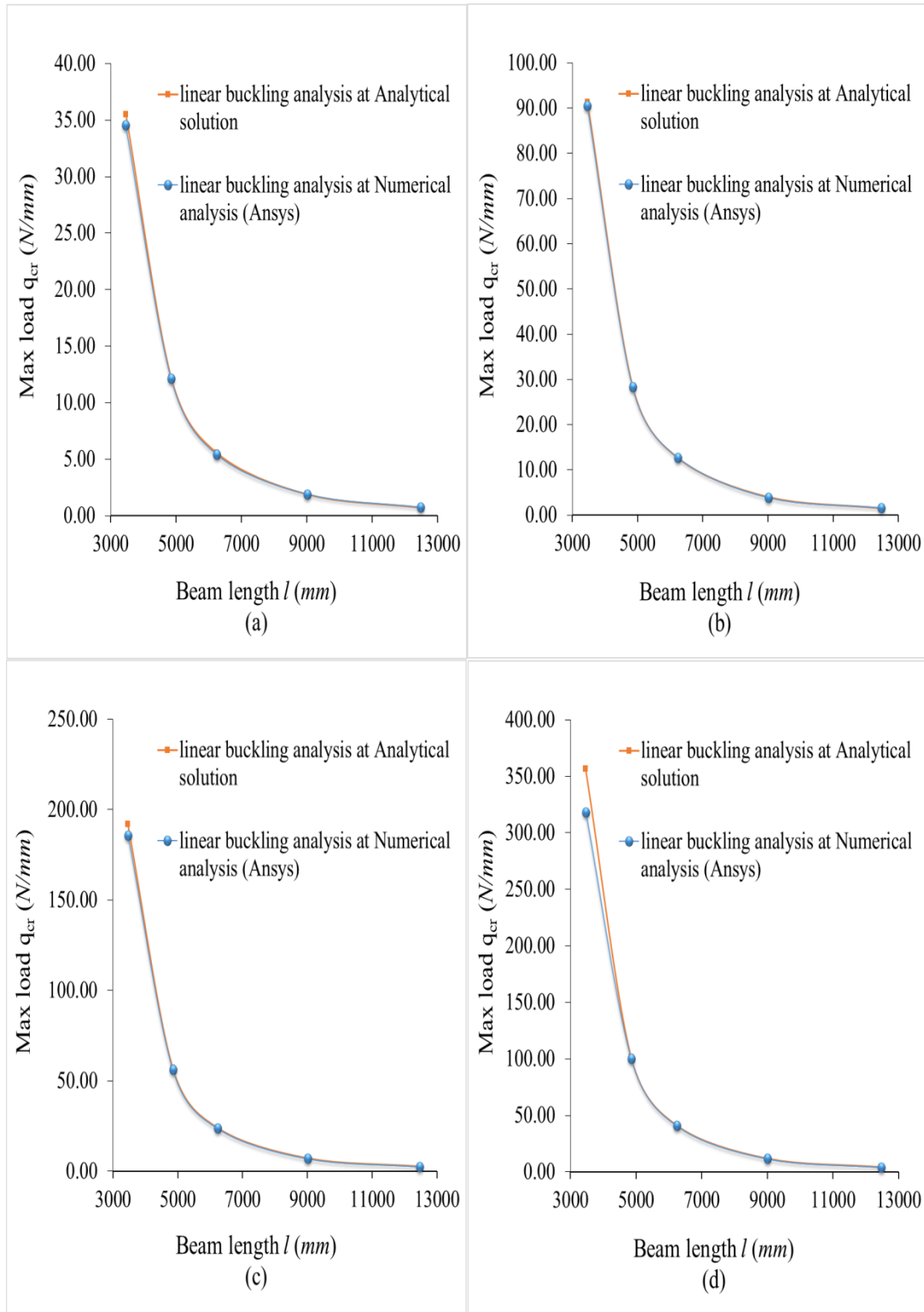
Figure 4-3 Critical elastic lateral-torsional buckling load (q_{cr}) of simply supported castellated beam subjected to a uniformly distributed load between analytical solutions and FEA numerical solution for different beam lengths with various flange widths (a) bf =100mm, (b) bf=150mm, (c) bf=200mm and (d) bf =250mm (h_w=300mm, t_f=10mm, t_w=8mm and a=100mm)
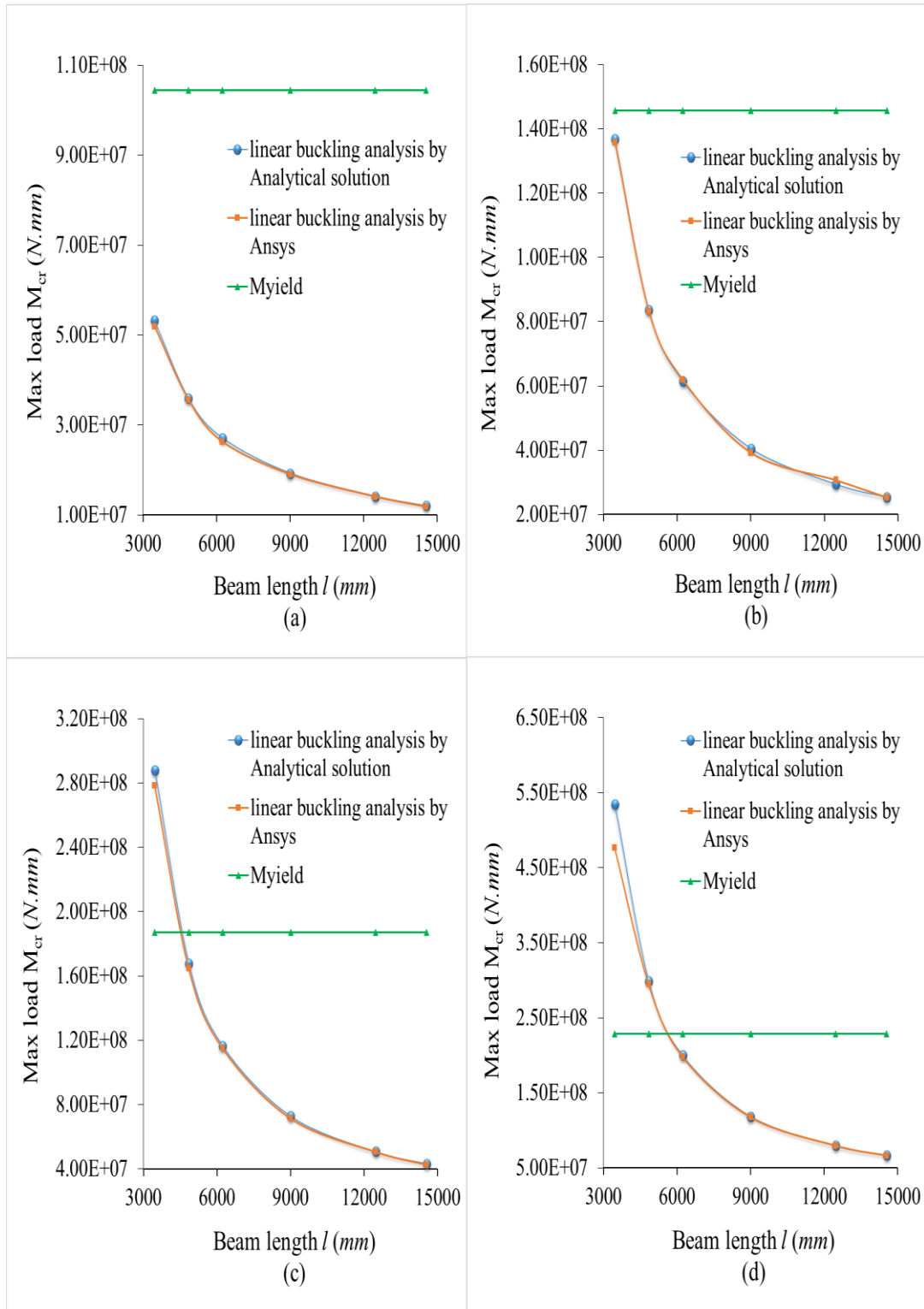
Figure 4-4 Critical elastic lateral-torsional buckling moment (M_{cr}) of simply supported castellated beam subjected to a uniformly distributed load between analytical solutions and FEA numerical solution for different beam lengths with various flange widths (a) bf =100mm, (b) bf=150mm, (c) bf=200mm and (d) bf =250mm (h_w=300mm, t_f=10mm, t_w=8mm and a=100mm)
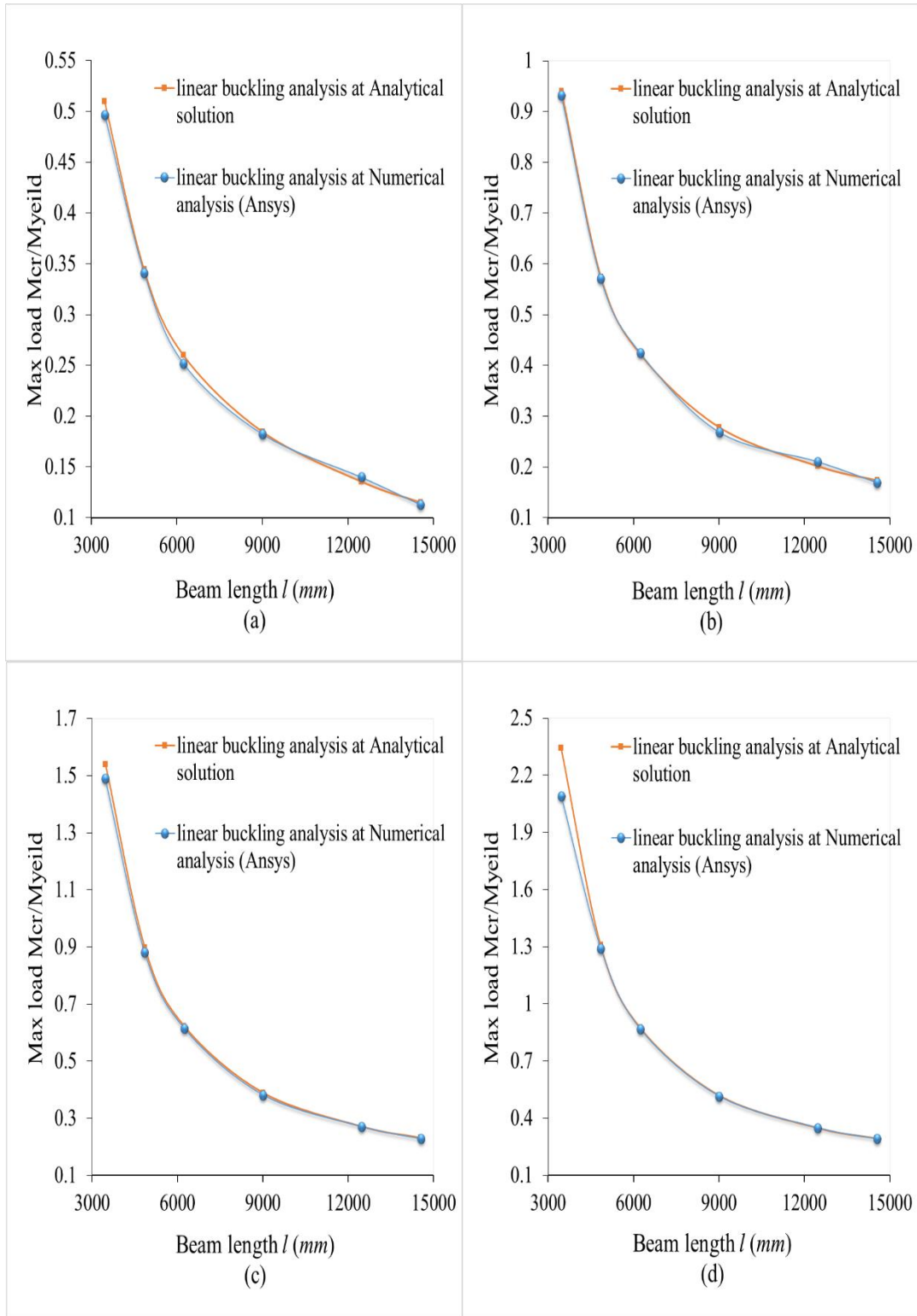
Figure 4-5 Critical elastic lateral-torsional buckling moment (M_{cr}/M_{yield}) of simply supported castellated beam subjected to a uniformly distributed load between analytical solutions and FEA numerical solution for different beam lengths with various flange widths (a) *bf* =100mm, (b) *bf*=150mm, (c) *bf*=200mm and (d) *bf* =250mm (h_w=*300mm, t_f*=10mm, *t_w*=8mm and *a*=100mm)

4.6.3.2. Linear lateral-torsional buckling stress results of pinned-fixed castellated beam due to uniformly distributed load act on top flange

Table (4-2) shows a comparison of the critical loads of lateral-torsional buckling of pinned-fixed castellated beams subjected to a uniformly distributed transverse load applying on its top flange between analytical solution and numerical analysis. The analytical solution was obtained directly from Eqs. (4-34) and (4-35), whereas the numerical result was obtained by using linear buckling analysis built in ANSYS software (APDL). The yield moment was calculated by using $M_{yield} = \frac{2\sigma_y I_{reduced}}{h_w + 2t_f}$ with $\sigma_y = 275 \frac{N}{mm^2}$ and $I_{reduced}$ was calculated using Eq. (3-17). The results of different castellated beam lengths with various flange widths (see Section 3.3.4) shown in **Table (4-2)** are also plotted in **Figures 4-6**, **4-7** and **4-8**, respectively

It can be seen from the figures that, in each group of flange width, the curves of the analytical solution and numerical analysis have a similar variation pattern. The analytical solution is in very good agreement with the numerical analysis for beams longer than 4.8 m. This indicates that the analytical model developed here for the castellated beam is appropriate for calculating the critical load of lateral-torsional buckling. In the case that the beam is shorter, the critical load obtained from the analytical solution is found to be larger than that obtained from the numerical analysis. This is because the critical mode of buckling for the shorter beam is not dominated by the lateral-torsional buckling. This is demonstrated by the critical buckling mode shown in **Figure 4-9** which was obtained from the numerical analysis for the beam of length (l = 3.5 m) and flange width (b_f = 200 mm). It is obvious that the critical buckling mode of this short beam not only involves the lateral-torsional buckling mode but also contains the modes of local buckling of compressed flange and shear buckling of web. The latter disappears with the increase of the beam length or the decreases of beam flanges (Kerdal and Nethercot, 1984). In the case that the beam is shorter (l < 3.5 m) and its flanges are wider (b_f=250mm), the critical buckling mode is no longer controlled by the lateral-torsional buckling and thus the difference between the analytical solution and numerical analysis becomes large (Ellobody, 2011).

Table 4-2 Comparison of results linear critical lateral-torsional buckling load (q_{cr}, M_{cr}) of pinned-fixed castellated beams with a uniformly distributed act on top flange

b_f mm	Name of beam	Myield N.mm x10^7	Linear buckling Analytical analysis			Linear buckling Numerical analysis (Ansys)		
			qcr N/mm	Mcr N.mm x10^7	$\frac{Mcr}{Myield}$	qcr N/mm	Mcr N.mm x10^7	$\frac{Mcr}{Myield}$
100	C1	10.44	80.43	12.06	1.16	79.31	11.90	1.14
	E1	10.44	25.79	7.58	0.73	26.02	7.65	0.73
	G1	10.44	11.55	5.61	0.54	11.78	5.73	0.55
	H1	10.44	3.80	3.89	0.40	4.12	4.17	0.41
	I1	10.44	1.49	2.89	0.28	1.59	3.13	0.30
	J1	10.44	0.92	2.43	0.23	0.91	2.40	0.23
150	C2	14.57	232.88	34.93	2.40	207.30	31.09	2.13
	E2	14.57	68.16	20.03	1.38	66.07	19.42	1.33
	G2	14.57	28.40	13.80	0.95	28.31	13.76	0.94
	H2	14.57	8.47	8.60	0.59	8.84	8.96	0.62
	I2	14.57	3.10	6.01	0.41	3.15	6.12	0.42
	J2	14.57	1.94	5.15	0.35	1.94	5.13	0.35
200	C3	18.70	523.73	78.55	4.20	372.75	55.91	3.00
	E3	18.70	146.39	43.04	2.30	134.80	39.63	2.12
	G3	18.70	58.30	28.33	1.52	56.53	27.48	1.47
	H3	18.70	16.17	16.39	0.88	16.57	16.80	0.90
	I3	18.70	5.58	10.84	0.58	5.60	10.88	0.58
	J3	18.70	3.44	9.10	0.49	3.43	9.07	0.48
250	C4	22.83	1000.72	150.11	6.57	391.17	58.67	2.60
	E4	22.83	272.99	80.25	3.52	230.52	67.77	2.97
	G4	22.83	105.84	51.44	2.25	101.64	49.40	2.16
	H4	22.83	27.89	28.27	1.24	28.11	28.51	1.25
	I4	22.83	9.16	17.80	0.78	9.12	17.73	0.78
	J4	22.83	5.53	14.63	0.64	5.75	15.21	0.67
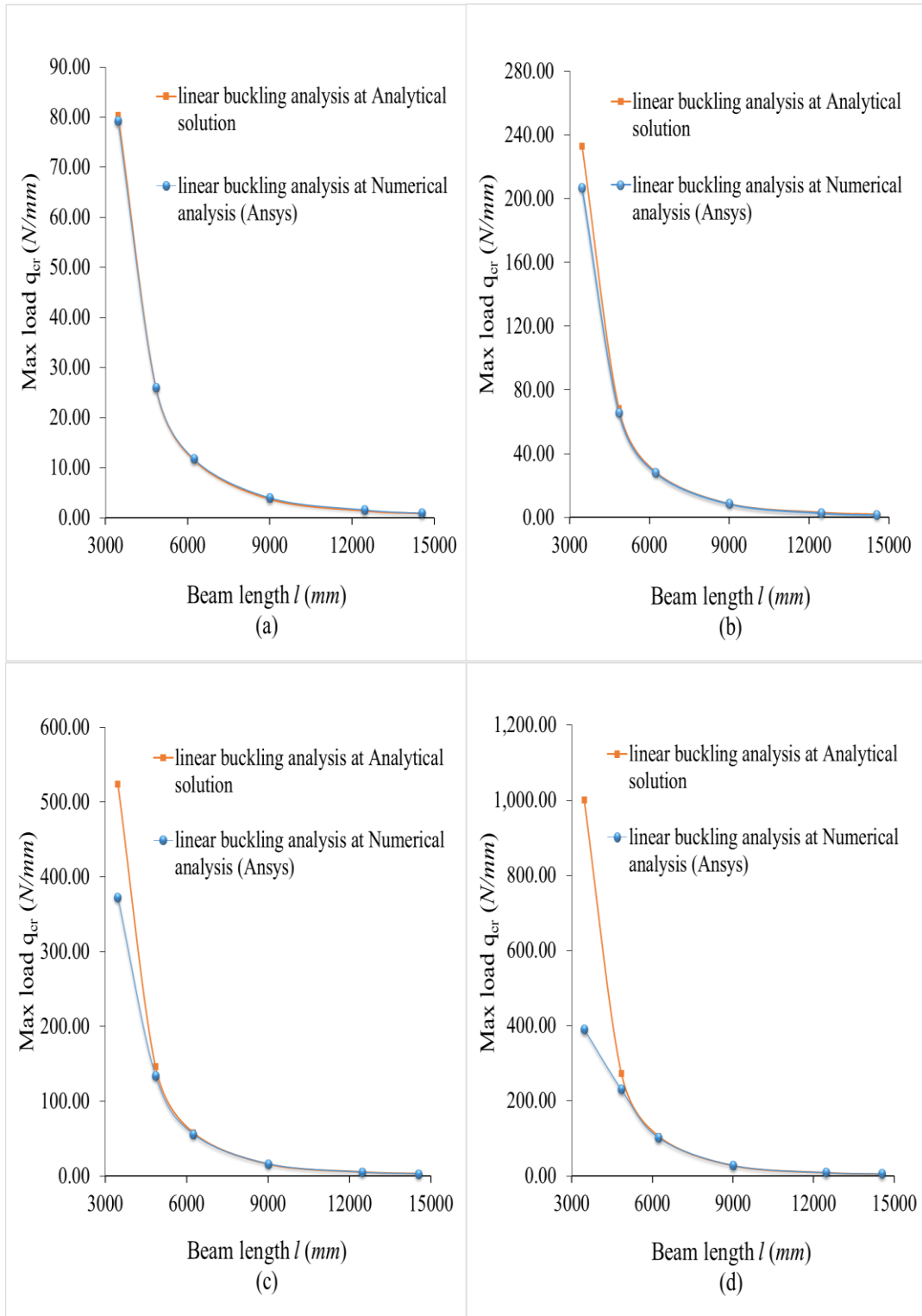
Figure 4-6 Critical elastic lateral-torsional buckling load (q_{cr}) of pinned-fixed castellated beam subjected to a uniformly distributed load between analytical solutions and FEA numerical solution for different beam lengths with various flange widths (a) bf =100mm, (b) bf=150mm, (c) bf=200mm and (d) bf =250mm (h_w=300mm, t_f=10mm, t_w=8mm and a=100mm)
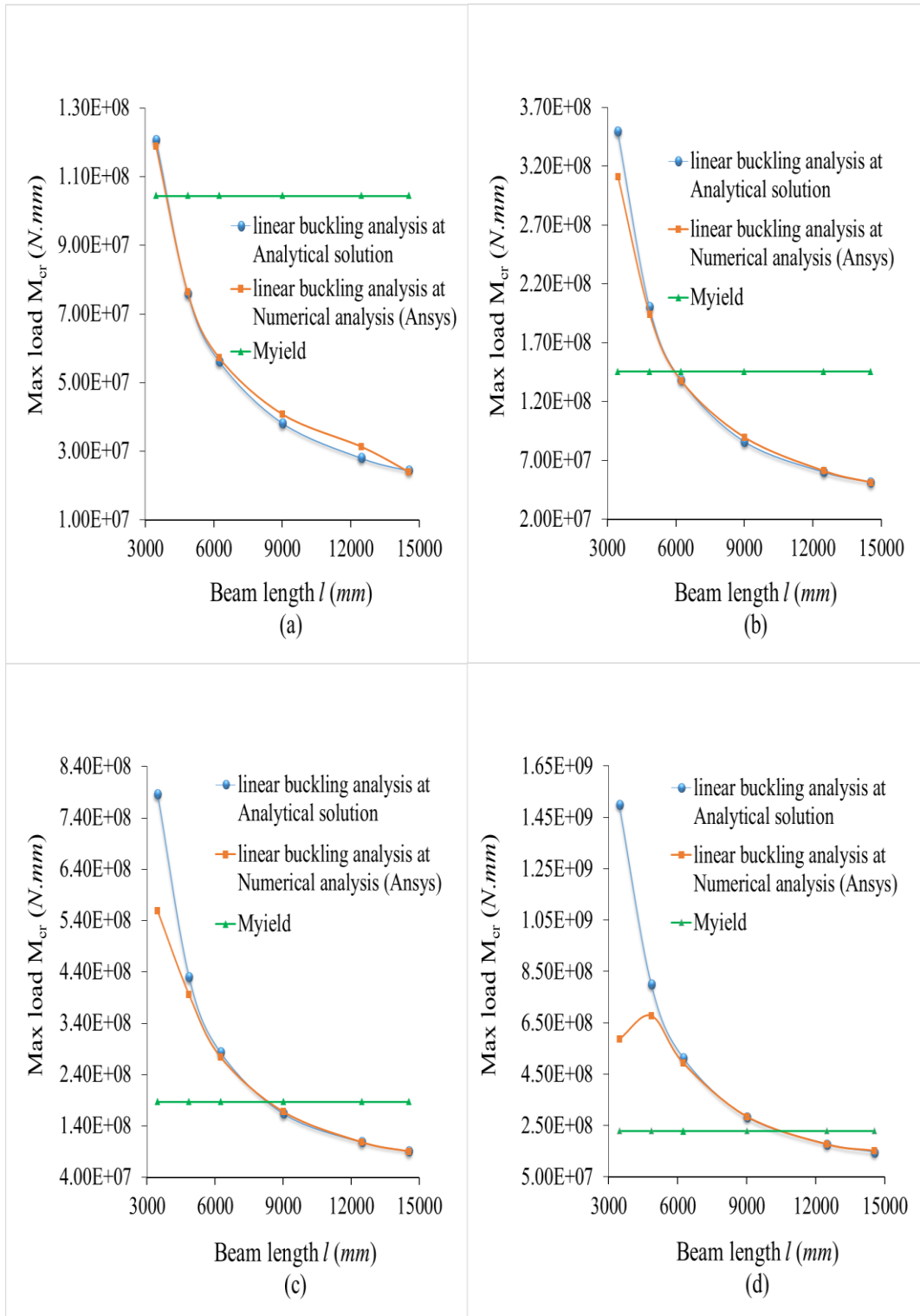
Figure 4-7 Critical elastic lateral-torsional buckling moment (M_{cr}) of pinned-fixed castellated beam subjected to a uniformly distributed load between analytical solutions and FEA numerical solution for different beam lengths with various flange widths (a) bf =100mm, (b) bf=150mm, (c) bf=200mm and (d) bf =250mm (h_w=300mm, t_f=10mm, t_w=8mm and a=100mm)
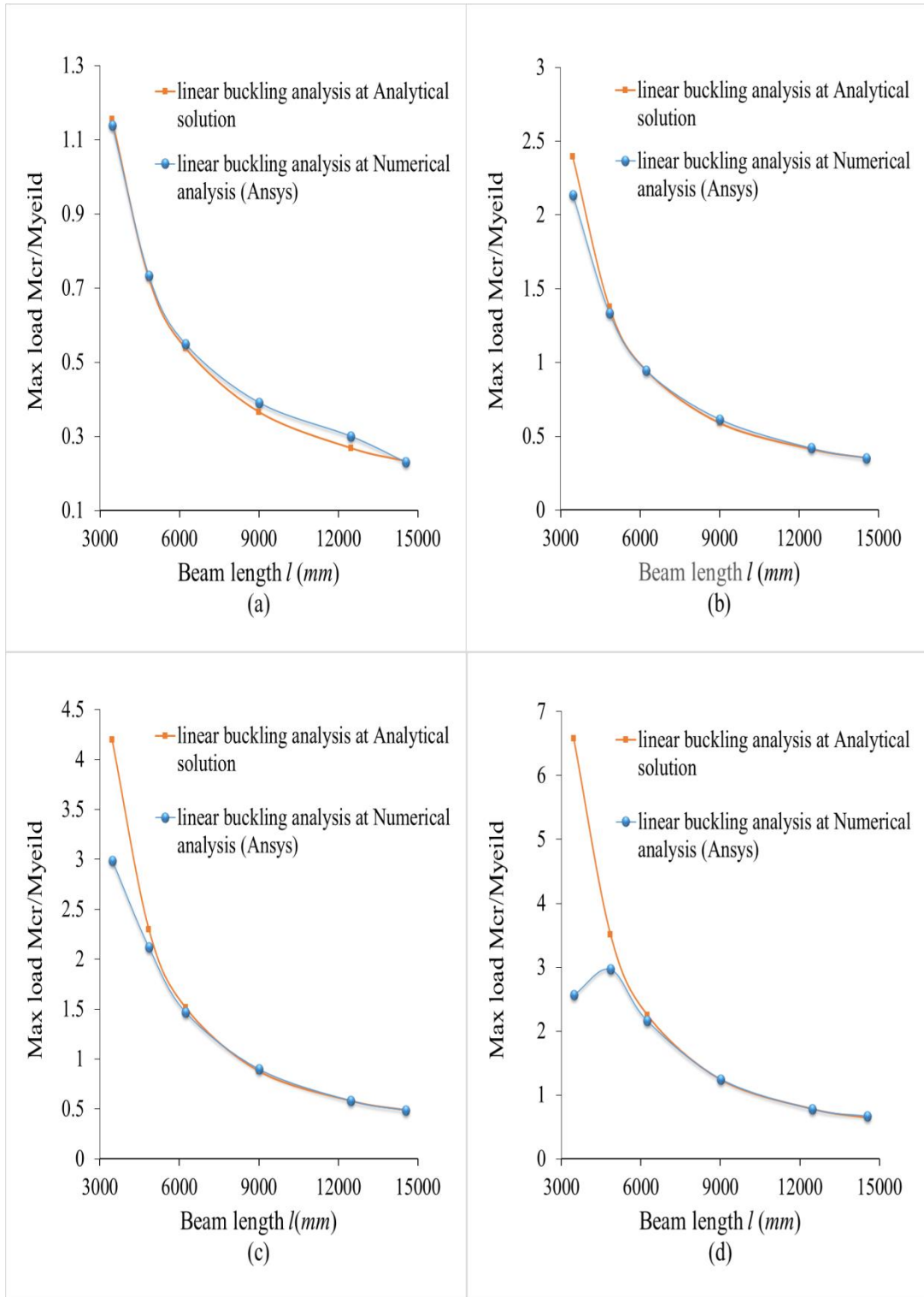
Figure 4-8 Critical elastic lateral-torsional buckling moment (M_{cr}/M_{yield}) of pinned-fixed castellated beam subjected to a uniformly distributed load between analytical solutions and FEA numerical solution for different beam lengths with various flange widths (a) bf =100mm, (b) bf=150mm, (c) bf=200mm and (d) bf =250mm (h_w=300mm, t_f=10mm, t_w=8mm and a=100mm)
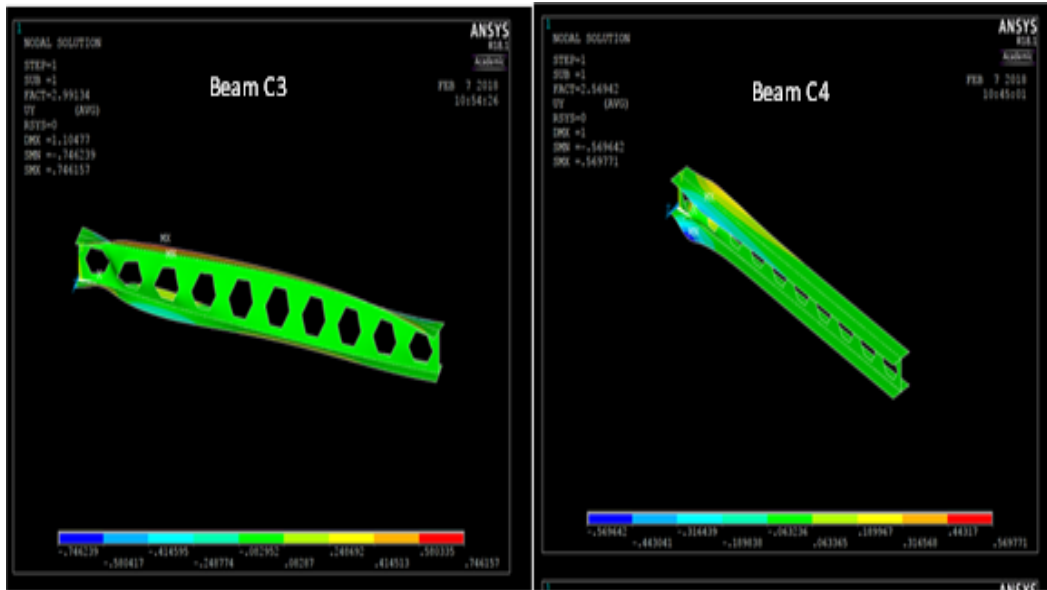
Figure 4-9 Combined modes failure of pinned-fixed castellated beam with a uniformly distributed load act on top flange for beam (C3 and C4) with two various flange widths *bf*=200mm and *bf*=250mm, obtained from the linear lateral-torsional buckling 3D finite element analysis using ANSYS software ($h_w=3$00mm, $t_f=$10mm, $t_w=$8mm and $a=$100mm).

4.7. Conclusions

In this chapter, the behaviour of lateral-torsional buckling of castellated beams subjected to a uniformly distributed load has been investigated using both analytical and numerical methods. The analytical study provides simplified equations for predicting the elastic critical load of lateral-torsional buckling. These equations have taken into account the web shear effect. FEA numerical analysis has been conducted using ANSYS commercial software to verify the analytical solution. From the comparison it can be concluded that:

➢ The torsional constant adopted for determining the critical lateral–torsional buckling load of castellated beams should be calculated by using the average torsional constant of the full and reduced section properties.

➢ The analytical solution and numerical solution have a similar variation pattern with the beam length. The analytical solution is in excellent agreement with the numerical analysis for middle and long length beams.

➢ For pinned-fixed castellated beams lateral-torsional buckling occurs only in long length beams. For beams shorter than 3.5 m with wider flanges, the buckling mode involves other modes and thus the critical load obtained from the lateral-torsional buckling analysis cannot represent the critical load of coupled buckling modes.

CHAPTER FIVE

5. *NONLINEAR ANALYSIS OF CASTELLATED BEAMS*

5.1. Introduction

This chapter is focusing on the effect of both the geometric and material nonlinearities on the bending and buckling behaviour of castellated beams under uniformly distributed transverse loads. The analysis is performed using finite element method with the use of ANSYS (APDL) commercial software.

Moreover, detailed comparisons of results obtained from the linear finite element analysis shown in Chapter three, the linear buckling analysis shown in chapter four, and the nonlinear finite element analysis shown in this Chapter are provided.

5.2. Nonlinear finite element analysis of castellated beam

The analysis of using elastic and small deflection theory provides a linear solution, in which any deflection is proportional to the externally applied load. This kind of analysis is correct only when the load is very small or the deflection is small. When the beam is subjected to a large external load, it may not behave linearly, in this case geometric nonlinearity and/or material nonlinearity may need to be considered. In general, when the beam has a large deflection, the geometric nonlinearity have to be considered; whereas when the stress occurred in the beam is near to the yield stress of the beam material the material nonlinearity has to be considered. In this section, we use the nonlinear analysis by considering both geometric and material nonlinearities. In the former large deflection is considered; while in the latter a bi-linear material model is employed for the constitutive relationship of the steel material.

Nonlinear finite element analysis is described in this section on the castellated beams that were considered in the analytical study in the previous chapters. The aim of this analysis is to study the large deflection and inelastic behaviour of castellated beams when subjected to a uniformly distributed load. The results of the nonlinear analysis are presented by using the load-deflection response curve, from which the failure load of the beam is also obtained. Moreover, an evaluation will be conducted of the critical value of load obtained by analytical buckling analysis and the critical load obtained by linear buckling analysis using finite element method.

ANSYS mechanical (APDL), that has technical potential, is employed to carry out both geometric and material nonlinear analysis of castellated beams. The geometric nonlinearity is to take into account the large deflection/displacement of the beams. The material nonlinearity is to consider the plasticity of steel material in which a bi-linear isotropic material model is used. The material properties used in the present nonlinear analysis are the modu1us of elasticity, E=2.1×10^5 MPa, yield stress, σ_y= 275 MPa, Poisson's ratio, $v = 0.3$, and the tangent modulus after the yield, E_t=0, that is the elastic-perfectly plastic material model is used (see **Figure 5-1**).
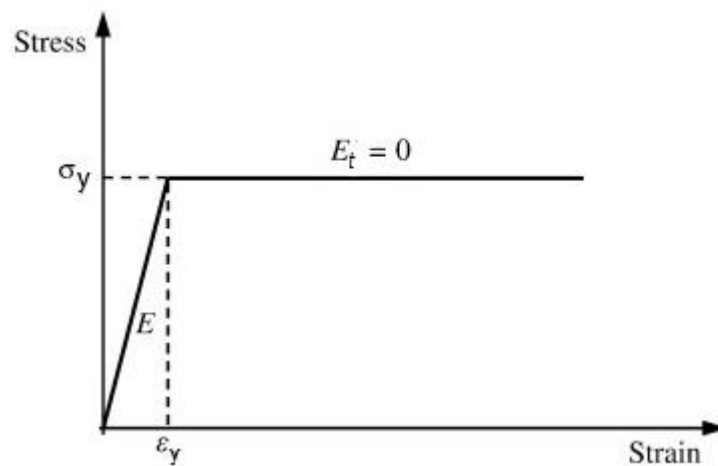
Figure 5-1 Elastic-perfectly plastic material model

5.2.1. Modelling, and boundary conditions

The modelling of castellated beams is carried out by using 3D 4-Node Thin Shell Elements (SHELL181) depicted in **Figure 3-5**. This element presents four nodes with six DOF per node, i.e., translations and rotations on the X, Y, and Z-axis, respectively.

The geometry of castellated beams is meshed by using 4-noded elements with maximum size not exceeding 10 mm. Two types of boundary conditions are considered herein; one is the simply support and the other is pinned-fixed, which are the same as those shown in Section 4.7.2

5.2.2. Apply loads gradually (incremental solution)

Similar to Chapter four, the external load is applied uniformly on the line between web and upper flange. This is done by applying the load to each node on the line. The nodal load applied is equal to the loading density multiplied by beam length and divided by the number of nodes on that line. In the early 1980's, the arc-length method was developed to improve Newton-Raphson method to make sure the convergence can be achieved for various different nonlinear problems (Crisfield, 1981). Note that, the Newton-Raphson method divides the load into a series of load increments to be applied over several load steps then evaluates convergence between the internal force and the applied loads; if the criteria of convergence are not convinced, the program attempts to resolve with a smaller load increment until the case converges. However, this method is suitable only for either load controlled, or displacement controlled nonlinear analysis. For a general nonlinear problem, the arc-length should be used as it combines the load and displacement increments in each iterative procedure. As a result, in the present study the equations of nonlinear equilibrium are solved by using the procedure of the Newton–Raphson method, in conjunction with Arc-Length Method.

5.3. Serviceability limit state

Structural serviceability indicates the limit states that are considered in the design of the structure. Therefore, to ensure that a building is safe, these conditions should be followed. The current standard serviceability design has different deflection limits which depend on the purpose of service as it is intended, and the material of the structure. The aim of this section is to validate the results of deflection that are calculated from the analytical linear method, linear, and nonlinear finite element

methods. In this study, the value of deflection under the serviceability load that was considered is $l/250$ because the structure is steel.

5.4. Investigating load-deflection response curve for castellated beams with different boundary conditions.

5.4.1. Investigating load-deflection response curve of simply supported beams with uniformly distributed loads

Figures 5-2, **5-3**, **5-4**, and **5-5** show a comparison of the curves of load versus deflection of simply supported castellated beam with a uniformly distributed load. This comparison involves the results of linear analytical solutions, which are developed in chapter three, nonlinear 3D finite element analysis using ANSYS software, and the deflection limit ($l/250$) to groups C, D, E, G, H, and I with different flange widths (see Section 3.3.4). The load is presented as the increments of load calculated following Eq. (3-31).

From these figures it can be noticed that the nonlinear behaviour of castellated beams, for the same flange width, drops continuously with the increase of beam length, whereas the behaviour of the beam towards linear behaviour progresses gradually. In contrast, the nonlinear behaviour of the castellated beams, for the same beam length, increases continuously with the increase of the flange width, thus the castellated beams will reach the yield point in the early stages of the loading process.

As expected, the reason for this is that the dimensions of castellated beams and the value of yield stress were taken account for calculating the value of uniformly distributed load, which was applied in this work (see Eq. (3-31)), where the yield stress value is constant for all groups of castellated beams, thus the load capacity of the beams is affected by changing the beam dimensions. Note that the uniformly distributed load with the same beam length increases when the flange width increases, which leads to being more susceptible to yielding in the early stages of the loading process. In contrast, the uniformly distributed load with the same flange width reduces when the beam length

increases, which leads to being less susceptible to yielding in the early stages of the loading process.

Table (5-1) presents the comparison of the critical value of loads (q_{cr}/q_{yield}) with the different beam lengths with various flange widths. The results are also plotted in **Figure 5-6**. For the purpose of comparison, the results obtained from the linear analytical solutions and the nonlinear 3D finite element analyses are evidence that the critical value of load is influenced by geometry, web openings and material beam. As a result, the designer should consider a nonlinear analysis of short castellated beams with wide flange width for the design.
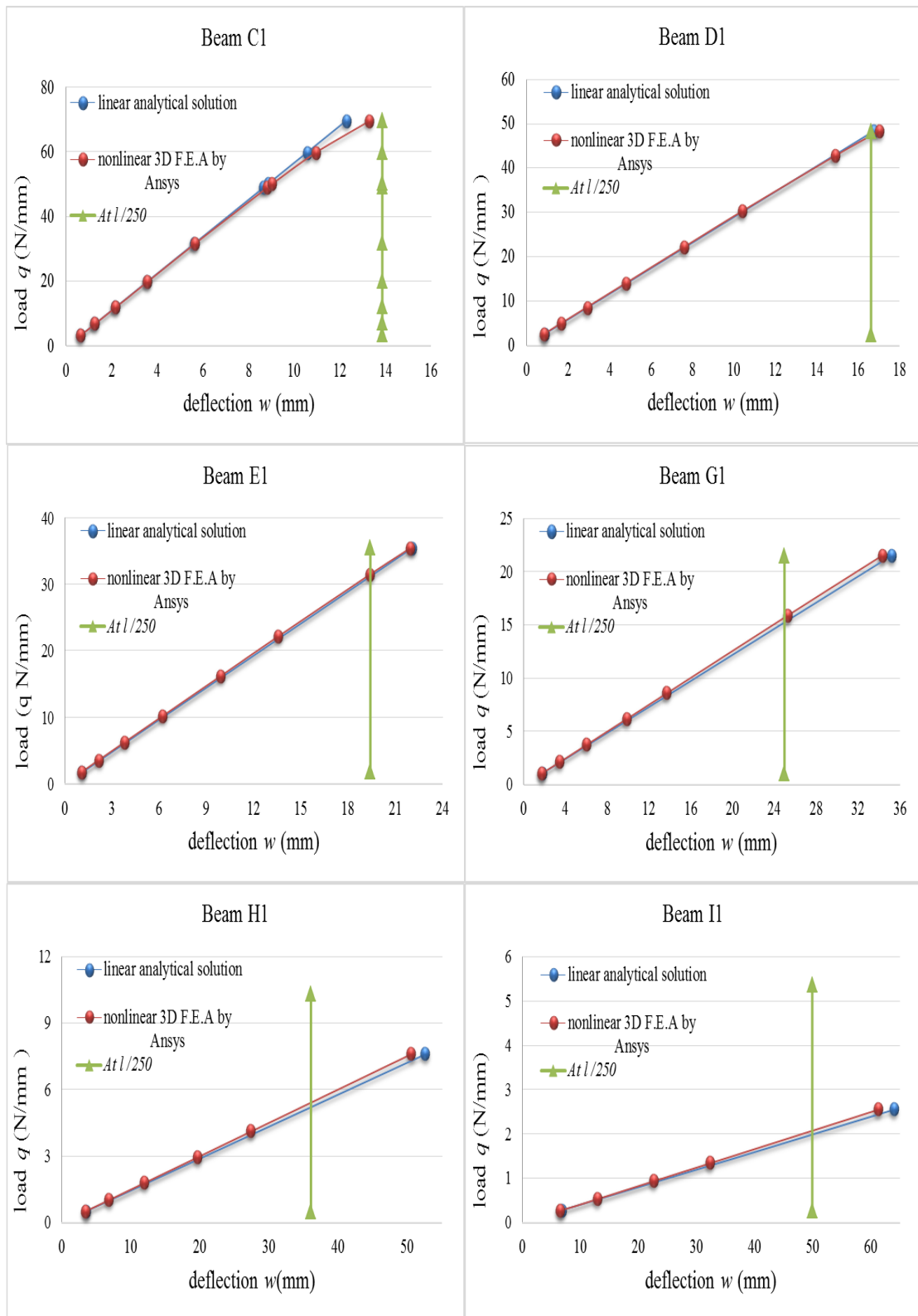
Figure 5-2 Comparison of the curves of load versus deflection of simply supported castellated beam with a uniformly distributed load obtained from linear analytical solutions, nonlinear 3D finite element analysis, and deflection limit (*l*/250) for beams C1, D1, E1, G1, H1, and I1.
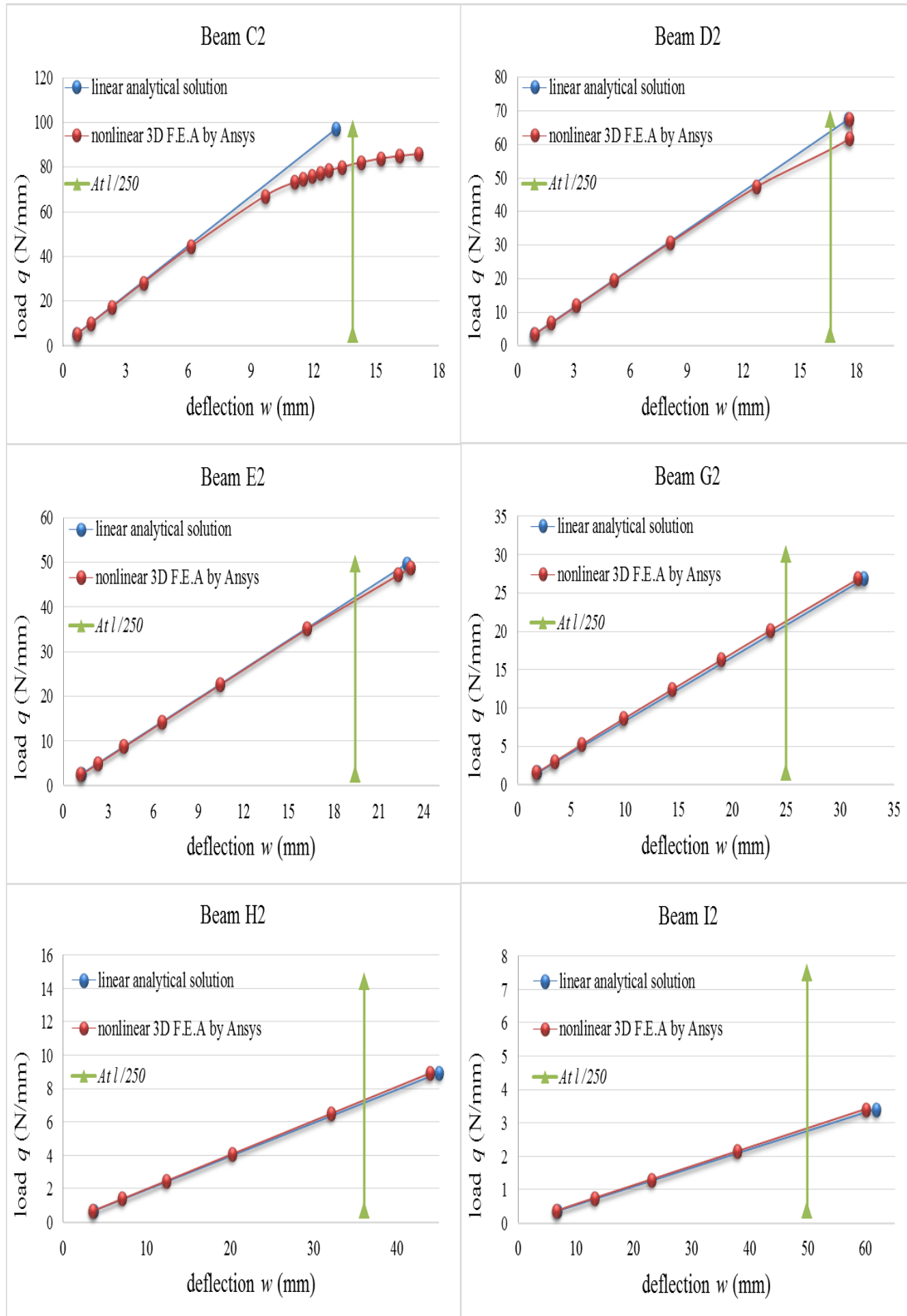
Figure 5-3 Comparison of the curves of load versus deflection of simply supported castellated beam with a uniformly distributed load obtained from linear analytical solutions, nonlinear 3D finite element analysis, and deflection limit (l/250) for beams C2, D2, E2, G2, H2, and I2.

Figure 5-4 Comparison of the curves of load versus deflection of simply supported castellated beam with a uniformly distributed load obtained from linear analytical solutions, nonlinear 3D finite element analysis, and deflection limit (l/250) for beams C3, D3, E3, G3, H3, and I3.

Figure 5-5 Comparison of the curves of load versus deflection of simply supported castellated beam with a uniformly distributed load obtained from linear analytical solutions, nonlinear 3D finite element analysis, and deflection limit ($l/250$) for beams C4, D4, E4, G4, H4, and I4.

Table 5-1 Comparison of results (q_{cr}/q_{yield}) between linear analytical solution and nonlinear 3D finite element analysis of simply supported castellated beams subjected to a uniformly distributed for groups C, D, E, G, H, and I with different flange widths.

b_f mm	Name of beam	q_{yield} N/mm	Linear analytical solution		Nonlinear 3D finite element analysis by Ansys	
			q_{cr} N/mm	$\dfrac{q_{cr}}{q_{yield}}$	q_{cr} N/mm	$\dfrac{q_{cr}}{q_{yield}}$
100	C1	69.59	69.59	1.00	59.94	0.86
	D1	48.33	48.33	1.00	47.85	0.99
	E1	35.51	35.51	1.00	35.51	1.00
	G1	21.48	21.48	1.00	21.48	1.00
	H1	10.29	10.29	1.00	10.29	1.00
	I1	5.37	5.37	1.00	5.37	1.00
150	C2	97.13	97.13	1.00	73.03	0.75
	D2	67.45	67.45	1.00	61.74	0.91
	E2	49.56	49.56	1.00	48.67	0.98
	G2	29.98	29.98	1.00	29.98	1.00
	H2	14.37	14.37	1.00	14.37	1.00
	I2	7.49	7.49	1.00	7.49	1.00
200	C3	124.67	124.67	1.00	75.99	0.61
	D3	86.57	86.57	1.00	66.06	0.76
	E3	63.61	63.61	1.00	56.66	0.89
	G3	38.48	38.48	1.00	38.48	0.99
	H3	18.44	18.44	1.00	18.44	1.00
	I3	9.62	9.62	1.00	9.62	1.00
250	C4	152.21	152.21	1.00	73.66	0.50
	D4	105.70	105.70	1.00	67.20	0.64
	E4	77.66	77.66	1.00	60.40	0.78
	G4	46.98	46.98	1.00	43.40	0.92
	H4	22.52	22.52	1.00	22.52	1.00
	I4	11.74	11.74	1.00	11.74	1.00

Figure 5-6 Critical values of simply supported castellated beams subjected to a uniformly distributed load, obtained from linear analytical solution and nonlinear 3D finite element analysis for groups C, D, E, G, H, and I with different flange widths (a) bf =100mm, (b) bf =150mm, (c) bf =200mm and (d) bf =250mm. (h_w=300mm, t_f=10mm, t_w=8mm and a=100mm)

5.4.2. Investigating load-deflection response curve of pinned-fixed beams subjected to uniformly distributed loads

Figures 5-7, 5-8, 5-9 and **5-10** show a comparison of the curves of load versus deflection of pinned-fixed castellated beams subjected to a uniformly distributed load. The comparison involves the results of linear analytical solutions, which is developed in chapter three, nonlinear 3D finite element analysis using ANSYS software, and deflection limit (l/250) for groups C, D, E, G, H, and I with different flange widths (see Section 3.3.4). The load is presented as the increments of load calculated following Eq. (3-31).

From these figures it can be seen that the nonlinear behaviour of castellated beams, with the same flange width, drops continuously with the increase of beam length, whereas the behaviour of the beam towards linear behaviour progresses gradually. In contrast, the nonlinear behaviour of the castellated beams with the same beam length increases continuously with the increase of the flange width, thus the castellated beams will reach the yield point in the early stages of the loading process.

As expected, the reason for this is that the dimensions of castellated beams and the yield stress were taken account for calculating the load capacity of the beams, which was applied in this work (see Eq. (3-31)), where the yield stress is identical for all groups of castellated beams. Thus, the loading capacity of the beams is affected by the change of the beam dimensions. Note that, the load for the same beam length increases when the flange width increases, which leads to being more susceptible to yielding in the early stages of the loading process. In contrast, the load with the same flange width reduces when the beam length increases, which leads to being less susceptible to yielding in the early stages of the loading process.

Table (5-2) presents the comparison of the critical value of loads (q_{cr}/q_{yield}) for beams with the different length for four groups with various flange widths. The results are also plotted in **Figure 5-11**. For the purpose of comparison, which include the results obtained from the linear analytical solutions and from the nonlinear 3D finite element analyses. It is evidence from the figure that the critical value of load is influenced by geometry, web openings and material beam. As a result, the designer

should consider to use a nonlinear analysis for short castellated beams with wide flange for design calculations.

For short beams or the beams with wide flanges, the overall deflections of these beams are rather small. Before the deflection of the beam reaches to the critical value of $l/250$, the material has already yielded, and in this case the material nonlinearity must be considered and the relationship between the deflection and the externally applied load is NOT linear.

Compare the results of the beams with simply support boundary, it is noted that the nonlinearity of the beams with pinned-fixed boundary is more sever because the deflection of simply supported beams is more than the deflection of the pinned-fixed beam.
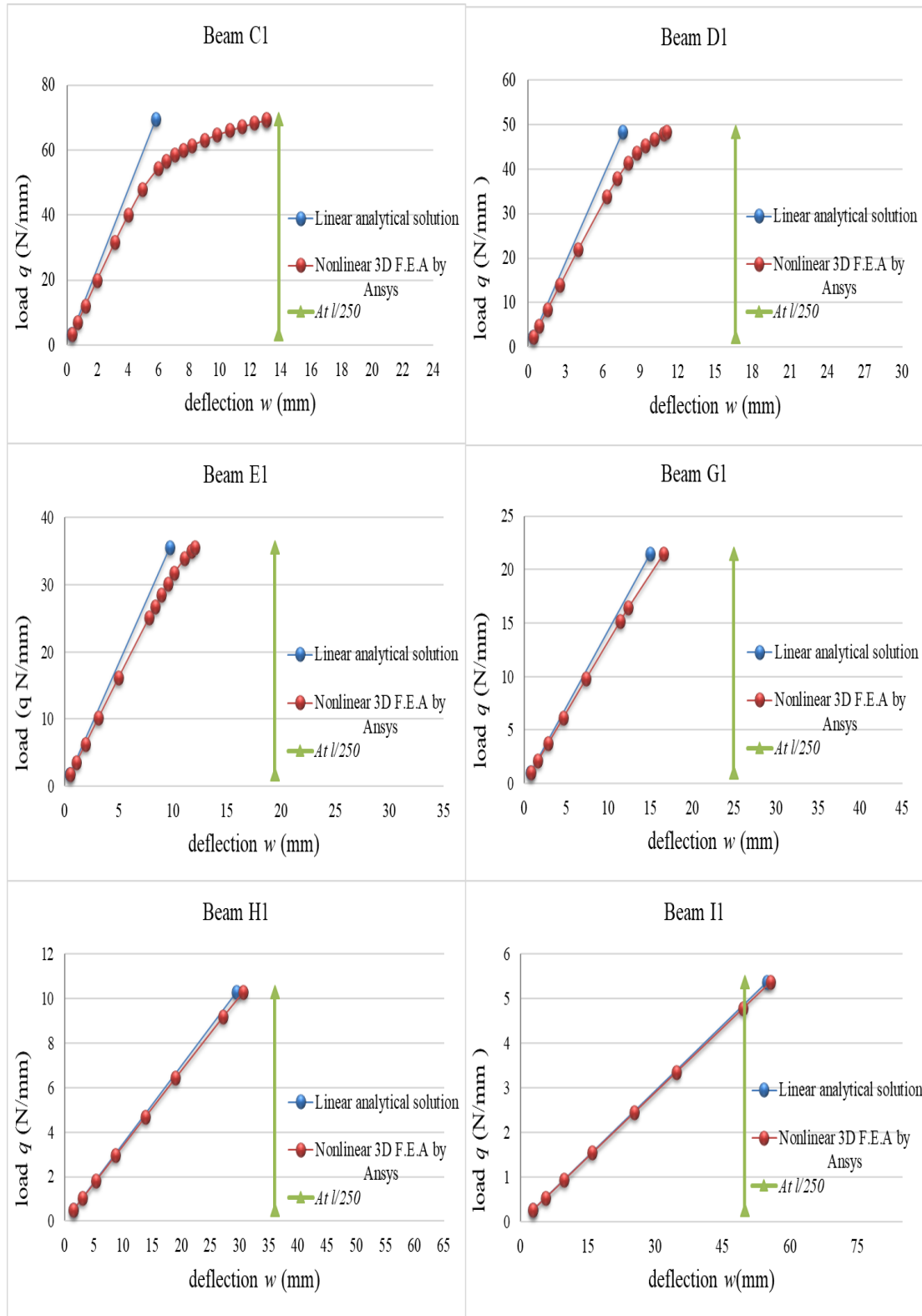
Figure 5-7 Comparison of the curves of load versus deflection of pinned-fixed castellated beams subjected to a uniformly distributed load, obtained from linear analytical solutions, nonlinear 3D finite element analysis, and deflection limit (*l*/250) for beams C1, D1, E1, G1, H1, and I1.
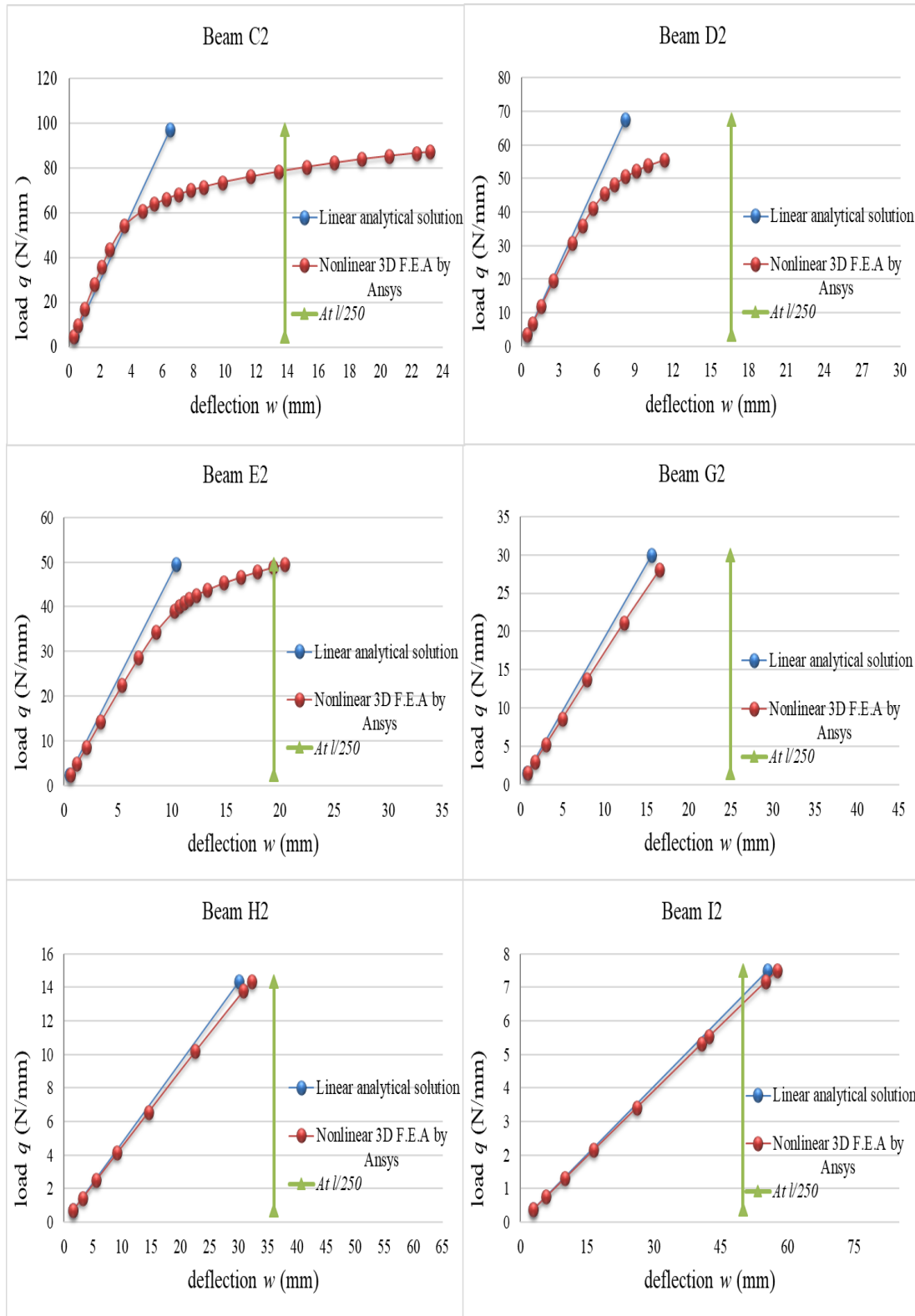
Figure 5-8 Comparison of the curves of load versus deflection of pinned-fixed castellated beam subjected to a uniformly distributed load, obtained from linear analytical solutions, nonlinear 3D finite element analysis, and deflection limit (*l*/250) for beams C2, D2, E2, G2, H2, and I2.
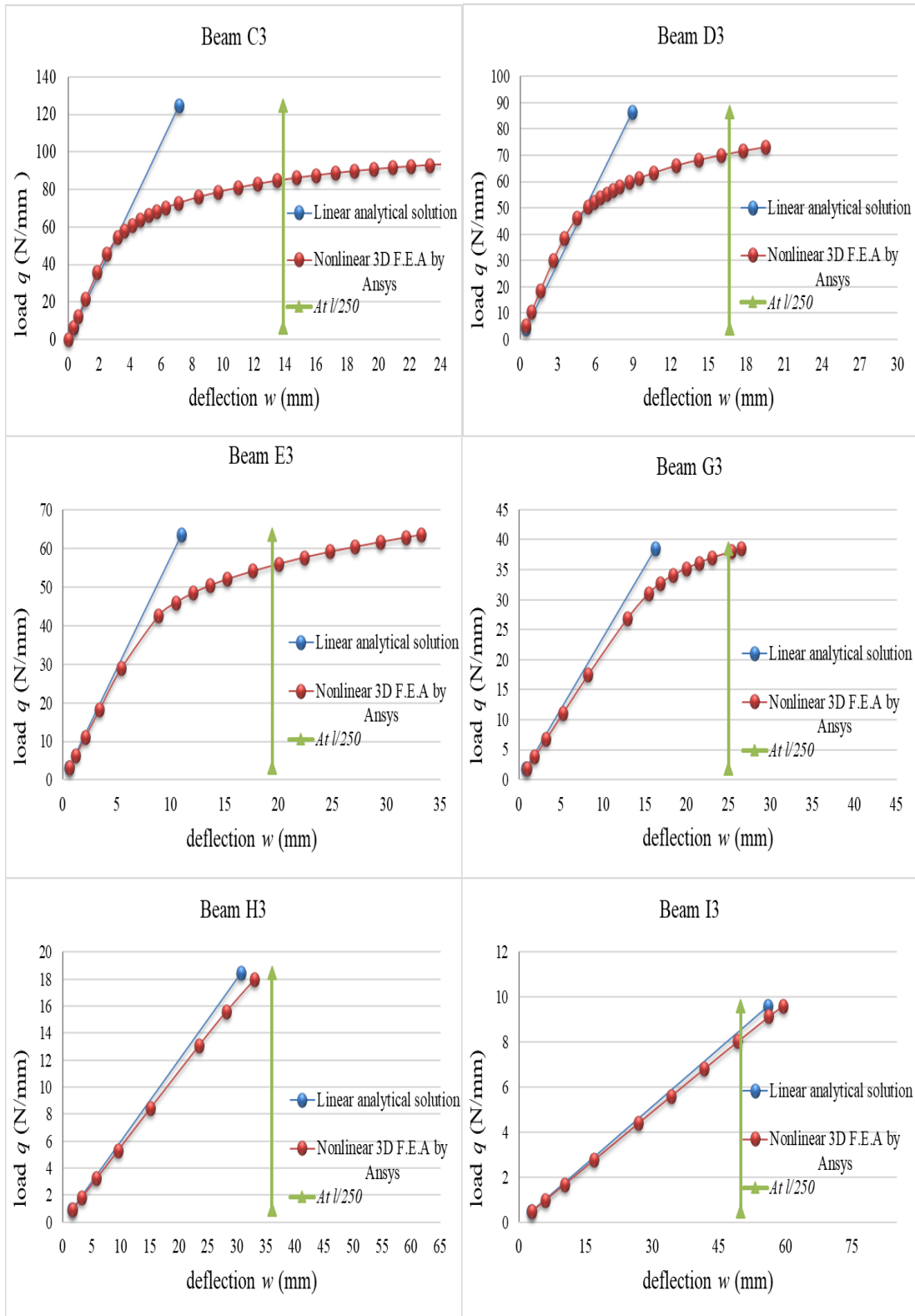
Figure 5-9 Comparison of the curves of load versus deflection of pinned-fixed castellated beam subjected to a uniformly distributed load, obtained from linear analytical solutions, nonlinear 3D finite element analysis, and deflection limit (*l*/250) for beams C3, D3, E3, G3, H3, and I3.
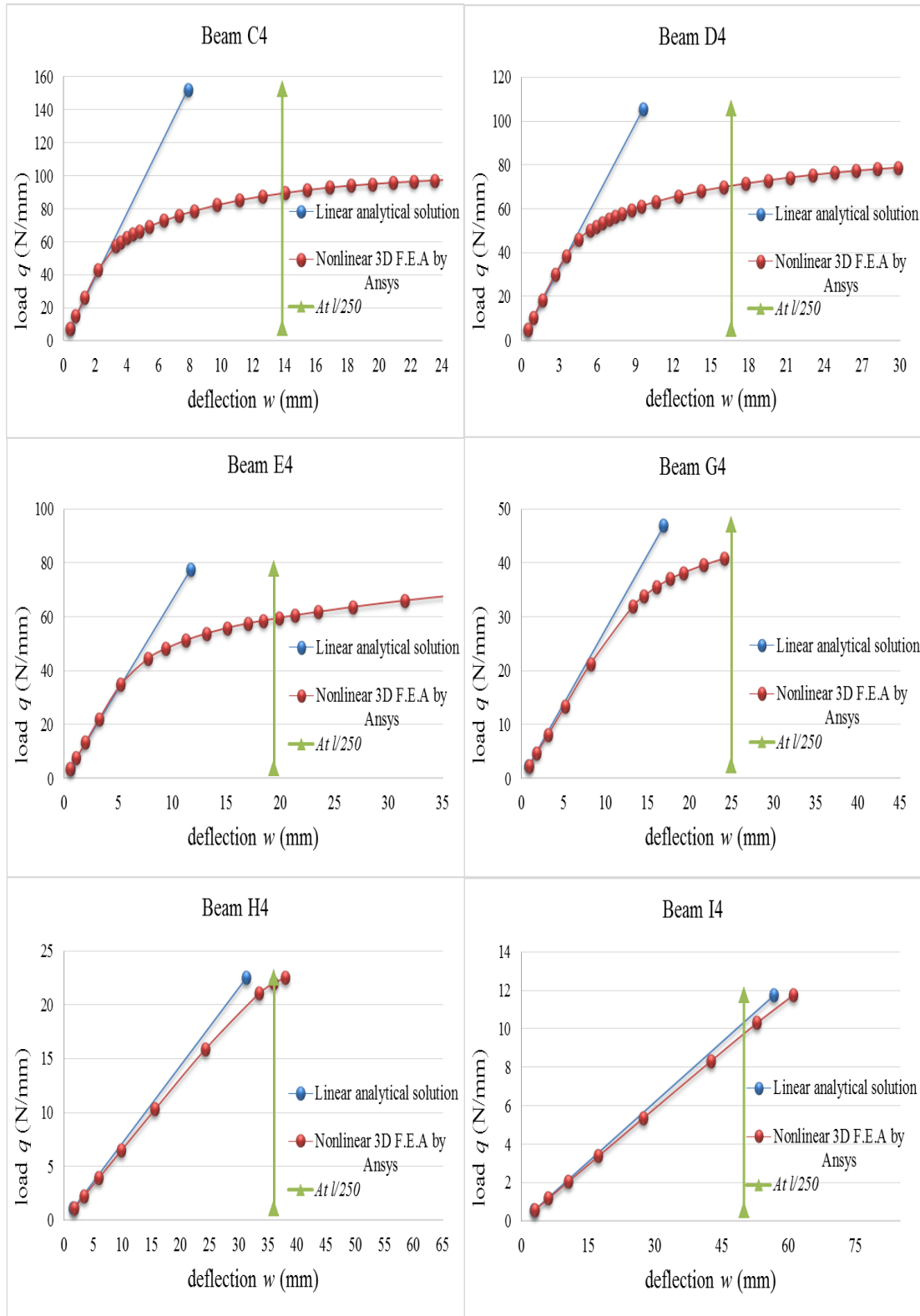
Figure 5-10 Comparison of the curves of load versus deflection of pinned-fixed castellated beam subjected to a uniformly distributed load, obtained from linear analytical solutions, nonlinear 3D finite element analysis, and deflection limit ($l/250$) for beams C4, D4, E4, G4, H4, and I4.
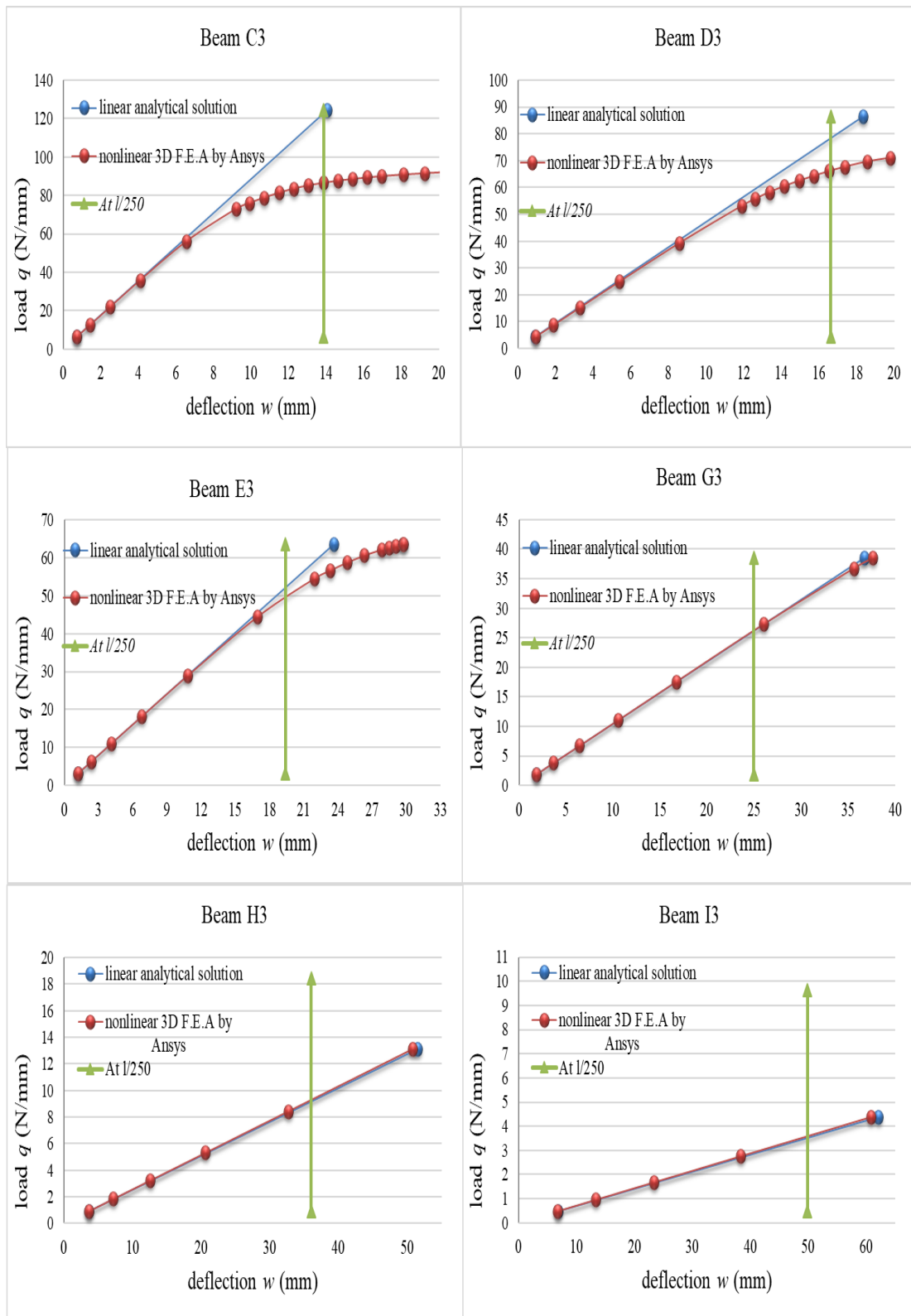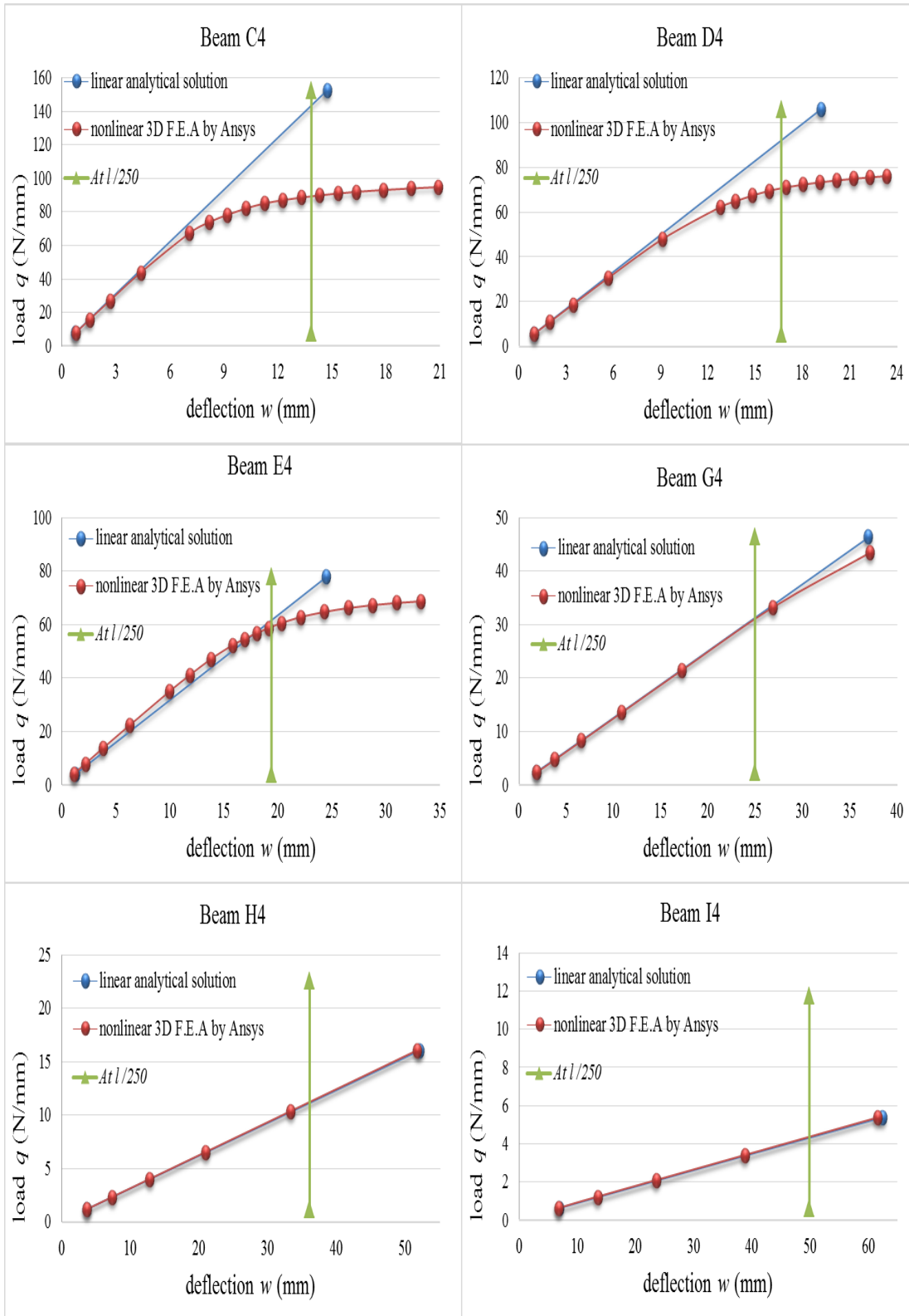
114

Table 5-2 Comparison of results (q_{cr}/q_{yield}) between linear analytical solution and nonlinear 3D finite element analysis of pinned-fixed castellated beams subjected to a uniformly distributed load, for groups C, D, E, G, H, and I beams with different flange widths.

b_f mm	Name of beam	q_{yield} N/mm	Linear analytical solution		Nonlinear 3D finite element analysis by Ansys	
			q_{cr} N/mm	$\dfrac{q_{cr}}{q_{yield}}$	q_{cr} N/mm	$\dfrac{q_{cr}}{q_{yield}}$
100	C1	69.59	69.59	1.00	48.40	0.70
	D1	48.33	48.33	1.00	41.49	0.86
	E1	35.51	35.51	1.00	33.92	0.96
	G1	21.48	21.48	1.00	21.48	1.00
	H1	10.29	10.29	1.00	10.29	1.00
	I1	5.37	5.37	1.00	5.37	1.00
150	C2	97.13	97.13	1.00	54.09	0.56
	D2	67.45	67.45	1.00	48.27	0.72
	E2	49.56	49.56	1.00	40.91	0.83
	G2	29.98	29.98	1.00	28.05	0.94
	H2	14.37	14.37	1.00	14.37	1.00
	I2	7.49	7.49	1.00	7.49	1.00
200	C3	124.67	124.67	1.00	54.54	0.44
	D3	86.57	86.57	1.00	50.40	0.58
	E3	63.61	63.61	1.00	42.51	0.67
	G3	38.48	38.48	1.00	31.03	0.81
	H3	18.44	18.44	1.00	17.96	0.97
	I3	9.62	9.62	1.00	9.62	1.00
250	C4	152.21	152.21	1.00	57.43	0.38
	D4	105.70	105.70	1.00	50.40	0.48
	E4	77.66	77.66	1.00	44.71	0.57
	G4	46.98	46.98	1.00	33.90	0.72
	H4	22.52	22.52	1.00	21.02	0.93
	I4	11.74	11.74	1.00	11.74	1.00

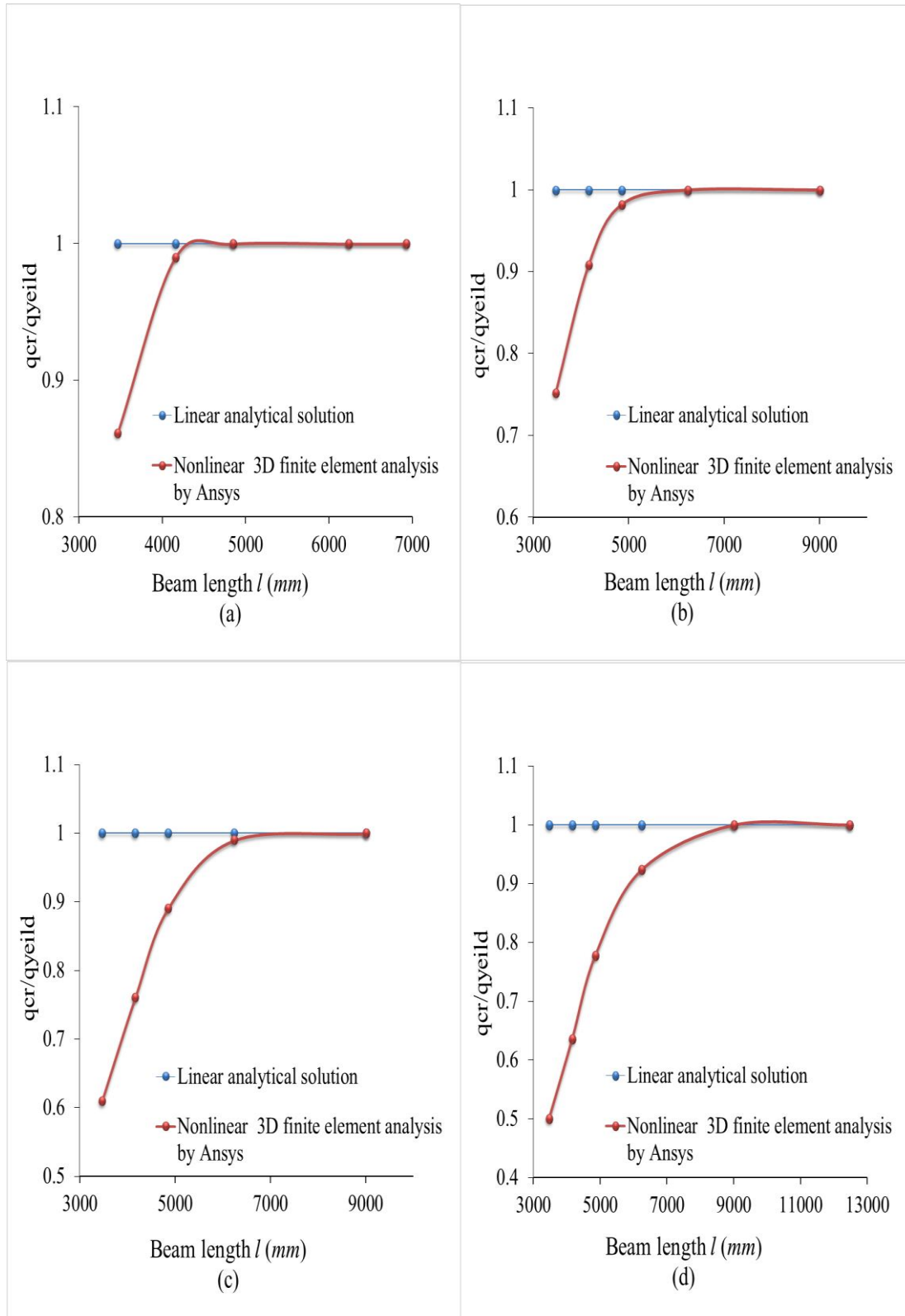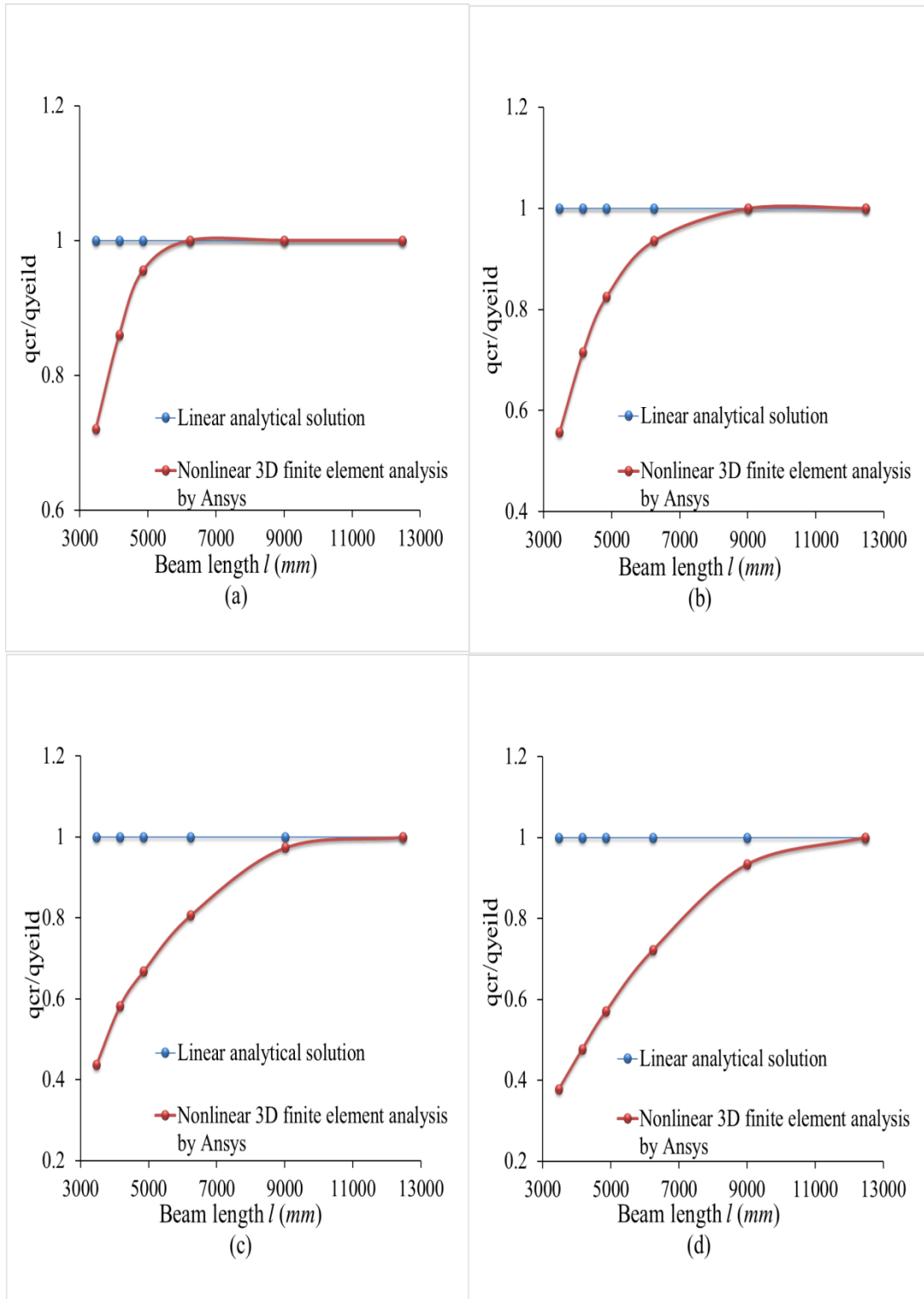**Figure 5-11** Critical values of pinned-fixed castellated beams subjected to a uniformly distributed load, obtained from linear analytical solution and nonlinear 3D finite element analysis for groups C, D, E, G, H, and I with different flange widths (a) bf =100mm, (b) bf =150mm, (c) bf =200mm and (d) bf =250mm. (h_w=300mm, t_f=10mm, t_w=8mm and a=100mm)

5.5. Nonlinear lateral-torsional buckling of castellated beams due to a uniformly distributed load

A nonlinear inelastic finite-element analysis is provided to examine inelastic lateral-torsional buckling behaviour of castellated beams subjected to uniformly distributed load act on the top flange. In this section, the analyses are carried out by using ANSYS mechanical (APDL) commercial software, which consider the effect of both the geometric nonlinear and material inelasticity of castellated beams for calculating the critical lateral-torsional buckling moment.

The analysis procedure is performed throughout two parts. Firstly, the manufacturing method of castellated beams causes initial geometrical imperfections that lead to the initial deformation. Therefore, linear lateral-torsional buckling is employed from which the lateral-torsional buckling mode is used as the initial geometric imperfection of the beam for the subsequent nonlinear analysis. Secondly, Newton-Raphson method with the large deflection method, in conjunction with Arc-Length Method is utilized for nonlinear lateral-torsional buckling analysis. The nonlinear analysis procedure used is exactly the same as that described in previous sections and thus is not provided here again.

5.5.1. Modelling, loading and boundary conditions

The modelling of castellated beams is carried out by using 3D 4-Node Thin Shell Elements (SHELL181) depicted in **Figure 3-5**. This element presents four nodes with six DOF per node, i.e. translations and rotations on the X, Y, and Z-axis, respectively. The geometric models of castellated beams are meshed by using elements with size not exceeding10 mm for both the pinned-pinned and pinned-fixed castellated beams. The load is applied at the junction line between the web and upper flange of the beam. The nodal load is calculated by the load density multiplied by beam length and divided by the number of nodes on that line. The mechanical properties and boundary conditions are the same as those described in the nonlinear analysis sections above.

5.5.2. Comparison of critical lateral-torsional bucking moment of simply supported beams due to uniformly distributed loads

Table (5-3) gives the comparison of critical moments of lateral-torsional buckling of simply supported castellated beams. This comparison involves the results of linear analytical solutions, which are developed in chapter four, linear buckling 3D finite element analysis using ANSYS, and nonlinear 3D finite element analysis (geometric nonlinear and material inelasticity) using ANSYS software for groups C, E, G, H, I, and J beams with different flange widths (see Section 3.3.4), in which the value of linear critical lateral-torsional buckling moment (M_{cr}) was obtained by Eq. (4-16), tabulated under term linear lateral-torsional buckling analytical analysis. The results that are determined by linear finite element analysis are tabulated under term linear lateral-torsional buckling analysis by ANSYS software and the results that are determined by nonlinear finite element analysis are tabulated under term nonlinear lateral-torsional buckling analysis by ANSYS software. Moreover, the yield moment is obtained by $M_{yield} = \frac{2\sigma_y I_{reduced}}{h_w + 2t_f}$, ($\sigma_y = 275 \frac{N}{mm^2}$,$I_{reduced}$ is obtained by following Eq. (3-17)), where it is tabulated under term.(M_{yield}) For the purpose of comparison, the results shown in the table is also plotted in **Figures 5-12** and **5-13** respectively.

From these figures, it can be seen that in each group of flange width, the curves of the analytical solution and numerical analysis of both linear and nonlinear have a similar variation pattern. In other words, the analytical solution is in excellent agreement with numerical analysis by ANSYS for all models of castellated beams. However, it is observed from these figures that in the case of nonlinear analysis of castellated beams, the critical lateral torsion buckling load (M_{cr}/M_{yield}) drops with the increase the flange width and the decrease of beam length. The previous studies mentioned that the reasons for this are because lateral-torsional buckling load of castellated beam is influenced by the lateral flexural and warping rigidities (Mohebkhah, 2011). In this study, the increasing flange width leads firstly to increase lateral flexural and warping rigidities, and secondly to increase applying moments on castellated beams. These issues indicate that the geometric nonlinear and material nonlinear lateral-torsional buckling resistance of castellated beams with short beam length is limited to the ultimate load carrying capacity, in which no lateral-torsional buckling occurs. In practice, $M_{cr} \gg M_{yield}$ will

not happen (it's not real) because the beam will fail by yield. When the M_{cr} is close to the M_{yield} there are some interactions between M_{yield} and M_{cr}, in which case $M_{cr} \gg M_{yield}$ needs to be considered. This is why in the plots the part of $M_{cr} \gg M_{yield}$ curves is included.

Figure 5-14 shows a comparison of the load-deflection curves of simply supported castellated beam subjected to a uniformly distributed load. This comparison involves the results of nonlinear 3D finite element analysis using ANSYS software, and deflection limit ($l/250$) to groups C, E, G, H, I and J beams with different flange widths (see Section 3.3.4). The load is presented as the increments of load calculated following by Eq. (3-31). This latter reflects that the critical lateral-torsional buckling for short beam length with wide flange is influenced by geometry, web openings and material beam. As a result, the designer should consider a nonlinear analysis for short castellated beam with wide flange width for design calculations.

Figure 5-15 presents the failure mode of the beam length ($l = 3.5$ m) with wide flange width (b_f=250mm) obtained from the numerical analysis. It can be observed that in the nonlinear analysis, the failure load is controlled by the plastic/buckling load, while the linear solution is controlled purely by the elastic buckling which is much higher than the yield load

Table 5-3 Comparison of lateral-torsional buckling results of simply supported castellated beams subjected to a uniformly distributed load obtained from linear and nonlinear analysis

b_f mm	Name of beam	Myield N.mm x10^7	Linear buckling analytical analysis			Linear buckling analysis by Ansys			Nonlinear buckling analysis by Ansys		
			qcr N/mm	Mcr N.mm x10^7	$\frac{Mcr}{Myield}$	qcr N/mm	Mcr N.mm x10^7	$\frac{Mcr}{Myield}$	qcr N/mm	Mcr N.mm x10^7	$\frac{Mcr}{Myield}$
	C1	10.44	35.50	5.33`	0.51	34.54	5.18	0.50	27.50	4.12	0.40
	E1	10.44	12.23	3.59	0.34	12.10	3.56	0.34	10.80	3.18	0.30
100	G1	10.44	5.58	2.76	0.26	5.40	2.63	0.25	5.34	2.60	0.25
	H1	10.44	1.90	1.93	0.18	1.88	1.90	0.18	1.93	1.96	0.19
	I1	10.44	0.73	1.41	0.14	0.72	1.41	0.13	0.77	1.73	0.15
	J1	10.44	0.45	1.20	0.11	0.45	1.18	0.11	0.45	1.19	0.11
	C2	14.57	91.28	13.69	0.94	90.56	13.58	0.93	58.00	8.70	0.60
	E2	14.57	28.44	8.36	0.57	28.29	8.32	0.57	23.22	6.83	0.47
150	G2	14.57	12.64	6.14	0.42	12.74	6.19	0.42	11.60	5.64	0.39
	H2	14.57	3.99	4.05	0.28	3.86	3.92	0.27	3.98	4.04	0.28
	I2	14.57	1.51	2.94	0.20	1.58	3.07	0.21	1.67	3.24	0.22
	J2	14.57	0.96	2.53	0.17	0.96	2.53	0.17	1.04	2.75	0.19
	C3	18.70	192.00	28.80	1.54	185.71	27.86	1.49	93.55	14.23	0.76
	E3	18.70	57.11	16.79	0.90	56.04	16.47	0.88	40.97	12.05	0.64
200	G3	18.70	23.97	11.65	0.62	23.67	11.51	0.62	20.19	9.79	0.52
	H3	18.70	7.18	7.28	0.39	7.04	7.14	0.38	6.96	7.05	0.38
	I3	18.70	2.61	5.07	0.27	2.61	5.07	0.27	2.50	4.86	0.26
	J3	18.70	1.64	4.33	0.23	1.61	4.26	0.23	1.72	4.54	0.24
	C4	22.83	356.67	53.50	2.34	317.97	47.70	2.09	96.35	14.45	0.63
	E4	22.83	101.70	29.90	1.31	100.22	29.46	1.29	60.59	17.81	0.78
250	G4	22.83	41.15	20.00	0.88	40.79	19.82	0.87	31.60	15.36	0.67
	H4	22.83	11.70	11.86	0.52	11.59	11.76	0.51	11.10	11.26	0.49
	I4	22.83	4.09	79.61	0.35	4.10	7.98	0.35	3.94	7.66	0.34
	J4	22.83	2.53	67.06	0.29	2.51	6.64	0.29	2.71	7.17	0.31
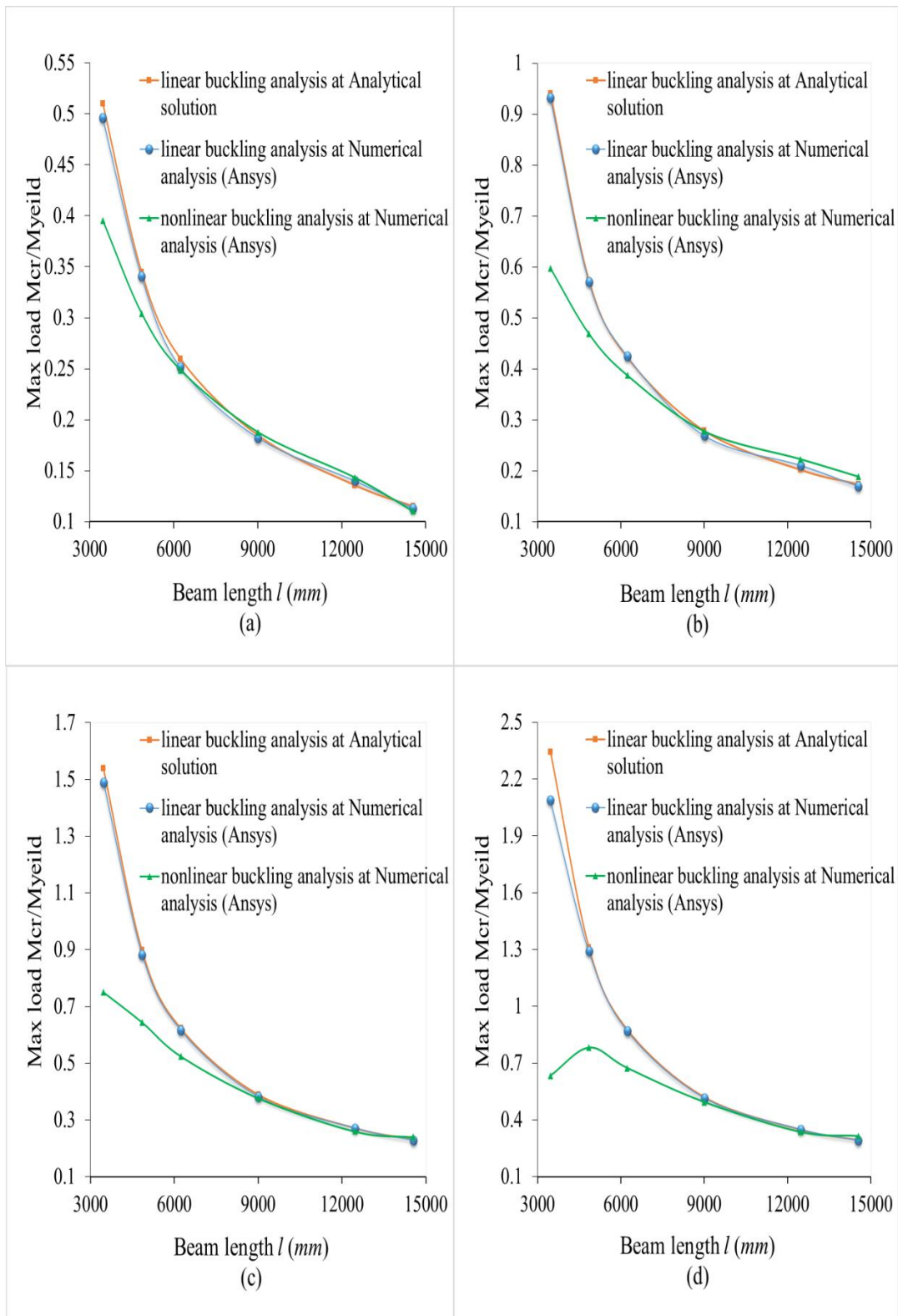
Figure 5-12 Comparison of critical moments (M_{cr}/M_{yield}) of lateral-torsional buckling of simply supported castellated beam subjected to a uniformly distributed load, obtained from linear analytical solutions, linear 3D finite element analysis using ANSYS, and nonlinear 3D finite element analysis (geometric nonlinear and material inelasticity) for groups C, E, G, H, I, and J beams with various flange widths (a) bf =100 mm , (b) bf =150 mm , (c) bf =200 mm , and (d) bf =250 mm)
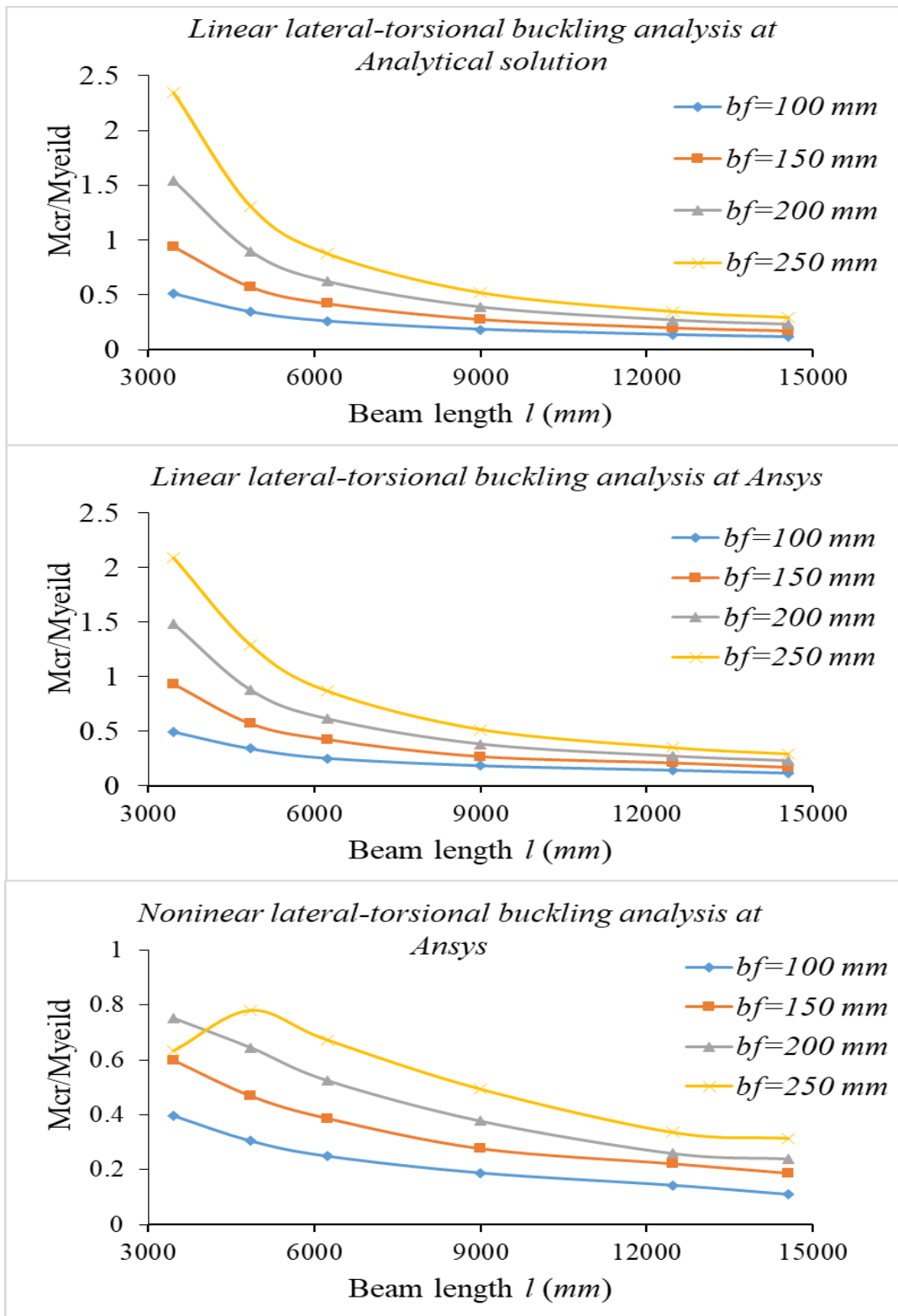
Figure 5-13 Comparison of critical moments (M_{cr}/M_{yield}) of lateral-torsional buckling of simply supported castellated beam subjected to a uniformly distributed load, obtained from linear analytical solutions, linear 3D finite element analysis using ANSYS, and nonlinear 3D finite element analysis (geometric nonlinear and material inelasticity) using ANSYS software for groups C, E, G, H, I, and J beams with various flange width.
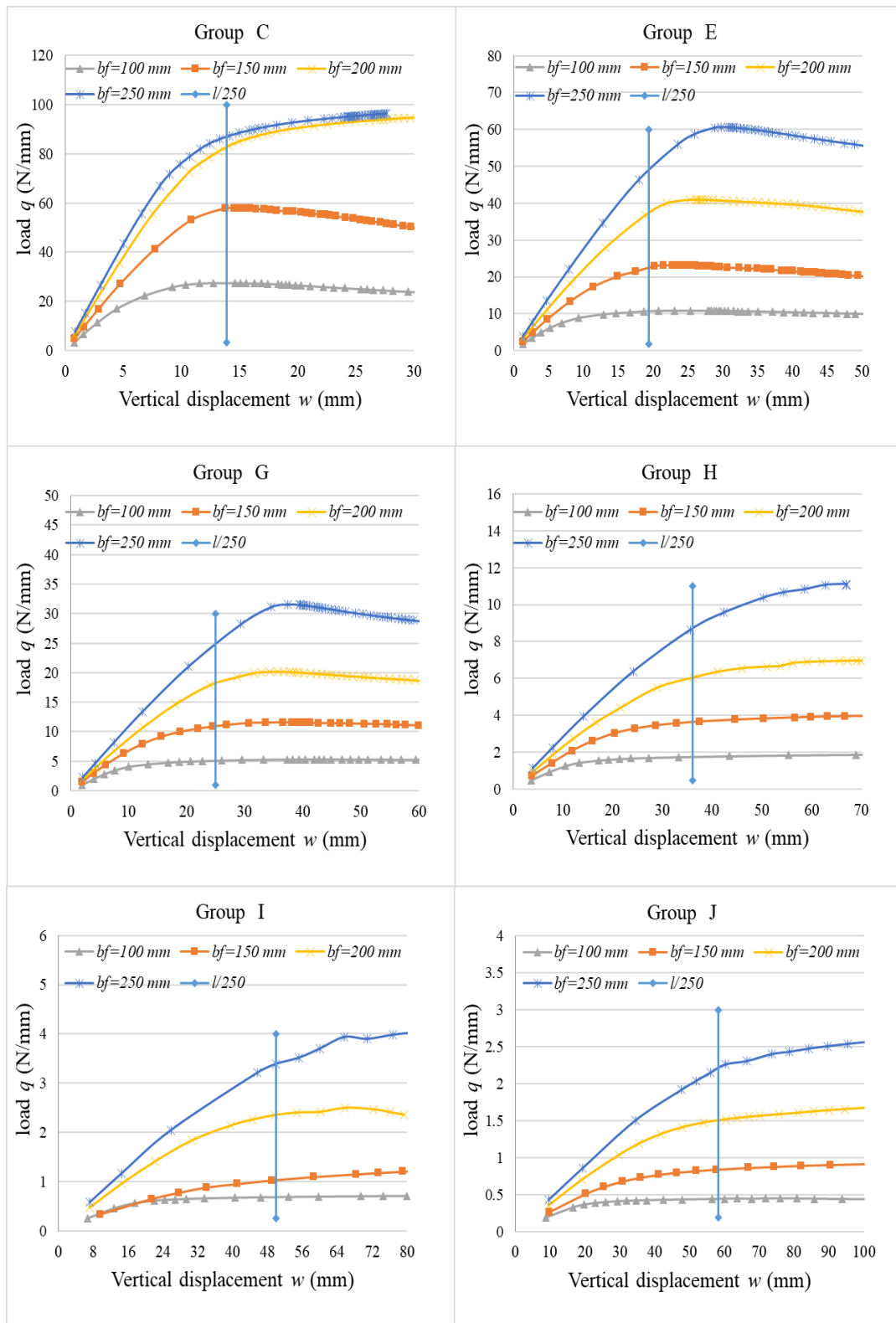
Figure 5-14 Comparison of the load-deflection curves of simply supported castellated beams subjected to a uniformly distributed load, obtained from nonlinear 3D finite element analysis and deflection limit (l/250) for groups C, E, G, H, I and J beams with various flange widths.
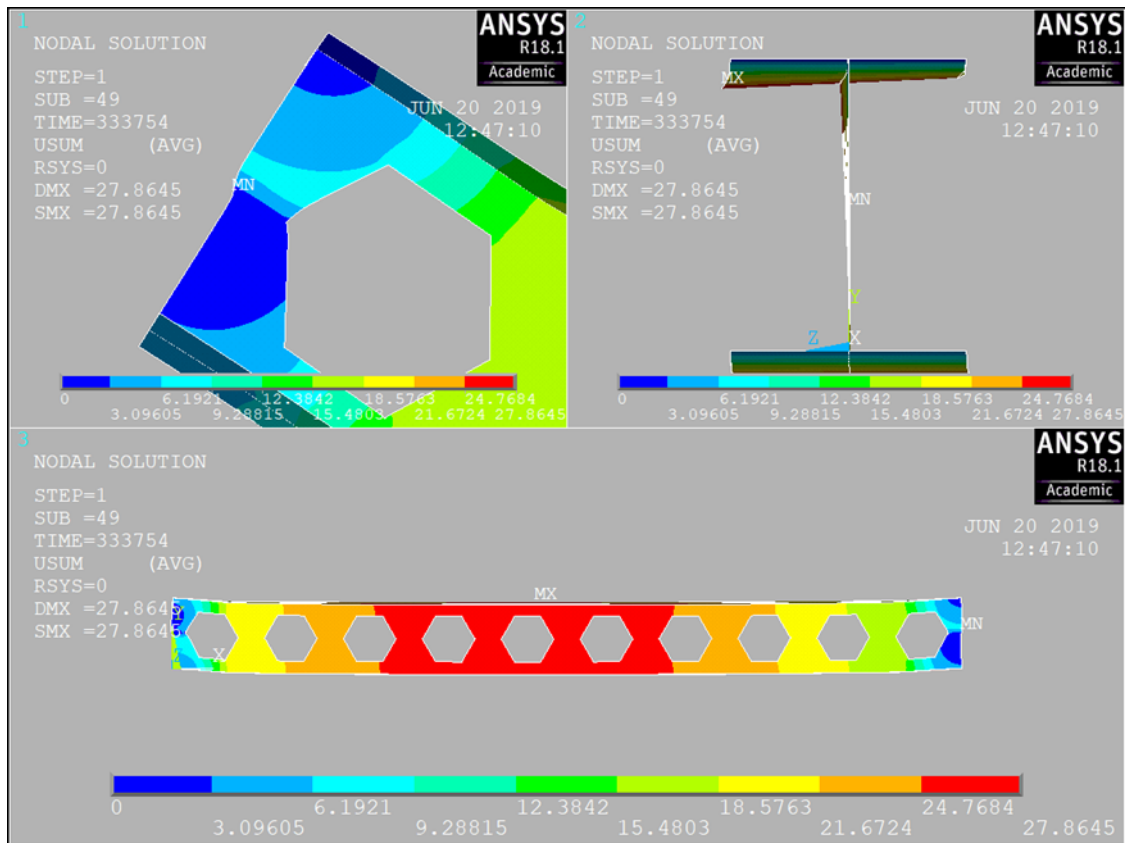
Figure 5-15 Failure mode of simply support castellated beam subjected to a uniformly distributed load (C4) with flange widths bf=250mm obtained from the nonlinear lateral-torsional buckling 3D finite element analysis using ANSYS software (h_w=$3$00mm, t_f=10mm, t_w=8mm and a=100mm)

5.5.3. Comparison of critical moments of lateral-torsional bucking of pinned-fixed beams subjected to uniformly distributed load

Table (5-4) shows the comparison of critical moments of lateral-torsional buckling of pinned-fixed castellated beams subjected to uniformly distributed load. This comparison involves the results of linear analytical solutions, which are developed in chapter four, linear 3D finite element analysis using ANSYS, and nonlinear 3D finite element analysis (geometric nonlinear and material inelasticity) using ANSYS software for groups C, E, G, H, I, and J beams with different flange widths (see Section 3.3.4), in which the value of linear critical lateral-torsional buckling moment (M_{cr}) was obtained by Eq. (4-34), tabulated under term linear lateral-torsional buckling analytical analysis. The results that are determined by linear finite element analysis are tabulated under term linear lateral-torsional buckling analysis by ANSYS software, and the results that are determined by nonlinear finite element analysis are tabulated under term nonlinear

lateral-torsional buckling analysis by ANSYS software. Moreover, the yield moment is obtained by $M_{yield} = \frac{2\sigma_y I_{reduced}}{h_w + 2t_f}$, ($\sigma_y = 275 \frac{N}{mm^2}$, $I_{reduced}$ is obtained by following Eq. (3-17)), where it is tabulated under term (M_{yield}).The results shown in table are plotted in **Figures 5-16** and **5-17**, respectively.

From these figures, it can be seen that in each group of flange width, the curves of the analytical solution and numerical analysis of both linear and nonlinear have a similar variation pattern. In other words, the analytical solution is in excellent agreement with numerical analysis by ANSYS for all models of castellated beams. However, it is observed from these figures that in the case of nonlinear analysis of castellated beams, the critical lateral-torsional buckling load (M_{cr}/M_{yield}) drops with the increase of the flange width and the decrease of beam length. The previous studies mentioned that the reason for this is that lateral-torsional buckling load is influenced by the lateral flexural and warping rigidities (Mohebkhah, 2011). In this study, the increasing flange width leads firstly to increase lateral flexural and warping rigidities, and secondly to increase the moments on castellated beams. These items indicate that the nonlinear lateral-torsional buckling resistance of castellated beams with short beam length is limited by the ultimate load carrying capacity, in which no lateral-torsional buckling occurs. In addition, the web opening under high loads makes the castellated beam more prone to compression buckling of web; and failure can occur in local loading areas or reaction force region (Kerdal and Nethercot, 1984).

Figure 5-18 shows a comparison of the load-deflection curves of pinned-fixed castellated beams. The comparison involves the results of nonlinear 3D finite element analysis using ANSYS software, and deflection limit (*l*/250) for groups C, E, G, H, I and J beams with different flange widths (see Section 3.3.4). The load is presented as the increments of load calculated following by Eq. (3-31). This latter reflects that the critical lateral-torsional buckling for short beam length with wide flange is influenced by geometry, web openings, boundary conditions, and material properties of the beam. As a result, the designer should consider a nonlinear analysis for short castellated beams with wide flange for design calculations. The failure mode of short castellated beams is dominated by the plastic failure, whereas the failure mode of long castellated beams is dominated by the lateral-torsional buckling failure mode, that is observed in

Figure 5-19 which obtained from the numerical analysis for the beam of length ($l = 3.5$ m) with wide flange width ($b_f = 200$ mm and $b_f = 250$mm).

The figures show there is a significant difference between the linear solution and nonlinear solution, particularly for short beams. The reason for this is because for the short beams the failure load predicted by the linear solution is controlled purely by the elastic buckling which is much higher than the yield load. While in the nonlinear analysis, the failure load is controlled by the plastic/buckling load. While the long beams usually fail by elastic buckling (the stress is lower than the yield stress) and this is why the linear and nonlinear solutions give almost the same result for long beams but not for the short beams.

Table 5-4 Comparison of lateral-torsional buckling results of pinned-fixed castellated beams subjected to a uniformly distributed load obtained from linear and nonlinear analysis

| b_f mm	Name of beam	Myield N.mm x10^7	Linear buckling analytical analysis			Linear buckling analysis by Ansys			Nonlinear buckling analysis by Ansys		
			qcr N/mm	Mcr N.mm x10^7	$\frac{Mcr}{Myield}$	qcr N/mm	Mcr N.mm x10^7	$\frac{Mcr}{Myield}$	qcr N/mm	Mcr N.mm x10^7	$\frac{Mcr}{Myield}$
100	C1	10.44	80.43	12.06	1.16	79.31	11.90	1.14	50.85	7.63	0.73
	E1	10.44	25.79	7.58	0.73	26.02	7.65	0.73	22.10	6.50	0.62
	G1	10.44	11.55	5.61	0.54	11.78	5.73	0.55	11.64	5.66	0.54
	H1	10.44	3.80	3.89	0.40	4.12	4.17	0.41	4.34	4.40	0.42
	I1	10.44	1.49	2.89	0.28	1.59	3.13	0.30	1.99	3.86	0.29
	J1	10.44	0.92	2.43	0.23	0.91	2.40	0.23	1.20	3.18	0.25
150	C2	14.57	233.13	34.97	2.40	207.30	31.09	2.13	81.97	12.30	0.84
	E2	14.57	68.29	20.08	1.38	66.07	19.42	1.33	41.66	12.25	0.84
	G2	14.57	28.47	13.84	0.95	28.31	13.76	0.94	22.47	10.90	0.75
	H2	14.57	8.50	8.62	0.59	8.84	8.96	0.62	8.41	8.53	0.59
	I2	14.57	3.10	6.03	0.41	3.15	6.12	0.42	3.10	6.03	0.41
	J2	14.57	1.95	5.17	0.35	1.94	5.13	0.35	1.98	5.24	0.36
200	C3	18.70	522.91	78.44	4.19	372.75	55.91	3.00	85.71	12.85	0.69
	E3	18.70	146.00	42.92	2.30	134.80	39.63	2.12	58.37	17.16	0.92
	G3	18.70	58.07	28.22	1.51	56.53	27.48	1.47	35.16	17.09	0.91
	H3	18.70	16.07	16.30	0.87	16.57	16.80	0.90	13.98	14.18	0.76
	I3	18.70	5.53	10.75	0.57	5.60	10.88	0.58	5.92	11.51	0.62
	J3	18.70	3.41	9.02	0.48	3.43	9.07	0.48	3.52	9.32	0.50
250	C4	22.83	998.80	149.82	6.56	391.17	58.67	2.60	87.40	13.11	0.57
	E4	22.83	272.04	79.98	3.50	230.52	67.77	2.97	69.84	20.53	0.90
	G4	22.83	105.29	51.17	2.24	101.64	49.40	2.16	48.11	23.38	1.02
	H4	22.83	27.64	28.03	1.23	28.11	28.51	1.25	22.36	22.67	0.99
	I4	22.83	9.04	17.57	0.77	9.12	17.73	0.78	9.29	18.06	0.79
	J4	22.83	5.55	14.68	0.64	5.75	15.21	0.67	5.18	13.71	0.60
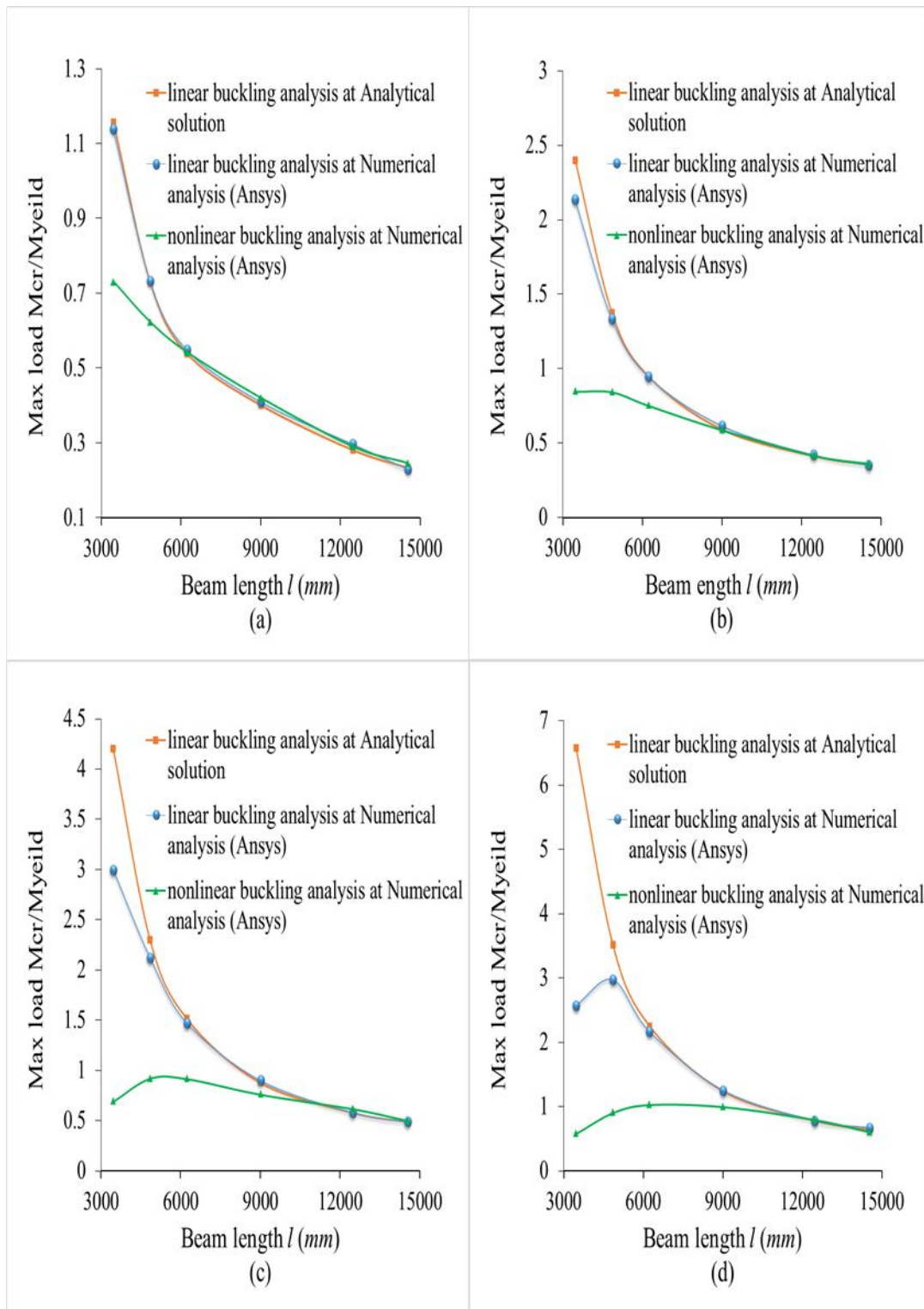
Figure 5-16 Comparison of critical moments (M_{cr}/M_{yield}) of lateral-torsional buckling of pinned-fixed castellated beams subjected to a uniformly distributed load, obtained from linear analytical solutions, linear 3D finite element analysis using ANSYS, and nonlinear 3D finite element analysis (geometric nonlinear and material inelasticity) using ANSYS software for groups C, E, G, H, I, and J beams with various flange widths (a) bf =100 mm ,(b) bf =150 mm ,(c) bf =200 mm , and (d) bf =250 mm
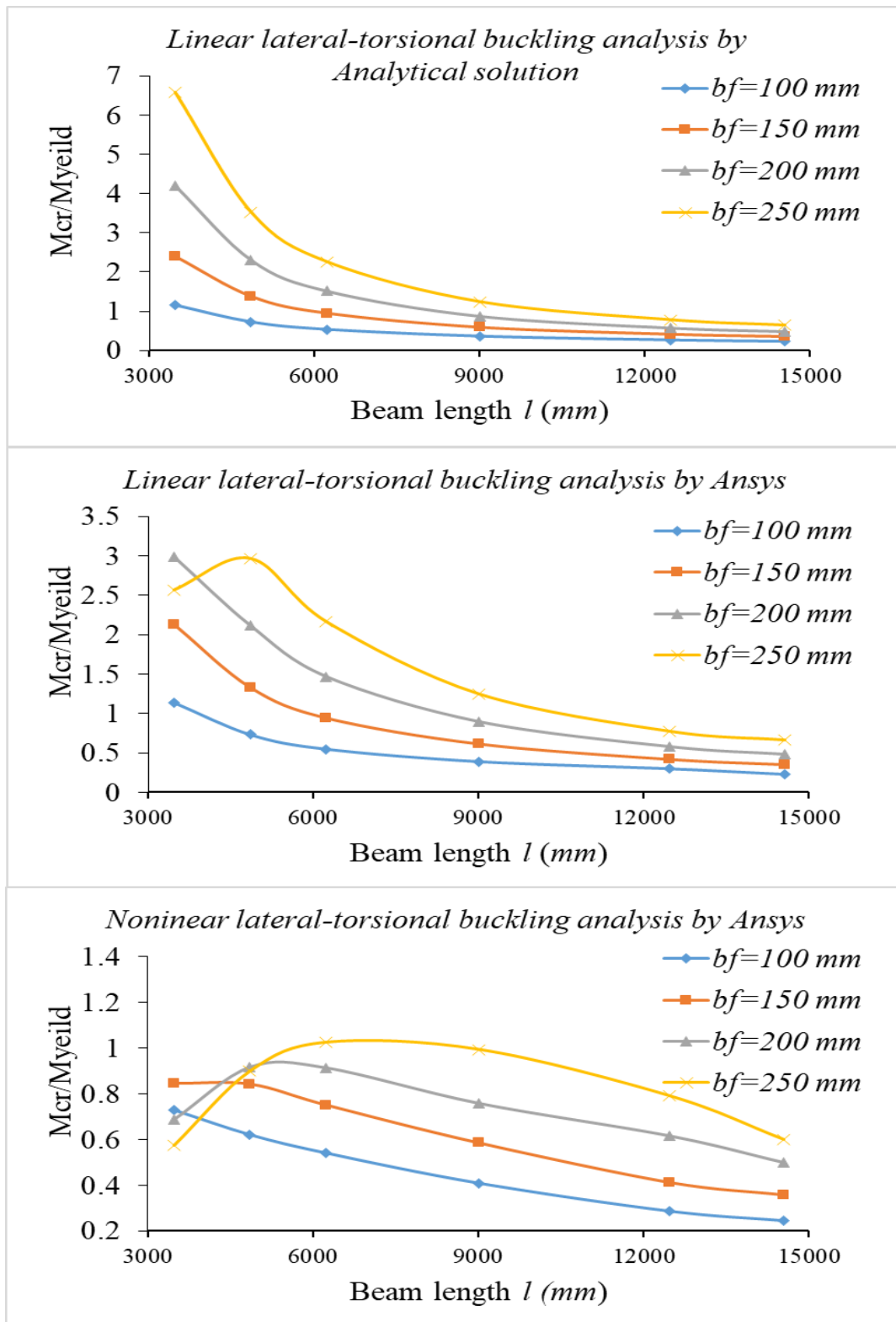
Figure 5-17 Comparison of critical moments (M_{cr}/M_{yield}) of lateral-torsional buckling of pinned-fixed castellated beams subjected to a uniformly distributed load, obtained from linear analytical solutions, linear 3D finite element analysis using ANSYS, and nonlinear 3D finite element analysis (geometric nonlinear and material inelasticity) using ANSYS software for groups C, E, G, H, I, and J beams with various flange widths.
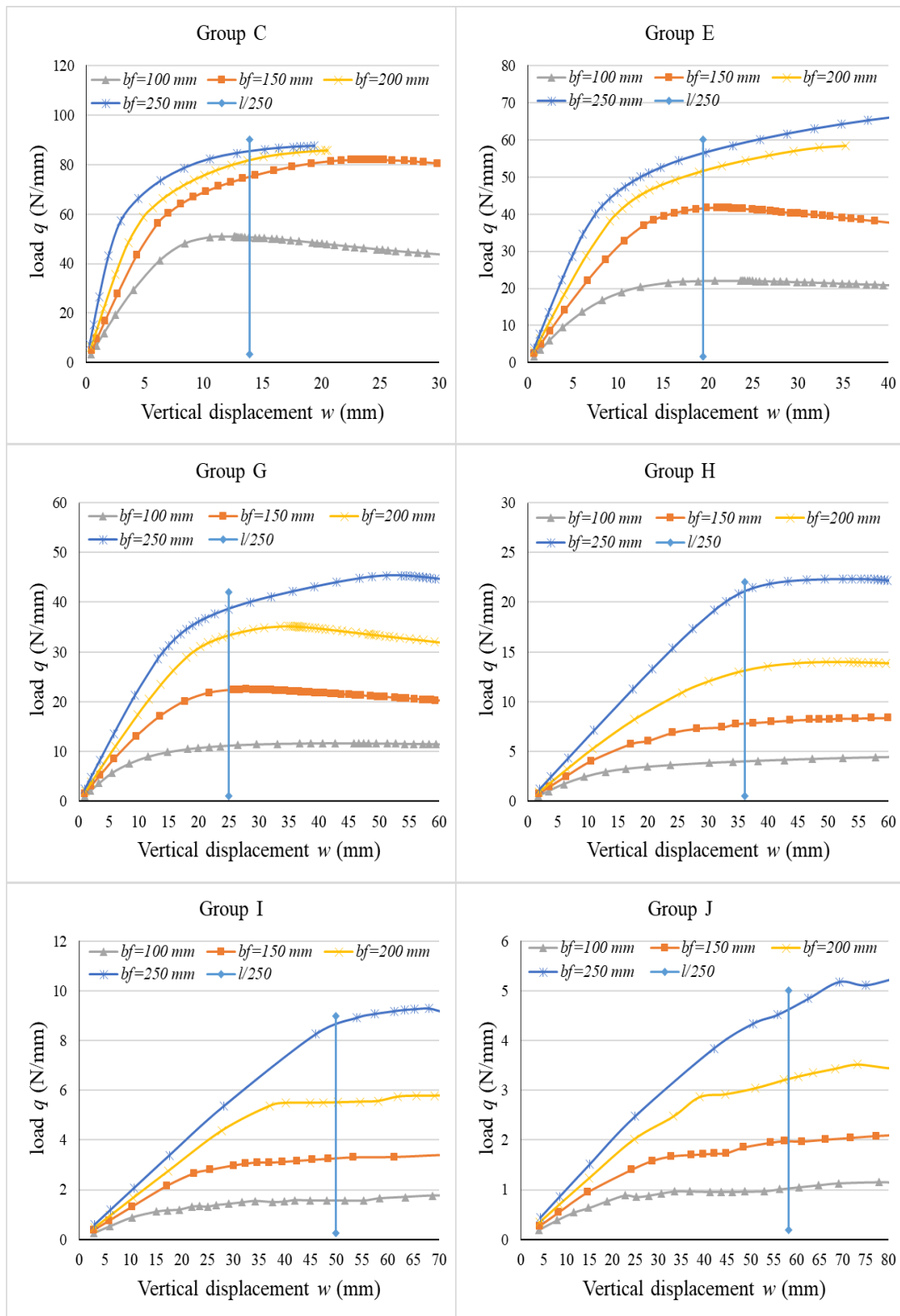
Figure 5-18 Comparison of the load-deflection curves of pinned-fixed castellated beams subjected to a uniformly distributed load, obtained from nonlinear 3D finite element analysis, and deflection limit (*l*/250) for groups C, E, G, H, I and J beams with various flange widths.
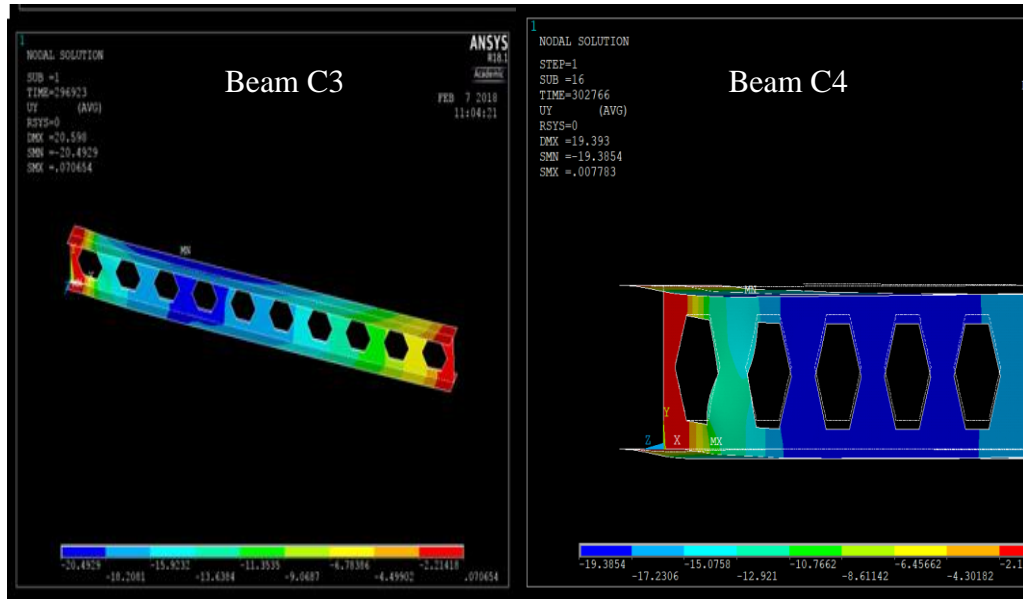
Figure 5-19 Combined failure modes of pinned-fixed castellated beams subjected to a uniformly distributed load (C3 and C4) with two flange widths bf=200mm and bf=250mm obtained from the nonlinear lateral-torsional buckling 3D finite element analysis using ANSYS software (h_w=300mm, t_f=10mm, t_w=8mm and a=100mm)

5.6. Conclusions

In this chapter, geometric nonlinear and material nonlinear analysis by using finite element method has been carried out to investigate the behaviour of pinned-pinned and pinned-fixed castellated beams subjected to uniformly distributed load at the inelastic range. Comparison has been made between the result of the linear and nonlinear analyses. The main conclusions can be summarized as follows:

➢ The load carrying capacity of castellated beams obtained by nonlinear 3D finite element analysis is influenced by the geometry, web openings, boundary conditions, and material properties of the beams.

➢ The load carrying capacity of castellated beams obtained by using the nonlinear 3D finite element analysis is generally less than that obtained by using the linear analysis method. This reflects that the elastic range is unsafe for short length beams with wide flange width.

➢ The critical moments of lateral-torsional buckling of castellated beams obtained by using nonlinear 3D finite element analysis are influenced by the geometry, web openings, boundary conditions, and mechanical properties of the beams.

➢ The critical moment of lateral-torsional buckling of castellated beams obtained by using nonlinear 3D finite element analysis are generally less than those obtained using the linear analysis methods. This indicates that the elastic range is unsafe for short length beams with wide flange.

➢ The nonlinear lateral-torsional buckling resistance of castellated beam with the short beam length under high loads is limited by the ultimate load carrying capacity of the beams, in which case no lateral-torsional buckling occurs.

➢ In nonlinear analysis, increasing castellated beam length leads to beam behaviour that will be similar to that in the linear analysis, and the lateral-torsional buckling mode will dominate the failure mode.

➢ When the serviceability is also considered, the deflection limit seems to be the dominant criterion in controlling the load in most of the beam length regions.

CHAPTER SIX

6. DYNAMIC INSTABILITY OF CASTELLATED BEAMS UNDER TRANSVERSE PERIODIC LOADING

6.1. Introduction

In this chapter, an analytical solution is developed to investigate the free vibration, static buckling and dynamic instability of castellated beams subjected to transverse periodic loading. Bolotin's method is used to perform the dynamic instability analysis that is utilized in this study. By assuming the instability modes, the mass, stiffness, and geometric stiffness matrices are derived using the kinetic energy, strain energy and potential of applied loads. Analytical equations for determining the free vibration frequency, critical buckling moment, and excitation frequency of castellated beams are derived, In addition, the influences of the flange width of the castellated beam and the static part of the applied load on the variation of dynamic instability zones are discussed.

6.2. The studies about dynamic instability

Literature survey on structural members shows that little research has been carried out on the dynamic instability of castellated beams when the applied load varies with time. In many countries, the static load still dominates the current designing of structures for castellated beams, in spite of the significance of the dynamic response to machinery loading and to extreme environmental loads, for example wind and earthquakes, that have been considered for some time. It is acknowledged that applying static load can lead to free vibration behaviour of the structural members, which causes a decrease in the critical load of buckling of the members. For this reason, we should understand the effect of applying the dynamic load on the structure behaviour to avoid resonance disasters due to the dynamic instability.

As a result, limited research and studies exist on the dynamics, especially the dynamic instability of the castellated beams subjected to transverse loading. Since 1960 research has been carried out on the vibration-induced buckling of beams. For instance:

Morris (1965) investigated the nonlinear vibration problem of a two hinged beam-column subjected to a harmonic load of any space distribution

In 1966, Hsu carried out the investigation of the dynamic stability of the elastic body with given initial conditions and reported the necessary and sufficient stability criteria in terms of trajectories in the phase space of finite dimension.

 Huang (1980) and Chen et al. (1991) used the Bolotin's method to examine the dynamic instability of generally orthotropic beams and thick bi-modulus beams subjected to periodic axial loads, respectively.

Huang and Hung (1984) used the averaging method and the Routh-Hurwitz stability to study the dynamic instability of a simply supported beam under periodic axial excitation. The coupling of the first two modes was considered to investigate the instability regions and vibration amplitudes.

Gürgöze (1985) conducted an investigation into the instability behaviour of a pre-twisted beam subjected to a pulsating axial force. They used the Mettler method and derived the equations describing the instability regions that could be applied with various different boundary conditions.

A finite element dynamic instability model of Timoshenko beams was introduced by Park (1987) that adopted the extended Hamilton's principle to build the equation of the beam transverse motion in the plane.

Kar and Sujata (1991) examined the dynamic instability of rotating beams with various different boundary conditions, subjected to a pulsating axial excitation. As well, they also discussed the effects of the boundary conditions, rotational speed on the static buckling loads and the regions of parametric instability.

Numerous of the papers Uang, and. Fan (2001); Yoon, and. Kim (2002) have been presented to study the influence of various different supporting boundary conditions on the dynamic instability behaviour of beams

Yeh et al. (2004) used both the finite element method and the harmonic balance method to present a study of the dynamic instability problem of a sandwich beam with a constrained layer and an electro rheological fluid core subjected to an axial dynamic force. Moreover, this study discussed the influences of the natural frequencies and static buckling loads on the dynamic instability behaviour.

Zhu et al. (2017) conducted an analytical solution to examine the free vibration, static buckling and dynamic instability of laterally-restrained zed-section purlin beams under uplift wind loading. They used the classical principle of minimum potential energy which assumed the instability modes, the kinetic energy and strain energy of the beam and the loss of the potential energy of the applied load are evaluated, from which the mass, stiffness and geometric stiffness matrices of the system are derived.

More recently, Zhu et al. (2018) presented a study on the dynamic buckling of cold-formed steel channel section beams under the action of uniformly distributed loading.

Gao et al. (2019) provided a nondeterministic dynamic stability assessment of Euler–Bernoulli beams using Chebyshev surrogate model.

6.3.   Governing equations for dynamic instability analysis of castellated beams

The analysis model used for this study is illustrated in **Figure 6-1 (a).** The cross-section of the castellated beam is assumed to be doubly symmetric, with the flange width and thickness as b_f and t_f, the web depth and thickness as h_w and t_w, and the half depth of hexagons as a. The half of the distance between the centroids of the two T-sections is e. The side length of the hexagonal opening is $\left(\frac{2a}{\sqrt{3}}\right)$, and the hexagonal opening height is $2a$, respectively.

According to **Figure 6-1 (b)**, the lateral and transverse displacements of the beam are assumed to be *v(x)*, *w(x)*, respectively, and the angle of twist of the cross-section is $\phi(x)$. In the linear situation, the strain energy of the beam involves two parts; the strain energy generated by the bending and the energy generated by the twist.

In order to consider the warping influence, the cross-section of the castellated beam is decomposed into three parts, two of which represent the top and bottom T-section, one of which represents the middle-part of the web. It is assumed that the displacements at the shear centers of the top and bottom T-sections are small and can be expressed as follows (see **Figure 6-1**) :(Kim et al., 2016)

$$v_1(x) = v(x) + \frac{h}{2}\phi(x) \qquad\qquad 6\text{-}1$$

$$v_2(x) = v(x) - \frac{h}{2}\phi(x) \qquad\qquad 6\text{-}2$$

$$w_1(x) = w + \frac{h}{2}(1 - cos\phi) \approx w \qquad\qquad 6\text{-}3$$

$$w_2(x) = w + \frac{h}{2}(1 - cos\phi) \approx w \qquad\qquad 6\text{-}4$$

where v_1 and v_2 are the lateral displacements of the shear centre of the top and bottom T-section, w_1 and w_2 are the transverse displacements of the shear centre of the top and bottom T-section, h is the distance between the shear centres of top and bottom T-sections. Hence, the kinetic energy T of castellated beam due to the transverse displacement, lateral displacement and rotation thus can be expressed as:

The kinetic energy for the top T- section:

$$T_{top} = \frac{\rho A_{tee}}{2}\int_0^l (\dot{v_1}^2 + \dot{w_1}^2)dx + \frac{\rho I_{ptop}}{2}\int_0^l \dot{\phi}^2\, dx \qquad\qquad 6\text{-}5$$

The kinetic energy for the bottom T- section:

$$T_{bot} = \frac{\rho A_{tee}}{2}\int_0^l (\dot{v_2}^2 + \dot{w_2}^2)dx + \frac{\rho I_{pbot}}{2}\int_0^l \dot{\phi}^2\, dx \qquad\qquad 6\text{-}6$$

The kinetic energy for the middle part between the two T- sections

$$T_{web} = \frac{\rho 2at_w}{2} \int_0^l (\dot{v}^2 + \dot{w}^2)dx + \frac{\rho I_{pweb}}{2} \int_0^l \dot{\phi}^2\, dx \qquad\qquad 6\text{-}7$$

Hence, the total kinetic energy of the beam is:

$$T = \frac{\rho}{2}\left[A_{tee}\left[\int_0^l (\dot{v_1}^2 + \dot{w_1}^2)dx + \int_0^l (\dot{v_2}^2 + \dot{w_2}^2)dx \right] \right.$$
$$\left. + at_w \int_0^l (\dot{v}^2 + \dot{w}^2)dx + I_p \int_0^l \dot{\phi}^2\, dx \right] \qquad\qquad 6\text{-}8$$

where ρ the density, l is the beam length, $A_{tee}=b_f t_f + t_w\left(\frac{h_w}{2} - a\right)$ is the cross-section area of the T-section, $I_p = I_{ptop} + I_{pweb} + I_{pbot}$ is the polar moment of inertia. Note that the dot above a symbol in above equations represents the derivative of the symbol with respect to time.

The strain energy of castellated beam that is determined based on the three parts due to the transverse displacement, lateral displacement and rotation. It thus can be written as follows:

$$U_s = \frac{1}{2}\int_0^l \left[EI_{y1}\left(\frac{d^2 w_1}{dx^2}\right)^2 + EI_{z1}\left(\frac{d^2 v_1}{dx^2}\right)^2 + GJ_1\left(\frac{d\phi}{dx}\right)^2 \right] dx$$
$$+ \frac{1}{2}\int_0^l \left[EI_{y2}\left(\frac{d^2 w_2}{dx^2}\right)^2 + EI_{z2}\left(\frac{d^2 v_2}{dx^2}\right)^2 + GJ_2\left(\frac{d\phi}{dx}\right)^2 \right] dx \qquad 6\text{-}9$$
$$+ \frac{1}{2}\int_0^l \left[EI_{y3}\left(\frac{d^2 w_3}{dx^2}\right)^2 + EI_{z3}\left(\frac{d^2 v_3}{dx^2}\right)^2 + GJ_3\left(\frac{d\phi}{dx}\right)^2 \right] dx$$

where U_s is the strain energy, E is the Young's modulus, G is the shear modulus. $I_{y1} = I_{y2}$ and $I_{z1} = I_{z2}$ are the second moments of the T- sectional area about the y and z axes. $J_1 = J_2$ is the torsional constant of the tee-section, I_{y3} and I_{z3} are the second moments of the cross-sectional area of the mid-part of the web about the y and z axes respectively, and J_3 is the torsional constant of the mid-part of the web.

Hence, the formula of the strain energy of castellated beam (top T- section, bottom T- section and mid-part of the web) can be written as follows:

$$U = \frac{1}{2} \int_0^l \left[2EI_{y1} \left(\frac{d^2w_1}{dx^2} \right)^2 + 2EI_{z1} \left(\frac{d^2v_1}{dx^2} \right)^2 \right.$$
$$\left. + \frac{h^2}{2} EI_{z1} \left(\frac{d^2\phi}{dx^2} \right)^2 + 2GJ_1 \left(\frac{d\phi}{dx} \right)^2 \right] dx$$
$$+ \frac{1}{2} \int_0^l \left[EI_{y3} \left(\frac{d^2w_2}{dx^2} \right)^2 + EI_{z3} \left(\frac{d^2v_2}{dx^2} \right)^2 + GJ_3 \left(\frac{d\phi}{dx} \right)^2 \right] dx \qquad \text{6-10}$$

According to **Figure 6-1**, I_{y1}, I_{z1} and J_1 are constants, whereas I_{y3}, I_{z3} and J_3 are the function of x and depending upon the location of the web openings. Hence, from the comparison between equation of the strain energy of an I-beam without web openings and Eq. (6-10), the following relations can be obtained:

$$I_y = 2I_{y1} + I_{y3} \qquad \text{6-11}$$

$$I_z = 2I_{z1} + I_{z3} \qquad \text{6-12}$$

$$I_w = \left(\frac{h}{2} \right)^2 I_z \approx \frac{h^2}{2} I_{z1} \qquad \text{6-13}$$

$$J = 2J_1 + J_3 \qquad \text{6-14}$$

$$I_p = I_y + I_z = 2I_{y1} + 2I_{z1} + kI_{y3} + kI_{z3} \qquad \text{6-15}$$

According to Kim.et al. (2016) k refers to the fraction of the volume of the solid and holes in the mid-part of the web. In castellated beams, because of matching of the areas and holes in the mid-part of the web, the value of k=0.5.

Assume that the transverse load is the periodic load applying on the top flange of castellated beam when the sheeting is fixed with the top flange (e.g. for wind-induced vibration). In this case, the loss of potential energy V of the transverse load q_z can be expressed as follows:

$$V = \int_0^l \left[M_y \phi \left(\frac{d^2v}{dx^2} \right) + \frac{a_z q_z}{2} \phi^2 \right] dx \qquad \text{6-16}$$

where q_z is the distribution load, M_y is the pre-buckling internal bending moment, and a_z refers to the z-coordinate of the loading point, which is equal to the distance between the loading point and the shear centre of the beam. In the present case, $a_z = \frac{h_w}{2} + t_f$ because the uniformly distributed load is applied on the top flange of the beam. The second term in Eq. (6-16) is attributed to the effect of loading position, which, in the present case, has a positive effect on the stability of the beam and thus will increase the critical buckling load.

According to the Lagrange method, the equations of motion describing the lateral-torsional buckling of the beam can be expressed as follows: (Massachusetts Institute of Technology, 2003)

$$\frac{d}{dt}\left(\frac{\partial L}{\partial \dot{q}}\right) - \frac{\partial L}{\partial q} = 0 \qquad \text{6-17}$$

where $L = T - (U - V)$ is the Lagrangian function and $q = \{q_1, q_2, q_3\}^T$ is the general displacement vector. Substituting Eqs (6-1)-(6-4), (6-8), (6-10) and (6-16) into (6-17), the governing equation for the dynamic instability analysis of a castellated beam is obtained, as follows: (Kratzig and Nawrotzki, 1991; Li, 1991; and Patel et al., 2006).

$$[\mathbf{M}]\{\ddot{\mathbf{q}}\} + [\mathbf{K}]\{\mathbf{q}\} - \lambda[\mathbf{K_g}]\{\mathbf{q}\} = \{\mathbf{0}\} \qquad \text{6-18}$$

where **[M]** is the mass matrix, **[K]** is the elastic stiffness matrix, **[Kg]** is the geometric stiffness matrix, $\{\ddot{\mathbf{q}}\}$ is the generalized acceleration vector, is the general displacement vector, and λ is the loading factor. The mass, stiffness, and geometric stiffness matrices are expressed as follows:

$$[\mathbf{M}] = \begin{bmatrix} \frac{\partial^2 T}{\partial \dot{q}_1^2} & \frac{\partial^2 T}{\partial \dot{q}_1 \partial \dot{q}_2} & \frac{\partial^2 T}{\partial \dot{q}_1 \partial \dot{q}_3} \\ \frac{\partial^2 T}{\partial \dot{q}_2 \partial \dot{q}_1} & \frac{\partial^2 T}{\partial \dot{q}_2^2} & \frac{\partial^2 T}{\partial \dot{q}_2 \partial \dot{q}_3} \\ \frac{\partial^2 T}{\partial \dot{q}_3 \partial \dot{q}_1} & \frac{\partial^2 T}{\partial \dot{q}_3 \partial \dot{q}_2} & \frac{\partial^2 T}{\partial \dot{q}_3^2} \end{bmatrix} \qquad \text{6-19}$$

$$[\mathbf{K}] = \begin{bmatrix} \dfrac{\partial^2 U}{\partial q_1^2} & \dfrac{\partial^2 U}{\partial q_1\, \partial q_2} & \dfrac{\partial^2 U}{\partial q_1\, \partial q_3} \\[2ex] \dfrac{\partial^2 U}{\partial q_2\, \partial q_1} & \dfrac{\partial^2 U}{\partial q_2^2} & \dfrac{\partial^2 U}{\partial q_2\, \partial q_3} \\[2ex] \dfrac{\partial^2 U}{\partial q_3\, \partial q_1} & \dfrac{\partial^2 U}{\partial q_3\, \partial q_2} & \dfrac{\partial^2 U}{\partial q_3^2} \end{bmatrix}$$

6-20

$$[\mathbf{K}_g] = \begin{bmatrix} \dfrac{\partial^2 V}{\partial q_1^2} & \dfrac{\partial^2 V}{\partial q_1\, \partial q_2} & \dfrac{\partial^2 V}{\partial q_1\, \partial q_3} \\[2ex] \dfrac{\partial^2 V}{\partial q_2\, \partial q_1} & \dfrac{\partial^2 V}{\partial q_2^2} & \dfrac{\partial^2 V}{\partial q_2\, \partial q_3} \\[2ex] \dfrac{\partial^2 V}{\partial q_3\, \partial q_1} & \dfrac{\partial^2 V}{\partial q_3\, \partial q_2} & \dfrac{\partial^2 V}{\partial q_3^2} \end{bmatrix}$$

6-21

Assume that the externally applied load q_z is periodic, in which case the loading factor can be divided into two parts as expressed as follows:

$$\lambda = \lambda_s + \lambda_t \, cos\Omega t$$

6-22

Where λ_s and λ_t are the amplitudes of the static and dynamic parts, respectively, Ω is the excitation frequency of the dynamic part of the load, and t is the time.

The dynamic instability regions of the structure described by Eq. (6-18) can be calculated by investigating periodic solutions with the periods of T=2π/Ω and 2T=4π/Ω. The solution with the period of 2T is of particular importance, representing the primary instability region of the structure, which can be expressed using the form of trigonometric series given by:

$$\{q\} = \sum_{k=1,3,\dots} \left[\{a_k\}sin\frac{k\Omega t}{2} + \{b_k\}cos\frac{k\Omega t}{2} \right]$$

6-23

where $\{a_k\}$ and $\{b_k\}$ are the vectors of coefficients of the assumed solution. Substituting Eqs. (6-22) and (6-23) into (6-18) and letting the coefficients of the series associated with sin (Ωt/2) and cos (Ωt/2) be zero, it yields:

$$\left([\mathbf{K}] - \frac{2\lambda_s - \lambda_t}{2} [\mathbf{K}_g] - \frac{\Omega^2}{4} [\mathbf{M}] \right) \{a_1\} = \{0\}$$

6-24

$$\left([\mathbf{K}] - \frac{2\lambda_s + \lambda_t}{2} [\mathbf{K}_g] - \frac{\Omega^2}{4} [\mathbf{M}] \right) \{b_1\} = \{0\} \qquad \text{6-25}$$

For given values of λ_s and λ_t one can calculate the two frequencies of Ω from Eqs. (6-24) and (6-25), which represent the boundary of dynamic instability region of the castellated beams under periodic loading.

6.4. Simply supported, doubly symmetric castellated beam subjected to periodic loads on top flange

For the calculation due to the dynamic lateral-torsional buckling, the displacement functions $w(x)$, $v(x)$, $\phi(x)$ and pre-buckling internal bending moment $M_y(x)$ that satisfy the boundary conditions of a simply supported beam can be assumed as follows:

$$v(x) = q_1(t)\sin\frac{\pi x}{l} \qquad \text{6-26}$$

$$w(x) = q_2(t)\sin\frac{\pi x}{l} \qquad \text{6-27}$$

$$\phi(x) = q_3(t)\sin\frac{\pi x}{l} \qquad \text{6-28}$$

$$M_y(x) = \frac{q_z x(l - x)}{2} \qquad \text{6-29}$$

where $q_i(t)$ ($i = 1,2,3$) are the functions of time.

Therefore, the mass, stiffness, and geometric stiffness matrices for simply supported beam are obtained from Eqs. (6-19)- (6-21) and are expressed as follows:

$$[\mathbf{M}] = \begin{bmatrix} m_{11} & 0 & 0 \\ 0 & m_{22} & 0 \\ 0 & 0 & m_{33} \end{bmatrix} \qquad \text{6-30}$$

where:

$$m_{11} = m_{22} = \rho l(at_w + A_{tee}) \ , \quad m_{33} = \rho l \left(\frac{A_{tee}h^2}{4} + \frac{I_p}{2} \right)$$

$$[\mathbf{K}] = \begin{bmatrix} \kappa_{11} & 0 & 0 \\ 0 & \kappa_{22} & 0 \\ 0 & 0 & \kappa_{33} \end{bmatrix}$$

6-31

where:

$$\kappa_{11} = \frac{El(2I_{z1} + kI_{z3})}{2} \left(\frac{\pi}{l}\right)^4$$

$$\kappa_{22} = \frac{El(2I_{y1} + kI_{y3})}{2} \left(\frac{\pi}{l}\right)^4$$

$$\kappa_{33} = \frac{EI_w l}{2} \left(\frac{\pi}{l}\right)^4 + \frac{Gl(2J_1 + kJ_3)}{2} \left(\frac{\pi}{l}\right)^2$$

$$[\mathbf{K}_g] = \begin{bmatrix} 0 & 0 & \kappa_{g13} \\ 0 & 0 & 0 \\ \kappa_{g31} & 0 & \kappa_{g33} \end{bmatrix}$$

6-32

where:

$$\kappa_{g13} = \kappa_{g31} = -\frac{q_z l}{8} \left(\frac{\pi^2}{3} + 1\right), \; \kappa_{g33} = -\frac{a_z q_z l}{2}$$

6.4.1. The free vibration analysis

The free vibration analysis frequency of the lateral-torsional vibration of the castellated beam can be determined using Eq. (6-33):

$$\|[\mathbf{K}] - \omega^2 [\mathbf{M}]\| = 0$$

6-33

where $\boldsymbol{\omega}$ is the free vibration frequency. Substituting Eqs. (6-30) and (6-31) into (6-33), the following frequency can be obtained:

$$\omega_1 = \left(\frac{\pi}{l}\right)^2 \sqrt{\frac{E(2I_{z1} + kI_{z3})}{2\rho(at_w + A_{tee})}}$$

6-34

$$\omega_2 = \left(\frac{\pi}{l}\right)^2 \sqrt{\frac{E(2I_{y1} + kI_{y3})}{2\rho(at_w + A_{tee})}}$$

6-35

$$\omega_3 = \left(\frac{\pi}{l}\right)^2 \sqrt{\frac{2\left(EI_w + \frac{Gl^2}{\pi^2}(2J_1 + kJ_3)\right)}{\rho\left(A_{tee}h^2 + 2I_p\right)}} \qquad \text{6-36}$$

I_{z3}^* can be negligible because in most of castellated beams $I_{z3}^* << 2I_{z1}$, then Eqs. (6-34), (6-35) and (6-36) can be simplified as follows: (Kim et al., 2016)

$$\omega_1 = \left(\frac{\pi}{l}\right)^2 \sqrt{\frac{E(2I_{z1})}{2\rho(at_w + A_{tee})}} \qquad \text{6-37}$$

$$\omega_2 = \left(\frac{\pi}{l}\right)^2 \sqrt{\frac{E\left(2I_{y1}\right)}{2\rho(at_w + A_{tee})}} \qquad \text{6-38}$$

$$\omega_3 = \left(\frac{\pi}{l}\right)^2 \sqrt{\frac{2\left(EI_w + \frac{Gl^2}{\pi^2}(2J_1 + kJ_3)\right)}{\rho\left(A_{tee}h^2 + 2(I_{z1} + I_{y1})\right)}} \qquad \text{6-39}$$

The above formulations (6-37), (6-38) and (6-39) calculate the natural frequencies, which are well known and can be found from many vibration textbooks. These equations represent the translational and rotational vibrations of castellated beams. Moreover, it indicates that the lateral vibration and torsional vibration modes are influenced by web openings.

6.4.2. Buckling analysis

The critical load of the lateral-torsional buckling of the castellated beam subjected to a static load can be calculated using Eq. (6-40):

$$\left\|[\mathbf{K}] - \lambda_{cr}[\mathbf{K}_g]\right\| = 0 \qquad \text{6-40}$$

where λ_{cr} is the loading factor and $q_{cr} = \lambda_{cr}q_o$ is the critical load for static buckling.

Substituting Eqs. (6-31) and (6-32) into (6-40), the following critical load is obtained:

$$\lambda_{cr} = -\frac{K_{11}K_{g33} \pm \sqrt{K_{11}^2 K_{g33}^2 + 4K_{g13}^2 K_{11} K_{33}}}{2K_{g13}^2} \qquad \text{6-41}$$

$$\left(\frac{q_z l^2}{8}\right)_{cr} = \frac{\left(\left(\frac{h_w}{2} + t_f\right) + \sqrt{\left(\frac{h_w}{2} + t_f\right)^2 + \frac{1}{4}\left(I_w + \frac{G(2J_1 + kJ_3)}{E}\left(\frac{l}{\pi}\right)^2\right)\left(\frac{\pi^2}{3} + 1\right)^2 \times \frac{1}{(2I_{z1} + I_{z3})}}\right)}{\left(\frac{1}{3} + \frac{1}{\pi^2}\right)^2} \qquad \text{6-42}$$
$$\times \frac{2E(2I_{z1} + I_{z3})}{l^2}$$

$$\left(\frac{q_z l^2}{8}\right)_{cr} = \frac{\left(\left(\frac{h_w}{2} + t_f\right) + \sqrt{\left(\frac{h_w}{2} + t_f\right)^2 + \frac{1}{4}\left(I_w + \frac{G(2J_1 + kJ_3)}{E}\left(\frac{l}{\pi}\right)^2\right)\left(\frac{\pi^2}{3} + 1\right)^2 \times \frac{1}{(2I_{z1})}}\right)}{\left(\frac{1}{3} + \frac{1}{\pi^2}\right)^2} \times \frac{2E(2I_{z1})}{l^2} \qquad \text{6-43}$$

It can be noticed that Eq. (6-43) is similar to the formulation of the critical load given in (Kim et al., 2016) for simply supported castellated beams when the load is applied at the top flange.

6.4.3. The dynamic instability

The dynamic instability region of the castellated beam can be calculated using Eq. (6-44):

$$\left\| [K] - \frac{2\lambda_s \pm \lambda_t}{2}[K_g] - \frac{\Omega^2}{4}[M] \right\| = 0 \qquad \text{6-44}$$

Substituting Eqs. (6-30), (6-31) and (6-32) into (6-44), it yields:

$$\frac{\Omega^2}{4} = \frac{(K_{33}^* m_{11} + K_{11} m_{33}) \pm \sqrt{(K_{11} m_{33} - K_{33}^* m_{11})^2 + 4\left(\frac{2\lambda_s \pm \lambda_t}{2}\right)^2 K_{g13}^2 m_{33} m_{11}}}{2m_{33} m_{11}} \qquad \text{6-45}$$

where

$$K_{33}^* = K_{33} - \frac{2\lambda_s \pm \lambda_t}{2} K_{g33}$$

It can be seen, four different equations given by Eq. (6-45) which represents four different Ω values can be obtained, where the value of Ω^2 is associated with vibration modes, which were illustrated in the free vibration analysis shown in Section 6.4.1.

6.4.4. Comparison of the dynamic instability of simply supported beams due to transverse periodic loading

Table (6-1) gives the dimensions and material properties of four various flange width, (*bf* =100 mm, *bf* =150 mm, *bf* =200 mm, and *bf* =250 mm) of castellated beams discussed herein. The analytical solution to determine the natural frequencies was obtained directly from Eqs. (6-37), (6-38) and (6-39) while the critical loads were obtained by Eq. (6-43).

Furthermore, Eq. (6-45) calculated the dynamic instability regions of castellated beam for various span lengths (small, middle, large and very large) (see **Table (6-1)**) under a transverse periodic load applied at the top flange of the beam. The results are plotted in **Figures 6-2, 6-3, 6-4, 6-5, 6-6, 6-7, 6-8** and **6-9** respectively.

Figures 6-2, 6-3, and **6-4** present the variation of the frequencies of lateral vibration, vertical vibration and rotational vibration of the beams of different flange widths versus the beam length. The three figures correspond to the 1st, 2nd and 3rd vibration modes.

From these figures it can be observed that, for each vibration mode, the frequency curves have a similar variation pattern. In addition, the beam length and the flange width influence the frequencies. Increasing the beam length causes reductions in the frequencies. In contrast, the larger flange width gives the greater frequencies. Furthermore, it can be seen from the figures that the frequency of the lateral vibration is slightly higher than the frequency of the rotational vibration of the beam but a little higher than the frequency of the vertical vibration of the castellated beam.

Figure 6-5 plots the critical load curves of the beams of different flange widths subjected to the transverse static load applying on the top flange, where the critical

moment has been calculated using the yield moment, is obtained by $M_{yield} = \frac{2\sigma_y I_{reduced}}{h_w + 2t_f}$, ($I_{reduced}$ is obtained by following Eq. (3-17)). It can be noticed, as expected, that for each beam the increase of beam length causes the reduction of the critical moment.

Figures 6-6, 6-7, 6-8, and **6-9** show the dynamic instability zones of the simply support castellated beam with four different flange widths, subjected to a transverse periodic load applied at the top flange of the beams, in which the geometric stiffness matrix is assessed using the static critical load, that is $(q_{yield} = q_{cr})$, where $(q_{yield} = \frac{2\sigma_y I_{reduced}}{l^2(h_w + 2t_f)})$. The four figures correspond to four different beam lengths as indicated in **Table (6-1)**. It can be observed from these figures that, the dynamic instability regions of the four beams all exhibit a "v" shape in despite of having different flange widths. With the increase of beam length, the dynamic instability zone not only moves towards to higher frequency side but its width is also expanded. In contrast, where the beam length is the same, the width of the dynamic instability zone decreases with the increase of the flange width.

The figures of the variation of the frequencies, curve of the critical load and the dynamic instability zones of castellated beams have the same patterns with those computed in previous studies by Plaut (2017); Zhu et al. (2017); and Zhu et al. (2018). However, a quantitative comparison is not mentioned because the beams are different between this study (castellated beams) and previous studies (cold-formed steel beams).

Table 6-1 Dimensions and properties of four various flange widths (*bf* =100 mm, *bf* =150 mm, *bf* =200 mm, and *bf* =250 mm) castellated beams[*]

t_f mm	h_w mm	t_w mm	a mm	E MPa	ρ kg/m^3	σ_y MPa	G MPa	v
10	300	8	100	2.1×10^5	7800	275	78750	0.3

Note[*]: Dynamic instability analysis uses four different beam lengths. They are 4.156m; 6.235 m; 9.006 m and 14.549 m
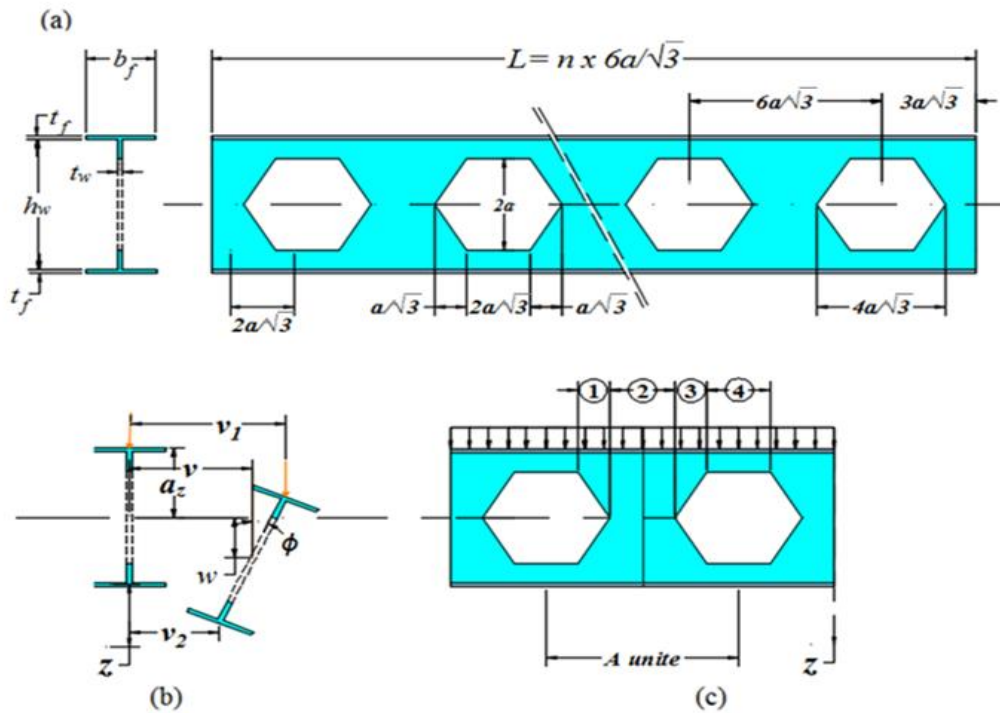
Figure 6-1 (a) Notations is used in castellated beams. **(b)** Loading and displacements of web and displacement of flanges when lateral–torsional buckling occurred **(c)** Section properties of middle-part of web in four different regions. $I_{y3} = I_{y3}^*$, $I_{z3} = I_{z3}^*$, $J_3 = J_3^*$ in region 2, in region 4,$I_{y3} = I_{z3} = J_3 = 0$, section properties vary with x in regions 1 and 3.
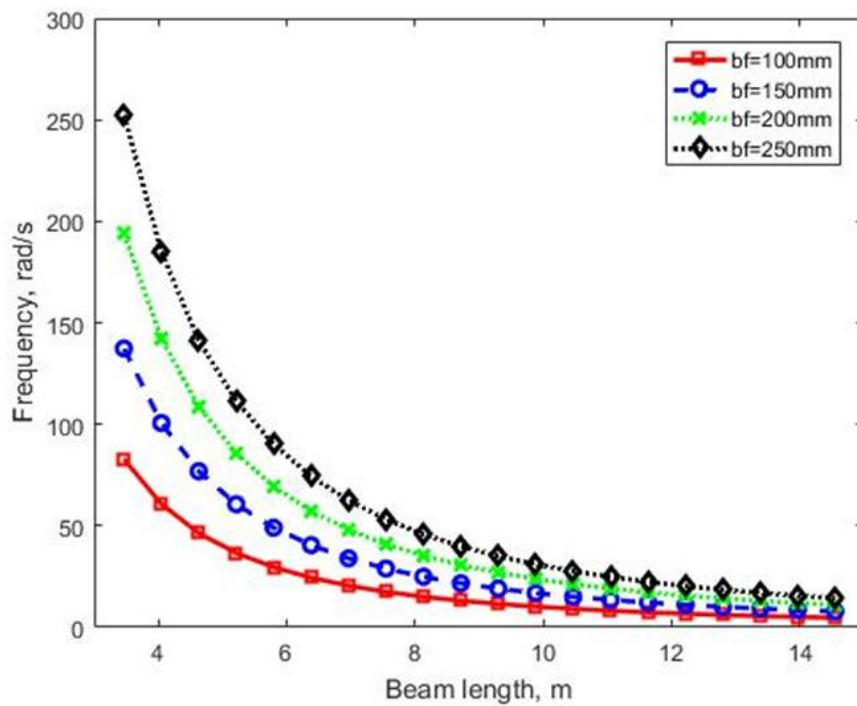
Figure 6-2 Comparison of frequencies of simply support castellated beams with different flange widths (1st mode)
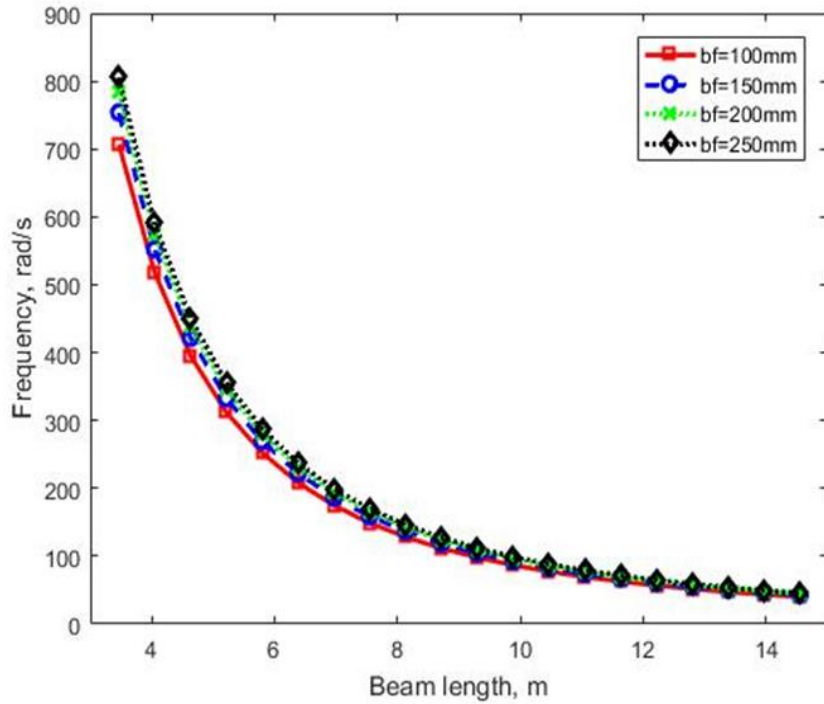
Figure 6-3 Comparison of frequencies of simply support castellated beams with different flange widths (2nd mode)
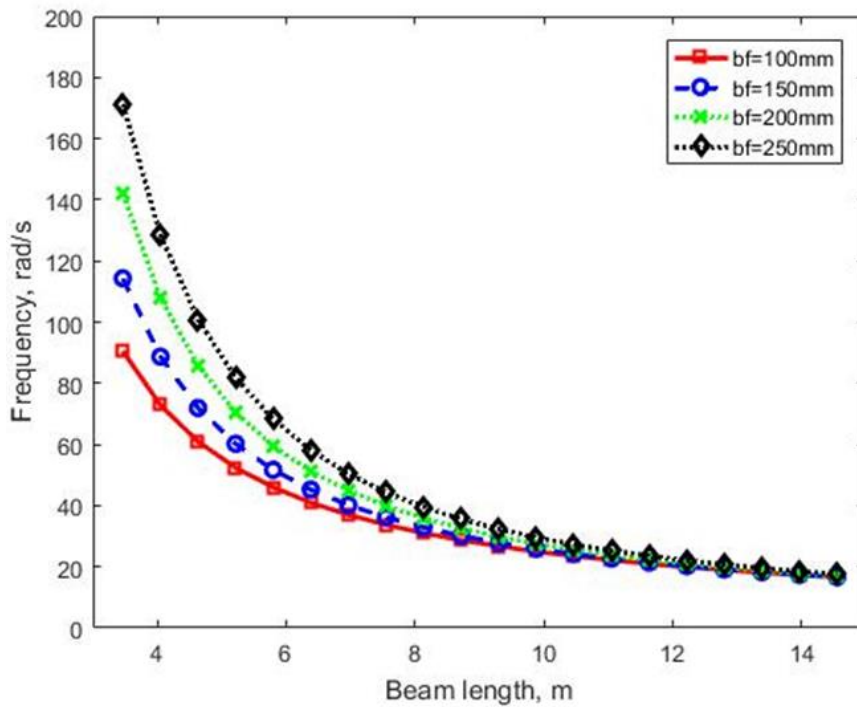
Figure 6-4 Comparison of frequencies of simply support castellated beams with different flange widths (3rd mode)
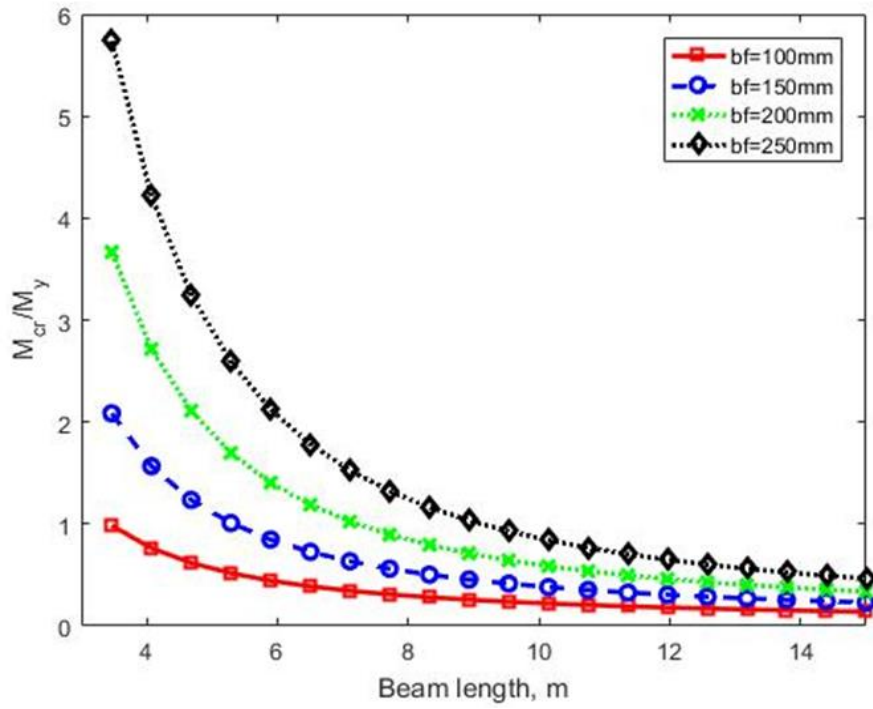
Figure 6-5 Comparison of critical buckling moments of simply support castellated beam with different flange widths
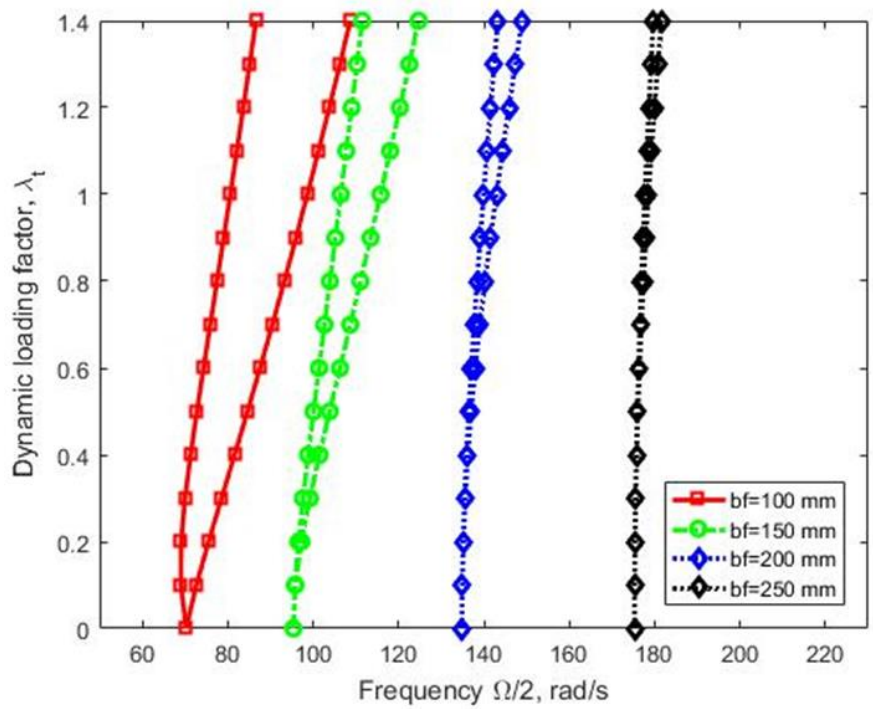
Figure 6-6 Comparison of dynamic instability regions of simply support castellated beam (l = 4.156 m) ($q_{yield} = q_{cr}$ and λ_s=0)
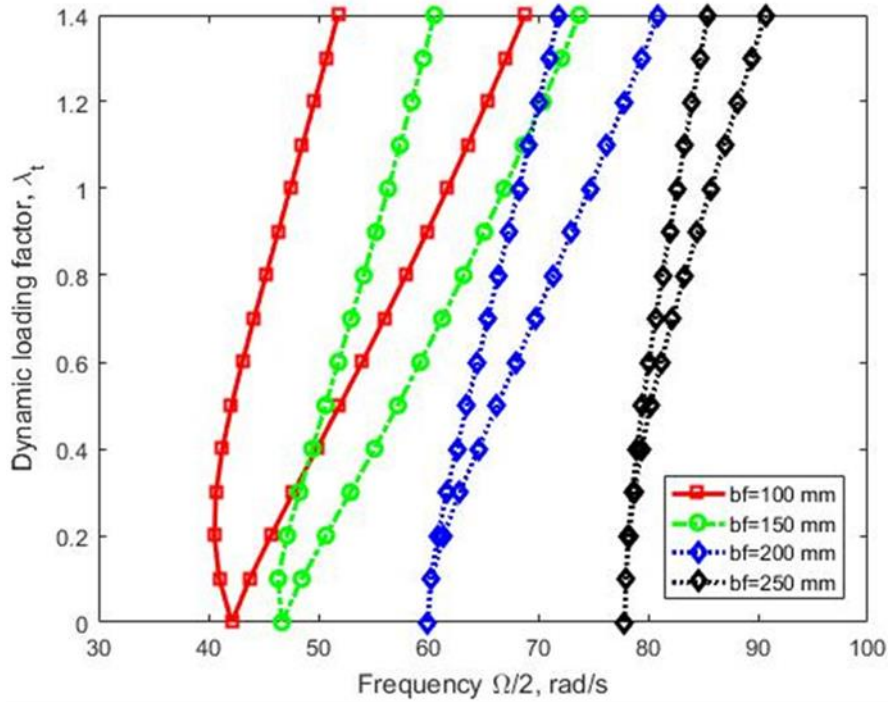
Figure 6-7 Comparison of dynamic instability regions of simply support castellated beam
(l = 6.235 m) ($q_{yield} = q_{cr}$ and λ_s=0)
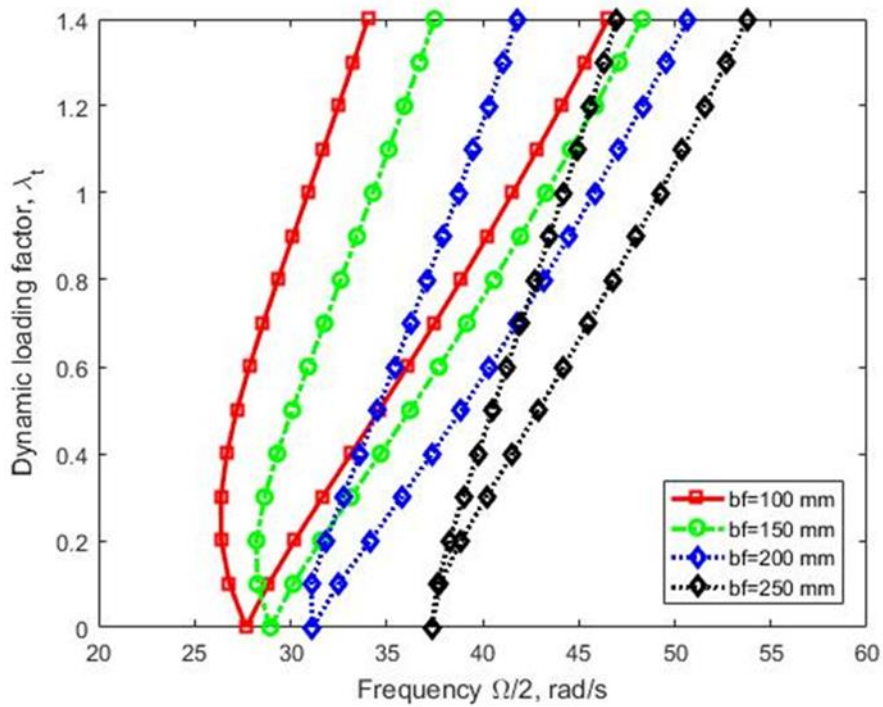
Figure 6-8 Comparison of dynamic instability regions of simply support castellated beam
(l = 9.006 m) ($q_{yield} = q_{cr}$ and λ_s=0)
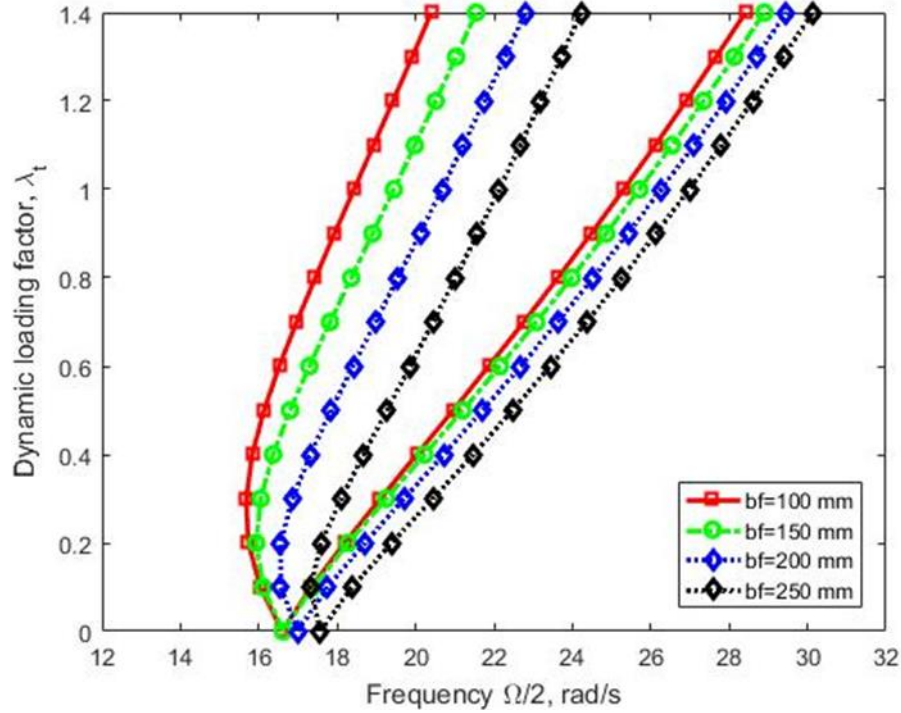
Figure 6-9 Comparison of dynamic instability regions of simply support castellated beam
($l = 14.549$ m) ($q_{yield} = q_{cr}$ and λ_s=0)

6.5. Pinned–fixed doubly symmetric castellated beam subjected to periodic loads on top flange

For the calculation due to the dynamic lateral-torsional buckling, the displacement functions $w(x)$, $v(x)$, $\phi(x)$ and pre-buckling internal bending moment $M_y(x)$ that satisfy the boundary conditions of a pinned-fixed beam can be assumed as follows:

$$v(x) = q_1(t)sin\frac{\pi(l-x)}{l}sin\frac{\pi(l-x)}{2l} \qquad\qquad 6\text{-}46$$

$$w(x) = q_2(t)sin\frac{\pi(l-x)}{l}sin\frac{\pi(l-x)}{2l} \qquad\qquad 6\text{-}47$$

$$\phi(x) = q_3(t)sin\frac{\pi(l-x)}{l}sin\frac{\pi(l-x)}{2l} \qquad\qquad 6\text{-}48$$

$$M_y(x) = \frac{q_z x}{2}\left(\frac{3l}{4} - x\right) \qquad\qquad 6\text{-}49$$

where $q_i(t)$ $(i = 1,2,3)$ are the functions of time.

Therefore, the mass, stiffness, and geometric stiffness matrices for pinned-fixed beam are obtained from Eqs. (6-19)- (6-21) and are expressed as follows:

$$[\mathbf{M}] = \begin{bmatrix} m_{11} & 0 & 0 \\ 0 & m_{22} & 0 \\ 0 & 0 & m_{33} \end{bmatrix} \qquad\qquad 6\text{-}50$$

where:

$$m_{11} = m_{22} = \frac{\rho l (a t_w + A_{tee})}{2} \quad, \quad m_{33} = \frac{\rho l}{2}\left(\frac{A_{tee} h^2}{4} + I_p\right)$$

$$[\mathbf{K}] = \begin{bmatrix} \kappa_{11} & 0 & 0 \\ 0 & \kappa_{22} & 0 \\ 0 & 0 & \kappa_{33} \end{bmatrix} \qquad\qquad 6\text{-}51$$

where:

$$\kappa_{11} = \frac{41El(2I_{z1} + kI_{z3})}{64}\left(\frac{\pi}{l}\right)^4$$

$$\kappa_{22} = \frac{41El\left(2I_{y1} + kI_{y3}\right)}{64}\left(\frac{\pi}{l}\right)^4$$

$$\kappa_{33} = \frac{41EI_w l}{64}\left(\frac{\pi}{l}\right)^4 + \frac{5Gl(2J_1 + kJ_3)}{16}\left(\frac{\pi}{l}\right)^2$$

$$[\mathbf{K}_g] = \begin{bmatrix} 0 & 0 & \kappa_{g13} \\ 0 & 0 & 0 \\ \kappa_{g31} & 0 & \kappa_{g33} \end{bmatrix} \qquad\qquad 6\text{-}52$$

where:

$$\kappa_{g13} = \kappa_{g31} = -\frac{q_z l}{8}\left(\frac{\pi^2}{3} + 1\frac{1}{8}\right), \kappa_{g33} = -\frac{a_z q_z l}{4}$$

6.5.1. The free vibration analysis

The free vibration analysis frequency of the lateral-torsional vibration of the castellated beam can be determined using Eq. (6-53):

$$\|[\mathbf{K}] - \omega^2[\mathbf{M}]\| = 0 \qquad\qquad 6\text{-}53$$

where $\boldsymbol{\omega}$ is the free vibration frequency. Substituting Eqs. (6-50) and (6-51) into (6-53), also, the following frequency can be obtained:

$$\omega_1 = \left(\frac{\pi}{l}\right)^2 \sqrt{\frac{41E(2I_{z1} + kI_{z3})}{32\rho(at_w + A_{tee})}} \qquad \text{6-54}$$

$$\omega_2 = \left(\frac{\pi}{l}\right)^2 \sqrt{\frac{41E(2I_{y1} + kI_{y3})}{32\rho(at_w + A_{tee})}} \qquad \text{6-55}$$

$$\omega_3 = \left(\frac{\pi}{l}\right)^2 \sqrt{\frac{41EI_w + 20\dfrac{Gl^2}{\pi^2}\left(2J_1 + kJ_3\right)}{8\rho\left(A_{tee}h^2 + 2I_p\right)}} \qquad \text{6-56}$$

I_{z3}^* can be negligible because in most of castellated beams $I_{z3}^* \ll 2I_{z1}$, then Eqs. (6-54), (6-55) and (6-56) can be simplified as follows:

$$\omega_1 = \left(\frac{\pi}{l}\right)^2 \sqrt{\frac{41E(2I_{z1})}{32\rho(at_w + A_{tee})}} \qquad \text{6-57}$$

$$\omega_2 = \left(\frac{\pi}{l}\right)^2 \sqrt{\frac{41E(2I_{y1})}{32\rho(at_w + A_{tee})}} \qquad \text{6-58}$$

$$\omega_3 = \left(\frac{\pi}{l}\right)^2 \sqrt{\frac{41EI_w + 20\dfrac{Gl^2}{\pi^2}\left(2J_1 + kJ_3\right)}{8\rho\left(A_{tee}h^2 + 2I_p\right)}} \qquad \text{6-59}$$

The above formulations (6-57), (6-58) and (6-59) give the natural frequencies, which are well known and can be found from many vibration textbooks. These equations represent the translational and rotational vibrations of castellated beams. Moreover, it indicates that the lateral vibration and torsional vibration modes are influenced by web openings.

6.5.2. Buckling analysis

The critical load of the lateral-torsional buckling of the castellated beam subjected to a static load can be calculated using Eq. (6-60):

$$\left\| [\mathbf{K}] - \lambda_{cr}[\mathbf{K}_g] \right\| = 0 \qquad\qquad 6\text{-}60$$

where λ_{cr} is the loading factor and $q_{cr} = \lambda_{cr}q_o$ is the critical moment for static buckling.

Substituting Eqs. (6-51) and (6-52) into (6-60), the following critical load is obtained:

$$\lambda_{cr} = -\frac{K_{11}K_{g33} \pm \sqrt{K_{11}^{2}K_{g33}^{2} + 4K_{g13}^{2}K_{11}K_{33}}}{2K_{g13}^{2}} \qquad\qquad 6\text{-}61$$

$$\left(\frac{q_z l^2}{8}\right)_{cr} = \frac{\left(\left(\frac{h_w}{2}+t_f\right) \;+\; \sqrt{\left(\frac{h_w}{2}+t_f\right)^2 + \left(\frac{5\pi^2+108}{192}\right)^2\left(I_w + \frac{20G(2J_1+kJ_3)}{41E}\left(\frac{l}{\pi}\right)^2\right)\times\frac{1}{(2I_{z1}+kI_{z3})}}\right)}{\left(\frac{5\pi^2+108}{96}\right)^2 l^2} \times \frac{41E(2I_{z1}+kI_{z3})}{32} \qquad\qquad 6\text{-}62$$

$$\left(\frac{q_z l^2}{8}\right)_{cr} = \frac{\left(\left(\frac{h_w}{2}+t_f\right) \;+\; \sqrt{\left(\frac{h_w}{2}+t_f\right)^2 + \left(\frac{5\pi^2+108}{192}\right)^2\left(I_w + \frac{20G(2J_1+kJ_3)}{41E}\left(\frac{l}{\pi}\right)^2\right)\times\frac{1}{(2I_{z1})}}\right)}{\left(\frac{5\pi^2+108}{96}\right)^2 l^2} \times \frac{41E(2I_{z1})}{32} \qquad\qquad 6\text{-}63$$

It can be noticed that Eq. (6-63) is similar to the formulation of the critical load given in this study Section 4.6.2 for pinned-fixed castellated beams when the load is applied at the top flange.

6.5.3. The dynamic instability

The dynamic instability region of the castellated beam can be calculated using Eq. (6-64):

$$\left\| [K] - \frac{2\lambda_s \pm \lambda_t}{2}[K_g] - \frac{\Omega^2}{4}[M] \right\| = 0 \qquad\qquad 6\text{-}64$$

Substituting Eqs. (6-50), (6-51) and (6-52) into (6-64), it yields:

$$\frac{\Omega^2}{4} = \frac{(K_{33}^* m_{11} + K_{11} m_{33}) \pm \sqrt{(K_{11} m_{33} - K_{33}^* m_{11})^2 + 4\left(\frac{2\lambda_s \pm \lambda_t}{2}\right)^2 K_{g13}^{\ 2} m_{33} m_{11}}}{2 m_{33} m_{11}} \qquad \text{6-65}$$

where

$$K_{33}^* = K_{33} - \frac{2\lambda_s \pm \lambda_t}{2} K_{g33}$$

It can be seen that, there are four different equations given by Eq. (6-65), which represent four different Ω values, where the value of Ω^2 is associated with vibration modes, which were illustrated in the free vibration analysis shown in Section 6.5.1

6.5.4. Comparison of the dynamic instability of pinned-fixed beams due to transverse periodic loading

Table (6-1) gives the dimensions and material properties of four various flange width, (*bf* =100 mm, *bf* =150 mm, *bf* =200 mm, and *bf* =250 mm) of castellated beams discussed herein. The analytical solution to determine the natural frequencies was obtained directly from Eqs. (6-57), (6-58) and (6-59), while the critical loads were obtained by Eq. (6-63).

Furthermore, Eq. (6-65) calculated the dynamic instability regions of castellated beam for various span lengths (small, middle, large and very large) (see **Table (6-1)** under a transverse periodic load applied at the top flange of the beam. The results are plotted in **Figures 6-10, 6-11, 6-12**, **6-13, 6-14, 6-15, 6-16** and **6-17** respectively.

Figures 6-10, 6-11, and **6-12** present the variation of the frequencies of lateral vibration, vertical vibration and rotational vibration of the beams of different flange widths versus the beam length of the pinned-fixed castellated beam. The three figures correspond to the 1st, 2nd and 3rd vibration modes.

From these figures it can be observed that, for each vibration mode, the frequency curves have a similar variation pattern. In addition, the beam length and the flange width influence the frequencies. Increasing the beam length causes reductions in the frequencies. In contrast, the larger flange width gives the greater frequencies. Furthermore, it can be seen from the figures that the frequency of the lateral vibration is slightly higher than the frequency of the rotational vibration of the beam but a little higher than the frequency of the vertical vibration of the castellated beam.

Figures 6-13 plots the critical loads curves of the pinned-fixed castellated beam subjected to the transverse periodic load applying on top flange versus the beam length for different flange widths, where the critical moment has been normalized using the yield moment ,$M_{yield} = \frac{2\sigma_y I_{reduced}}{h_w + 2t_f}$, ($I_{reduced}$ is obtained by following Eq. (3-17)). It can be noticed, as expected, that for each beam the increase of beam length causes the reduction of the critical moment.

Figures 6-14, 6-15, 6-16 and **6-17** show the dynamic instability zones of the pinned-fixed castellated beam with four different flange widths, subjected to a transverse periodic load applied at the top flange of the beams, in which the geometric stiffness matrix is assessed using the static critical load that is $(q_{yield} = q_{cr})$ where $(q_{yield} = 16\frac{\sigma_y I_{reduced}}{l^2(h_w + 2t_f)})$. The four figures correspond to four different beam lengths as indicated in **Table (6-1)** It can be observed from these figures that, the dynamic instability regions of the four beams all exhibit a "v" shape in despite of having different flange widths. With the increase of beam length, the dynamic instability zone not only moves towards to higher frequency side but its width is also expanded. In contrast, where the beam length is the same, the width of the dynamic instability zone decreases with the increase the flange width.

The figures of the variation of the frequencies, curve of the critical load and the dynamic instability zones of castellated beams have the same patterns with those computed in previous studies by Plaut (2017); Zhu et al. (2017); and Zhu et al. (2018). However, I did not make a quantitative comparison. This is because the beams are different between ours (castellated beams) and others (cold-formed steel beams).
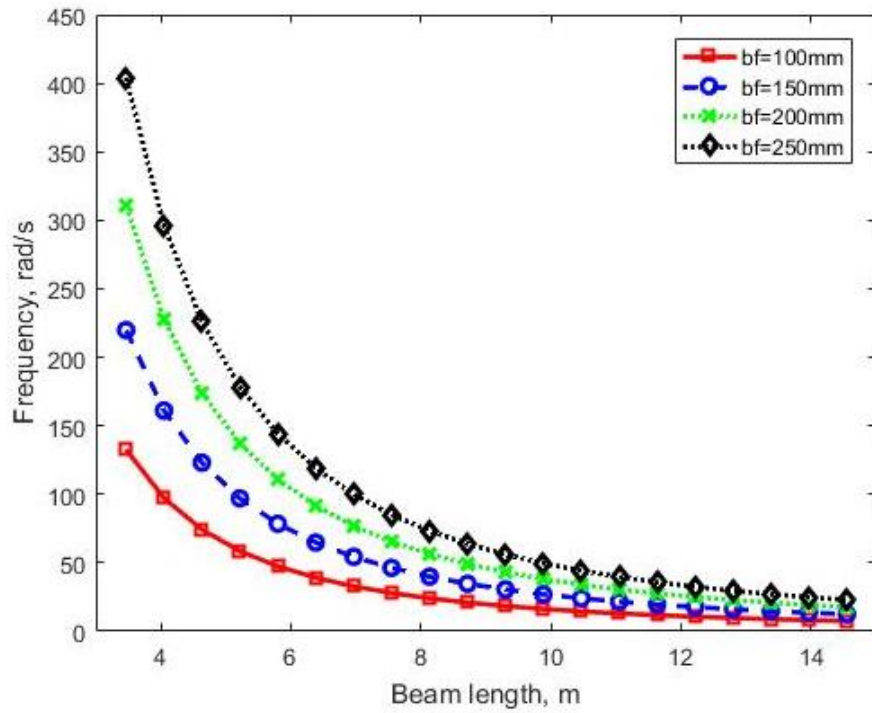
Figure 6-10 Comparison of frequencies of pinned-fixed castellated beams with different flange widths (1st mode)
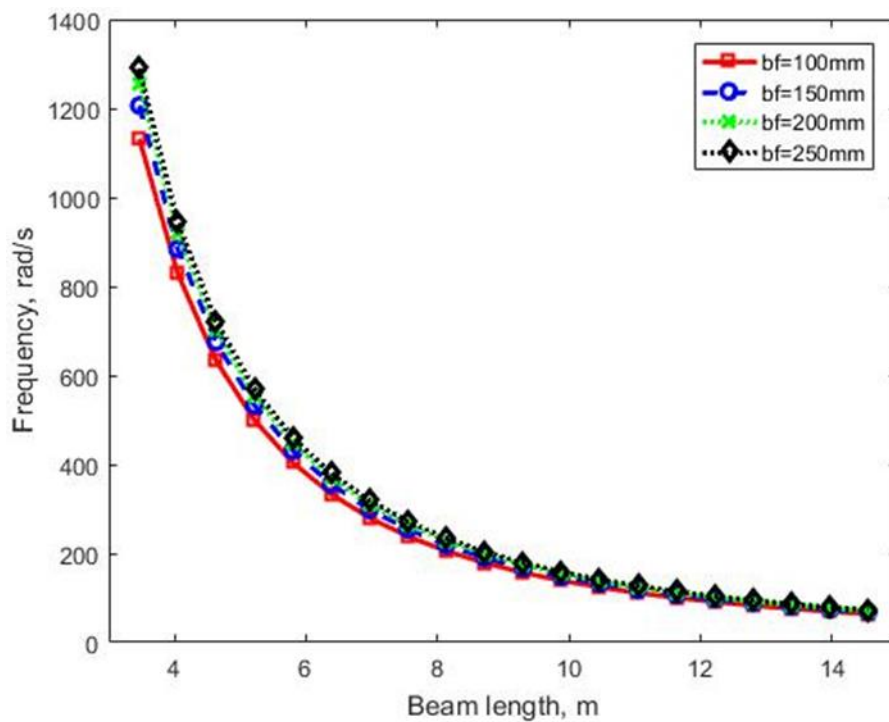
Figure 6-11 Comparison of frequencies of pinned-fixed castellated beams with different flange widths (2nd mode)
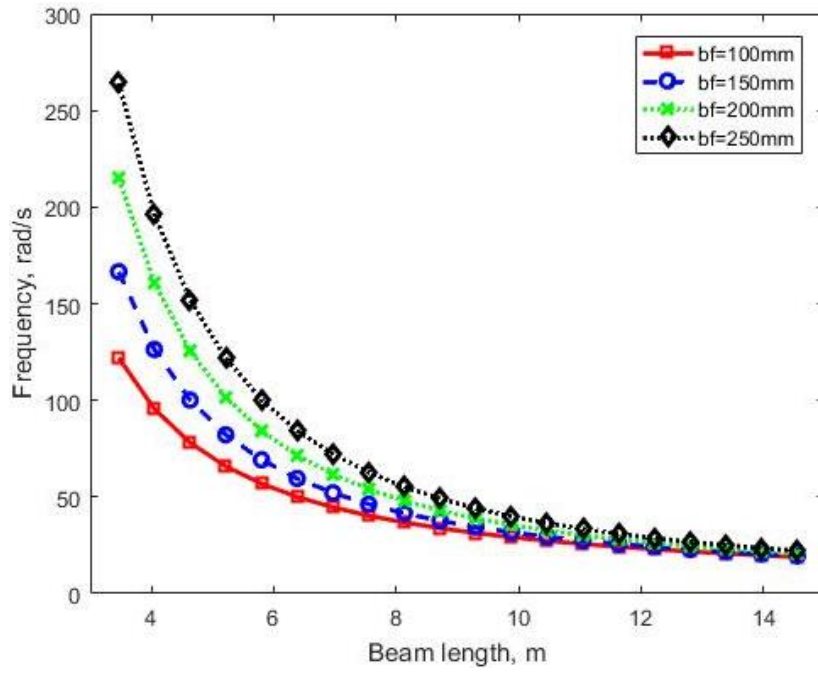
Figure 6-12 Comparison of frequencies of pinned-fixed castellated beams with different flange widths (3rd mode)
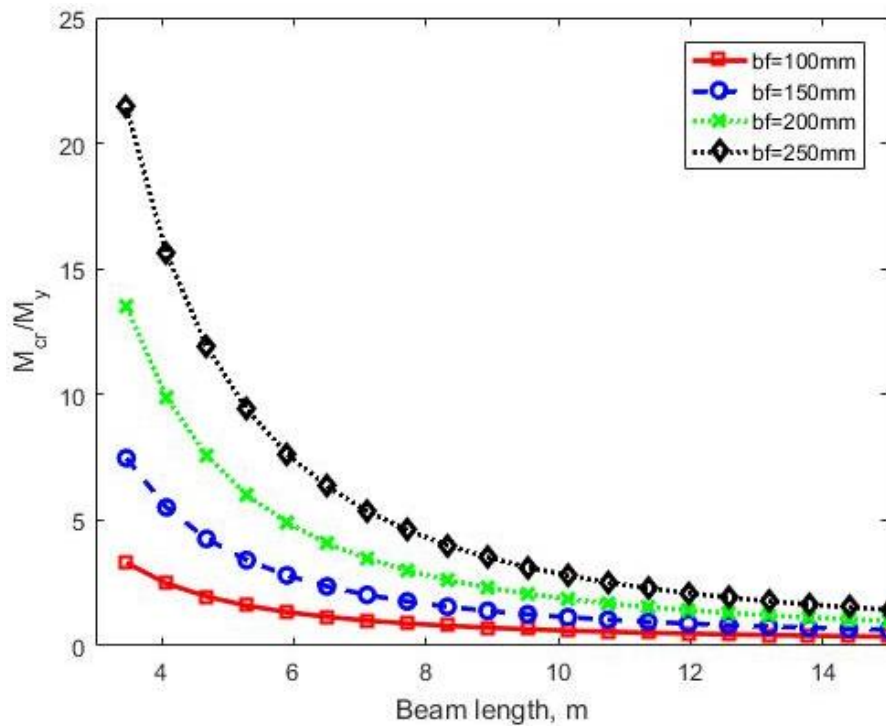
Figure 6-13 Comparison of critical buckling moments of pinned-fixed castellated beam with different flange widths
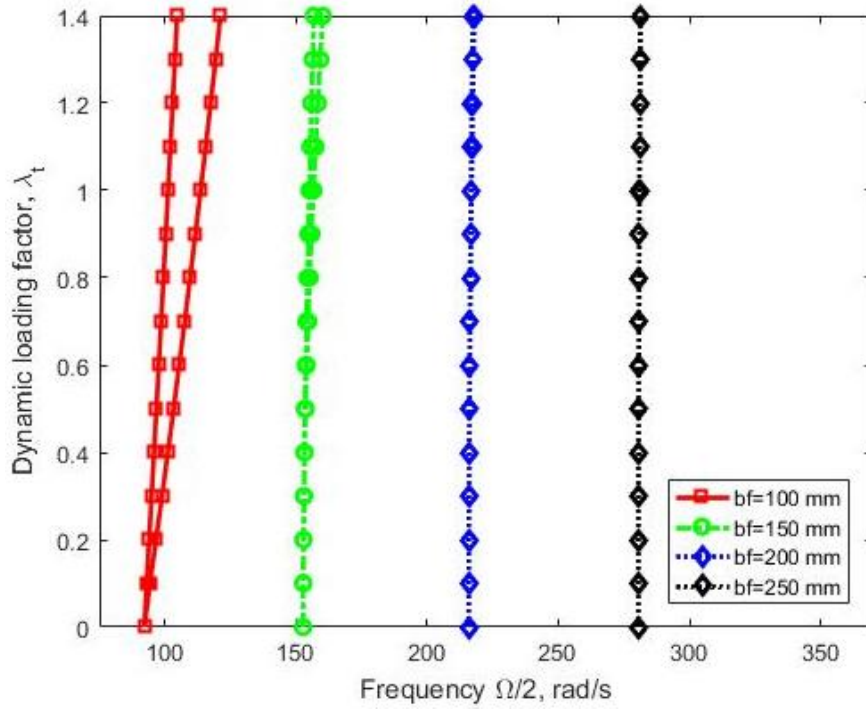
Figure 6-14 Comparison of dynamic instability regions of pinned-fixed castellated beam ($l = 4.156$ m) ($q_{yield} = q_{cr}$ and λ_s=0)
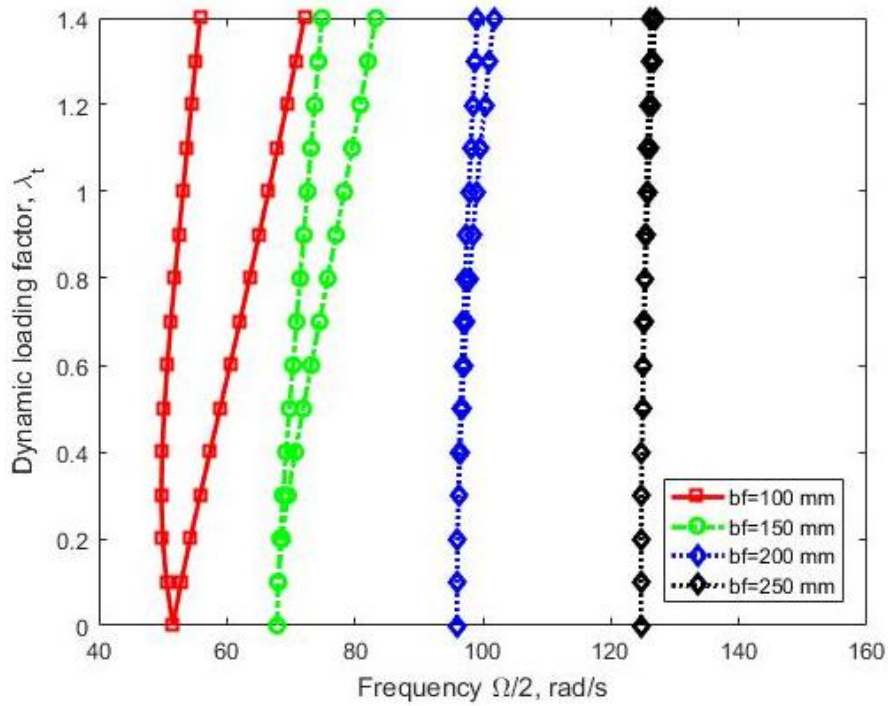
Figure 6-15 Comparison of dynamic instability regions of pinned-fixed castellated beam (l =6.235 m) ($q_{yield} = q_{cr}$ and λ_s=0)
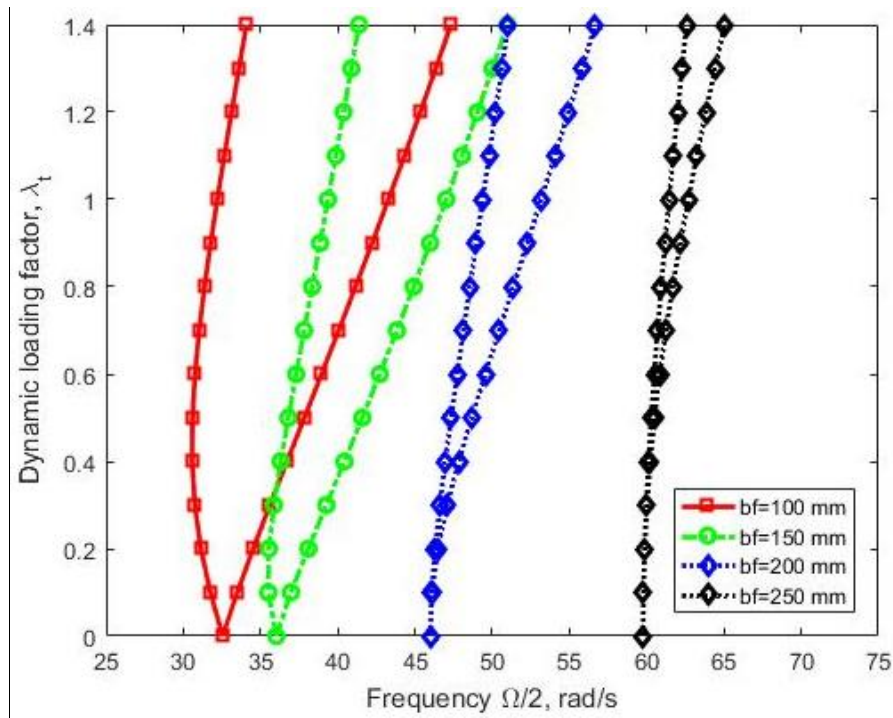
Figure 6-16 Comparison of dynamic instability regions of pinned-fixed castellated beam (l = 9.006 m) ($q_{yield} = q_{cr}$ and λ_s=0)
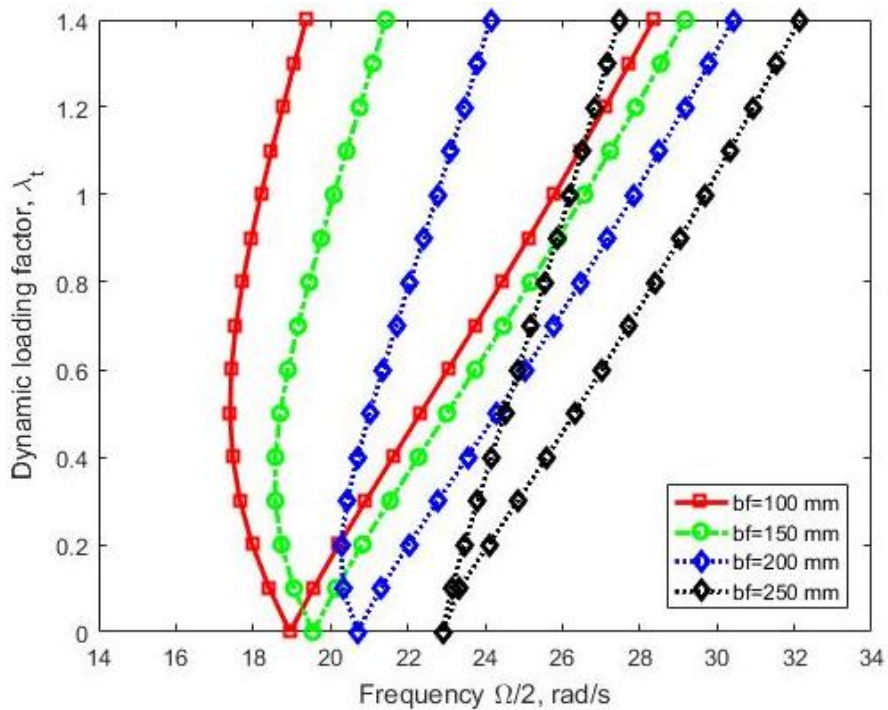
Figure 6-17 Comparison of dynamic instability regions of pinned-fixed castellated beam (l =14.549 m) ($q_{yield} = q_{cr}$ and λ_s=0)

6.6. Conclusions

This chapter has presented an analytical study on the dynamic instability of castellated beams subjected to transverse periodic loading at top flange. The dynamic instability analysis employed in the present study uses Bolotin's method, while the mass, stiffness, and geometric stiffness matrices are derived using the kinetic energy, the strain energy and the potential of applied loads, which are used for conducting the analytical of the frequency of free vibration, the critical load of lateral torsional buckling, and the excitation frequency of dynamic instability region.

From the obtained results the following conclusions can be drawn:

➢ The free vibration, static buckling and dynamic instability analyses of castellated beams subjected to transverse periodic loading at the top flange are influenced by the coupling between the translational and rotational modes.

➢ Increasing the flange width of beam leads to increase both of the frequency and critical buckling moment. However, increasing beam length reduces this effect.

➢ The dynamic instability zone of the castellated beam will move towards to high-frequency side and the corresponding width of the dynamic instability zone decreases when its flanges become wide.

➢ The effect of lateral-torsional buckling on the dynamic instability zone becomes more significant in the short beam than in the long beam, and also in the wide flange beam than in the narrow flange beam.

CHAPTER SEVEN

7. *CONCLUSIONS AND FUTURE STUDIES*

7.1. Conclusions

Despite the widespread use of castellated beams in the structural field, the current design specifications of steel structure do not provide design provisions for the beam. The designing procedure of castellated beams needs to consider three different issues. The first issue is the strength, the second is the deflection and the last one is the lateral torsional buckling. In the castellated beam, these issues are affected by web openings.

The aims of this thesis were to investigate the effect of web openings on the transverse deflection and lateral-torsional buckling of castellated beams and to focus on the effect of both the geometric nonlinear and material inelasticity on castellated beams under uniformly distributed load with different boundary conditions. In addition, the free vibration, static buckling and dynamic instability of castellated beams subjected to transverse periodic loading has been also discussed by developing analytical solutions.

Numerous researches have been conducted to investigate the castellated beams where various methods have been adopted such as experimental, analytical, and numerical methods to predict the calculations' design of the beams. However, these methods differ in terms of safety and accuracy. Some of them need efficiency in using, and are furthermore very expensive.

Both analytical and numerical methods were used to achieve the aims of this thesis. The purpose of developing analytical methods is for the design and practical use,

while the numerical methods developed are for the validation of the analytical methods. The analytical solution is developed using the classical principle of minimum potential energy, whereas the numerical solutions are obtained using the commercial software ANSYS. Bolotin's method is used to perform the dynamic instability analysis.

The conclusions drawn from the analytical and numerical investigations carried out in this research can be summarized as follows:

➢ The present analytical results are in excellent agreement with those obtained from the finite element analysis, which demonstrates the appropriateness of proposed approach.

➢ The shear-induced deflection is proportional to the cross-section area of the two T-sections but inversely proportional to castellated beam length.

➢ The web shear effect on the deflection of castellated beams is very important, particularly for short and medium length beams. In contrast, increasing the beam length reduces the web shear effect on the deflection.

➢ Non-uniform material properties caused by the non-uniform temperature affect the maximum deflection of the castellated beam when the shear effect is considered.

➢ For the same average temperatures, the maximum deflection of the castellated beam under non-uniform temperature distribution with transverse distributed load is directly proportional to the amount of difference in temperatures between the two T- sections of the beam.

➢ For lateral-torsional buckling of the castellated beam, one can ignore the lateral flexural rigidity of the web openings and use the average torsional constant of the full and reduced section properties in the calculation of the critical moment of lateral–torsional buckling of castellated beams.

➢ For linear behaviour, the lateral-torsional buckling results' curves of the analytical solution and numerical analysis have a similar variation pattern.

➢ The failure mode of short castellated beams is dominated by the plastic failure, whereas the failure mode of long castellated beams is dominated by the lateral-torsional buckling failure mode.

➢ The non-linear behaviour showed the critical load of lateral-torsional buckling of castellated beams is influenced by the beam size, web openings, boundary conditions, and material properties of the beam.

➢ The critical loads of flexural and lateral-torsional buckling of castellated beams obtained by using nonlinear 3D finite element analysis are generally less than those obtained from the linear analyses, particularly for beams with short lengths and wide flanges. This indicates that the elastic range is unsafe for short length beam with wide flanges.

➢ The lateral-torsional buckling resistance of castellated beams with short length and/or wide flanges is limited by the ultimate load carrying capacity, in which no lateral-torsional buckling occurs.

➢ When the serviceability is also considered, the deflection limit seems to be the dominant criterion in controlling the load in most of the beam length regions.

➢ The longer the beam, the closer the critical load obtained from the linear lateral-torsional buckling analysis to the failure load obtained from of the full nonlinear analysis.

➢ The longer the beam, the less importance of the nonlinearity need to be considered.

➢ The free vibration, static buckling and dynamic instability analyses of castellated beams subjected to transverse periodic loading at the top flange are influenced by the coupling between the translational and rotational modes.

➢ The frequency and critical buckling moment load are directly proportional to the flange width of castellated beams. However, increasing length of the beam reduces this effect.

➢ The dynamic instability zone of the castellated beam will move towards to high-frequency side and the corresponding width of the dynamic instability zone decreases when its flanges become wide.

➢ The effect of lateral-torsional buckling on the dynamic instability zone becomes more significant in the short beam than in the long beam, and also in the wide flange beam than in the narrow flange beam.

7.2. Future studies

The main conclusions that have been discussed above have presented the primary aims of this thesis, which clearly confirm the need for additional researches, which are recommended as follows:

➢ The analytical method which was developed in this research to calculate the maximum deflections of castellated beams in three different fire scenarios with a uniformly distributed load, needs to enhance the understanding of the fire performance of castellated beams by carrying out an experimental investigation, also to validate the results.

➢ Fire safety is an important aspect that should be considered in the design of the structure because it refers to the protection of the building from the risk of fire. Therefore, further research should focus on the method of calculation of the fire resistance of the castellated beam which is influenced by the cross-sectional geometry, depth and the material of the beam. Additionally, conduct investigations to identify the most suitable fire protection materials insulate of the castellated beam due to the effects of the high temperatures.

➢ In this thesis the material model of the castellated beam is limited to grade 275 MPa, other materials should be studied.

➢ Dynamic instability regions of a castellated beam subjected to non-uniform periodic bending moment with damping can be investigated in future.

➢ The effect of live load on floor vibration may also can be studied.

APPENDIX A

A.1. Web combined stiffness

As for material model castellated beam of steel grade S275, this is assumed to be constructed of linear elastic material with Young's modulus E = 2.1 × 10⁵ MPa, Poisson's ratio v =0.3 and yield stress σ_y=275 MPa.

3D linear shell finite element (SHELL181) is adopted to calculate shear rigidity factor (K_{sh}), which was formed at Eq. (3-27).**Table (A-1)** presents the value of the combined stiffness of the mid part of the web of the castellated beam caused by the bending and shear for groups A,B,C,D,E,F,G,H,I and J (see Section 3.3.4) are obtained by Eq. (3-28) is tabulated under term (K_{b1}); based on: (Yuan et al, 2016) is tabulated under term (K_{b2}); (Yuan et al, 2014) is tabulated under term (K_{b3}).

Table A-1.Web combined stiffness of castellated beams considered

Group	Name of beam	b_f mm	K_{b1} N/mm	K_{b2} N/mm	K_{b3} N/mm
A	A1	100	172257.90	218238.40	279792.80
	A2	150	152065.62	218238.40	279792.80
	A3	200	131873.32	218238.40	279792.80
	A4	250	111681.01	218238.40	279792.80
B	B1	100	199181.01	218238.40	279792.80
	B2	150	192450.24	218238.40	279792.80
	B3	200	185719.47	218238.40	279792.80
	B4	250	178988.70	218238.40	279792.80
C	C1	100	204565.62	218238.40	279792.80
	C2	150	200527.16	218238.40	279792.80
	C3	200	196488.70	218238.40	279792.80
	C4	250	192450.24	218238.40	279792.80
D	D1	100	205911.78	218238.40	279792.80
	D2	150	202546.39	218238.40	279792.80
	D3	200	199181.01	218238.40	279792.80
	D4	250	195815.62	218238.40	279792.80
E	A1	100	172257.90	218238.40	279792.80
	A2	150	152065.62	218238.40	279792.80
	A3	200	131873.32	218238.40	279792.80
	A4	250	111681.01	218238.40	279792.80
F	F1	100	207594.47	218238.40	279792.80
	F2	150	205070.43	218238.40	279792.80
	F3	200	202546.39	218238.40	279792.80
	F4	250	200022.35	218238.40	279792.80
G	G1	100	208155.37	218238.40	279792.80
	G2	150	205911.78	218238.40	279792.80
	G3	200	203668.19	218238.40	279792.80
	G4	250	201424.60	218238.40	279792.80

Group	Name of beam	b_f mm	K_{b1} N/mm	K_{b2} N/mm	K_{b3} N/mm
H	H1	100	209536.04	218238.40	279792.80
	H2	150	207982.78	218238.40	279792.80
	H3	200	206429.53	218238.40	279792.80
	H4	250	204876.27	218238.40	279792.80
I	I1	100	210398.96	218238.40	279792.80
	I2	150	209277.16	218238.40	279792.80
	I3	200	208155.37	218238.40	279792.80
	I4	250	207033.57	218238.40	279792.80
J	J1	100	210719.45	218238.40	279792.80
	J2	150	209757.93	218238.40	279792.80
	J3	200	208796.39	218238.40	279792.80
	J4	250	207834.985	218238.40	279792.80

BIBLIOGRAPHY

ABNT NBR 8800:2008 (2008)."Design of Steel Structures and Mixed Structures of Steel and Concrete Buildings." Brazilian Association of Technical Standards, Rio de Janeiro.

Abreu, L.M.P., Fakury, R.H. and Castro e Silva, A.L.R. (2010). "Determination of Bending Moment Resistance to Lateral Buckling with Torsion of Cellular Steel Beams." Associacao Argentina de Mecanica Computacional, Buenos Aires, XXIX: 7255-7271.

Aglan, A.A. and Redwood, R.G. (1974). "Web buckling in castellated beams." Proceedings of the Institution of Civil Engineers Part 2, Research and Theory,(57): 307-320.

Ahnlén, M. and Westlund, J. (2013). "Lateral Torsional Buckling of I-Beams. A Parametric Study of Elastic Critical Moments in Structural Design Software". Master of Science Thesis in the Master's Programme Structural Engineering and Building Technology. Department of Civil and Environmental Engineering, Division of Structural Engineering, Steel and Timber Structures, Chalmers University of Technology, Göteborg, Sweden.

Altifillisch, M. D., Cooke, R. B. and Toprac, A. A. (1957). "An investigation of open web expanded beams." Welding Research Council Bulletin, New York, 47: 307-320.

American Institute of Steel Construction (AISC) (2011). "ANSI/AISC 360–10 specification for structural buildings14th ed.", Chicago, Illinois, USA.

BIBLIOGRAPHY

Aminian, P., Niroomand, H., Gandomi, A. H., Alavi, A. H. and Arab Esmaeili, M. (2013). "New design equations for assessment of load carrying capacity of castellated steel beams: a machine learning approach." Neural Computing and Applications, 23(1): 119-131.

ANSYS User's Manual. (2017). "ANSYS Mechanical APDL Technology Demonstration Guide." Release 18.1, Canonsburg, USA: ANSYS Inc.

Anupriya, B. and Jagadeesan, D. K. (2014). "Shear strength of castellated beam with and without stiffeners using FEA (Ansys 14)." International Journal of Engineering and Technology (IJET), 6(4): 1970-1981.

ArcelorMittal. (2008). ArcelorMittal Europe: Long products sections and merchant bars ACB. Cellular Beams.

Badke-Neto, A., Calenzani, A.F. G. and Ferreira, W. G. (2015). "Study of methods for the design of cellular composite steel and concrete beams." Ibracon structures and material Journal, 8(6): 827-859.

Bake, S. M. (2010)."Cellular beams at ambient and elevated temperatures." PhD. dissertation, The University of Manchester, Manchester, UK.

Bolotin, V.V. (1964). "The dynamic stability of elastic systems." San Francisco, CA: Holden-day, Inc.

Boyer, J. P. (1964). "Castellated Beam- A New Development Castellated beams-new developments." AISC Engineering, 1(3): 104-108.

Bradley, T. P. (2003). "Stability of Castellated Beams During Erection." Master's Thesis, Thesis submitted to the Faculty of the Virginia Polytechnic Institute and State University, Blacksburg.

British Standards Institution (BSI). (2000). ".BS5950-1 structural use of steelwork in buildings-Part 1, code of practice for design rolled and welded sections." ,England.

Chang, C-S. and Hodges, D.H. (2009). "Stability studies for curved beams." Journal of Mechanics of Materials and Structures, Journal of Mechanical Material and Structures, 4(7, 8):1257-70.

Chen, L. Y., Lin, P. D. and Chen, L. W. (1991). "Dynamic stability of thick bimodulus beams)." Computers & Structures, 41(2): 257-263.

Chung, K., Liu, T. and Ko, A. (2001). "Investigation on Vierendeel mechanism in steel beams with circular web openings." Journal of Constructional Steel Research, 57(5a): 467-490.

Crisfield, M.A. (1981). "A fast incremental/iterative solution procedure that handles snap-through." Computer & Structures, 13:55-62.

Demirdjian, S. (1999). "Stability of castellated beam webs." PhD, McGill University Montreal, Canada.

Durif, S., Bouchaïr, A. and Vassart, O. (2013). "Experimental tests and numerical modeling of cellular beams with sinusoidal openings." Journal of Constructional Steel Research, 82: 72-87.

Durif, S., Vassart, O., Bouchaïr, A. and Muzeau, J. P. (2011). "Modèle mécanique pour les poutres à larges ouvertures d'âmes de section variable." In XXIXe Rencontres Universitaires de Génie Civil, AUGC, Tlemcen, 1(29): 345-355.

El-Sawy, K. M., Sweedan, A. M. and Martini, M. I. (2009). "Major-axis elastic buckling of axially loaded castellated steel columns." Thin-Walled Structures, 47(11): 1295-1304.

Ellobody, E. (2011). "Interaction of buckling modes in castellated steel beams." Journal of Constructional Steel Research, 67(5): 814-825.

Ellobody, E. and Young, B. (2015). "Nonlinear analysis of composite castellated beams with profiled steel sheeting exposed to different fire conditions." Journal of Constructional Steel Research, 113: 247-260.

Erdal, F. and Saka, M. P. (2013). "Ultimate load carrying capacity of optimally designed steel cellular beams." Journal of Constructional Steel Research, 80: 355-368.

Erdal, F., Tunca, O. and Tas, S. (2015). "Nonlinear finite element analysis of optimally designed steel cellular beams." Research on Engineering Structures and Materials 2(2): 59-66.

European Committee for Standardization EN1993-1-1 (2005). "Eurocode 3. Design of steel structures, Part1.1: General rules and rules for building."

Forde, B. D. R. and Stiemer, S. F. (1987) "Improved Arc Length Orthogonality Methods for Nonlinear Finite Element Analysis." Computers and & Structures, 27(5): 625-630.

Gandomi, A. H., Tabatabaei, S. M., Moradian, M. H., Radfar, A. and Alavi, A. H. (2011). "A new prediction model for the load capacity of castellated steel beams." Journal of Constructional Steel Research, 67(7): 1096-1105.

Gao, K., Gao, W., Wu, BH. and Song, CM. (2019). "Nondeterministic dynamic stability assessment of Euler–Bernoulli beams using Chebyshev surrogate model." Applied Mathematical Modelling, 66, 1-25.

Gholizadeh, S., Pirmoz ,A. and Attarnejad, R. (2011). "Assessment of load carrying capacity of castellated steel beams by neural networks." Journal of Constructional Steel Research, 67(5): 770-779.

Gürgöze, M. (1985). "On the dynamic stability of a pre-twisted beam subject to a pulsating axial load." Journal of Sound and Vibration, 102(3): 415-422 (1985).

Halleux, P. (1967). "Limit Analysis of Castellated Beams." Acier-Stahl-Steel, 3: 133-144.

Harper, C. (1991). "Design in steel 4: castellated & cellular beams." British Steel.

Hosain, M., Cheng, W. and Neis, V. (1974). "Deflection analysis of expanded open-web steel beams." Computers & Structures, 4(2): 327-336.

Hosain, M. and Spiers, W. (1971). "Failure of Castellated Beams due to Rupture of Welded Joints." Acier-Stahl-Steel, 36(1):34-40

Hosain, M. and Spiers, W. (1973). "Experiments on castellated steel beams." American Welding Society, Welding Research Supplement, 52(8): 329S-342.

Hsu, C.S. (1966). "On dynamic stability of elastic bodies with prescribed initial conditions." International Journal of Engineering Science, 4 (1):1-21.

Huang, C. C. (1980). "Dynamic stability of generally orthotropic beams." Fibre Science and Technology, 13(3): 187-198.

Huang, J.S. and Hung, L.H. (1984). "Dynamic stability for a simply supported beam under periodic axial excitation." International Journal of Non-Linear Mechanical, 19(4):287-301.

Jovic, M. (2015). "Lateral torsional buckling analysis of multiple laterally restrained I-beams in bending." Master thesis A-2015.102. Eindhoven University of Technology Department of the Built Environment Structural Design

Kar, R. and Sujata, T. (1991). "Dynamic stability of a rotating beam with various boundary conditions." Computers & Structures, 40(3): 753-773.

Kerdal, D. (1982). "Lateral-torsional buckling strength of castellated beams." PhD thesis, Civil and Structural Engineering, Faculty of Engineering (Sheffield), University of Sheffield, Sheffield, UK.

Kerdal, D. and Nethercot, D. (1984). "Failure modes for castellated beams." Journal of Constructional Steel Research, 4(4): 295-315.

Kim, B., Li, L. and Edmonds, A. (2016). "Analytical Solutions of Lateral–Torsional Buckling of Castellated Beams." International Journal of Structural Stability and Dynamics, 16(8): 1-16 (1550044).

Knowles, P. R. (1991). "Castellated beams." Proceeding of the Institution of Civil Engineers, ICE, London, UK 90(Part 1): 521-536.

Kohnehpooshi, O. and Showkati, H. (2009). "Numerical Modeling and Structural Behavior of Elastic Castellated Section", European Journal of Scientific Research, 31(2):306–18.

Korrani, H. K., Kabir, M. and Molanaei, S. (2010). "Lateral-Torsional Buckling of Castellated Beams under End Moments." International Journal. of Recent Trends in Engineering and Technology, 3(5): 16-19.

Kratzig, WB, Li L. and Nawrotzki, P. (1991). "Stability conditions for non-conservative dynamical systems." Computational Mechanics, 8(3):145-51.

Kwani,S. and Wijaya, P. K. (2017). "Lateral torsional buckling of castellated beams analyzed using the collapse analysis." Procardia Engineering, 171: 813-820.

Lawson, R. M. and Hicks, S. J. (2011). "Design of composite beams with large web openings." (SCI P355), The Steel Construction Institute Publication.

Lei, J. S., Yuan, W. B. and Li, L. Y. (2017). "Axial compression buckling of castellated columns at elevated temperatures." International Journal of Structural Stability and Dynamics, 17(3): 1750034

Li, L. Y. (1991). "Interaction of forced and parametric loading vibrations." Computers & Structures, 40(3):615-618.

Li, L. Y., Ren, C. and Yang, J. (2012). "Theoretical analysis of partially restrained zed-purlin beams subjected to up-lift loads." Journal of Constructional Steel Research, 70: 273-279.

Liu, T. and Chung, K. (2003). "Steel beams with large web openings of various shapes and sizes: finite element investigation." Journal of Constructional Steel Research, 59(9): 1159-1176.

Maalek, S. (2004). "Shear deflections of tapered Timoshenko beams." International Journal of Mechanical Sciences, 46(5): 783-805.

Martins, C.H., Fer-reira, F.P.V., Rossi, A. and Trentini, E.V.W. (2017)." Numerical Analysis of Physical and Geometrical Imperfections in Cellular Beams." Open Journal of Civil Engineering, 7: 116-129.

Menkulasi, F., Moen, C., Eatherton, M. and Kuruppuarachchi, D. (2015). "Investigation of Stiffener Requirements in Castellated Beams."

Structural Stability Research Council Annual Stability Conference SSRC.

Mohebkhah, A. (2004). "The moment-gradient factor in lateral-torsional buckling on inelastic castellated beams." Journal of Constructional Steel Research, 60(10): 1481-1494.

Mohebkah, A. (2011), "Lateral buckling resistance of inelastic I-beams under off-shear center loading." Thin-Walled Structures, 49: 431-436.

Mohebkhah, A. and Showkati, H. (2005). "Bracing requirements for inelastic castellated beams." Journal of Constructional Steel Research, 61(10): 1373-1386.

Morkhade, S. G. and Gupta, L.M. (2015). "An experimental and parametric study on steel beams with web openings." International journal of advanced structural engineering, Springer, 7(3):249-260.

Morris, N. F (1965). "The dynamic stability of beam-columns with a fixed distance between supports." Journal of the Franklin Institute, 280(2): 163-173.

Müller, C., Hechler, O., Bureau , A., Bitar, D., Joyeux, D., Cajot , L-G., Demarco, T., Lawson, M., Hicks, S., Devine, P., Lagerqvist, O., Hedman-Pétursson, E., Unosson, E. and Feldmann, M. (2006). "Large web openings for service integration in composite floors." Design Guide (en), Technical steel report.

Nethercot D.A and Kerdal, D. (1982). "Lateral-torsional Buckling of Castellated Beams." The Structural Engineer, 60B (3):53-61.

New steel construction technical report. (2006). "Lateral torsional buckling and slenderness." NSC, October: 30-34.

Nseir, J., Lo, M., Sonck, D., Somja, H., Vassart, O. and Boissonnade, N. (2012). "Lateral torsional buckling of cellular steel beams." Proceedings of the Annual Stability Conference, Structural Stability Research Council, Grapevine, Texas, April 18-21.

BIBLIOGRAPHY

Okubo, T. and Nethercot, D. (1985). "Web post strength in castellated steel beams." Proceedings of the Institution of Civil Engineers, Part 2: Research and Theory, 79: 533-557.

Pachpor, P.D., Gupta, L.M. and Deshpande, N.V. (2014). "Analysis and design of cellular beam and its verification", International Conference on Applied Computing, Computer Science and Computer Engineering, IERI Procardia, 7: 120-127.

Panedpojaman, P. (2015). "Investigation on lateral torsional buckling resistance of ec3 for cellular beam." International Journal of Advances in Mechanical and Civil Engineering, 2(4) ISSN: 389-399.

Panedpojaman, P. and Rongram, T. (2014). "Design equations for Vierendeel bending of steel beams with circular web openings." Proceedings of the World Congress on Engineering (WCE 2014), vol. II, July 2-4, London, UK.

Park, Y.P. (1987). "Dynamic stability of a free Timoshenko beam under a controlled follower force." Journal of Sound and Vibration, 113(3):407-15.

Patel, S.N, Datta, P.K. and Sheikh, A.H. (2006). "Buckling and Dynamic Instability Analysis of Stiffened Shell Panels." Thin-Walled Struct, 44: 321-333.

Pattanayak, U. and Chesson, E. (1974). "Lateral Instability of Castellated Beams." AISC Engineering Journal, 11(3): 73-79.

Pourbehi, P. and Pirmoz, A. (2015). "Shear response of castellated steel beams." International Journal of Steel Structures, 15(2): 389-399.

Radić., I. and Markulak, D. (2007). "Lateral buckling of castellated beams. " Technical Gazette, 14(1, 2): 25-35.

Redwood, R. and Demirdjian, S. (1998). "Castellated Beam Web Buckling in Shear." Journal of Structural Engineering (ASCE), 124(10): 1202-1207.

Sehwail, M.M. (2013). "Lateral Torsional Buckling of steel I-section Cellular Beams." Gazimagusa, Estern Mediterranean University.

Sherbourne, A. and Van Oostrom, J. (1972). "Plastic analysis of castellated beams—I interaction of moment, shear and axial force." Computers & Structures, 2(1): 79-109.

Showkati, H (2008). "Lateral-Torsional Buckling of Castellated Beams." Iranian Journal of Science & Technology, Transaction B, Engineering, 32:153-156.

Showkati, H., Ghazijahani, T. G., Noori, A. and Zirakian, T. (2012). "Experiments on elastically braced castellated beams." Journal of Constructional Steel Research, 77: 163-172.

Soltani, M. R., Bouchaïr, A. and Mimoune, M. (2012). "Nonlinear FE analysis of the ultimate behavior of steel castellated beams." Journal of Constructional Steel Research, 70: 101-114.

Sonck, D. (2014). "Global buckling of castellated and cellular steel beams and columns." Ph.D. dissertation, Ghent Univ., Ghent, Belgium.

Sonck, D. and Belis, J. (2016). "Lateral-Torsional Buckling Resistance of Castellated Beams." Journal of Constructional Steel Research, 105: 119-128.

Sonck, D., Kinget, L. and Belis, J. (2015). "Deflections of cellular and castellated beams." Future Visions (International Association for Shell and Spatial Structures), Proceedings (pp. 1–12). Presented at the Future Visions (International Association for Shell and Spatial Structures) (IASS2015), Amsterdam, The Netherlands: Koninklijk Instituut van Ingenieurs, Nederland.

Sonck, D., Van Impe, R. and Belis, J. (2014). "Experimental investigation of residual stresses in steel cellular and castellated members." Journal of Construction and Building Materials, 54: 512-519.

Srimani, S. S. and Das, P. (1978). "Finite element analysis of castellated beams." Computers & structures, 9(2): 169-174.

Standards Australia (SA) (1998). "AS 4100 Steel Structures."Sydney, Australia.

Sweedan, A. (2011). "Elastic lateral stability of I-shaped cellular steel beams." Journal of Constructional Steel Research, 67 (2): 151-163.

Timoshenko, S. P. and Gere, J. M. (1961). "Theory of elastic stability." McGrawHill-Kogakusha Ltd, Tokyo.

Toprac, A. and Cooke, B. (1959). "The plastic behavior of castellated beams." Welding Research Council Bulletin, New York, 47: 1-10.

Tsavdaridis, K. D. and D'Mello,C. (2011). "Web buckling study of the behaviour and strength of perforated steel beams with different novel web opening shapes." Journal of Constructional Steel Research, 67(10): 1605-1620.

Tsavdaridis, K. D. and D'Mello, C. (2012). "Vierendeel Bending Study of Perforated Steel Beams with Various Novel Web Opening Shapes through Nonlinear Finite-Element Analyses." Journal of Structural Engineering, 138(10): 1214-1230.

Yeh, J. Y., Chen, L. W. and Wang, C. C. (2004). "Dynamic stability of a sandwich beam with a constrained layer and electro rheological fluid core". Composite Structures, 64(1): 47-54.

Yoon, S. J.and Kim, J. H. (2002) "A concentrated mass on the spring unconstrained beam subjected to a thrust." Journal of Sound and Vibration, 254(4): 621-634.

Yuan, W.B., Kim, B. and Li, L.Y. (2014). "Buckling of axially loaded castellated steel columns." Journal of Constructional Steel Research, 92: 40-45.

Yuan, W. B., Yu, N.T., Bao, Z.S. and Wu, L.P. (2016). "Deflection of castellated beams subjected to uniformly distributed transverse loading." International Journal of Steel Structures, 16(3): 813-821.

Uang, C.M. and Fan, C.C. (2001). "Cyclic stability criteria for steel moment connections with reduced beam section." Journal of Structural Engineering, 127(9): 1021-1027.

Van Oostrom, J. and Sherbourne, A. (1972). "Plastic analysis of castellated beams—II Analysis and tests." Computers & Structures, 2(1-2): 111-140.

Wang, P., Ma, Q. and Wang, X. (2014). "Investigation on Vierendeel mechanism failure of castellated steel beams with fillet corner web openings." Engineering Structures, 74: 44-51.

Wang, P., Ma, N. and Wang, X. (2014). "Numerical studies on large deflection behaviors of restrained castellated steel beams in a fire." Journal of Constructional Steel Research, 100: 136-145.

Wang, P., Wang, X. and Ma, N. (2014). "Vertical shear buckling capacity of web-posts in castellated steel beams with fillet corner hexagonal web openings." Engineering Structures, 75: 315-326.

Ward, J. K. (1990)."Design of composite and non-composite cellular beams." The Steel Construction Institute Publication, SCI publications 100.

Zaarour, W. and Redwood, R. (1996). "Web buckling in thin webbed castellated beams." Journal of Structural Engineering, 122(8): 860-866.

Zirakian, T. and Showkati, H. (2006). "Distortional buckling of castellated beams." Journal of Constructional Steel Research, 62(9): 863-871.

Zhu, J., Qian, S. and Li, L.Y. (2017). "Dynamic instability of laterally-restrained zed-purlin beams under uplift loading." International Journal of Mechanical Sciences, 131–132: 408–413.

Zhu, J., Qian, S. and Li, L.Y. (2018). "Dynamic instability of channel-section beams under periodic loading." Mechanics of Advanced Materials and Structures (in press) (https://doi.org/10.1080/15376494.2018.1501521).